Inclusive Neutron Analysis in MIPP Experiment

a technical report on the neutron analysis

Turgun Nigmanov, Michael Longo, Durga Rajaram, Dick Gustafson

University of Michigan

November 3, 2010

Abstract

We demonstrate that the Main Injector Particle Production (MIPP) experiment has the ability to detect neutrons with good energy resolution [1]. The most comprehensive measurements of inclusive neutron production cross sections were recently made by the NA49 collaboration using pp collisions at 158 GeV/c [2]. Using the Fermilab Main Injector proton beam we study the neutron production spectra at 58 GeV/c and 120 GeV/c with liquid hydrogen, beryllium, carbon, bismuth and uranium targets. This note describes the detailed analysis procedure for inclusive neutron production cross section measurements using data from the MIPP experiment.

Contents

1 Introduction

The neutron analysis is based on MIPP experimental data processed with MIPP software release "pass4f".

2 Interaction Targets

The target properties shown on Table 1.

name	A	d, cm	m, g	AD, g/cm^2	IL, %	$n_t \times 10^{23}$cm^{-2}	ρ(db)	ρ(MC)
H_2 liquid	1.008	14.0		0.991		5.922		
Beryllium	9.012	0.399	14.4	0.71	0.94	0.4744	1.779	1.848
Carbon	12.011	1.003	34.0	1.677	1.94	0.8408	1.672	2.000
Bismuth	208.98	0.173	34.25	1.69	0.87	0.0487	9.769	9.780
Uranium	238.03	0.1	38	1.875	?	0.0474	18.75	18.95

Table 1: The targets and their properties, where d - thickness in cm, m - mass in g, AD - areal density in g/cm^2, IL - interaction length and n_t is a number of nucleus per cm^2.

The n_t quantity in Table was calculated as:

$$n_t = \frac{N_A \times density \times thickness}{A},$$

where N_A is Avogadro number, density $\times$ thickness is an areal density AD and A is a target atomic weight.

Figure 1 shows the nuclear target positions within the "target wheel" vs run number for 58 GeV/c (on left) and 120 GeV/c (on right) data.

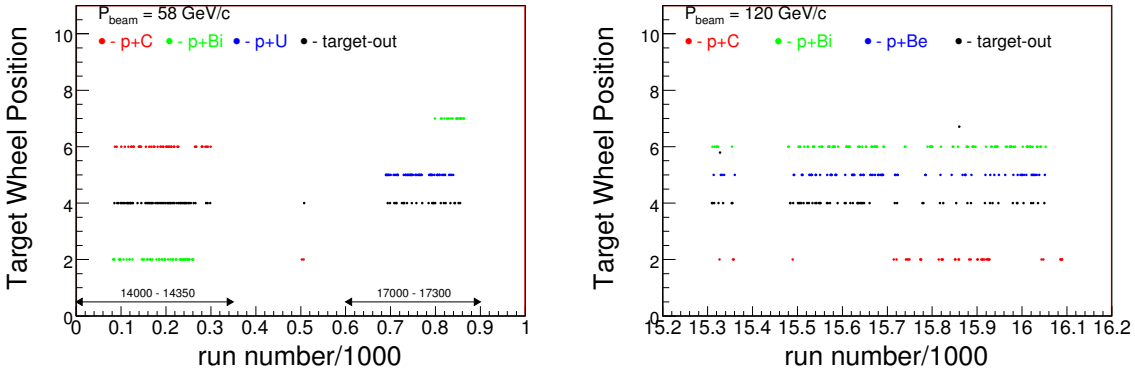

Figure 1: The nuclear target positions within the "target wheel" vs run number for 58 GeV/c (on left) and 120 GeV/c (on right) data.

3 Event Selection

The neutron analysis was done using a "good" event sample. It means that each event should pass some preliminary conditions:

- No more than 30 tracks per event
- EMCAL and HCAL detectors status should have readout
- "Good" beam track
- Trigger scintillator is on
- Use events with reliable tracking conditions

Each event was tested for "clean" conditions: no more than 30 tracks and valid EMCAL and HCAL status. We used data when "SciHi" scintillator trigger was available and it's conditions (HV, threshold) were stabilized. According to [3] such conditions are started from run number 13267. Efficiencies for each above mentioned cuts are summarized in Tables 3 and 4.

3.1 Selection of "good" beam track

The beam track selection was done according to following criteria:

- Use events with single beam track
- Reduce unreconstructed second beam tracks: nBeamCrossings$\leq$4
- Apply beam track time cut
- Use beam track segment "xbc3[3]" and track slopes
- Project it to Z_{tgt} and apply a specific spot size cut depending on the target type and beam momenta
- Beam divergence cut

The proton beam track time distributions are presented in Figure 2 for 58 GeV/c and 120 GeV/c momenta. Plots clearly shows the presence of the bucket structure, with about 19 ns separation and half width of 9.5 ns. Buckets closest to central bucket are at -12 ns and at 24 ns. Hence we set cuts at -2 ns and at 15 ns.

The fraction of events when the beam track is off-time is 2.5%. The time gates for the tracking system and calorimeters are wider than for the BC1-3 beam chambers. Hence the actual contribution to the neutron candidates from other buckets might be more significant.

Selection of the transverse position cut for the incident beam is based on the beam spot at the center of the target. This is a good approach for the thin target data. But

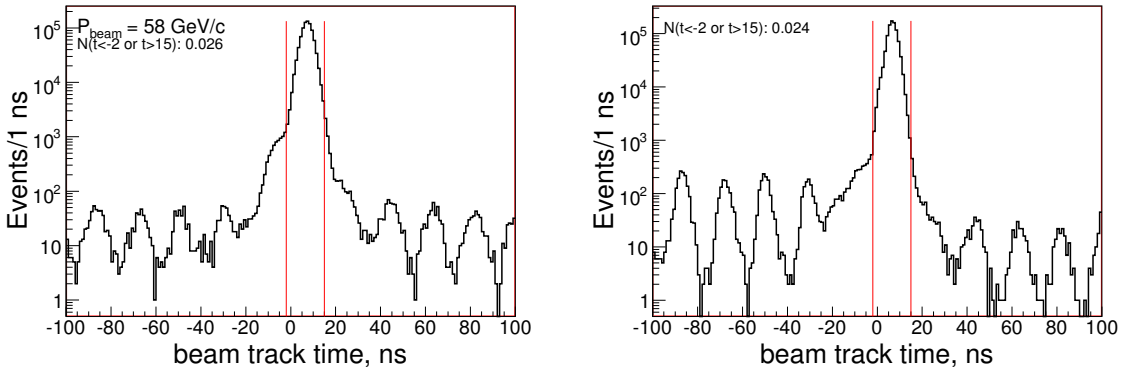

Figure 2: The beam track time distributions for 58 GeV/c (on left) and for 120 GeV/c protons (on right). The time info is based on the beam chambers. The red lines illustrate the selected time cut: time should be within -2 ns $< t <$ 15 ns.

for the liquid hydrogen data we need to follow the LH2 tube position and its radius. We also found that part of the transport pipes are shadowing the LH2 volume. For the shadowed area we might expect that the beam track with some probability might interact with pipe and disappear. Then the incident beam might be overestimated. The best solution is to drop the beam tracks in this area. The details on this matter are described in Appendix A.

In order to calculate the beam spot we used the beam track segment "xbc3" and its slopes. We assumed that these parameters are less biased to the tracks downstream of the target. The beam positions shown in Figure 3 for 58 GeV/c and in Figure 5 for 120 GeV/c protons at Z of the thin target. The red lines show what was selected as the beam spot center, (X_o and Y_o). We used a cut of R $\leq$ 2.0 cm for 58 GeV/c and R $\leq$ 0.8 cm for 120 GeV/c beam, in order to eliminate the beam halo. This cut drops about 3% of events (using 120 GeV/c). The beam spot position for 58 GeV/c data was considered as run dependent (see Fig. 6).

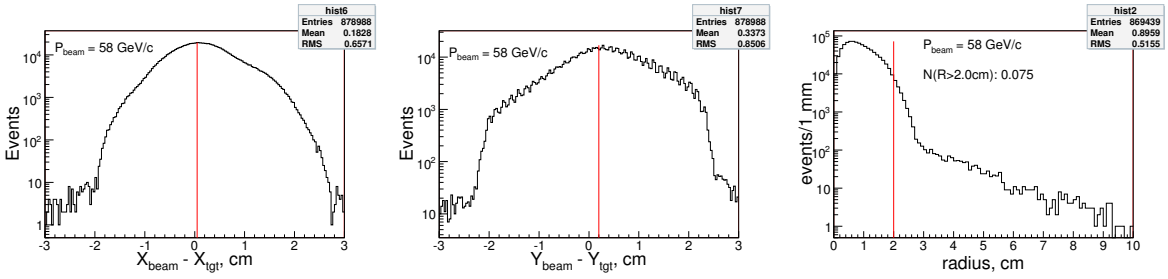

Figure 3: The beam track position distributions at Z of thin target using 58 GeV/c protons. The red lines on left and in middle plots illustrate the average beam spot center, X_o and Y_o. The right plot shows the distance between target center and the position of the particle. The red line there shows the radius cut position.

The 58 GeV/c beam divergences shown in Figure 4.

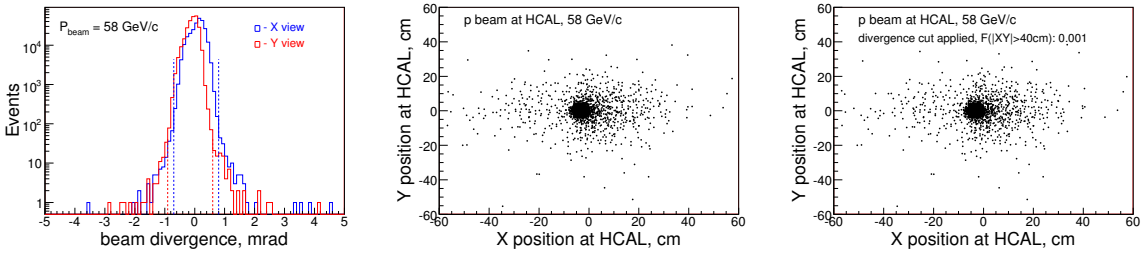

Figure 4: Left plot: the beam track divergence distributions for 58 GeV/c protons. Middle plot: track projections at HCAL for beam triggers and single track events. Right plot: same as on middle except that the divergence cut applied: from -0.7 up to 0.8 mrad in X-view and from -0.9 up to 0.6 mrad in Y-view.

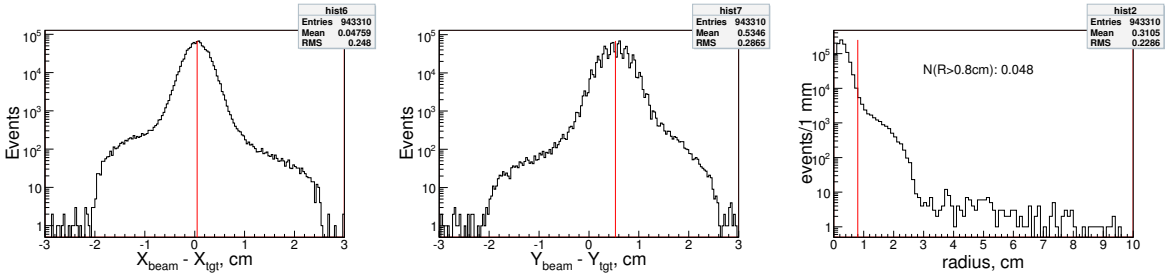

Figure 5: The beam track position distributions at Z of carbon (2%) target using 120 GeV/c protons. The red lines on left and in middle plots illustrate the selected beam spot center, X_o and Y_o. The right plot shows the distance between beam center and the position of the particle. The red line there shows the radius cut position.

Selected beam spot centers (X_o,Y_o) and radius values for the different beam settings and targets are presented in Table 2.

The beam track transverse position and the width variations at the Z Z_{tgt} vs run number presented in Figure 6. So, we required that both distances: from the beam mean position up to the particle and particles distance from the beam axis should be less than 2.0 cm.

3.2 Trigger Scintillator

Our neutron analysis would be based on the trigger scintillator. Figure 7 illustrates the scintillator trigger behavior vs the run number.

The left plot in Fig. 7 is "SciHi" rate vs run number for 58 GeV/c data, right plot - for 120 GeV/c data. By viewing "SciHi" rates we conclude that some runs are not useful for the neutron analysis: runs where rate is equal to 0 or below of the

beam momentum	X_o,cm	$Y_o$cm	Radius, cm	ϵ_{beam}
58 GeV/c, LH				
58 GeV/c, thin	0.05	-0.2	2.0	0.92
84 GeV/c, LH				
120 GeV/c, thin	0.05	0.53	0.8	0.95

Table 2: Selected spot center (X_o,Y_o) and radius values used as the transverse position cut for counting of incident protons. Last column represents the combined efficiency of the beam track time, divergence and radius cuts.

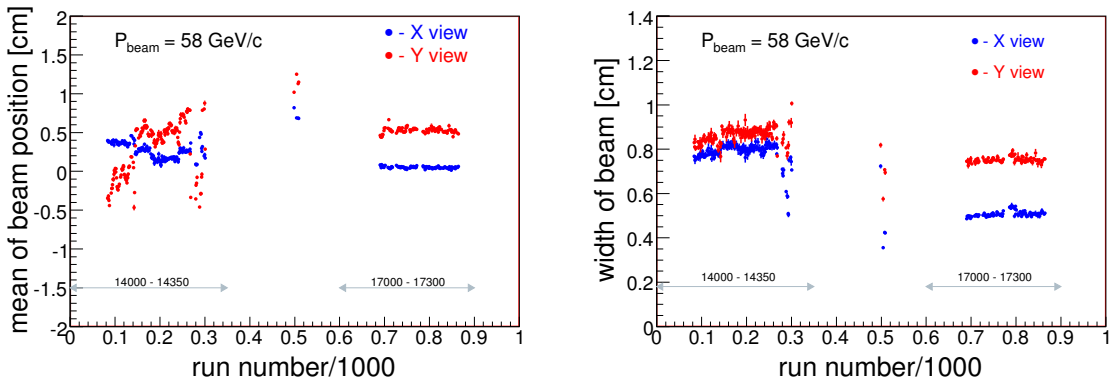

Figure 6: The beam track transverse position (on left) and width (on right) distributions vs run number at Z of thin target using 58 GeV/c protons.

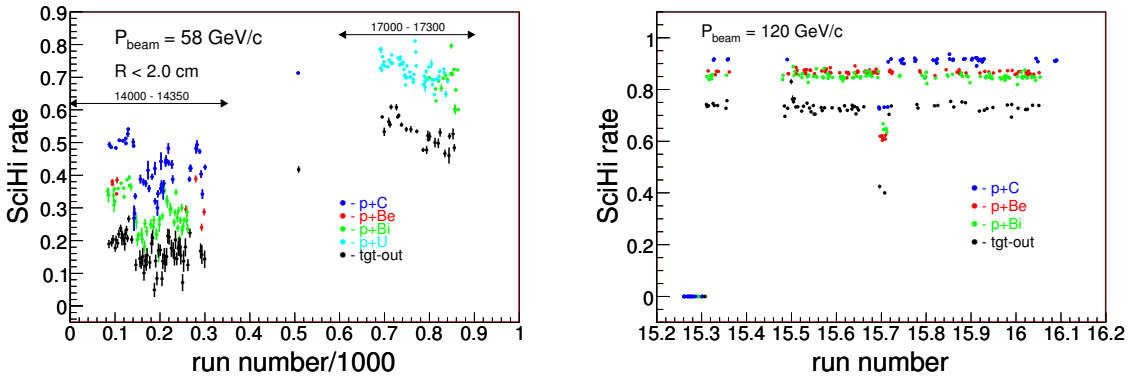

Figure 7: "SciHi" fires normalized per single proton interaction vs the run number: at 58 GeV/c (on left) and at 120 GeV/c (on right).

respective band. For 58 GeV/c data (left plot) we see that "SciHI" rate in run range between 14060 and 14300 are systematically lower by at least factor of 2 than for data with runs above 17000. What is a reason for that? Study shows that if we require a reasonable Z cut on 58 GeV/c data, then the "SciHi" rate would be more uniform. Figure 8 illustrates the case when -4cm< Z_{vtx} <2cm requirements made for the 58 GeV/c data. The remained run dependence can be explained by the beam width and the transverse position variations.

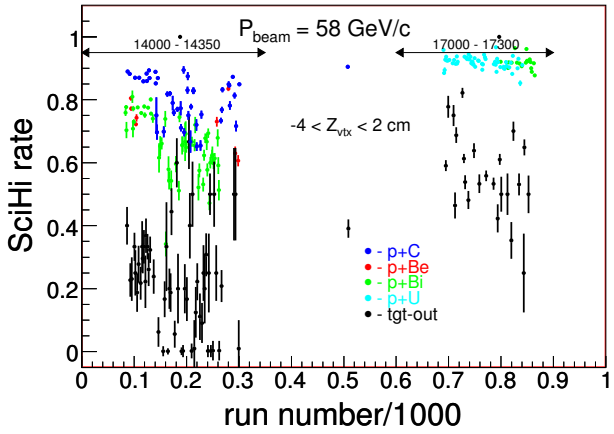

Figure 8: "SciHi" fires rate per proton interactions vs the run number, 58 GeV/c data

Figure 9 illustrates the scintillator trigger rate per single incident proton beam vs the run number.

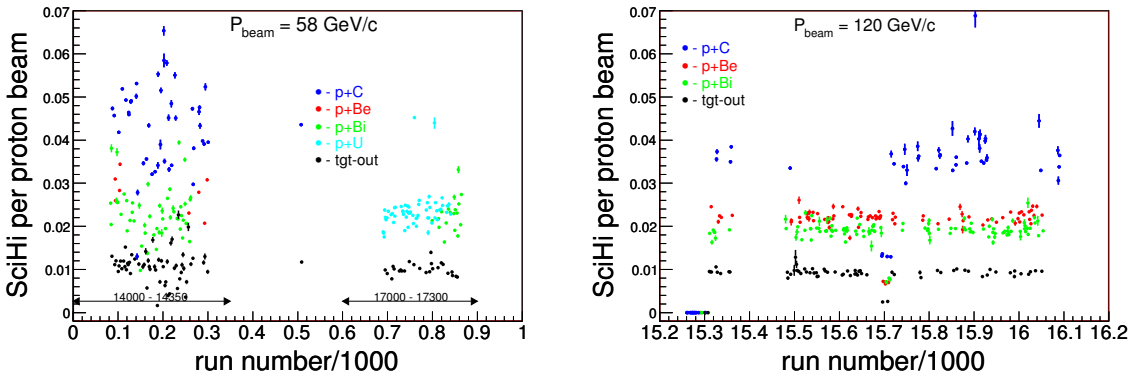

Figure 9: "SciHi" fires normalized per single incident proton beam vs the run number. Left plot - 58 GeV/c, right - 120 GeV/c data.

3.3 Selection of events with reliable tracking conditions

We found that in a relatively small fraction of events the sum of momenta of tracks is significantly higher than the beam momentum. Figure 10 illustrates the sum of momenta of the charged tracks in event using 120 GeV/c proton beam incident on carbon 2% target. The tracks from the primary vertex were used to make this plot.

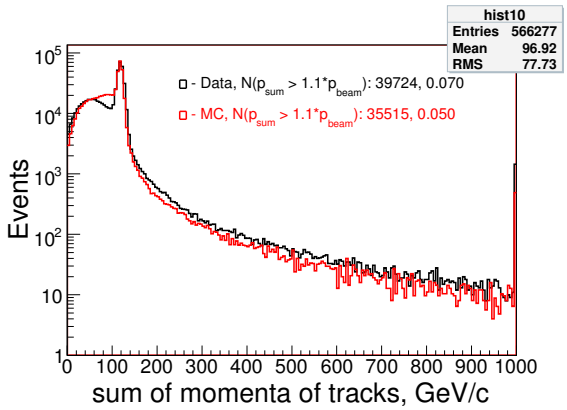

Figure 10: The sum of momenta of the charged tracks in event using the p+C interactions at 120 GeV/c for data (black) and Monte Carlo (red). Calculated sum based on the tracks which belong to the primary vertex.

The fraction of the events when the sum of momenta exceeds $1.1p_{beam}$ are 7.0% data and 5.0% for Monte Carlo. It is obvious that events, where the momentum conservation law is violated, might be useful for special studies, but not for cross section measurements. Thus, we identified a special category of events in which MIPP detector and software do not allow us to perform physics analysis. Speaking of the neutron analysis momentum conservation is one of the key requirements. Hence we drop those events before counting of the incident protons.

3.4 Beam track selection cut efficiencies

Beam track selection cut efficiencies are summarized in two Tables: Table 3 for the thin target data and Table 4 for the liquid hydrogen data.

3.5 Counting of incident protons

The counting of incident protons was done for events which passed all above discussed selection requirements. The incident proton counting was based on two methods: the proton beam prescalers (rs→trigps[6]+1) and direct scalers (spill→gatedTrigBit[6]), where "rs" represents the run summary pointer and "spill" - spill summary. First proton counter was incremented by each "good" event times the proton beam prescaler, second - direct accumulating of given scaler. If beam trigger event was failed by

cut name	N(58-thin)	EFF(58-thin)	N(120-thin)	EFF(120-thin)
Total events	1667211		2615429	
nTrks>30	1543447	0.926	2518598	0.963
Calo status	1543447	1.000	2518592	1.000
Is beam trk?	1477568	0.957	2470960	0.981
Single beam trk	869439	0.558	2011903	0.814
nCrossing < 5	685526	0.788	1674480	0.832
radius-1<2.0cm	670633	0.978	1618680	0.967
radius-2<2.0cm	653655	0.975	1618680	1.000
track time	646536	0.989	1610870	0.995
trk divergence	645172	0.998	1610784	1.000
P<1.1P_{beam}	602133	0.933	1509270	0.937
Total efficiency		0.361		0.577
Proton fraction	246413	0.409	1499105	0.993

Table 3: Beam track selection cut efficiencies and proton fractions for the thin target data.

cut name	N(58-LH2)	EFF(58-LH2)	N(84-LH2)	EFF(84-LH2)
Total events	802616		916581	
nTrks>30	772373	0.962	847790	0.925
Calo status	772373	1.000	847787	1.000
Is beam trk?	745447	0.965	826374	0.975
Single beam trk	480130	0.644	590770	0.715
nCrossing < 5	386237	0.804	492143	0.833
ellipse cut	300063	0.777	364479	0.741
track time	291234	0.971	363265	0.997
trk divergence	290707	0.998	362342	0.997
P<1.1P_{beam}	275275	0.947	328733	0.907
Total efficiency		0.343		0.359
Proton fraction	92414	0.336	202371	0.616

Table 4: Beam track selection cut efficiencies and proton fractions for the liquid hydrogen data.

some reasons: the track time is off or the calorimeter status is not readable, then the scaler subtraction was applied. For the test purpose we count the incident protons in two ways: in first - without subtraction applied (in Table 5) and second - with the correction for those protons which was rejected by some reason(s) - in Table 6.

target	$p_{beam}, GeV/c$	prescaler bit	direct scalers	ratio
H_2	20	6863900	6712290	1.023
Empty Cryo	20	1077263	1055900	1.020
H_2	58	55527097	55046896	1.009
Empty Cryo	58	12250227	11941328	1.026
Beryllium	58	4435167	4448628	0.997
Carbon	58	16159654	16011182	1.010
Bismuth	58	33625880	32735965	1.027
Uranium	58	71706424	69833283	1.027
Empty thin	58	26332939	25641913	1.027
H_2	84	71645485	69168883	1.036
Empty Cryo	84	24199480	22290732	1.086

Table 5: The number of incident protons calculated with two methods: accumulating the direct scaler and using the proton prescaler. Data selection: all data events without any rejections.

4 Vertex Method Selection

MIPP software has two options for fitting of the interaction point - a vertex. They are "dafit" and "confit". The first one has an advantage on the transverse and total momentum resolution. The second option, "confit", uses what was done by the first method and then refits incoming and outgoing track parameters simultaneously. We select this method because it has a better resolution in Z direction. Using the "confit" method we are better able to reduce (subtract) backgrounds due to interactions with the trigger scintillator. The neutron analysis is not sensitive to the track momentum resolution, which might be gained by using the "dafit" method, because the neutron momentum resolution is defined by the calorimeter.

For the neutron analysis we required that the incident protons should interact within the target region. This case was named as "primary vertex" selection. We applied both transverse and longitudinal vertex position cuts. For the transverse position cut we used the same cut as for the beam track with a slightly bigger radius to account the possible multiple scattering of the incident particle between DC3 and the target. But there are some vertices's with the transverse positions are way off (2-3 cm and more away from the edge of the beam spot). This effect is present for the multi track (n$\geq$5) vertices's too. At this moment we have only one explanation: misreconstracted vertex and or tracking.

target	p_{beam}, GeV/c	prescaler bit	direct scalers	ratio
H_2	20*	2215467	2063857	1.07
Empty Cryo	20*	397364	376001	1.06
H_2	58	26205872	16572320	1.03
Empty Cryo	58	5585745	2740163	1.05
Beryllium	58	2207422	2220883	0.99
Carbon	58	8751838	8603366	1.02
Bismuth	58	17164512	16274597	1.05
Uranium	58	32643688	30770547	1.06
Empty thin	58	12397130	11706104	1.06
H_2	84	31372847	28896245	1.09
Empty Cryo	84	10962656	9053908	1.21
Beryllium	120	19864149		0.08
Carbon	120	5542062		0.07
Bismuth	120	21559032		0.08
Empty thin	120	8004477		0.15

Table 6: The number of incident protons calculated with two methods: accumulating the direct scaler and using the proton prescaler. Results presented for different momenta and targets. Both results were corrected for protons which was rejected by some reason(s). Last column represents the ratio of two approaches. For 120 GeV/c it was estimated using runs, where the spill info was reliable. *Note: studies with RICH detector indicates that the pion contamination on 20 GeV/c proton beam is about 25%.

The fraction of the off-spot events for different beam momenta and targets are presented in Table 7. Using this data we might assign the systematic uncertainty or apply correction?

p_{beam} / target	H_2	Be	C	Bi	U
58 GeV/c	0.066	0.093	0.072	0.067	0.046
84 GeV/c	0.114				
120 GeV/c		0.019	0.015	0.021	

Table 7: The fraction of events when the transverse position of primary vertex was out of the beam spot.

The longitudinal (along Z direction) position cut depends on the length of the target. The vertex resolution in Z direction for the track multiplicity of 2 is about 3 cm (half width). Hence we are not capable of separating the interactions with the target from the interactions with the trigger scintillator, (about 2 cm from each other). Thus, we selected as the Z cut for the thin target -4 cm upstream of the target center and +4 cm downstream of the trigger scintillator. For the liquid hydrogen target data the Z cut was ±15 cm around the center of liquid hydrogen tube. The Z cut was applied for the primary vertexes with any charged track multiplicity except single straight through track. In the primary vertex with the multiplicity of 1 the track is considered as a straight through if momentum was greater than 15 GeV/c. Figure 11 shows the longitudinal position distribution for the 120 GeV/c protons striking the carbon 2% target using both "dafit" and "confit" vertex methods. The trigger conditions: both proton beam and proton interaction triggers were used to make these plots.

The peak at about 0.4 cm represents the interactions with carbon 2% target, the peak at 2.5 cm indicates the interactions with trigger scintillator. The dashed plot illustrates the target-out only case. One can see from the plots that "confit" has sharper peaks. Due to of that we decided that it is better for the neutron analysis. The captions in plots allow to tell what is the fraction of interactions within the target region and downstream of the trigger scintillator. For example, using the "confit" plot we can read that the occupancy of both peaks (-2.5$< Z <$5.0 cm) is about 53%. The events with Z<-2 cm has occupancy of 36%. They represent the single beam track events where the Z value was assigned to be from -17 cm through -2 cm. The interactions downstream of the trigger scintillator are of 11%. They represent the interactions within the TPC volume. The surviving rate of events after both transverse and longitudinal vertex position cuts for this beam and target are 0.892 with "confit" and 0.887 with "dafit" vertex methods, respectively.

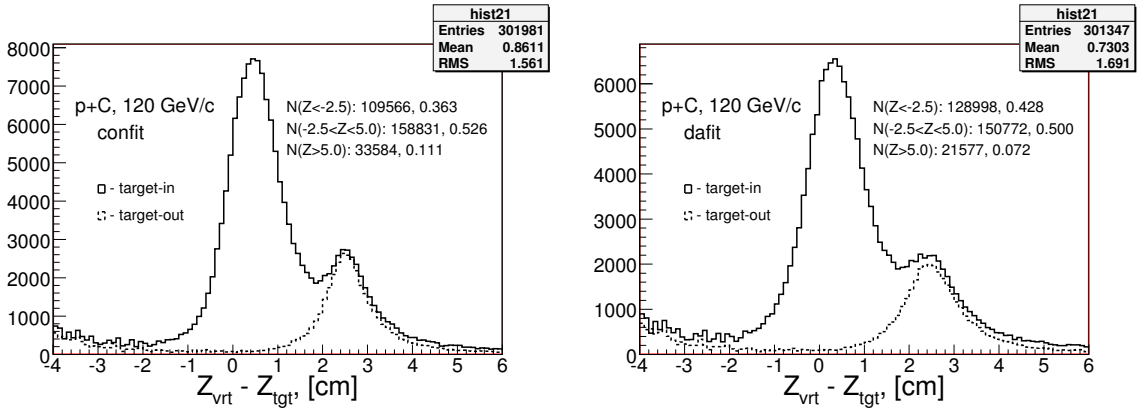

Figure 11: The longitudinal (along Z direction) position distribution for the 120 GeV/c protons striking the carbon 2% target with "confit" (on left) and "dafit" (on right) vertex fit methods. The solid line plot illustrates the target-in and dashed - target-out data. One can see from these plots that the "dafit" method has broader signal and background peaks.

5 Sum of Momenta: "confit" vs "dafit"

We knew that the "confit" vertex method drops an off-time track from the primary vertex list. It raised questions: how valid the time assignment for the track? What would be with the sum of momenta of tracks in case if this assignment is false? Remind that value of sum in use for the neutron selection. How to distinguish cases when drop was true and when it false? If it is the false then how recognize a right track in an unused list and bring it to the momentum balance?

Below we describe the study we performed in order to answer above questions. We select a control sample, run 15742 p+C interactions at 120 GeV/c. This control sample was processed with both "confit" and "dafit" vertex methods. We trying to see what are differences between these approaches. A comparison made on the event-by-event basis considering tracks from the primary vertex only. Figure 12 shows two plots: the sum of momenta of tracks (on left) and the differences for the sum between "confit" and "dafit".

The left plot on Figure 12 shows that the "confit" has a little higher occupancy at a peak and it below of "dafit" at low p_{sum} region. Plot indicates that the Δp_{sum} in 6% of cases might exceed 10 GeV/c. Due to of drop one might expect to see a tail on negative side. But the distribution tells that the tail on the positive side is not less, but a little higher. What is an explanation on that? An analysis shows that the major part of events are due to some issues with the "dafit" method. Remaining part caused by the reforming of the vertex. Figure 13 show the track multiplicity and the multiplicity differences for the same primary vertex between the both vertex methods.

Figure 13 right plots clearly shows the track drops by "confit". For drop the

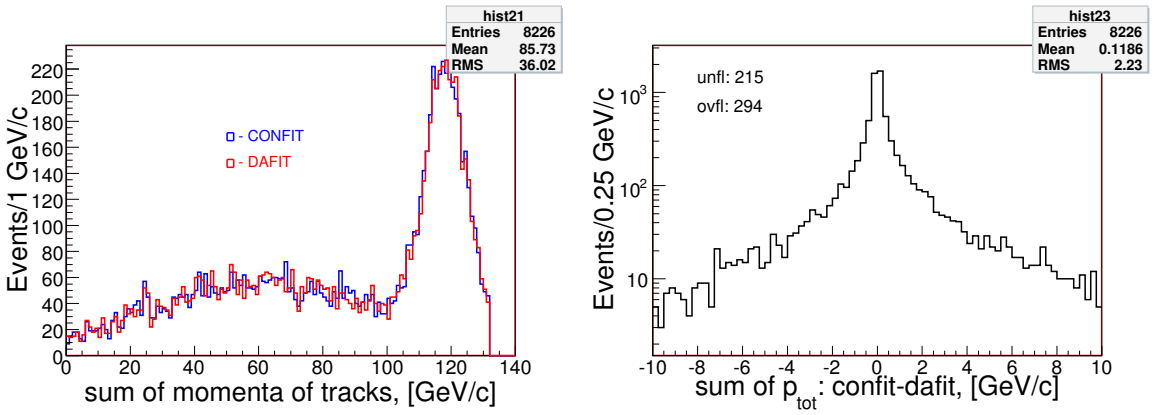

Figure 12: Left plot represents the sum of momenta of tracks. Right plot shows the differences for the sum of momenta of tracks between "confit" and "dafit"

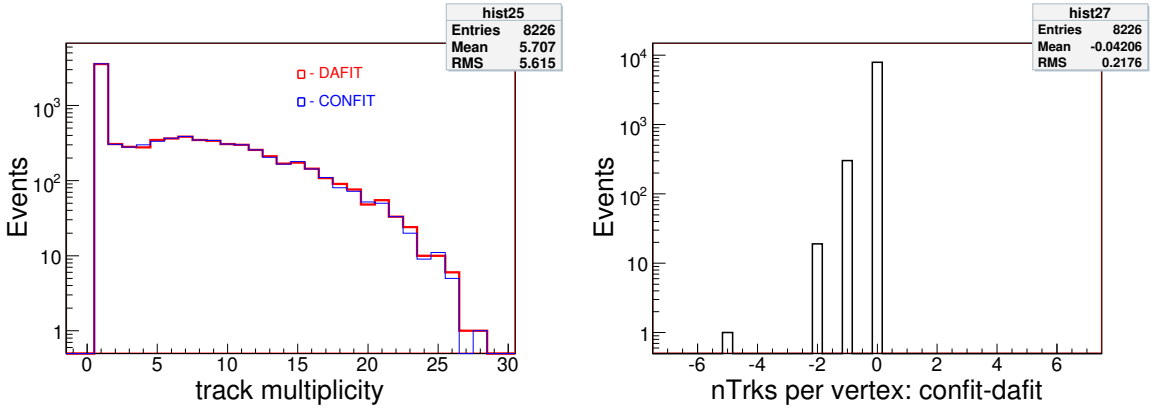

Figure 13: Left plot - the track multiplicity distributions for the primary vertex with "dafit" and "confit" methods. Right plot - multiplicity difference distribution.

difference became negative. We identified 323 multiplicity changes for 8226 considerations, about 4%. Drops occur in 303 events for 1, in 19 events for 2 and in 1 event for 5 tracks. Thus, the "confit" method slightly reduce the multiplicity of the charged tracks, but in another hand it keeps the momentum balance same as "dafit". However, our concerns are events on the negative tail, including underflows. By viewing the underflow events - 24 candidates, which associated with track drops, we found: 11 out of 24 - are looks a real off-time tracks, they have no match with RICH. We knew that RICH has a tight, ±50 ns, time gate. 22 events out of 24 are cases when dropped track(s) used to form another vertex with different the vertex position. One event out of 24 is case when one off-time track is present in the vertex, but another off-time was dropped. Finally, we bring the dropped track back to the primary vertex list, if it has match with RICH ring position within ±3 cm and has match with vertex within 0.8 cm in the transverse plane. For an example, in p+C interaction run 15359 event 2499 has a track with time 494 ns and momentum of 84 GeV/c which was dropped from the primary vertex. We found that for this track there is an unused RICH ring within 2.2 cm. Also, the track - vertex distance appear to be 0.3 cm. Figure 14 shows the track multiplicity per the primary vertex (blue plot). A red plot shows the multiplicity when "off-time" track was brought back to the vertex and it was in match with RICH ring. The distribution made using p+C interactions at 120 GeV/c. The fraction of events when the multiplicity was updated is 2.3%.

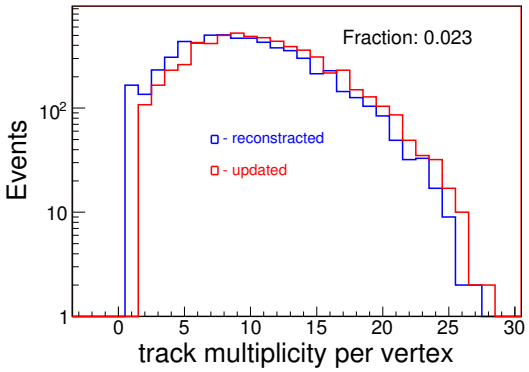

Figure 14: The track multiplicity per the primary vertex (blue plot). Red plot shows the multiplicity when the "off-time" track was brought back to the vertex and it was in match with RICH ring. The distribution was made using p+C interactions at 120 GeV/c.

6 Segment 456 Track Usage

What is a tracking efficiency? We have no information on this matter so far. But by viewing the neutron candidates on an "event display" tool we found a few missing

tracks. In one of such events we found that if we will use an unused track from the downstream segment track, then it would perfectly match with the EMCAL hits and unused RICH ring. Hence we decided to include to our track collection unused tracks from the downstream segment, which was named as a segment 456 track. There are some code modifications was needed to achieve this goal [4]. Since "pass4c" processed DST data has such option. Now we will discuss how to use it for the neutron analysis.

The problem with the segment 456 track is that the momentum information is not supported by the MIPP software. But RICH - track match procedure require the knowledge of the particle momentum vector, which used to pass the light through set of mirrors. We can assign a Pz momentum component for the track using the missing momentum in event. It can be done only if there is a single segment 456 track. Px and Py values can by calculated using the track slopes. Then the RICH ring and segment 456 track match procedure is following:

- Select single track events
- Assign Pz from the missing momentum in the primary vertex: p_{beam} - $\sum p_{trk}$
- Calculate Px and Py using Pz and track slopes
- Apply the RICH ring position prediction function - PredictRingCenter
- Use average mirror offsets in X and Y views
- Test for the segment 456 track - RICH ring match (within 2 cm)

Figure 15 shows two plots: the RICH ring (on left) and the segment 456 track (on right) multiplicities. Both plots illustrate what was reconstructed by these detectors but did not fall into the global track stream.

For the given p+C interaction data at 120 GeV/c on average the segment 456 track and the unused RICH ring availabilities are about 32% and 22%, respectively. The numbers from captions on Figure 15 allow to calculate the segment 456 track - RICH ring match efficiency: $\epsilon = 7944 / 28249 = 0.281$. The low efficiency indicates that the segment 456 track in most of the cases is a fake. For example, the fraction of events, when the number of hits on this track equal to 8, is about 45%. In this subsample the track can be made using 4 hits from DC4, nothing from PWC5 and 4 hits from PWC6. Another example, if we require 9 hits on the segment 456 track, then the match efficiency rises to 36%. But some of the fake tracks survive. The main reason for the fakes is that PWC6 is very noisy. Thus, we might accept only those segment 456 tracks, which match with the RICH ring position. Only those tracks were considered for the neutron analysis. For an example, in p+C interaction run 15327 event 2441 for the single segment 456 track particle momentum of 97 GeV/c was assigned. Then it was found to be in match with RICH ring within 0.8 cm and with the EMCAL shower too. Figure 16 shows the assigned momentum distribution for the segment 456 tracks when match with RICH ring is on. The distribution made using p+C interactions at 120 GeV/c. The fraction of such events is 2.3%.

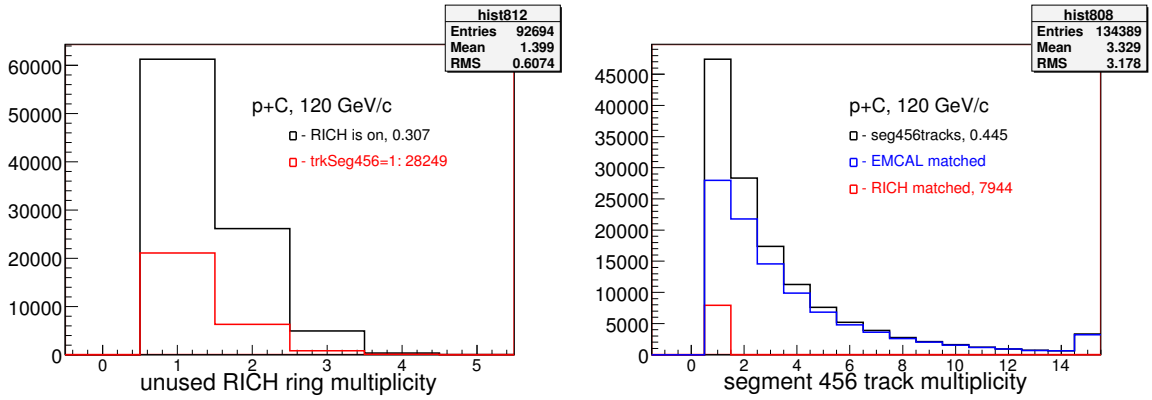

Figure 15: Left plot represents the RICH ring multiplicity: black plot indicates the multiplicity of unused rings (rate is about 0.22), the red plot shows cases when it associated with a single segment 456 track. The right plot shows the segment 456 track multiplicity: the black plot represents the total occupancy (rate is about 0.32). The blue and red plots show cases when it matches with EMCAL and RICH respectively.

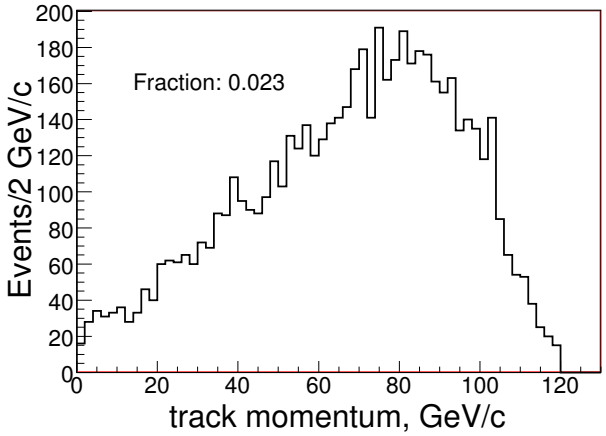

Figure 16: The assigned momentum distribution for segment 456 tracks when it matches with a RICH ring. The distribution was made using p+C interactions at 120 GeV/c..

7 Missing Total Momentum

Before discussing the neutron selection we might try to answer the question: is there any room for the neutrons in our data? We can answer this question by viewing the missing momentum distribution. Figure 17 represents the missing momentum for two proton beam momenta: 58 GeV/c (on left) and 120 GeV/c (on right). The missing momentum is $\Delta p = p_{beam} - \sum p_{trk}$ quantity, where $\sum p_{trk}$ is based on tracks from the primary vertex.

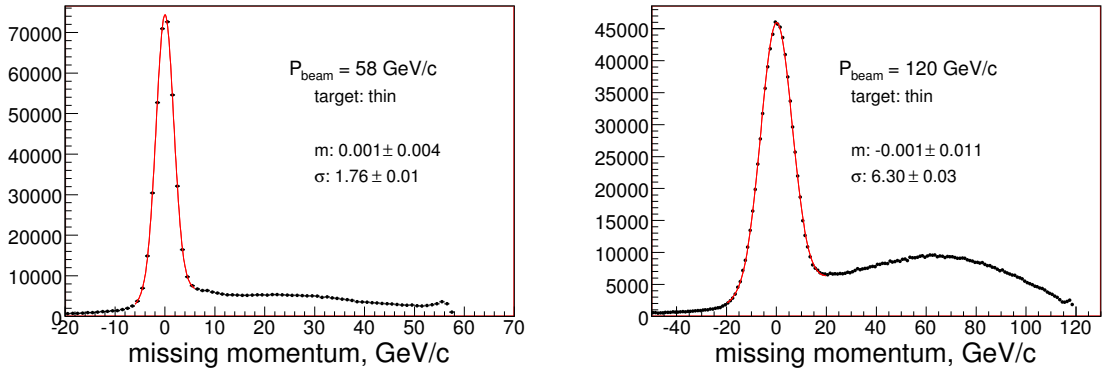

Figure 17: The missing total momentum distributions for two proton beam momenta: 58 GeV/c (on left) and 120 GeV/c (on right). The missing total momentum represents $\Delta p = p_{beam} - \sum p_{trk}$ quantity, where $\sum p_{trk}$ is based on tracks from the primary vertex.

The negative tail of the distribution in Figure 17 represents the cases when $\sum p_{trk}$ is significantly higher than the beam momentum. The peak represents cases when $p_{beam} \approx \sum p_{trk}$. The width of the peak reflects the momentum resolution integrated over all outgoing tracks. The cases with p_{missed} >7 GeV/c (on left) and p_{missed} >20 GeV/c (on right) represents the room for neutrals in the event. According to this data almost every third event for left plot and every second event for right plot are associated with neutrals production, where neutrons are a subsample of these neutrals.

8 Missing Transverse Momentum

Here we like to find out that is any an advantage on the neutron selection by using the missing transverse momentum value? Figure 18 represents the p_T differences between the combined transverse momentum of all outgoing tracks in the primary vertex and incoming beam track. Plots made using the p+C interactions at 120 GeV/c for the different bin size in Δp_T: 0.25 GeV/c (on left) and 0.01 GeV/c (on right).

The blue plot in Fig. 18 made for events after the vertex Z position cut applied, the red plot - events passed the neutron selection requirements (details are on next

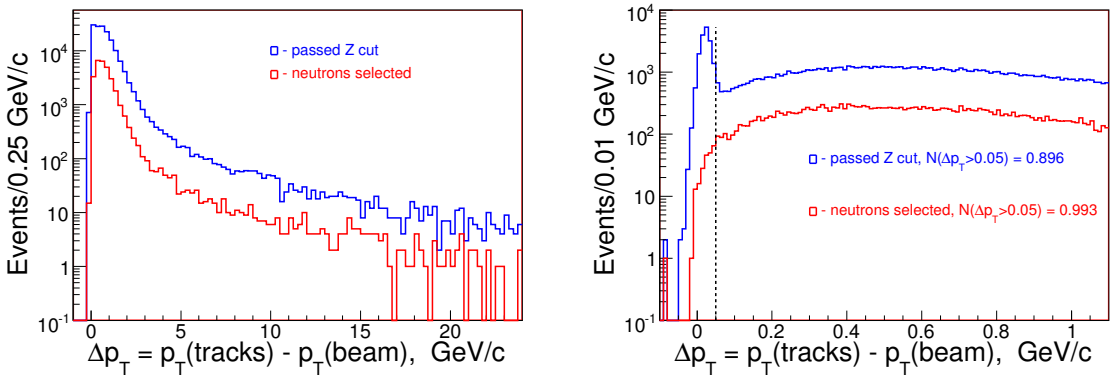

Figure 18: The missing transverse momentum distributions using the p+C interactions at 120 GeV/c. The missing transverse momentum represents $\Delta p_T = p_T^{trk}$ - p_T^{beam} quantity, where p_T^{trk} is based on tracks from the primary vertex. Left plot done with 0.25 GeV/c and right with 0.01 GeV/c bin sizes, respectively.

section). Plots illustrate that with and without the neutron selection requirements behavior of distributions are pretty much similar, except $0 < \Delta p_T < 0.05$ GeV/c region. The peak at low missed momentum region illustrate the presence of the beam straight through events. Plots made with interaction trigger and SciHi suggests that by applying the $\Delta p_T > 0.05$ GeV/c cut we might exclude the beam straight throughs. The caption in the right plot tells that 89.6% of events would survive this cut. While it cutting only 0.7% of neutron sample.

How this peak will looks like for the unbias data (beam triggers without SciHi requirement)? Figure 19 represents such cases for 58 GeV/c (on left) and for 120 GeV/c (on right) using all thin targets data.

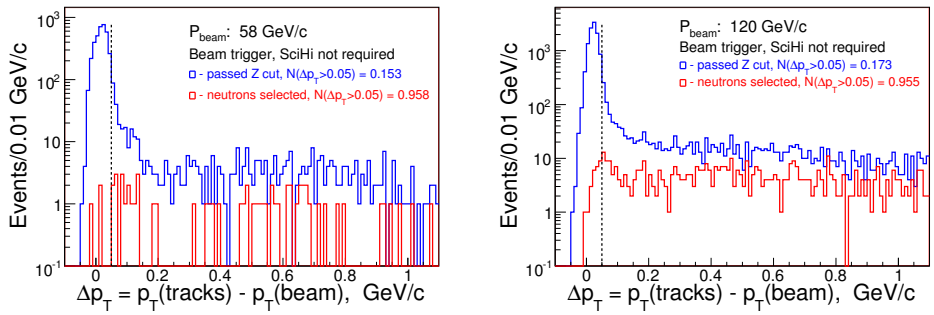

Figure 19: The missing transverse momentum distributions using the thin targets at 58 GeV/c (on left) and at 120 GeV/c (on right). Plots suggests that the straight through partially will remain there. Most effective cut might be 0.15 GeV/c.

We do not expect that the transverse momentum cut would be useful for Monte

Carlo samples. As indicated in Figure 20 by applying this cut we just slightly reducing the statistics.

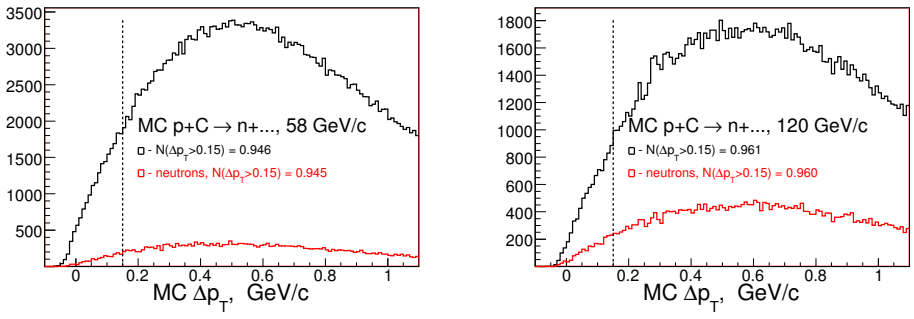

Figure 20: The missing transverse momentum distributions for Monte Carlo samples at 58 GeV/c (on left) and at 120 GeV/c (on right).

9 Neutron Selection Requirements

Below we summarize cuts applied after the event selection listed in Section 3.

- use the primary vertex only
- transverse position of vertex for thin targets is same as radius of the incoming beam: 0.8cm for 120 GeV/c and 2.0cm for 58 GeV/c
- longitudinal position is within -4cm $< Z_{vtx} <$ 6cm for thin targets and $\pm$15 cm for the liquid hydrogen target
- missing transverse momentum cut: Δp >0.15 GeV/c

Finally, neutron selection requirements are:

- Proton interaction bit in the prescaled trigger word is on
- "SciHi" trigger bit in the raw trigger word should be on
- Choose the lowest momentum value of neutron $P_n(min)$ for given beam settings using the missing momentum distribution.
- There is no charged track with P>0.7*P_{beam}
- Include the segment 456 track to the momentum balance if it points to HCAL and matches with a RICH ring

- Momentum balance requirement: $(\sum P_{tracks} + P_n - P_{trkHcal}) < 1.2 * P_{beam}$, where $\sum P_{tracks}$ is the total momentum of all charged tracks in event, P_n is the neutron momentum and $P_{trkHcal}$ is the combined momentum of charged tracks pointing to the HCAL. Term $P_{trkHcal}$ is a subsample of $\sum P_{tracks}$ and it needs to be subtracted in order to avoid double counting.

- Candidate should have sufficient deposition to calorimeter compared with the sum of momenta of tracks pointing to calorimeter: $(P_n - P_{trkHcal}) > 3\sigma$, where σ represents the HCAL energy resolution

The neutron momentum is: $P_n = E_{hcal} + E_{emcal} - (P_{trkHcal} - E_{trksEmcal})$, where E_{hcal} is an energy deposition into HCAL, E_{emcal} is projected energy losses of neutrons in EMCAL, $P_{trkHcal}$ is tracks momentum pointing to HCAL and $E_{trksEmcal}$ is track energy lost in EMCAL. The neutron energy scale normalization and the estimated E_{emcal} values based on protons are described in Appendix B.

Neutron counting: each candidate event accumulated with a weight, where weight is the proton interaction prescaler on run-by-run basis.

What is the minimum neutron momentum to choose? To answer for this question we will review more closely the missing total momentum distribution. Figure 21 represents the missing momentum for two proton beam momenta: 58 GeV/c (on left) and 120 GeV/c (on right) with different cuts.

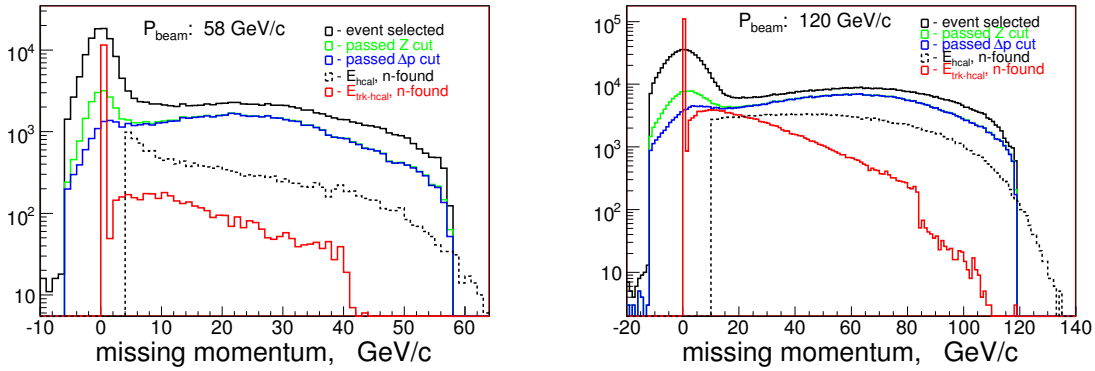

Figure 21: The missing total momentum distributions for two proton beam momenta: 58 GeV/c (on left) and 120 GeV/c (on right) with different cuts. Black plot - events passed the selection requirements discussed in section 3. Green plot - passed the vertex Z position cut, blue plot - passed the transverse momentum cut. Dashed black plot - energy deposited into HCAL for the neutron sample. Red plot - sum of tracks momenta pointing to HCAL fiducial.

Figure 22 shows the neutron spectrum with carbon target at 58 and 120 GeV/c, where the neutron minimum momentum selected as 4 GeV/c and 10 GeV/c, respectively.

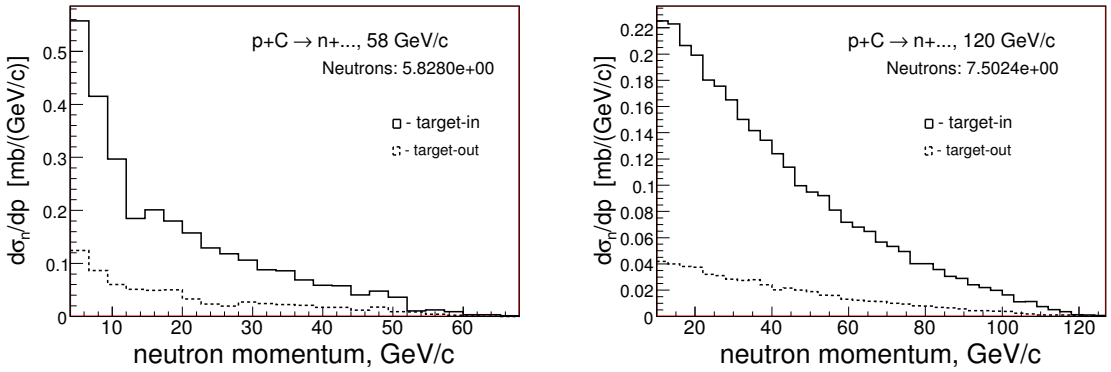

Figure 22: The neutron momentum distributions using p+C interactions at 58 GeV/c and 120 GeV/c, where the neutron minimum momentum selected as 4 GeV/c and 10 GeV/c, respectively.

10 Neutron Uncorrected Spectra

Below we present the uncorrected neutron spectra from various targets using 20 GeV/c, 58 GeV/c, 84 GeV/c and 120 GeV/c proton beams. The measurements were done using liquid hydrogen, Beryllium, Carbon, Bismuth and Uranium targets. Uncorrected means that we have not applied yet the trigger efficiency, calorimeter acceptance, and other corrections.

Our longitudinal vertex position resolution not allow to distinguish interactions at target versus interactions with the trigger scintillator. Due to of that we measured the neutron spectra also with the target-out case and then applied the subtraction procedure. For proper subtraction both target-in and target-out samples are normalized to same number of the incident proton beam particles.

10.1 Nominal neutron selection

The nominal neutron selection means that all selection cuts mentioned on the previous section has been applied. Figure 23 shows the neutron spectrum with liquid hydrogen target at 20 GeV/c.

Figure 24 shows the neutron spectrum with liquid hydrogen target at 58 GeV/c.

Figure 25 shows the neutron spectrum with beryllium target at 58 GeV/c.

Figure 26 shows the neutron spectrum with carbon target at 58 GeV/c.

Figure 27 shows the neutron spectrum with bismuth target at 58 GeV/c.

Figure 28 shows the neutron spectrum with uranium target at 58 GeV/c.

Figure 29 shows the neutron spectrum with liquid hydrogen target at 84 GeV/c.

Using 120 GeV/c protons we measured the neutron production from interactions with beryllium, carbon and bismuth targets. Figure 30 shows the neutron spectrum

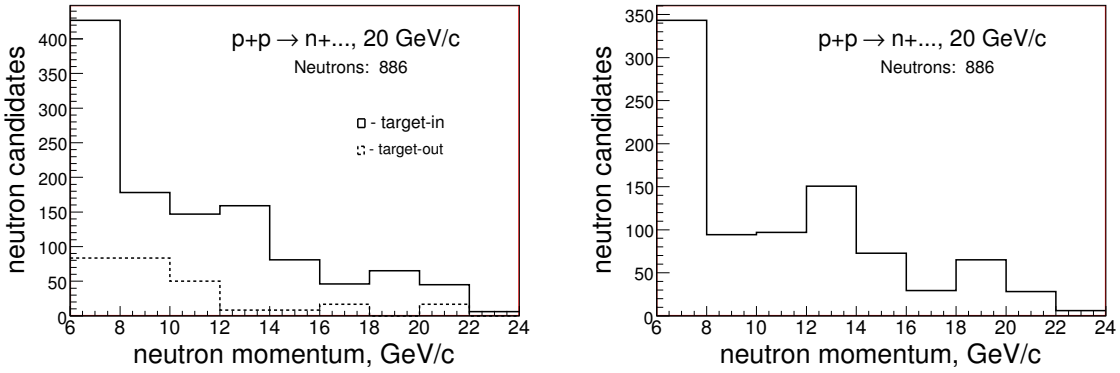

Figure 23: The neutron momentum distributions using p+p interactions at 20 GeV/c. Left plot represents both the target-in and target-out data. The right plot shows the neutron spectrum when the target-out subtraction was applied.

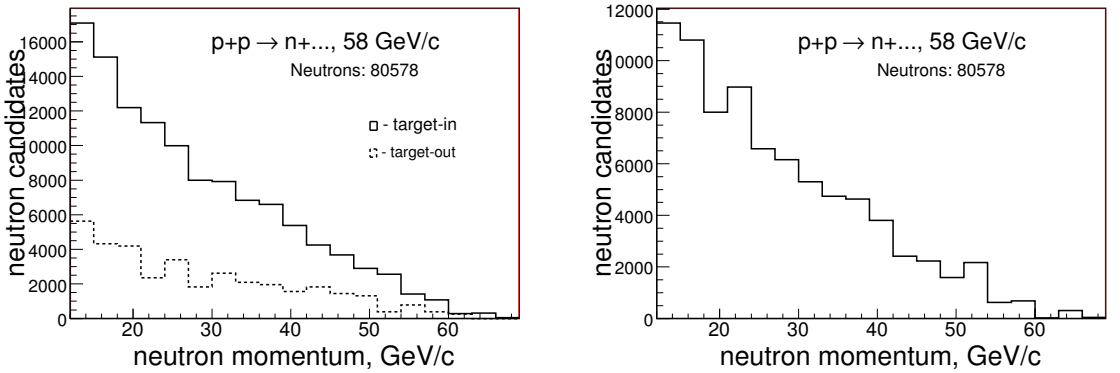

Figure 24: The neutron momentum distributions using p+p interactions at 58 GeV/c. Left plot represents both the target-in and target-out data. The right plot shows the neutron spectrum when the target-out subtraction was applied.

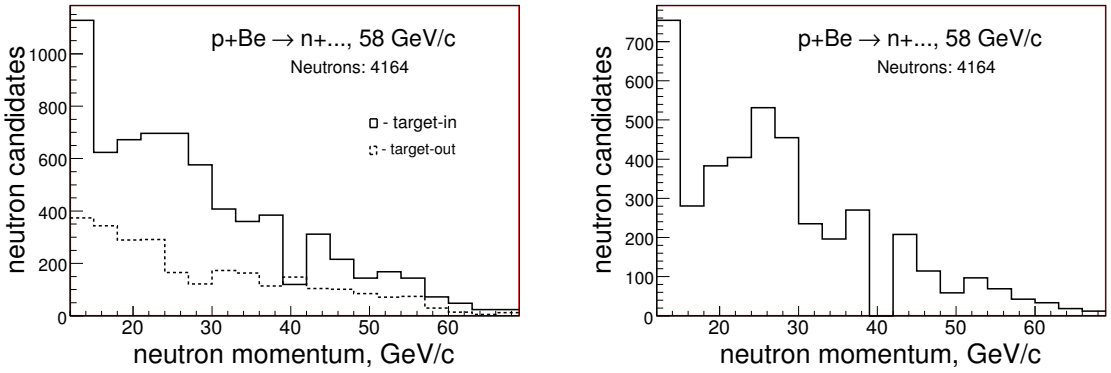

Figure 25: The neutron momentum distributions using p+Be interactions at 58 GeV/c. Left plot represents both the target-in and target-out data. The right plot shows the neutron spectrum when the target-out subtraction was applied.

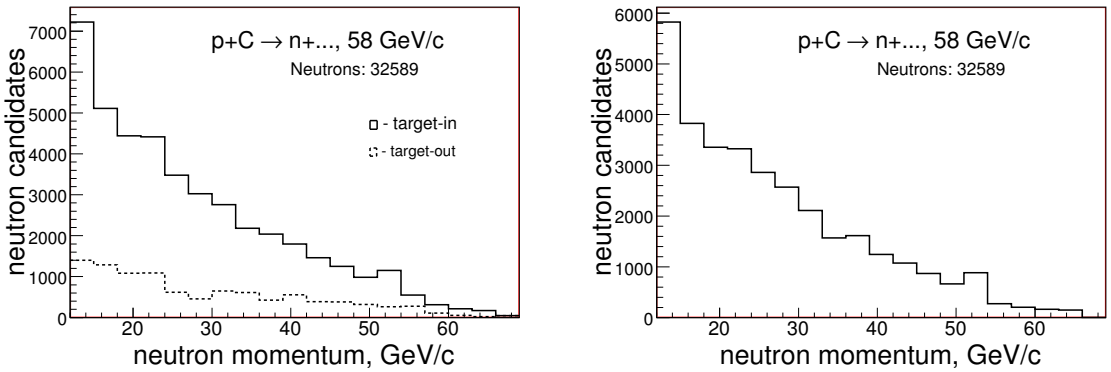

Figure 26: The neutron momentum distributions using p+C interactions at 58 GeV/c. Left plot represents both the target-in and target-out data. The right plot shows the neutron spectrum when the target-out subtraction was applied.

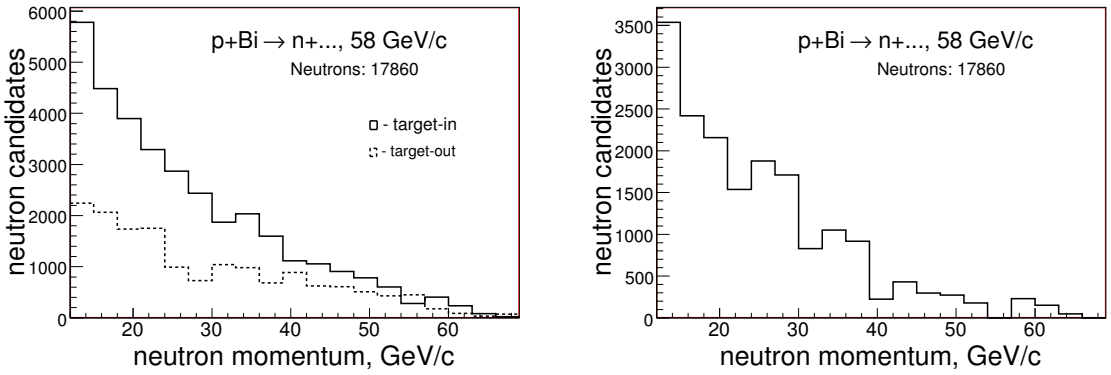

Figure 27: The neutron momentum distributions using the p+Bi interactions at 58 GeV/c. Left plot represents both the target-in and target-out data. The right plot shows the neutron spectrum when the target-out subtraction was applied.

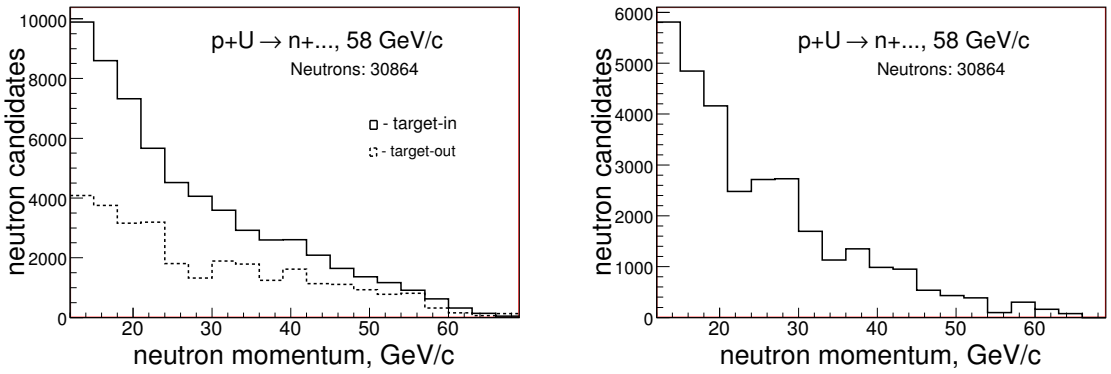

Figure 28: The neutron momentum distributions using the p+U interactions at 58 GeV/c. Left plot represents both the target-in and target-out data. The right plot shows the neutron spectrum when the target-out subtraction was applied.

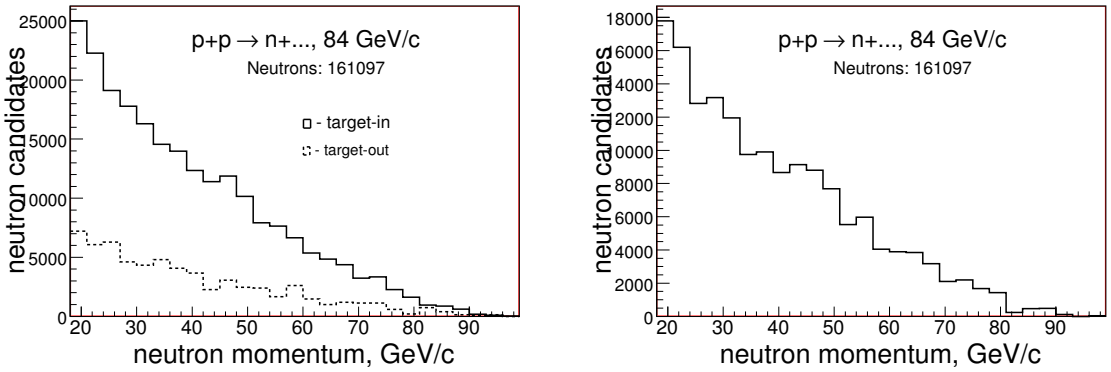

Figure 29: The neutron momentum distributions using p+p interactions at 84 GeV/c. Left plot represents both the target-in and target-out data. The right plot shows the neutron spectrum when the target-out subtraction was applied.

with beryllium target. Figure 31 shows the neutron spectrum with carbon target. Figure 32 shows the neutron spectrum with bismuth target.

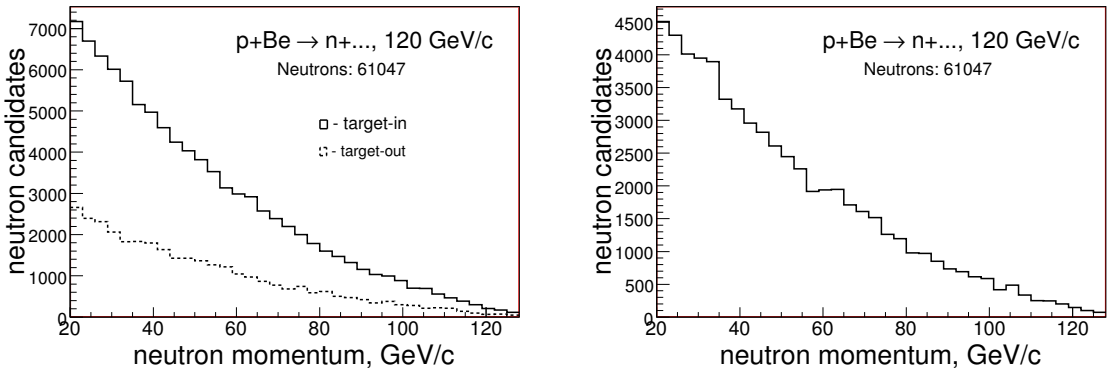

Figure 30: The neutron momentum distributions using the p+Be interactions at 120 GeV/c. Left plot represents both the target-in and target-out data. The right plot shows the neutron spectrum when the target-out subtraction was applied.

Table 8 represents the summary of the neutron sample size.

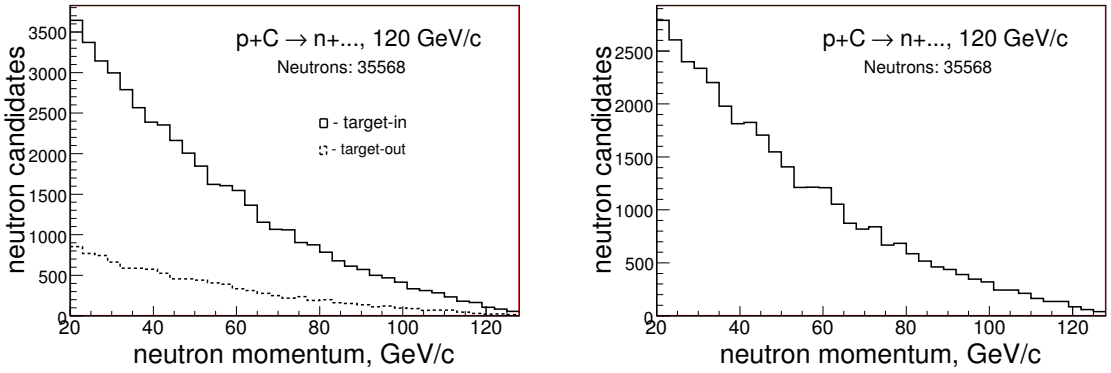

Figure 31: The neutron momentum distributions using the p+C interactions at 120 GeV/c. Left plot represents both the target-in and target-out data. The right plot shows the neutron spectrum when the target-out subtraction was applied.

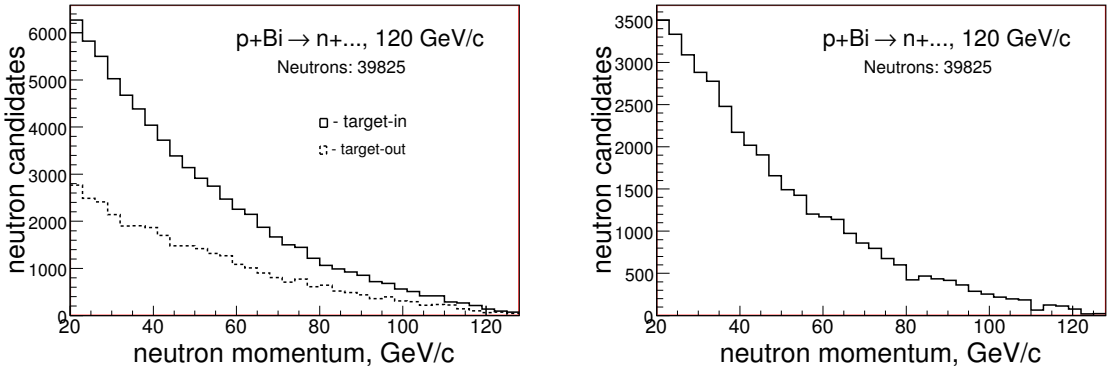

Figure 32: The neutron momentum distributions using the p+Bi interactions at 120 GeV/c. Left plot represents both the target-in and target-out data. The right plot shows the neutron spectrum when the target-out subtraction was applied.

	N_n	growth
H_2-20 GeV/c	886±48	
H_2-58 GeV/c	80578±1154	1.16
Be-58 GeV/c	4164±247	1.16
C-58 GeV/c	32589±773	1.19
Bi-58 GeV/c	17860±405	1.21
U-58 GeV/c	30864±421	1.20
H_2−84 GeV/c	161097±1517	-
Be-120 GeV/c	61047±199	1.15
C-120 GeV/c	35568±165	1.15
Bi-120 GeV/c	39825±146	1.17

Table 8: The summary of the neutron sample size. Growth column represents the increase factor relative to the previous neutron energy scale.

10.2 Neutrons from beam trigger events only

Below we present the neutron candidates when the beam trigger events used only. There is no SciHi requirement for neutrons.

Figure 33 shows the neutron spectrum using the beam trigger events only from p+p interactions at 58 GeV/c.

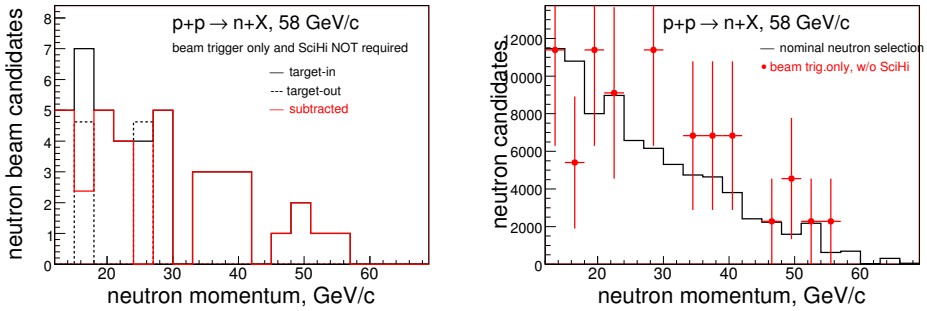

Figure 33: The neutron momentum distributions using the p+p interactions at 58 GeV/c. Left: using the beam trigger events only, right - both approaches.

Figure 34 shows the neutron spectrum using the beam trigger events only from p+U interactions at 58 GeV/c.

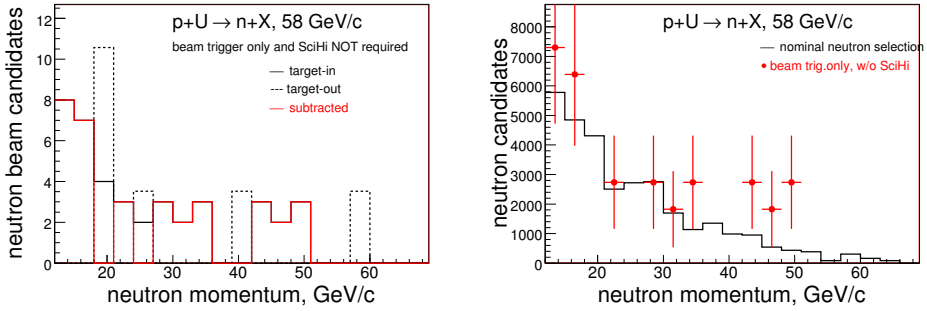

Figure 34: The neutron momentum distributions using the p+U interactions at 58 GeV/c. Left: using the beam trigger events only, right - both approaches.

Figure 35 shows the neutron spectrum using the beam trigger events only from p+p interactions at 84 GeV/c.

Figure 36 shows the neutron spectrum using the beam trigger events only from p+Be interactions at 120 GeV/c.

Figure 37 shows the neutron spectrum using the beam trigger events only from p+C interactions at 120 GeV/c.

Figure 38 shows the neutron spectrum using the beam trigger events only from p+Bi interactions at 120 GeV/c.

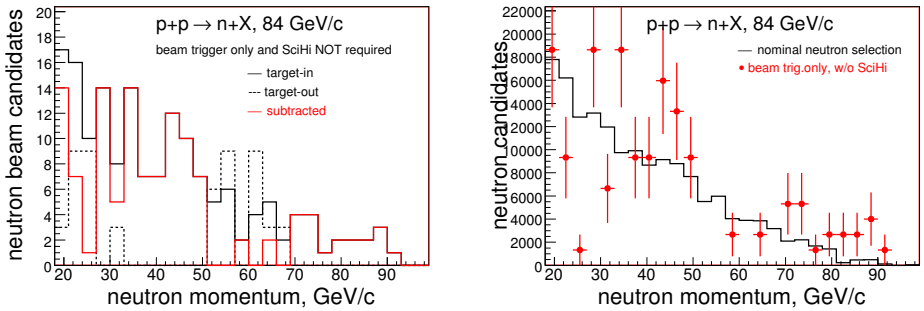

Figure 35: The neutron momentum distributions using the p+p interactions at 84 GeV/c. Left: using the beam trigger events only, right - both approaches.

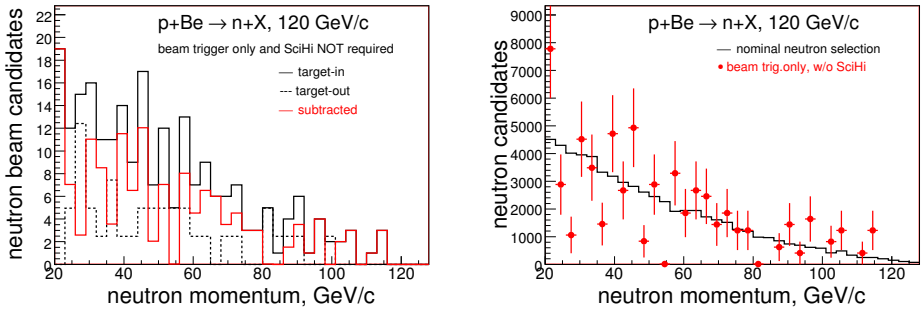

Figure 36: The neutron momentum distributions using the p+Be interactions at 120 GeV/c. Left: using the beam trigger events only, right - both approaches.

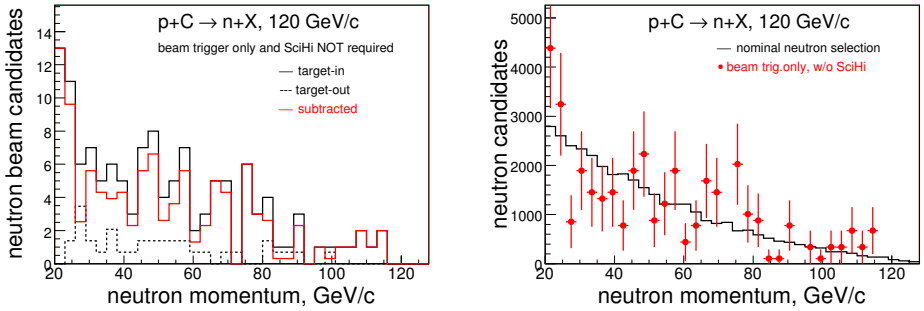

Figure 37: The neutron momentum distributions using the p+C interactions at 120 GeV/c. Left: using the beam trigger events only, right - both approaches.

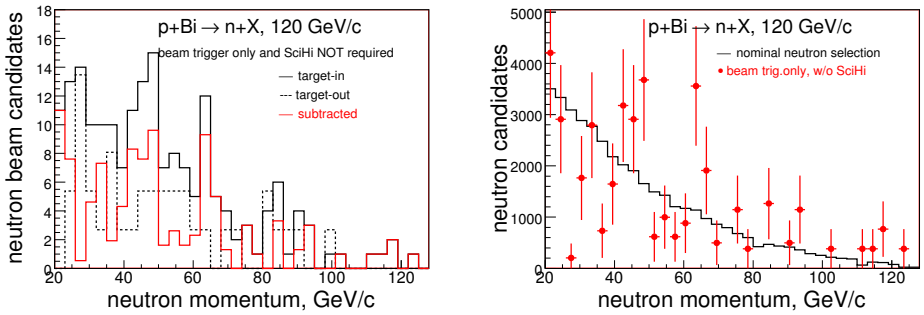

Figure 38: The neutron momentum distributions using the p+Bi interactions at 120 GeV/c. Left: using the beam trigger events only, right - both approaches.

11 Vertex Z distributions for neutron samples

Before to look on the Z vertex distribution for the neutron samples we might want to see once how the Z positions looks like for data prior of the trigger scintillator was installed. Figure 39 shows Z position distributions for $\pi/K/p$ incident beams interacting with Be (on left), Bi (on middle) and target-out (on right) at 58 GeV/c.

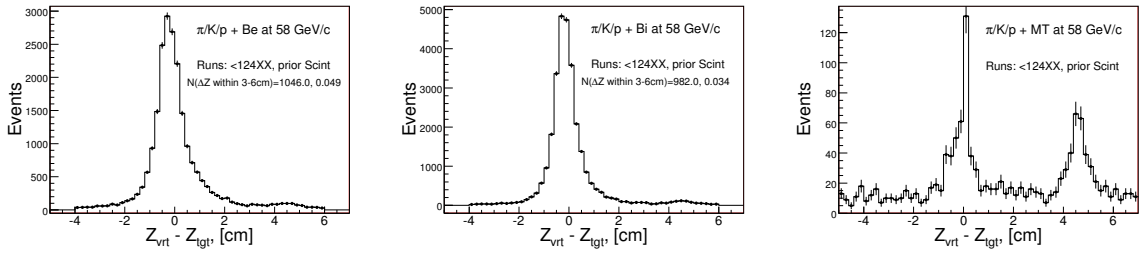

Figure 39: Z position distributions for $\pi/K/p$ incident beams interacting with Be (on left), Bi (on middle) and target-out (on right) at 58 GeV/c. The distributions with Be and Bi targets indicates the interactions around Z=4.5 cm. Target-out distribution shows same bump, but more pronounce. This peak represents interactions with TPC wall. For data with the scintillator installed the distance between the target center and TPC wall is about 7.5 cm

Below we will discuss the results of the target-out subtraction. Prior subtraction the target-out samples were normalized to same number of incident proton beam particles as in the target-in samples. Even so, the peak on the scintillator with target-out data appear to be slightly below than for the same peak on the target-in data.

Figure 40 shows the longitudinal vertex position distributions for the neutron candidates based on the interactions with the liquid hydrogen at 20 GeV/c beam momentum using the proton interaction triggers.

Figure 41 shows the longitudinal vertex position distributions for the neutron candidates based on the interactions with the liquid hydrogen at 58 GeV/c beam momentum using the proton interaction triggers.

Figure 42 shows the longitudinal vertex position distributions for the neutron candidates based on the interactions with the liquid hydrogen at 84 GeV/c beam momentum using the proton interaction triggers.

Figure 43 shows the longitudinal vertex position distributions for the neutron candidates based on the interactions with the Be target at 58 GeV/c beam momentum using the proton interaction triggers.

Figure 44 shows the longitudinal vertex position distributions for the neutron candidates based on the interactions with the C target at 58 GeV/c beam momentum using the proton interaction triggers.

Figure 45 shows the longitudinal vertex position distributions for the neutron

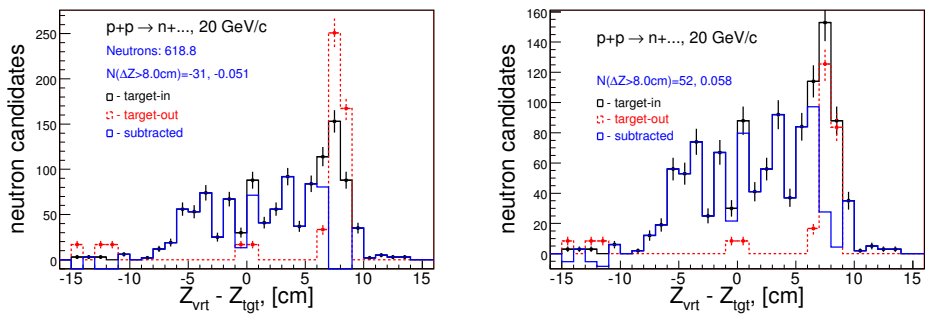

Figure 40: The longitudinal vertex position distributions for the neutron candidates based on the interactions with the liquid hydrogen at 20 GeV/c: without (on left) and with (on right) correction to the target-out size normalization. The correction factor is 1.7

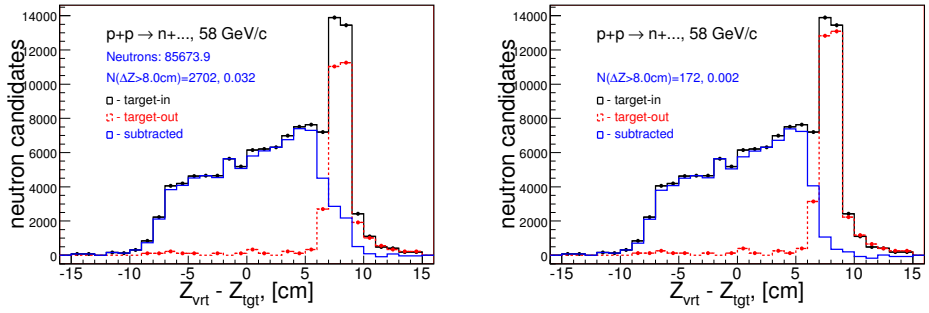

Figure 41: The longitudinal vertex position distributions for the neutron candidates based on the interactions with the liquid hydrogen at 58 GeV/c: without (on left) and with (on right) correction to the target-out size normalization. The correction factor is 1.11

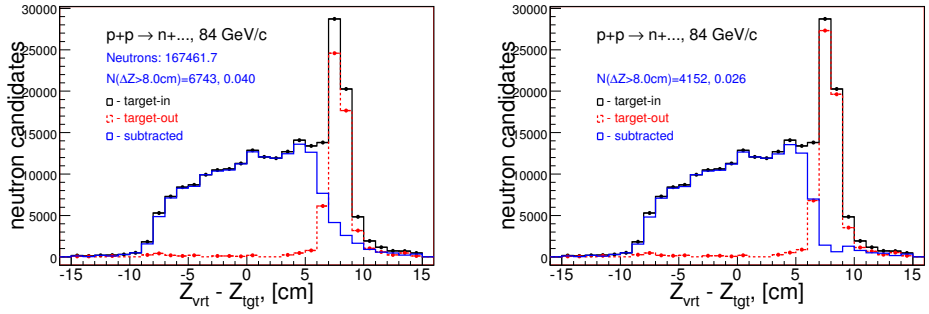

Figure 42: The longitudinal vertex position distributions for the neutron candidates based on the interactions with the liquid hydrogen at 84 GeV/c: without (on left) and with (on right) correction to the target-out size normalization. The correction factor is 1.18

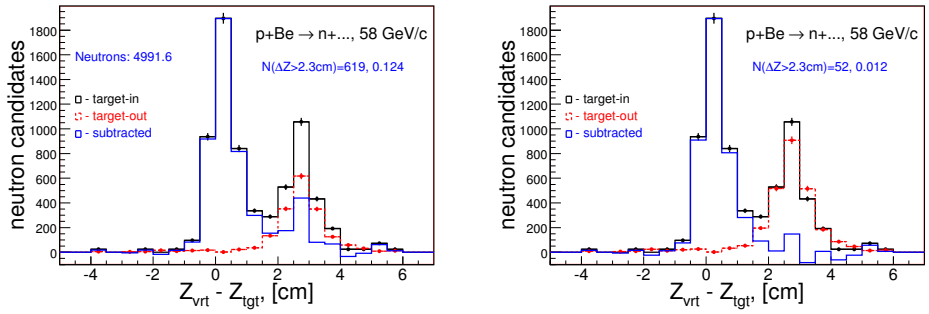

Figure 43: The longitudinal vertex position distributions for the neutron candidates based on the interactions with the Be target at 58 GeV/c: without (on left) and with (on right) correction to the target-out size normalization. The correction factor is 1.33

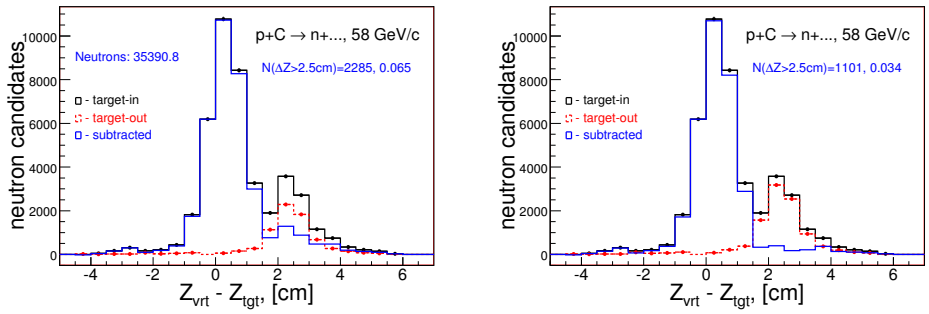

Figure 44: The longitudinal vertex position distributions for the neutron candidates based on the interactions with the C target at 58 GeV/c: without (on left) and with (on right) correction to the target-out size normalization. The correction factor is 1.33

candidates based on the interactions with the Bi target at 58 GeV/c beam momentum using the proton interaction triggers.

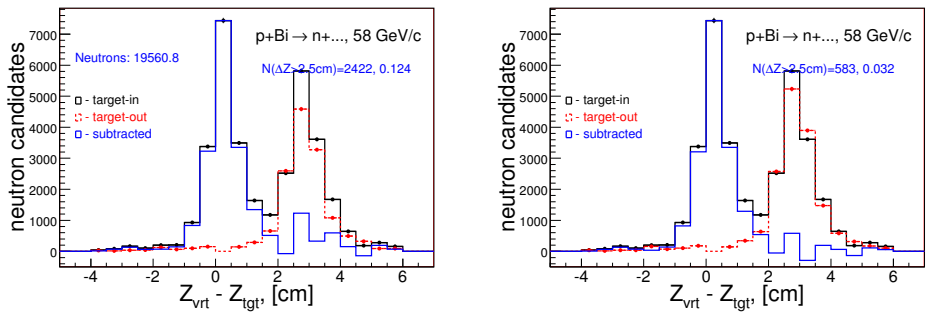

Figure 45: The longitudinal vertex position distributions for the neutron candidates based on the interactions with the Bi target at 58 GeV/c: without (on left) and with (on right) correction to the target-out size normalization. The correction factor is 1.14

Figure 46 shows the longitudinal vertex position distributions for the neutron candidates based on the interactions with the U target at 58 GeV/c beam momentum using the proton interaction triggers.

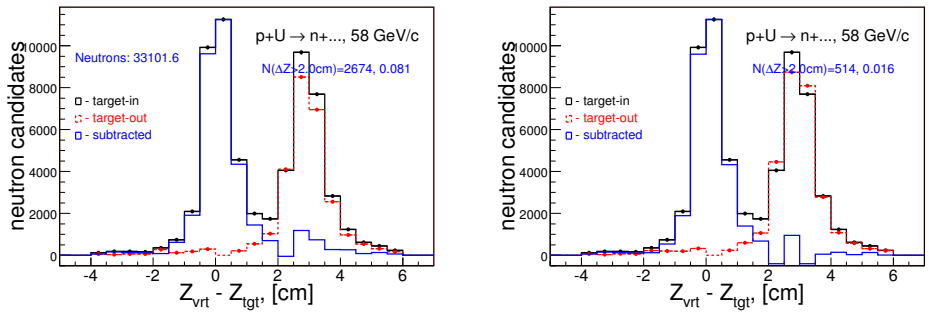

Figure 46: The longitudinal vertex position distributions for the neutron candidates based on the interactions with the U target at 58 GeV/c: without (on left) and with (on right) correction to the target-out size normalization. The correction factor is 1.09

Figure 47 shows the longitudinal vertex position distributions for the neutron candidates based on the interactions with the Be target at 120 GeV/c beam momentum using the proton interaction triggers.

Figure 48 shows the longitudinal vertex position distributions for the neutron candidates based on the interactions with the C target at 120 GeV/c beam momentum using the proton interaction triggers.

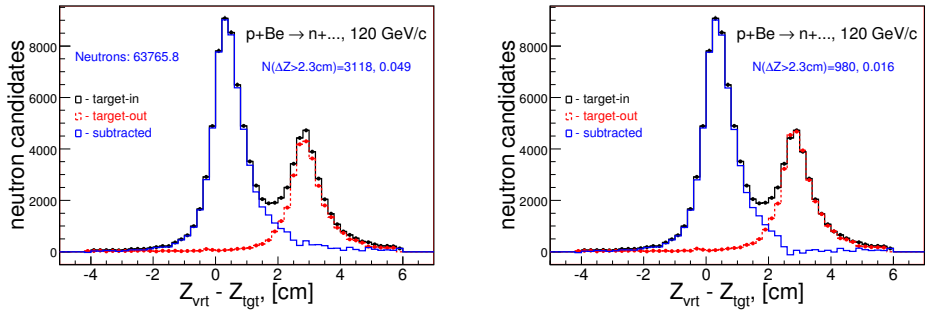

Figure 47: The longitudinal vertex position distributions for the neutron candidates based on the interactions with the Be target at 120 GeV/c: without (on left) and with (on right) correction to the target-out size normalization. The correction factor is 1.087

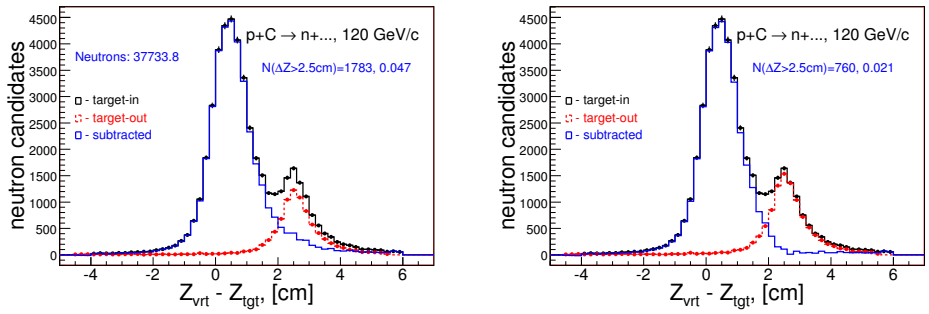

Figure 48: The longitudinal vertex position distributions for the neutron candidates based on the interactions with the C target at 120 GeV/c: without (on left) and with (on right) correction to the target-out size normalization. The correction factor is 1.25

Figure 49 shows the longitudinal vertex position distributions for the neutron candidates based on the interactions with the Bi target at 120 GeV/c beam momentum using the proton interaction triggers.

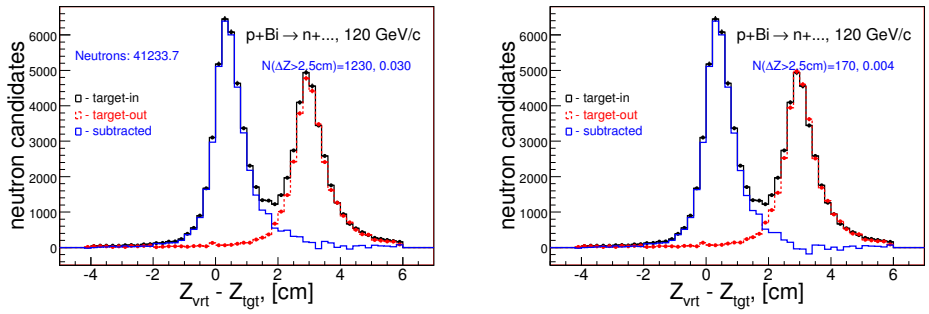

Figure 49: The longitudinal vertex position distributions for the neutron candidates based on the interactions with the Bi target at 120 GeV/c: without (on left) and with (on right) correction to the target-out size normalization. The correction factor is 1.042

Table 9 represents the number of neutrons calculated with and without corrections applied to the target-out size.

p_{beam}	MT-CF	N_n(MT-uncorr)	N_n(MT-corr)	$\Delta N_n/N_n$
H_2-20 GeV/c	-	-	886	
H_2-58 GeV/c	1.16	85674	80578	0.06
Be-58 GeV/c	1.47	4992	4164	0.20
C-58 GeV/c	1.38	35391	32589	0.09
Bi-58 GeV/c	1.14	19561	17860	0.09
U-58 GeV/c	1.09	33102	30864	0.07
H_2−84 GeV/c	1.11	167462	161097	0.04
Be-120 GeV/c	1.09	63766	61047	0.04
C-120 GeV/c	1.25	37734	35568	0.06
Bi-120 GeV/c	1.04	41234	39825	0.04

Table 9: The number of neutrons with and without corrections applied to the target-out size.

Figure 50 shows the neutron yields vs the run number.
The neutron yield calculated as:

$$\mathrm{Y}_n = \mathrm{nc}_{run} \times \frac{1}{N_{beam-run}} \times \frac{1}{A} \times \frac{1}{n_t} \times \mathrm{ipr} \times 10^4$$

where, nc_{run} and $N_{beam-run}$ are both represents what was accumulated for given run. The target-out subtraction procedure is not applicable for this study. 58 GeV/c

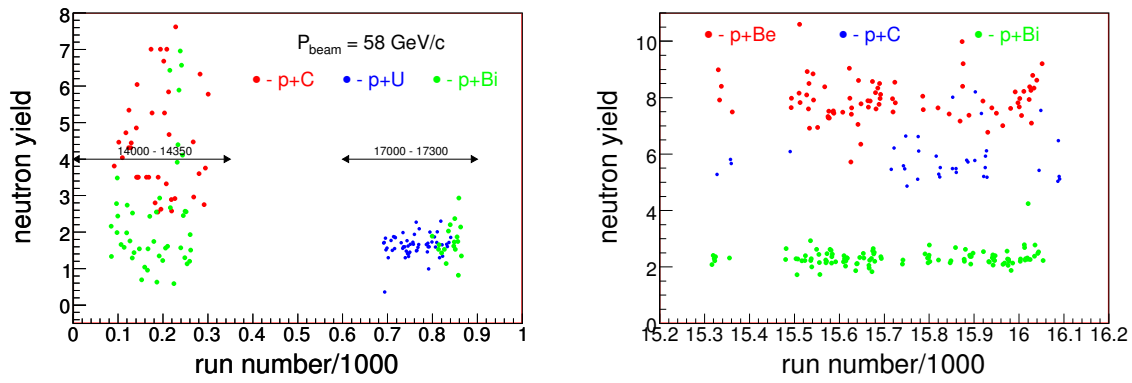

Figure 50: The neutron yield vs run number: 58 GeV/c data (on left) and 120 GeV/c data (on right). The target-out subtraction procedure is not applicable for this study.

data shows a great spread for the early runs. What is a reason for that? Possible an explanation is due to a big discrete beam and interaction prescalers for those runs. Figure 51 shows the beam and the interactions prescalers vs run number.

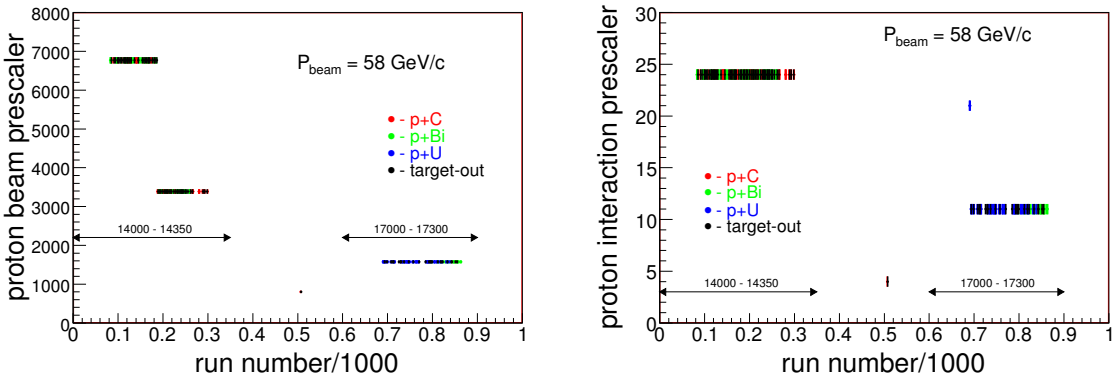

Figure 51: The proton beam and interaction prescalers values vs run number for the 58 GeV/c data

12 Neutron uncorrected spectrum: data vs MC

Below we compare data vs MC raw spectrum - when ONLY target-out subtraction was applied. Figure 52 illustrates the comparison for p+A interactions at 58 GeV/c.

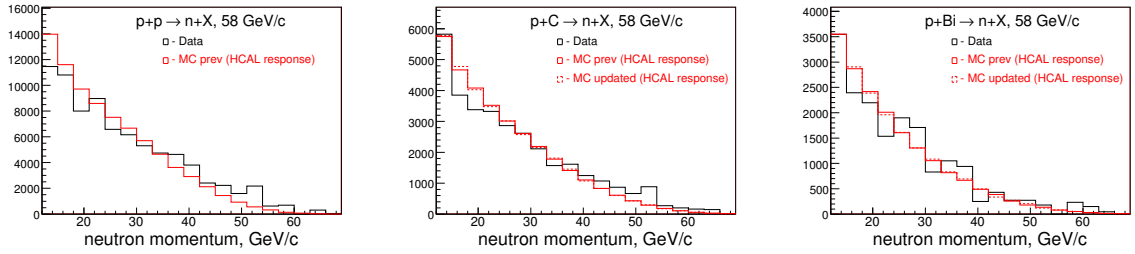

Figure 52: Comparison of the raw neutron spectrum, when ONLY target-out subtraction was applied. Distributions are based on HCAL responses for p+A interactions at 58 GeV/c. Area values under both distributions are same.

Figure 53 illustrates the comparison for p+A interactions at 84 and at 120 GeV/c.

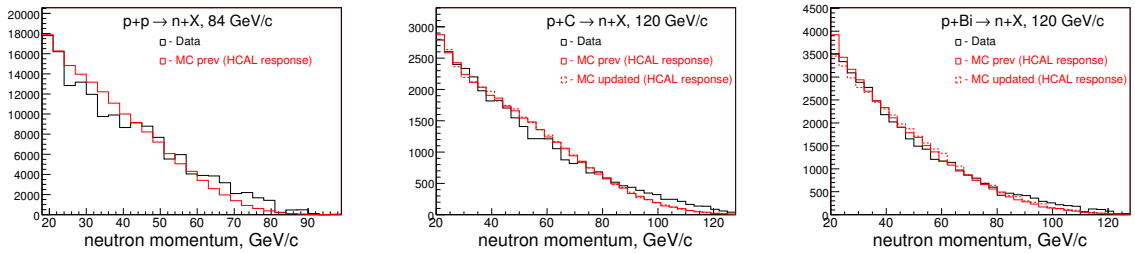

Figure 53: Comparison of the raw neutron spectrum, when ONLY target-out subtraction was applied. Distributions are based on HCAL responses for p+A interactions at 84 and at 120 GeV/c. Area values under both distributions are same.

We do not know what the true spectrum look like in data. But we see that the raw spectrum in MC is much differ from the true one. Why it so distorted? Because the background is accumulated through whole sample, which represents the total inelastic cross section. While the neutron cross section is relatively small sample (10-20%) in compare with the total inelastic cross section. Table 10 illustrates the inelastic and neutron production cross sections in Monte Carlo.

	σ_{inel}	σ_n MC
H_2-58	31.0 mb	4.4 mb (0.14)
C-58	286 mb	29.0 mb (0.10)
Bi-58	1875 mb	123.7 mb (0.07)
H_2-84	31.4 mb	6.0 mb (0.19)
C-120	287 mb	53.0 mb (0.18)
Bi-120	1880 mb	273.5 mb (0.15)

Table 10: Comparison of the total inelastic and neutron cross sections.

13 Neutron uncorrected cross section

The neutron production cross section when ONLY target-out subtraction applied calculated in data as:

$$\frac{d\sigma_n}{dp} = \frac{N_n(t-in) - N_n(t-out)}{N_{beam} \times \Delta p} \times \frac{1}{n_t} \times 10^4, \text{ mb/(GeV/c)}$$

in Monte Carlo as:

$$\frac{d\sigma_n}{dp} = \frac{N_n \times \sigma_{tot}}{N_{tot} \times \Delta p}, \text{ mb/(GeV/c)}$$

where N_n is number of neutron candidates detected by HCAL in given p_i bin, σ_{tot} is pA total cross section and N_{tot} is MC total events.

Figure 54 illustrates the comparison for p+A interactions at 58 GeV/c.

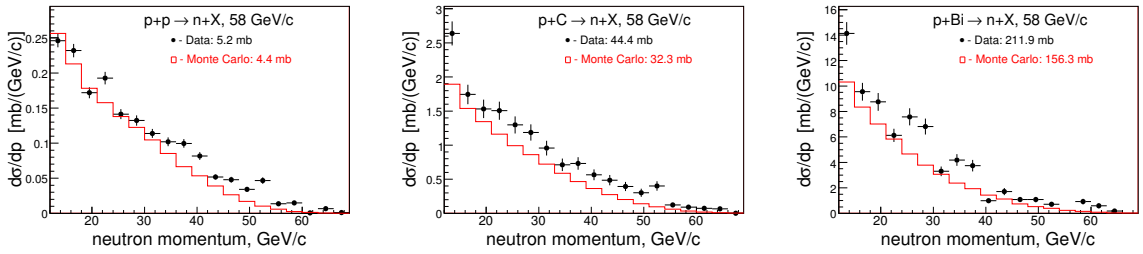

Figure 54: Comparison of the uncorrected neutron production cross section for p+A interactions at 58 GeV/c. Data: only target-out subtraction was applied. MC: no any corrections. Uncertainties are statistical.

Figure 55 illustrates the comparison for p+A interactions at 84 and 120 GeV/c.

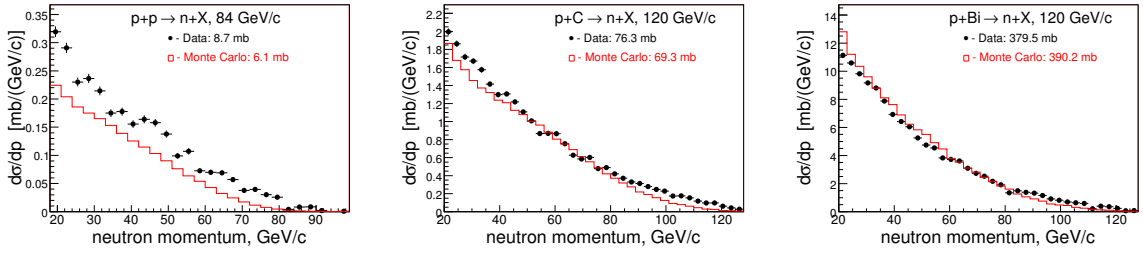

Figure 55: Comparison of the uncorrected neutron production cross section for p+A interactions at 84 and 120 GeV/c. Data: only target-out subtraction was applied. MC: no any corrections. Uncertainties are statistical.

Figure 56 illustrates the comparison for p+Be interactions at 58 and 120 GeV/c.

Summary of the uncorrected neutron production cross for data and Monte Carlo are summarized in Table 11

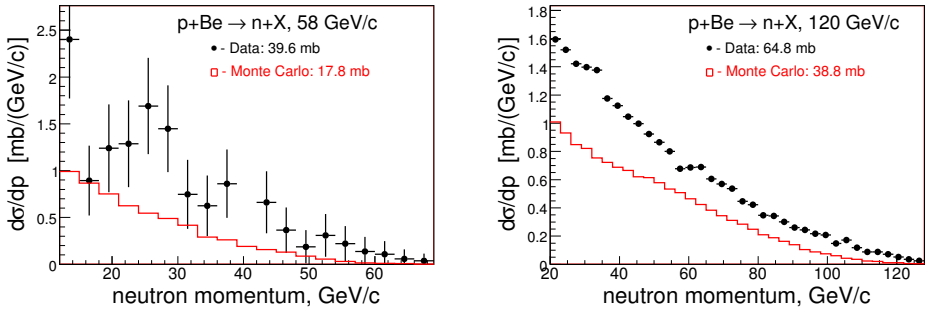

Figure 56: Comparison of the uncorrected neutron production cross section for p+Be interactions at 58 and 120 GeV/c. Data: only target-out subtraction was applied. MC: no any corrections. Uncertainties are statistical.

	DATA	Monte Carlo
H_2-20	0.7 mb	0.4 mb
H_2-58	5.2 mb	4.4 mb
Be-58	39.6 mb	17.8 mb
C-58	44.4 mb	32.3 mb
Bi-58	211.9 mb	156.3 mb
U-58	199.9 mb	180.8 mb
H_2-84	8.7 mb	6.1 mb
Be-120	64.8 mb	38.8 mb
C-120	76.3 mb	69.3 mb
Bi-120	379.5 mb	390.2 mb

Table 11: Summary of the uncorrected neutron production cross for data and Monte Carlo.

14 Trigger Efficiency

We study the trigger efficiency on both ways: using the unbias beam triggers in data and using Monte Carlo. We use the data sample consisting of the proton beam triggers and all requirements for the neutron selection applied, except "SciHi" (trigger) fires. As a supporting information, the track multiplicities for the proton interaction triggers are given in Appendix D.

Figure 57 shows the trigger scintillator pulse height distributions for the p+p interactions at 20 GeV/c using the liquid hydrogen target data for target-in (on left) and target-out subtraction applied (on right), respectively.

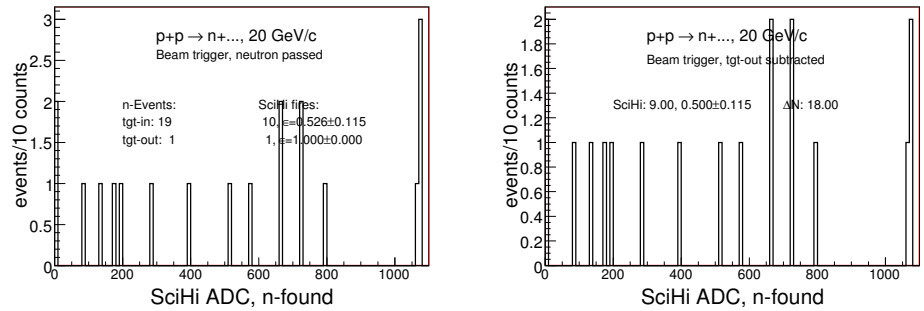

Figure 57: The "SciHi" pulse height distributions for the liquid hydrogen target data using 20 GeV/c proton beam triggers for target-in (on left) and target-out subtraction applied (on right), respectively.

Figure 58 shows the charged track multiplicities for the p+p interactions at 20 GeV/c.

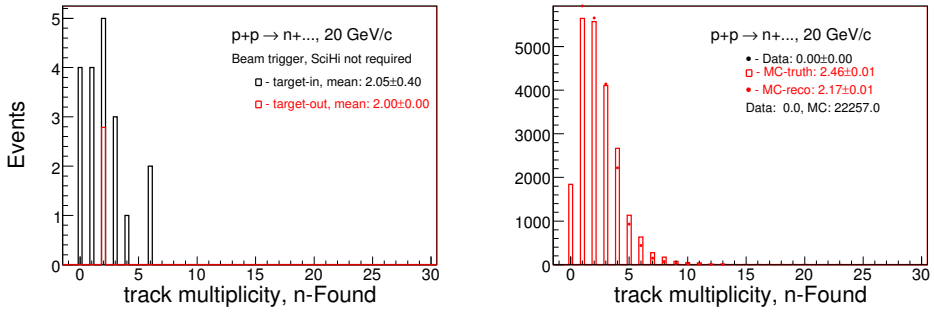

Figure 58: The charged track multiplicities for the liquid hydrogen target using 20 GeV/c proton beam triggers for data (left) and Monte Carlo (right), respectively.

Figure 59 shows the trigger efficiency as a function of the neutron momentum for p+p interactions at 20 GeV/c.

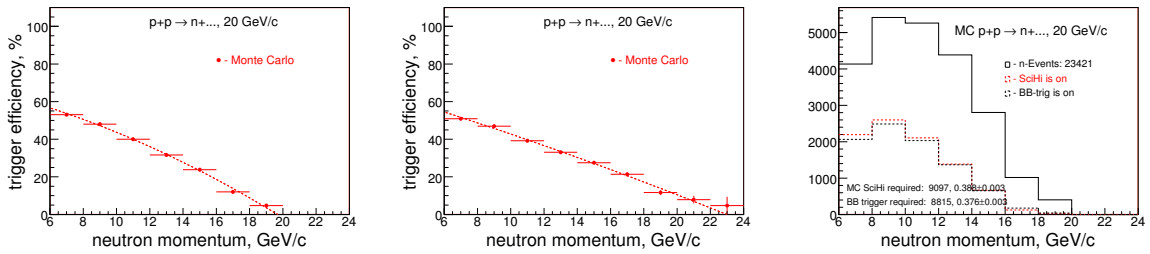

Figure 59: The trigger efficiency as a function of the neutron momentum for p+p interactions at 20 GeV/c: Monte Carlo efficiency dependence without (left) and with (middle) the neutron momentum smearing applied and MC average trigger efficiency (right).

The trigger efficiency study for p+p interactions at 20 GeV/c are summarized in Table 12.

N_{evt}	ϵ_{trig}(data)	ϵ_{trig}(MC-BB)	ϵ_{trig}(MC-SciHi)	ϵ_{trig}(final)	$\Delta\epsilon_{trig}$
19(1)	0.53(0.50)±0.12	0.38±0.003	0.39±0.003	0.46	±0.10

Table 12: Summary of the trigger efficiency studies for p+p interactions at 20 GeV/c. Last two columns represent assigned the final trigger efficiency and the systematic uncertainty.

Figure 60 shows the trigger scintillator pulse height distributions for the p+p interactions at 58 GeV/c using the liquid hydrogen target data for target-in (on left) and target-out subtraction applied (on right), respectively.

Figure 61 shows the charged track multiplicities for the p+p interactions at 58 GeV/c.

Figure 62 shows the trigger efficiency as a function of the neutron momentum for p+p interactions at 58 GeV/c.

The charged track multiplicities passing through the trigger scintillator for p+p interactions at 58 GeV/c are summarized in Table 13.

N_{trk}(beam-tr)	N_{trk}(intr-tr)	N_{trk}(MC-true)	N_{trk}(MC-reco)
4.9(5.1)±0.47	4.81(4.62)±0.05	4.55±0.01	4.26±0.01

Table 13: Summary of the charged track multiplicities for p+p interactions at 58 GeV/c. The difference between N_{trk}(MC-true) and N_{trk}(MC-reco) are mainly due to of TPC acceptance.

The trigger efficiency study for p+p interactions at 58 GeV/c are summarized in Table 14.

Figure 63 shows the trigger scintillator pulse height distributions for the p+Be and p+C interactions at 58 GeV/c.

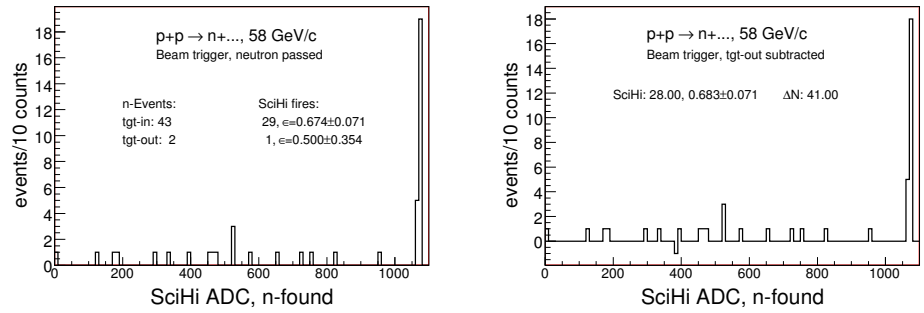

Figure 60: The "SciHi" pulse height distributions for the liquid hydrogen target data using 58 GeV/c proton beam triggers for target-in (on left) and target-out subtraction applied (on right), respectively.

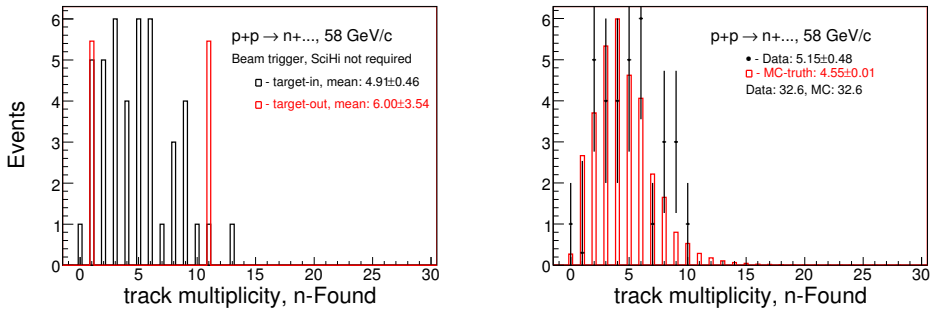

Figure 61: The charged track multiplicities for the liquid hydrogen target using 58 GeV/c proton beam triggers for data (left) and Monte Carlo superimposed (right), respectively.

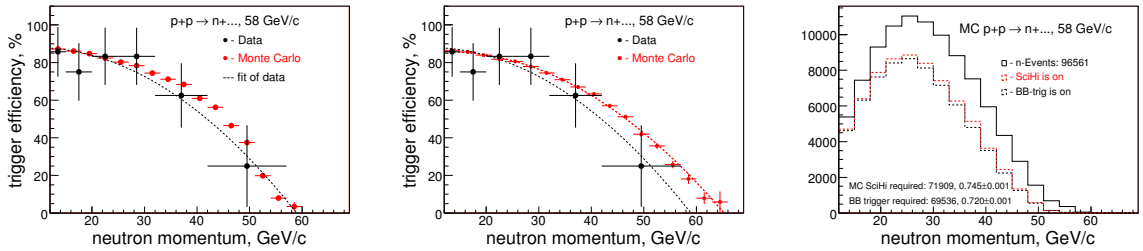

Figure 62: The trigger efficiency as a function of the neutron momentum for p+p interactions at 58 GeV/c: Monte Carlo efficiency dependence without (left) and with (middle) the neutron momentum smearing applied and MC average trigger efficiency (right).

N_{evt}	ϵ_{trig}(data)	ϵ_{trig}(MC-BB)	ϵ_{trig}(MC-SciHi)	ϵ_{trig}(final)	$\Delta\epsilon_{trig}$
43(2)	0.67(0.68)±0.07	0.72±0.001	0.74±0.001	0.71	±0.10

Table 14: Summary of the trigger efficiency studies for p+p interactions at 58 GeV/c. Last two columns represent assigned the final trigger efficiency and the systematic uncertainty.

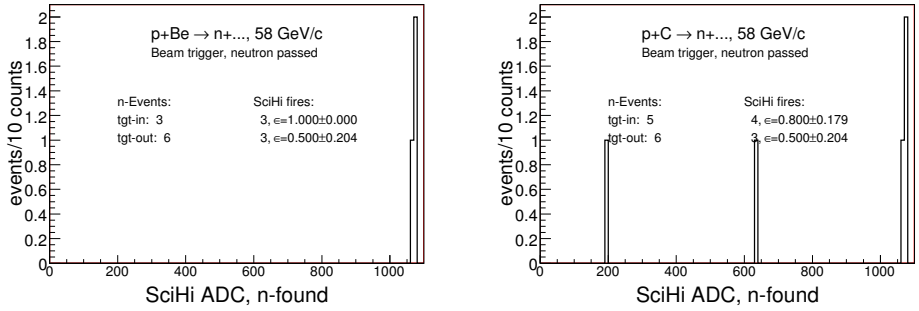

Figure 63: The "SciHi" pulse height distributions for p+Be (left) and p+C (right) interactions with 58 GeV/c proton beam triggers, respectively.

Figure 64 shows MC charged track multiplicities for the p+Be and p+C interactions at 58 GeV/c using interaction triggers.

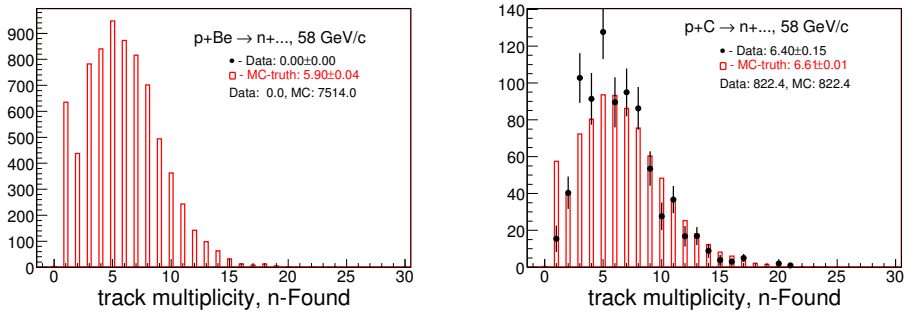

Figure 64: Monte Carlo charged track multiplicities for p+Be (left) and p+C interactions at 58 GeV/c. Since the multiplicities for the beam trigger requirements are not available, then compasion made for the interaction trigger cases.

Figure 65 shows Monte Carlo the average trigger efficiencies for p+Be and p+C interactions at 58 GeV/c.

Figure 66 shows Monte Carlo the trigger efficiency as a function of the neutron momentum for p+Be and p+C interactions at 58 GeV/c.

The charged track multiplicities passing through the trigger scintillator for p+Be and p+C interactions at 58 GeV/c are summarized in Table 15.

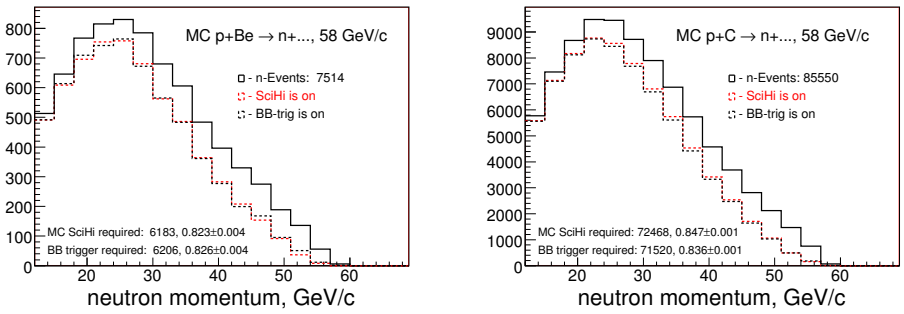

Figure 65: Monte Carlo the average trigger efficiencies for p+Be (left) and p+C (right) interactions at 58 GeV/c.

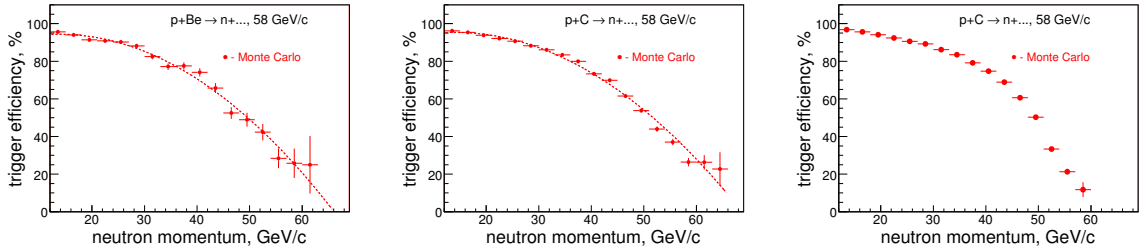

Figure 66: Monte Carlo the trigger efficiency as a function of the neutron momentum for p+Be (left) and p+C (middle and right) interactions at 58 GeV/c. Monte Carlo efficiency dependence with (middle) and without (right) the neutron momentum smearing applied.

	N_{trk}(beam-tr)	N_{trk}(intr-tr)	N_{trk}(MC-true)	N_{trk}(MC-reco)
Be, 58 GeV/c	n/a	6.03(6.23)±0.21	5.90±0.04	5.71±0.04
C, 58 GeV/c	n/a	6.10(6.40)±0.11	6.61±0.01	5.96±0.01

Table 15: Summary of the charged track multiplicities for p+Be and p+C interactions at 58 GeV/c

The trigger efficiency study for p+Be and p+C interactions at 58 GeV/c are summarized in Table 16.

	N_{evt}	ϵ_{trig}(data)	ϵ_{trig}(MC-BB)	ϵ_{trig}(MC-SciHi)	ϵ_{trig}(final)	$\Delta\epsilon_{trig}$
Be, 58 GeV/c	3(6)	1.00(?)±?	0.83±0.004	0.82±0.004	0.82	±0.10
C, 58 GeV/c	5(6)	0.80(?)±0.18	0.85±0.001	0.84±0.001	0.84	±0.10

Table 16: Summary of the trigger efficiency studies for p+Be and p+C interactions at 58 GeV/c. Last two columns represent assigned the final trigger efficiency and the systematic uncertainty.

Figure 67 shows the trigger scintillator pulse height distributions for the p+Bi and p+U interactions at 58 GeV/c.

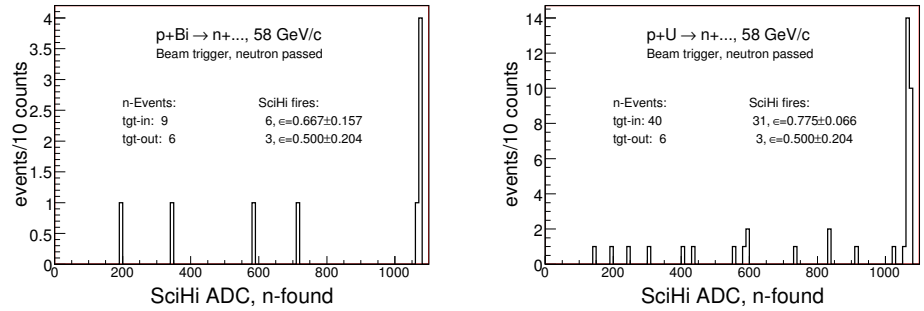

Figure 67: The "SciHi" pulse height distributions for p+Bi (left) and p+U (right) interactions with 58 GeV/c proton beam triggers, respectively.

Figure 68 shows the charged track multiplicities for the p+U interactions at 58 GeV/c.

Figure 69 shows the trigger efficiency as a function of the neutron momentum for p+Bi interactions at 58 GeV/c.

Figure 70 shows the trigger efficiency as a function of the neutron momentum for p+U interactions at 58 GeV/c.

The charged track multiplicities passing through the trigger scintillator for p+Bi and p+U interactions at 58 GeV/c are summarized in Table 17.

	N_{trk}(beam-tr)	N_{trk}(intr-tr)	N_{trk}(MC-true)	N_{trk}(MC-reco)
Bi, 58 GeV/c	n/a	6.96(8.87)±0.19	9.76±0.04	8.31±0.03
U, 58 GeV/c	5.30(6.25)±0.50	6.65(7.29)±0.07	10.06±0.04	8.52±0.03

Table 17: Summary of the charged track multiplicities for p+Be and p+C interactions at 58 GeV/c. For U target MC multiplicity is 8.52/6.25=1.36 times higher than in data. Due to of that the MC trigger efficiency could be overestimated.

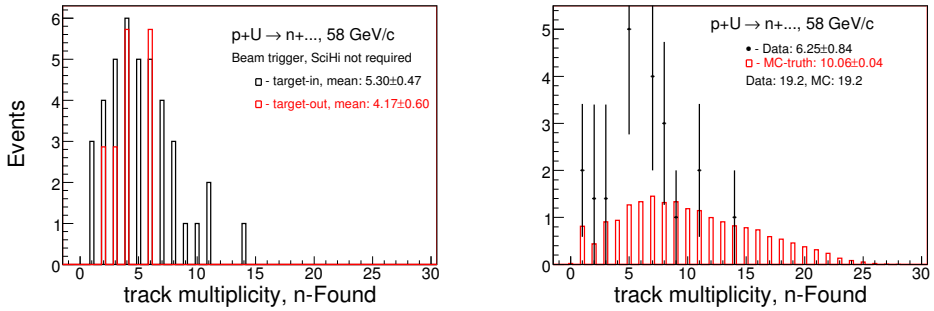

Figure 68: The charged track multiplicities for p+U interactions using 58 GeV/c proton beam triggers for data (left) and Monte Carlo superimposed (right), respectively.

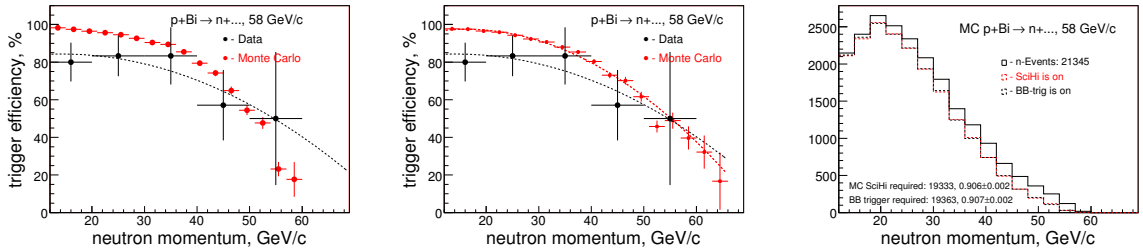

Figure 69: The trigger efficiency as a function of the neutron momentum for p+Bi interactions at 58 GeV/c: Monte Carlo efficiency dependence without (left) and with (right) the neutron momentum smearing applied and MC average trigger efficiency (right).

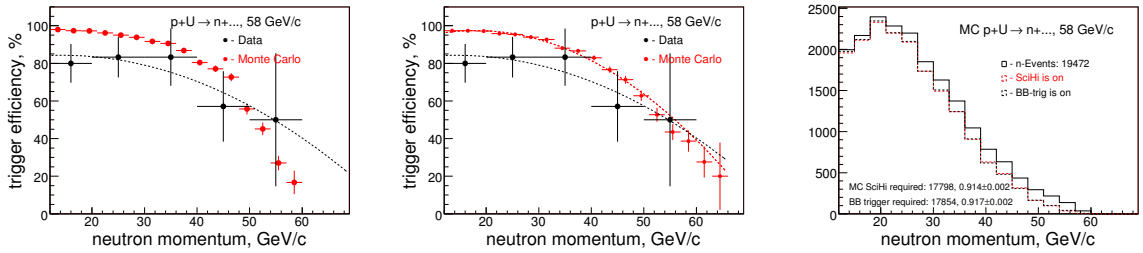

Figure 70: The trigger efficiency as a function of the neutron momentum for p+U interactions at 58 GeV/c: Monte Carlo efficiency dependence without (left) and with (right) the neutron momentum smearing applied and MC average trigger efficiency (right).

The trigger efficiency study for p+Bi and p+U interactions at 58 GeV/c are summarized in Table 18.

	N_{evt}	ϵ_{trig}(data)	ϵ_{trig}(MC-BB)	ϵ_{trig}(MC-SciHi)	ϵ_{trig}(final)	$\Delta\epsilon_{trig}$
Bi, 58 GeV/c	9(6)	0.67(?)±0.16	0.91±0.002	0.91±0.002	0.845	±0.10
U, 58 GeV/c	40(6)	0.78(?)±0.07	0.92±0.002	0.91±0.002	0.845	±0.10

Table 18: Summary of the trigger efficiency studies for p+Bi and p+U interactions at 58 GeV/c. Note: the efficiencies based on data have high level of statistical uncertainties. Last two columns represent the final trigger efficiency and the systematic uncertainty.

Figure 71 shows the trigger scintillator pulse height distributions for the p+p interactions at 84 GeV/c using the liquid hydrogen target data for target-in (on left) and target-out subtraction applied (on right), respectively.

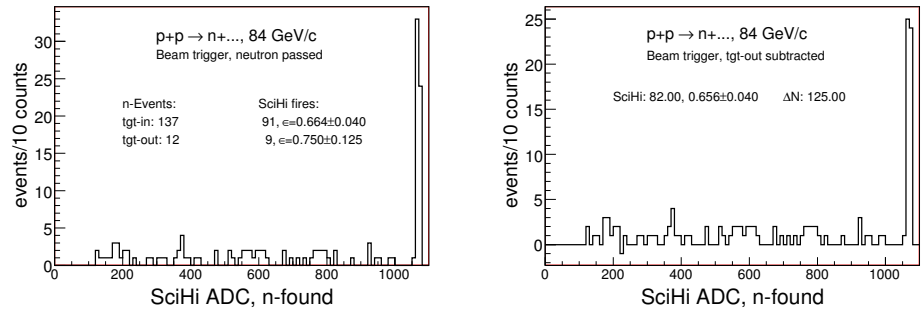

Figure 71: The "SciHi" pulse height distributions for the liquid hydrogen target data using 20 GeV/c proton beam triggers for target-in (on left) and target-out subtraction applied (on right), respectively.

Figure 72 shows the charged track multiplicities for the p+p interactions at 84 GeV/c.

Figure 73 shows the trigger efficiency as a function of the neutron momentum for p+p interactions at 84 GeV/c.

The trigger efficiency study for p+p interactions at 84 GeV/c are summarized in Table 19.

N_{evt}	ϵ_{trig}(data)	ϵ_{trig}(MC-BB)	ϵ_{trig}(MC-SciHi)	ϵ_{trig}(final)	$\Delta\epsilon_{trig}$
137(12)	0.66(0.66)±0.04	0.82±0.001	0.80±0.001	0.73	±0.10

Table 19: Summary of the trigger efficiency studies for p+p interactions at 84 GeV/c. Last two columns represent assigned final trigger efficiency and systematic uncertainty.

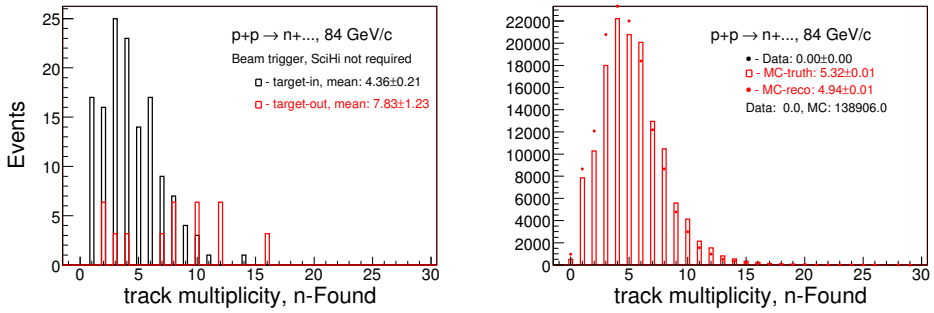

Figure 72: The charged track multiplicities for the liquid hydrogen target using 84 GeV/c proton beam triggers for data (left) and Monte Carlo (right), respectively.

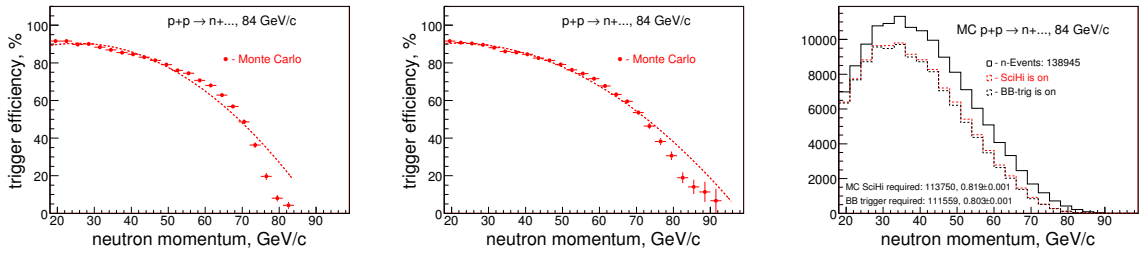

Figure 73: The trigger efficiency as a function of the neutron momentum for p+p interactions at 84 GeV/c: Monte Carlo efficiency dependence without (left) and with (middle) the neutron momentum smearing applied and MC average trigger efficiency (right).

Why the trigger efficiency at 84 GeV/c is lower than at 58 GeV/c? Let's compare SciHi rates for these two datasets. Figure 74 shows the SciHi fires rate as a function of the dataset number for both 58 and 84 GeV/c datasets using the beam triggers.

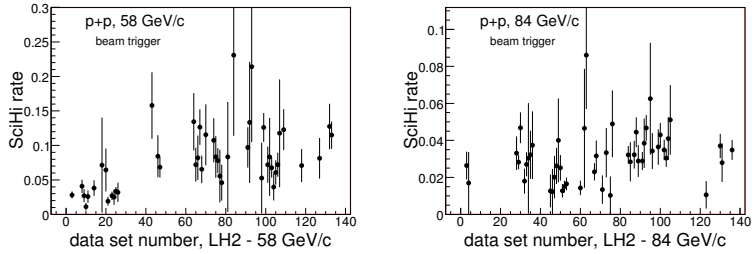

Figure 74: The SciHi fires rate as a function of the dataset number for both 58 GeV/c (left) and 84 GeV/c (right) using the beam triggers. Each data point on figures represents a single run number. Plots indicates that the SciHi fires at 84 GeV/c occurs at least twice lower than at 58 GeV/c.

Figure 75 shows the SciHi fires rate as a function of the dataset number for both 58 and 84 GeV/c datasets using the proton interaction triggers.

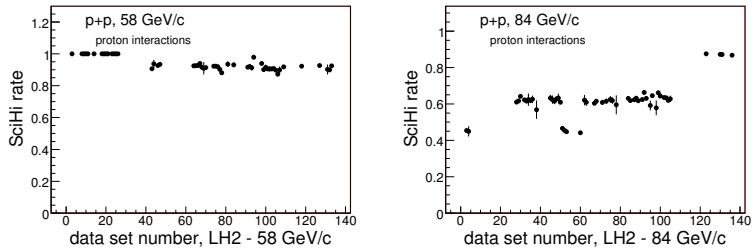

Figure 75: The SciHi fires rate as a function of the dataset number for both 58 GeV/c (left) and 84 GeV/c (right) using the proton interaction triggers. Each data point on figures represents a single run number. Plots indicates that the SciHi fires at 84 GeV/c occurs about 30% lower than at 58 GeV/c.

Figure 76 shows the SciHi ADC distributions for 58 and 84 GeV/c data using the beam triggers.

Figure 77 shows the SciHi ADC distributions for 58 and 84 GeV/c data using the beam triggers.

Figure 78 shows the trigger scintillator pulse height distributions for the p+Be interactions at 120 GeV/c.

Figure 79 shows the trigger efficiency as a function of the neutron momentum for p+Be interactions at 120 GeV/c.

Figure 80 shows the charged track multiplicities for the p+Be interactions at 120 GeV/c.

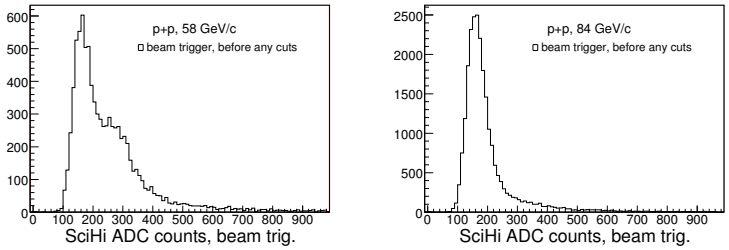

Figure 76: The SciHi ADC distributions for 58 (left) and 84 GeV/c (right) data using the beam triggers.

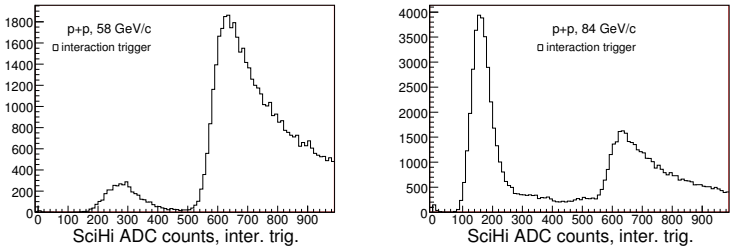

Figure 77: The SciHi ADC distributions for 58 (left) and 84 GeV/c (right) data using the proton interaction triggers. Left plot indicates that the trigger at 58 GeV mainly caused by SciHi with small straight through contamination. While 84 GeV data (right) mainly was triggered by iDC and it highly populated with the straight through. That can lead to the lower efficiency at 84 GeV in compare with 58 GeV data. Unfortunately, Monte Carlo could not able to reproduce these effects. Due to of that as the central value of trigger efficiency we used what was derived from data, while the momentum dependence follows according to Monte Carlo curve. So, Monte Carlo trigger efficiency function values were scaled down by coefficient of 0.82

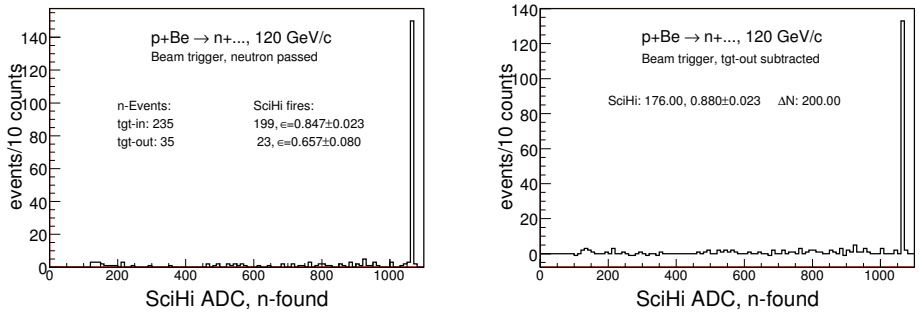

Figure 78: The "SciHi" pulse height distributions for p+Be interactions at 120 GeV/c: for target-in (left) and target-out subtraction applied (right), respectively.

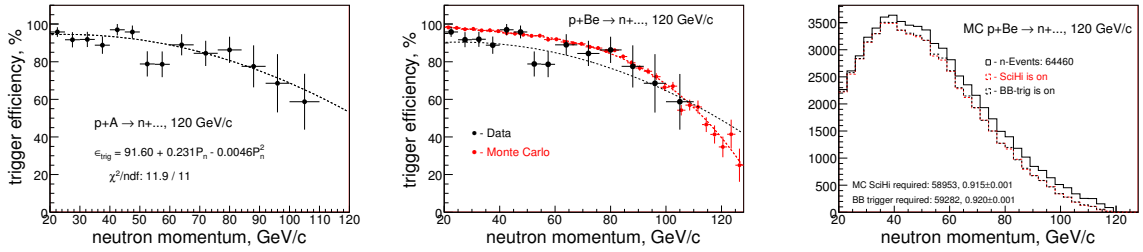

Figure 79: The trigger efficiency as a function of the neutron momentum for p+Be interactions at 120 GeV/c. Combined fit, Be and Bi data values are scaled to the C (left), predicted MC behavior (middle) and the average MC predictions (right). Monte Carlo efficiency dependence was made with the neutron momentum smearing applied.

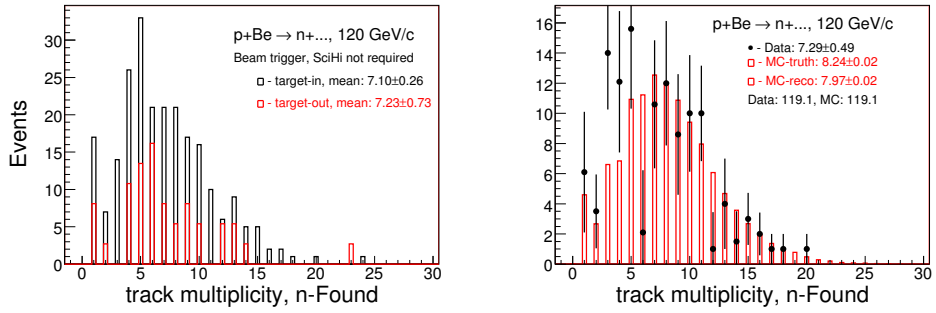

Figure 80: The charged track multiplicities for p+Be interactions at 120 GeV/c for data (left) and Monte Carlo superimposed (right), respectively.

The charged track multiplicities passing through the trigger scintillator for p+Be interactions at 120 GeV/c are summarized in Table 20.

N_{trk}(beam-tr)	N_{trk}(intr-tr)	N_{trk}(MC-true)	N_{trk}(MC-reco)
7.10(7.3)±0.49	7.9(7.8)±0.02	8.2±0.02	8.0±0.02

Table 20: Summary of the charged track multiplicities for p+Be interactions at 120 GeV/c. MC multiplicity is 8.0/7.3=1.1 times higher than in data. Both multiplicities and MC average efficiency suggests that ϵ_{trig}=0.99 looks unreasonable.

The trigger efficiency study for p+Be interactions at 120 GeV/c are summarized in Table 21.

N_{evt}	ϵ_{trig}(data)	ϵ_{trig}(MC-BB)	ϵ_{trig}(MC-SciHi)	ϵ_{trig}(final)	$\Delta\epsilon_{trig}$
235(35)	0.85(0.88)±0.03	0.92±0.001	0.92±0.001	0.885	±0.07

Table 21: Summary of the trigger efficiency studies for p+Be interactions at 120 GeV/c. What to use as the average trigger efficiency: 0.84(data) or 0.92(MC)? The value 0.84 is way off, however MC average is slightly overestimated. We might use MC value and assign 0.08 as systematic uncertainty.

Figure 81 shows the trigger scintillator pulse height distributions for the p+C interactions at 120 GeV/c.

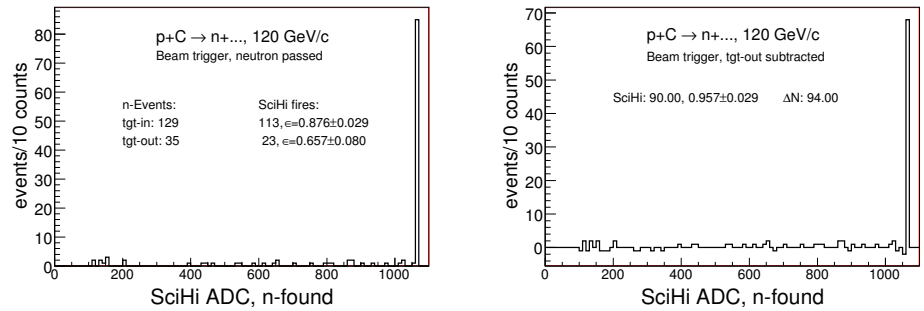

Figure 81: The "SciHi" pulse height distributions for p+C interactions at 120 GeV/c: for target-in (left) and target-out subtraction applied (right), respectively.

Figure 82 shows the trigger efficiency as a function of the neutron momentum for p+C interactions at 120 GeV/c.

Figure 83 shows the charged track multiplicities for the p+C interactions at 120 GeV/c.

The charged track multiplicities passing through the trigger scintillator for p+C interactions at 120 GeV/c are summarized in Table 22.

The trigger efficiency study for p+C interactions at 120 GeV/c are summarized in Table 23.

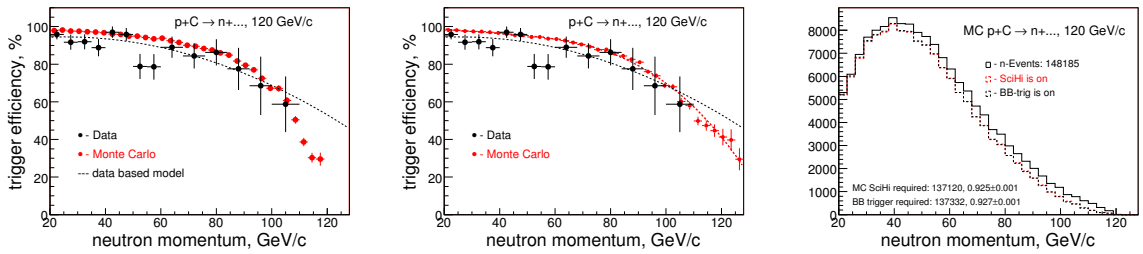

Figure 82: The trigger efficiency as a function of the neutron momentum for p+C interactions at 120 GeV/c: Monte Carlo efficiency dependence without (left) and with (right) the neutron momentum smearing applied and MC average trigger efficiency (right).

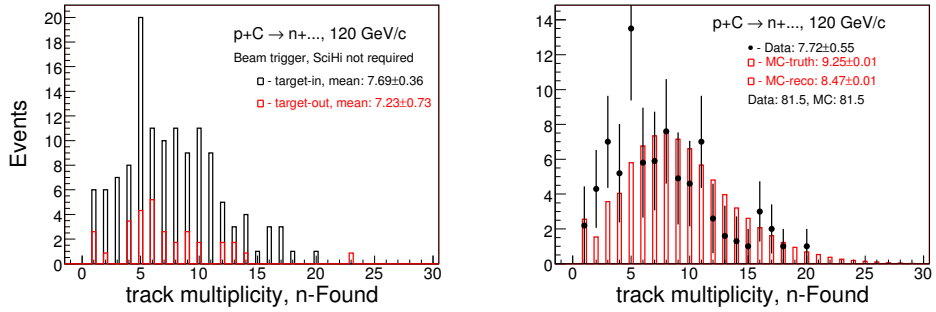

Figure 83: The charged track multiplicities for p+C interactions at 120 GeV/c for data (left) and Monte Carlo superimposed (right), respectively.

N_{trk}(beam-tr)	N_{trk}(intr-tr)	N_{trk}(MC-true)	N_{trk}(MC-reco)
7.7(7.7)±0.55	8.3(8.4)±0.02	9.3±0.01	8.5±0.01

Table 22: Summary of the charged track multiplicities for p+C interactions at 120 GeV/c. MC multiplicity is 8.5/7.7=1.1 times higher than in data. Both multiplicities and MC average efficiency suggests that ϵ_{trig}=0.96 looks unreasonable.

N_{evt}	ϵ_{trig}(data)	ϵ_{trig}(MC-BB)	ϵ_{trig}(MC-SciHi)	ϵ_{trig}(final)	$\Delta\epsilon_{trig}$
129(35)	0.88(0.96?)±0.03	0.93±0.001	0.93±0.001	0.905	±0.05

Table 23: Summary of the trigger efficiency studies for p+C interactions at 120 GeV/c. Last two columns represent assigned the final trigger efficiency and the systematic uncertainty.

Figure 84 shows the trigger scintillator pulse height distributions for the p+Be interactions at 120 GeV/c.

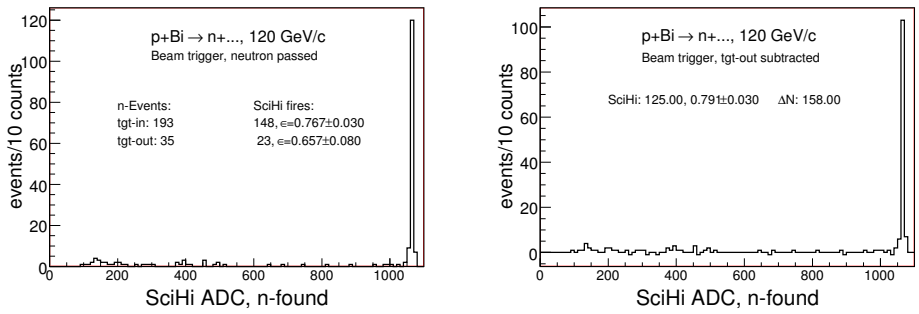

Figure 84: The "SciHi" pulse height distributions for p+Be interactions at 120 GeV/c: for target-in (left) and target-out subtraction applied (right), respectively.

Figure 85 shows the trigger efficiency as a function of the neutron momentum for p+Bi interactions at 120 GeV/c.

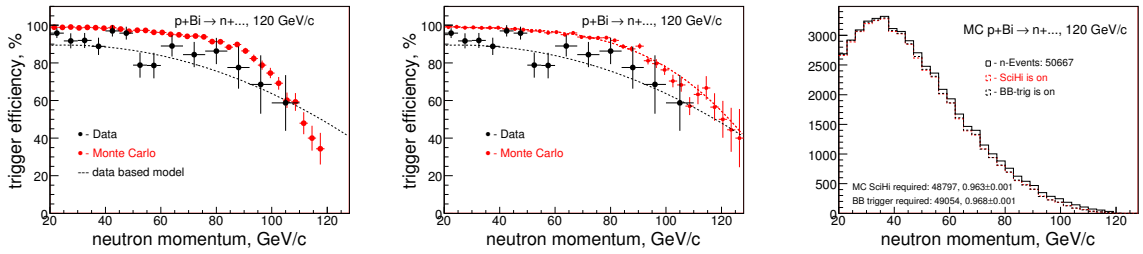

Figure 85: The trigger efficiency as a function of the neutron momentum for p+Bi interactions at 120 GeV/c: Monte Carlo efficiency dependence without (left) and with (right) the neutron momentum smearing applied and MC average trigger efficiency (right).

Figure 86 shows the charged track multiplicities for the p+Bi interactions at 120 GeV/c.

The charged track multiplicities passing through the trigger scintillator for p+Bi interactions at 120 GeV/c are summarized in Table 24.

The trigger efficiency study for p+Bi interactions at 120 GeV/c are summarized in Table 25.

The charged particles multiplicities for the Monte Carlo non-neutron samples are given in Appendix E.

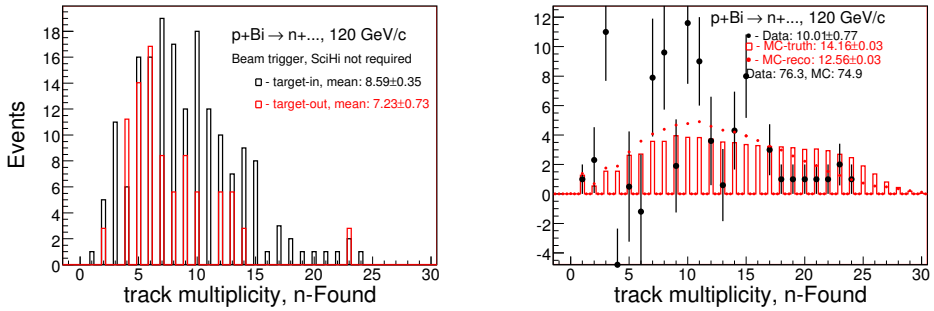

Figure 86: The charged track multiplicities for p+Bi interactions at 120 GeV/c for data (left) and Monte Carlo superimposed (right), respectively.

N_{trk}(beam-tr)	N_{trk}(intr-tr)	N_{trk}(MC-true)	N_{trk}(MC-reco)
8.6(10.0)±0.77	9.6(11.0)±0.05	14.23±0.03	12.62±0.03

Table 24: Summary of the charged track multiplicities for p+Bi interactions at 120 GeV/c. MC multiplicity is 12.62/10.0=1.26 times higher than in data. Due to of that the MC trigger efficiency could be overestimated.

N_{evt}	ϵ_{trig}(data)	ϵ_{trig}(MC-BB)	ϵ_{trig}(MC-SciHi)	ϵ_{trig}(final)	$\Delta\epsilon_{trig}$
193(35)	0.77(0.79)±0.03	0.96±0.001	0.97±0.001	0.87	±0.10

Table 25: Summary of the trigger efficiency studies for p+Bi interactions at 120 GeV/c. Last two columns represent assigned the final trigger efficiency and the systematic uncertainty.

15 Particles production cross sections from FLUKA

Particles production cross sections from FLUKA presented in Table 26.

	$\pi^{\pm}$	$K^{\pm}$	$p/\bar{p}$	n
H_2-20	47.5	3.6	33.0	17.6
H_2-58	92.8	8.6	33.4	18.6
H_2-84	111.2	10.6	34.2	19.1
Be-58	408.3	35.4	268.3	100.9
C-58	768.3	68.0	359.3	190.9
Bi-58	6218.8	593.0	3829.0	1777.5
U-58	7167.6	683.1	4263.5	2068.3
Be-120	573.3	52.9	275.4	106.2
C-120	1076.0	100.5	372.7	201.2
Bi-120	7878.7	779.4	3815.7	1692.8

Table 26: Particles production cross sections (everything in mb). Momentum threshold: 1 GeV/c

Figure 87 shows the particles production cross sections as a function of the target atomic weight.

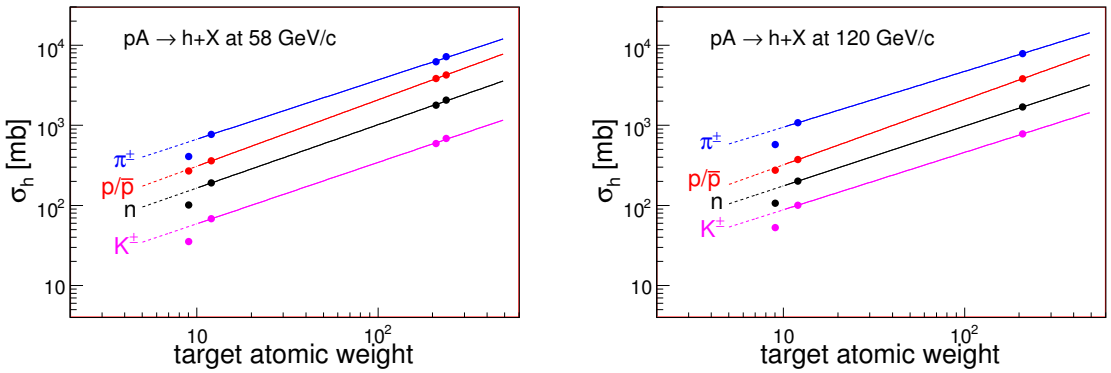

Figure 87: The particles production cross sections as a function of the target atomic weight. Plots made for both beam momenta: 58 GeV/c (left) and 120 GeV/c (right), respectively

Plots clearly indicates that the production rates from Be target has at least a factor two drop in compare with the predictions from other targets. This feature observable for charged pions, kaons and neutrons. Proton production looks reasonable. Is it possible that this feature because of low the total cross section implemented to Be target? Figure 88 shows the total cross sections as a function of the target atomic weight.

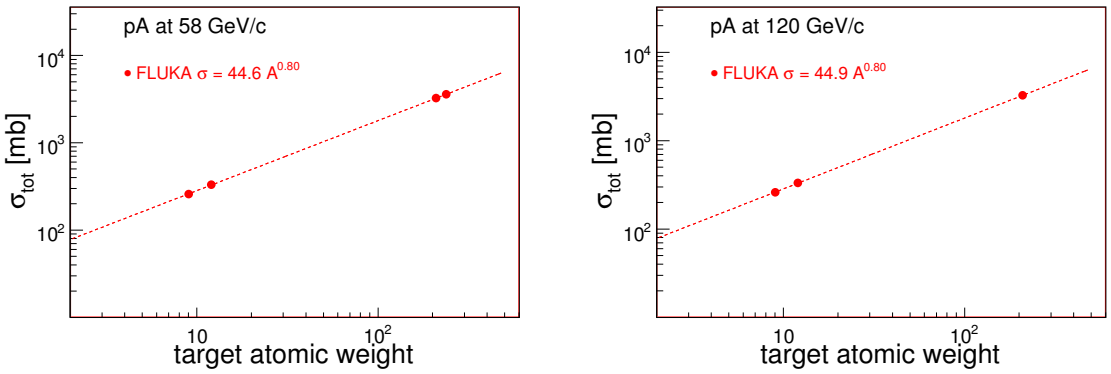

Figure 88: Total cross sections as a function of the target atomic weight implemented by FLUKA generator. Plots made for both beam momenta: 58 GeV/c (left) and 120 GeV/c (right), respectively

16 Neutron Production Properties Depending on Generator

We considered the particles production multiplicities, the true neutron spectra and the neutron an angular distribution. Comparison made for FLUKA/DPMJET and LAQGSM generators. DPMJET used for p+p interactions at 58 GeV/c only.

16.1 General particle multiplicities

Below we compare the particle production multiplicities of FLUKA and LAQGSM [5, 6, 7] generators calculated per single p+A interaction.

The particles multiplicity production from p+p, p+C and p+Bi interactions at 58 GeV/c using Fluka and LAQGSM models are shown in Table 27.

58 GeV/c	p+p		p+C		p+Bi	
	DPMJET	LAQGSM	FLUKA	LAQGSM	FLUKA	LAQGSM
π^+	2.71	1.81	2.05	2.84	1.97	5.35
π^-	2.00	1.28	1.82	2.50	1.89	5.81
K^+	0.21	0.15	0.16	0.25	0.16	0.48
K^-	0.11	0.10	0.09	0.15	0.09	0.20
p	1.59	1.41	1.65	2.86	3.10	11.01
n	0.68	0.52(0.51)	1.49	2.61(1.20)	3.20	32.27(4.49)
Total (charged)	6.62	4.75	5.77	8.60	7.21	22.85

Table 27: The particles multiplicity production from p+p, p+C and p+Bi interactions at 58 GeV/c using Fluka and LAQGSM generators. The multiplicities are calculated per single interaction. The number of neutrons in parenthesis represents yield with p_n >100 MeV/c threshold.

The particles multiplicity production from p+p, p+C and p+Bi interactions at 120 GeV/c using Fluka and LAQGSM models are shown in Table 28.

16.2 MC neutron production per single p+A interaction

Figure 89 shows the neutron production spectra and rates normalized per single p+p interactions at 20, 58 and 84 GeV/c.

Figure 90 shows the neutron production spectra and rates normalized per single p+Be or p+C interactions at 58 GeV/c.

Figure 91 shows the neutron production spectra and rates normalized per single p+Bi or p+U interactions at 58 GeV/c.

Figure 92 shows the neutron production spectra and rates normalized per single p+Be, p+C or p+Bi interactions at 120 GeV/c.

120 GeV/c	p+p		p+C		p+Bi	
	DPMJET	LAQGSM	FLUKA	LAQGSM	FLUKA	LAQGSM
π^+	-	2.36	2.56	3.87	2.53	7.72
π^-	-	1.82	2.33	3.53	2.46	8.24
K^+	-	0.25	0.21	0.41	0.22	0.79
K^-	-	0.18	0.13	0.28	0.14	0.39
p	-	1.39	1.67	2.97	2.92	11.88
n	-	0.54(0.52)	1.53	2.74(1.26)	3.16	33.69(4.99)
Total (charged)	-	6.00	6.90	11.06	8.27	29.02

Table 28: The particles multiplicity production from p+p, p+C and p+Bi interactions at 120 GeV/c using Fluka and LAQGSM generators. The multiplicities are calculated per single interaction. The number of neutrons in parenthesis represents yield with p_n >100 MeV/c threshold.

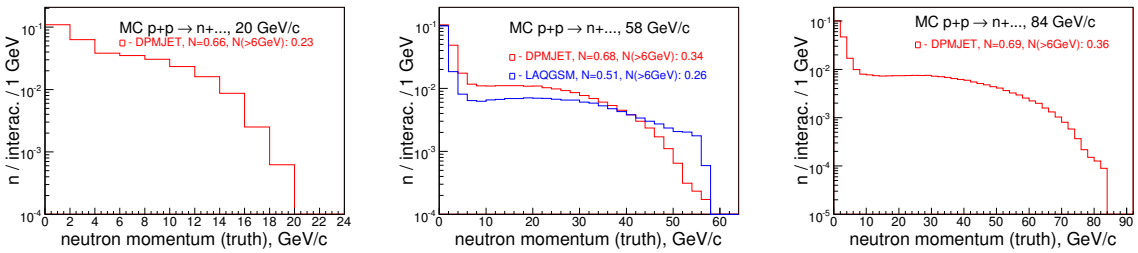

Figure 89: The neutron production spectra and rates normalized per single p+p interactions at 20 GeV/c (left), 58 GeV/c (middle) and 84 GeV/c (right) using FLUKA and LAQGSM (if possible).

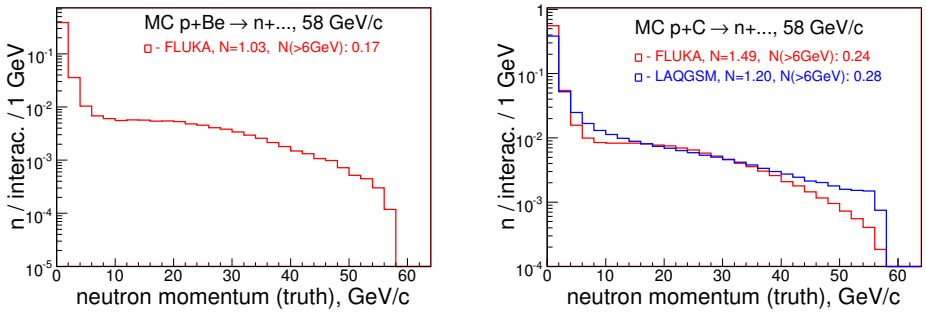

Figure 90: The neutron production spectra and rates normalized per single p+Be (left) or p+C (right) interactions at 58 GeV/c using FLUKA and LAQGSM (if possible).

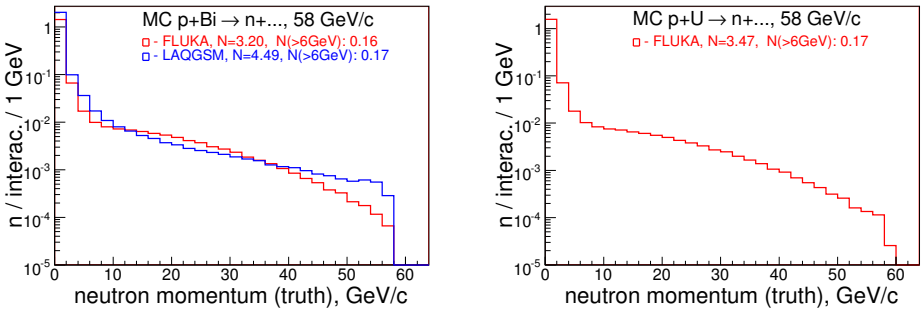

Figure 91: The neutron production spectra and rates normalized per single p+Bi (left) and p+U (right) interactions at 58 GeV/c using FLUKA and LAQGSM (if possible).

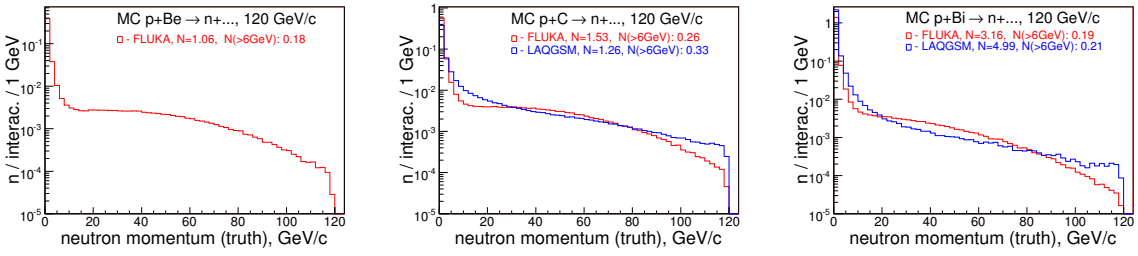

Figure 92: The neutron production spectra and rates normalized per single p+Be (left), p+C (middle) and p+Bi (right) interactions at 120 GeV/c using FLUKA and LAQGSM (if possible).

Table 29 illustrates Monte Carlo neutron production rates per single p+A interaction with p_n >100 MeV/c threshold.

	FLUKA	LAQGSM
H_2-20	0.66	
H_2-58	0.68	0.51
Be-58	1.03	
C-58	1.49	1.20
Bi-58	3.20	4.49
U-58	3.47	
H_2-84	0.69	
Be-120	1.06	
C-120	1.53	1.26
Bi-120	3.16	4.99

Table 29: Summary of Monte Carlo neutron production rates per single p+A interaction with p_n >100 MeV/c threshold. FLUKA column for H_2 target actually done with DPMJET generator.

Figure 93 shows the neutron p_T spectra normalized per single p+A interactions at 58 and 120 GeV/c.

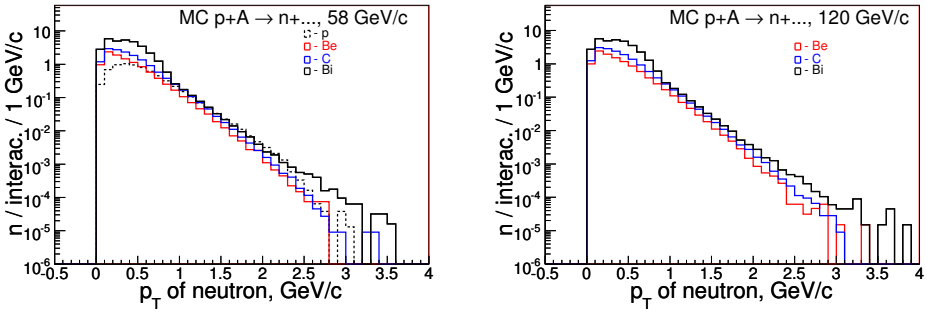

Figure 93: The neutron p_T spectra normalized per single p+A interactions at 58 (left) and 120 GeV/c (right) using FLUKA generator. Prediction for p target at 58 GeV/c was done by DPMJET.

16.3 Neutron spectra with $p_n > p_{min}$

Figure 94 shows the true neutron production spectra from p+p interactions at 20, 58 and 84 GeV/c using FLUKA and LAQGSM models.

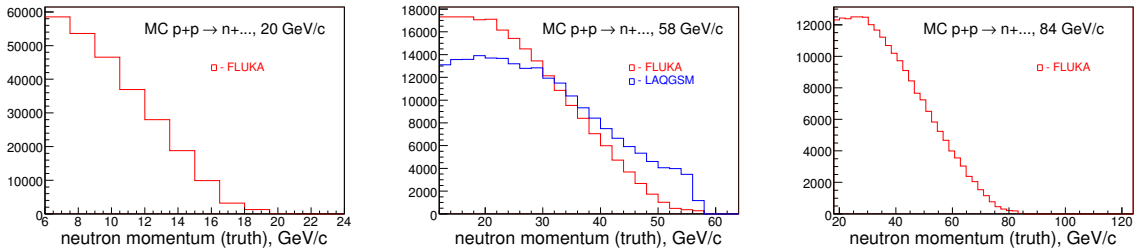

Figure 94: The true neutron production spectra from the p+p interactions at 20 GeV/c (left), 58 GeV/c (middle) and 84 GeV/c using FLUKA and LAQGSM (where it was possible) models.

Figure 95 shows the true neutron production spectra from p+Be and p+C interactions at 58 GeV/c using FLUKA and LAQGSM models.

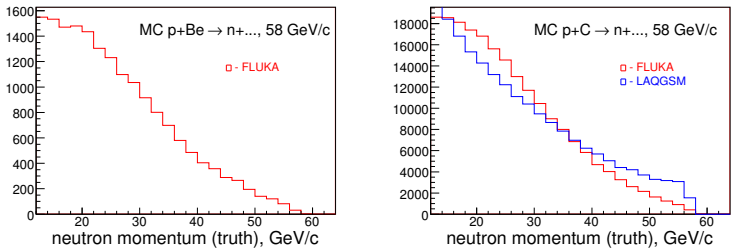

Figure 95: The true neutron production spectra from the p+Be (left) and p+C (right) interactions at 58 GeV/c using FLUKA and LAQGSM models.

Figure 96 shows the true neutron production spectra for the p+Bi and p+U interactions at 58 GeV/c using FLUKA and LAQGSM models.

Figure 97 shows the true neutron production spectra from p+Be, p+C and p+Bi interactions at 120 GeV/c using FLUKA and LAQGSM models.

16.4 Neutron an angular distribution

The neutron angular distribution effecting the calorimeter acceptance. Below we compare the neutron exit angle, a p_T/p_{tot} variable, from Fluka and LAQGSM [5, 6, 7] generators.

Figure 98 shows the p_T/p_{tot} quantity distributions for p+p at 20, 58 and 84 GeV/c using Fluka and LAQGSM models (where it was available).

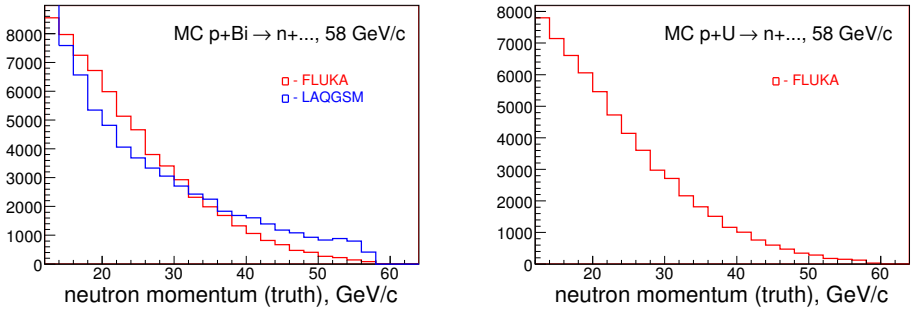

Figure 96: The true neutron production spectra from p+Bi (left) and p+U (right) interactions at 58 GeV/c using FLUKA and LAQGSM models.

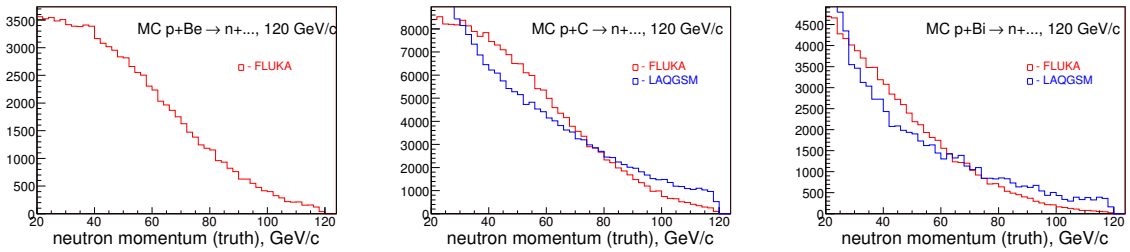

Figure 97: The true neutron production spectra from p+Be (left), p+C (middle) and p+Bi (right) interactions at 120 GeV/c using FLUKA and LAQGSM models.

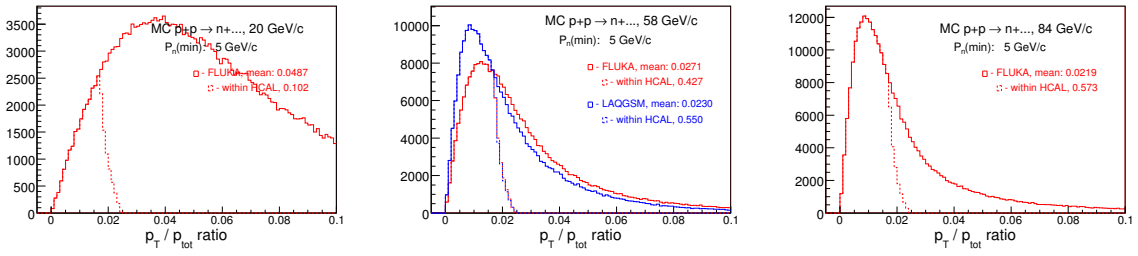

Figure 98: The p_T/p_{tot} distributions for neutrons from p+p at 20 GeV/c (left), 58 GeV/c (middle) and 84 GeV/c (right) using Fluka and LAQGSM models.

Figure 99 shows the p_T/p_{tot} quantity distributions for p+Be and p+C interactions at 58 GeV/c using Fluka and LAQGSM models.

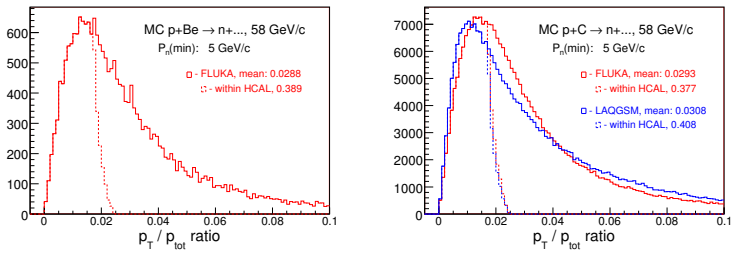

Figure 99: The p_T/p_{tot} distributions for neutrons from p+Be (left) and p+C (right) interactions at 58 GeV/c using Fluka and LAQGSM models.

Figure 100 shows the p_T/p_{tot} quantity distributions for p+Bi and p+U interactions at 58 GeV/c using Fluka and LAQGSM models.

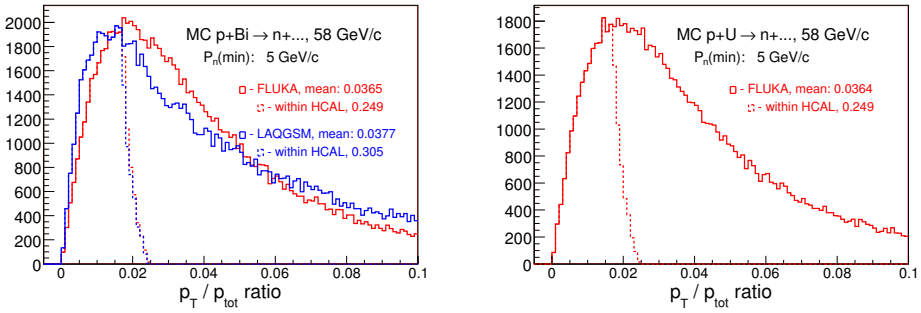

Figure 100: The p_T/p_{tot} distributions for neutrons from p+Bi (left) and p+U (right) interactions at 58 GeV/c using Fluka and LAQGSM models.

Figure 101 shows the p_T/p_{tot} quantity distributions for p+Be. p+C and p+U interactions at 120 GeV/c using Fluka and LAQGSM models..

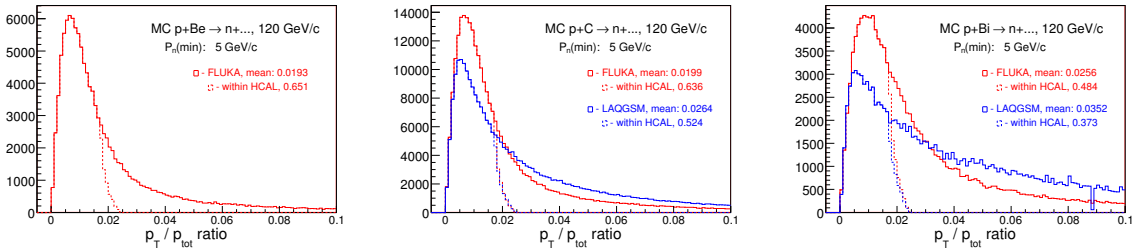

Figure 101: The p_T/p_{tot} distributions for neutrons from p+Be (left), p+C (middle) and p+Bi (right) interactions at 120 GeV/c using Fluka and LAQGSM models.

16.5 Neutron transverse momentum distribution

Figure 102 shows the neutron's p_T distributions using p+p, p+Be and p+C interactions at 58 GeV/c generated by Fluka.

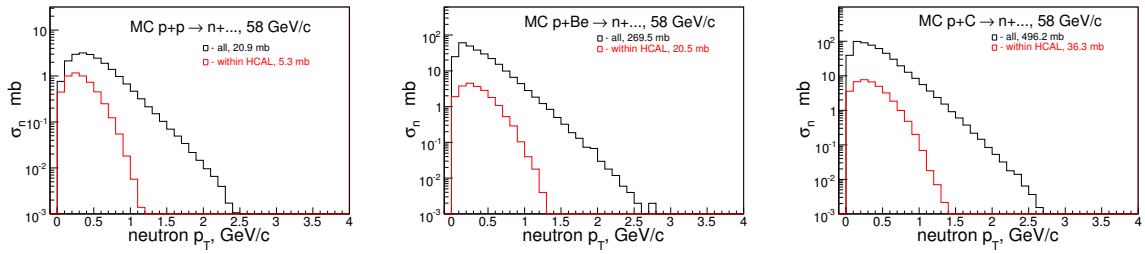

Figure 102: The neutron's p_T distributions using p+p (left), p+Be (middle) and p+C (right) interactions at 58 GeV/c generated by Fluka. Plots illustrates two cases: all neutrons (black) and within HCAL (red).

Figure 103 shows the neutron's p_T distributions using p+Bi and p+U at 58 GeV/c and p+p interactions at 84 GeV/c generated by Fluka.

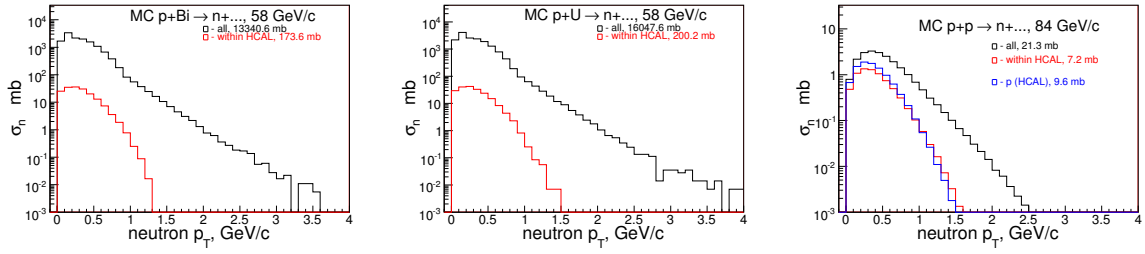

Figure 103: The neutron's p_T distributions using p+Bi (left) and p+U (middle) interactions at 58 GeV/c and p+p (right) interactions at 84 GeV/c generated by Fluka. Plots illustrates two cases: all neutrons (black) and within HCAL (red).

Figure 104 shows the neutron's p_T distributions using p+Be, p+C and p+Bi interactions at 120 GeV/c generated by Fluka.

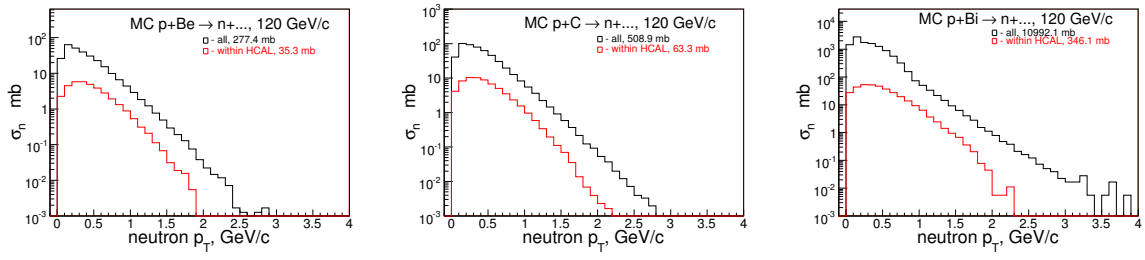

Figure 104: The neutron's p_T distributions using p+Be (left), p+C (middle) and p+Bi (right) interactions at 120 GeV/c generated by Fluka. Plots illustrates two cases: all neutrons (black) and within HCAL (red).

16.6 Neutron mean transverse momentum vs the total momentum

Figure 105 shows the neutron's mean p_T vs the total momentum distributions using p+p, p+Be and p+C interactions at 58 GeV/c generated by Fluka.

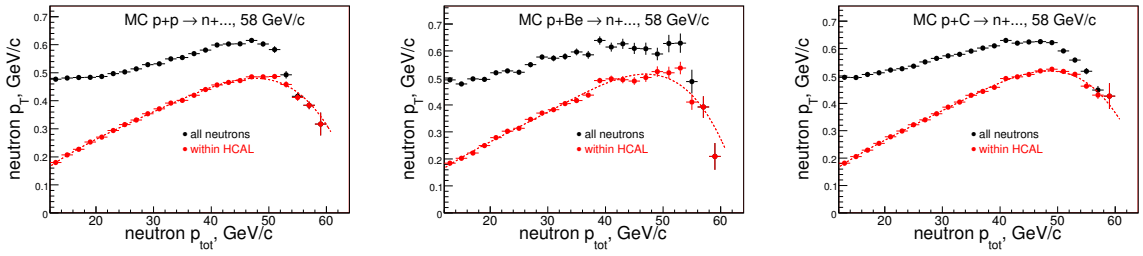

Figure 105: The neutron's mean p_T vs the total momentum distributions using p+p (left), p+Be (middle) and p+C (right) interactions at 58 GeV/c generated by Fluka. Plots illustrates two cases: all neutrons (black) and within HCAL (red).

Figure 106 shows the neutron's mean p_T vs the total momentum distributions using p+Bi and p+U at 58 GeV/c and p+p interactions at 84 GeV/c generated by Fluka.

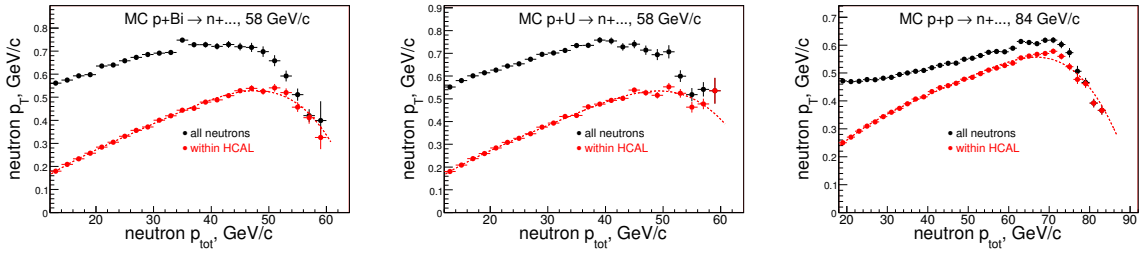

Figure 106: The neutron's mean p_T vs the total momentum distributions using p+Bi (left) and p+U (middle) interactions at 58 GeV/c and p+p (right) interactions at 84 GeV/c generated by Fluka. Plots illustrates two cases: all neutrons (black) and within HCAL (red).

Figure 107 shows the neutron's mean p_T vs the total momentum distributions using p+Be, p+C and p+Bi interactions at 120 GeV/c generated by Fluka.

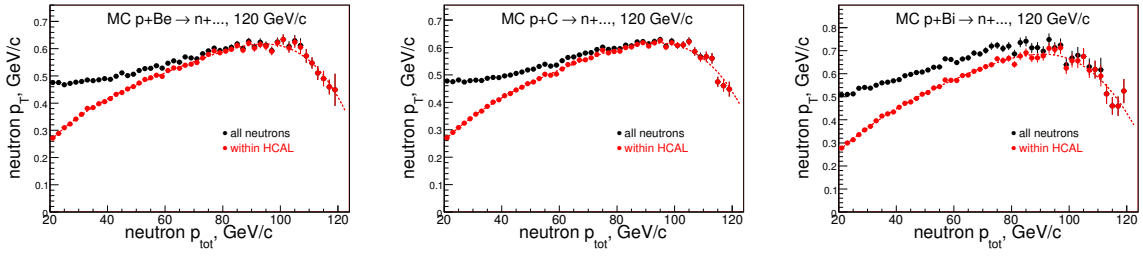

Figure 107: The neutron's mean p_T vs the total momentum distributions using p+Be (left), p+C (middle) and p+Bi (right) interactions at 120 GeV/c generated by Fluka. Plots illustrates two cases: all neutrons (black) and within HCAL (red).

17 Neutron Yields: data vs Monte Carlo

Table 30 illustrates the summary of data and Monte Carlo neutron production properties. Neutron fractions were calculated per single p+A interactions with $p_n > p_{min}$ requirements.

	N_{intr}(d)	F_n(data)	F_n(FL)	F_n(LA)	F_{non}(FL)
H_2-20	208786	0.0042±0.0002	0.014	-	0.502
H_2-58	2001048	0.0346±0.0005	0.111	0.109	0.450
Be-58	575635	0.0063±0.0004	0.104	-	0.154
C-58	1258291	0.0217±0.0005	0.102	0.099	0.156
Bi-58	1383354	0.0107±0.0003	0.066	0.047	0.091
U-58	1426534	0.0180±0.0003	0.067	-	0.094
H_2-84	2710439	0.0594±0.0003	0.162	-	0.438
Be-120	607457	0.0874±0.0003	0.201	-	0.151
C-120	319103	0.0966±0.0005	0.201	0.095	0.153
Bi-120	587048	0.0582±0.0002	0.156	0.042	0.105

Table 30: Summary of data and Monte Carlo neutron production properties. Neutron fractions were calculated per single p+A interactions with $p_n > p_{min}$ requirements.

18 Study of MC neutron losses in setup material

Figure 108 illustrates the primary neutron production and interaction Z positions with the setup material, the resulting spectrum in front face of EMCAL and neutron surviving probability. The primary neutrons are from p+C at 58 GeV/c.

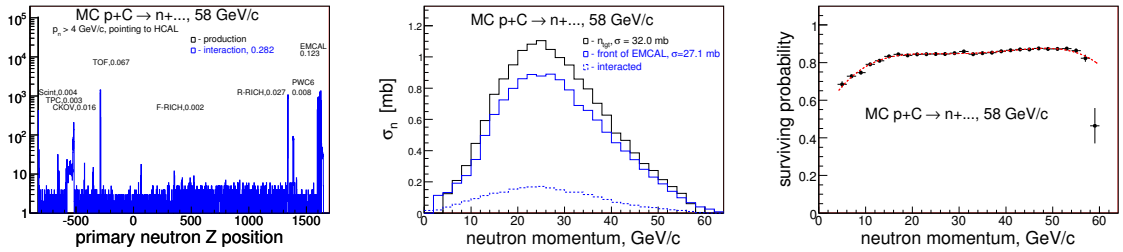

Figure 108: The primary neutron production/interaction Z positions with the setup material (left). Middle plot illustrates the primary neutron spectrum from the target and resulting spectrum in front face of EMCAL. Neutron surviving probability - right plot. The primary neutrons are from p+C at 58 GeV/c.

Figure 109 illustrates the primary neutron production and interaction Z positions with the setup material, the resulting primary neutron spectrum in front face of

EMCAL and neutron surviving probability. The primary neutrons are from p+Bi at 58 GeV/c.

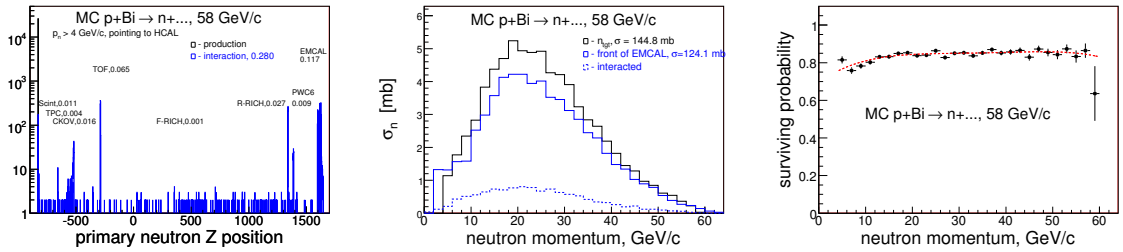

Figure 109: The primary neutron production/interaction Z positions with the setup material - left. Middle plot illustrates the primary neutron spectrum from the target and resulting spectrum in front face of EMCAL. Neutron surviving probability - right plot. The primary neutrons are from p+C at 58 GeV/c.

Figure 110 illustrates the primary neutron production and interaction Z positions with the setup material, the resulting primary neutron spectrum in front face of EMCAL and neutron surviving probability. The primary neutrons are from p+C at 120 GeV/c.

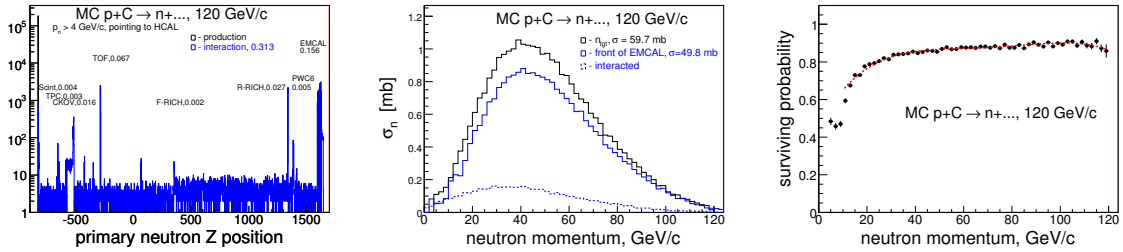

Figure 110: The primary neutron production/interaction Z positions with the setup material - left. Middle plot illustrates the primary neutron spectrum from the target and resulting spectrum in front face of EMCAL. Neutron surviving probability - right plot. The primary neutrons are from p+C at 120 GeV/c.

Figure 111 illustrates the primary neutron production and interaction Z positions with the setup material, the resulting primary neutron spectrum in front face of EMCAL and neutron surviving probability. The primary neutrons are from p+Bi at 120 GeV/c.

19 Hadron calorimeter's solid angle

The solid angle, Ω, subtended at the center of a sphere of radius r by a portion of the surface S of the sphere is defined as: $\Omega = \frac{S}{r^2}$, where S is area of calorimeter in

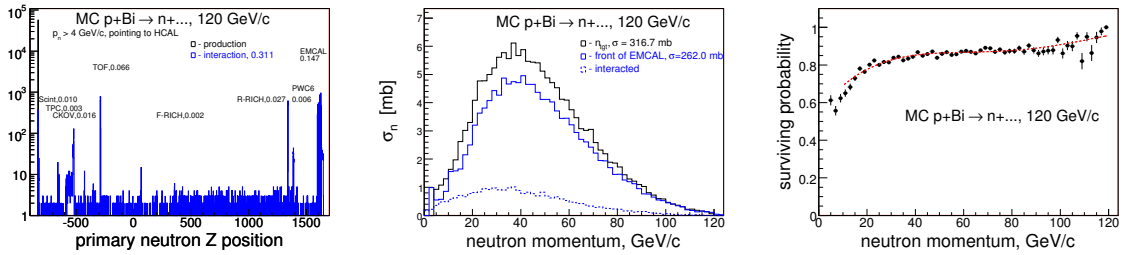

Figure 111: The primary neutron production/interaction Z positions with the setup material - left. Middle plot illustrates the primary neutron spectrum from the target and resulting spectrum in front face of EMCAL. Neutron surviving probability - right plot. The primary neutrons are from p+C at 120 GeV/c.

m^2, r = Z is a distance from the reconstructed interaction vertex up to HCAL front surface in m.

Calorimeter's designed surface area size is equal to S = 0.989 × 0.979 = 0.968 m^2. An active surface area size can be estimated by Monte Carlo.

At this moment the Monte Carlo information about the neutron passage simulation and it's position at HCAL front surface is not available. But we have the projected positions. We applied following cuts to the neutron sample in Monte Carlo:

- select events when there only single high momentum neutron being generated, $p_n > p_{min}$
- require that the high momentum neutron directed toward downstream of the beam line, within ±80 cm from beam line in both views at Z equal to the the Z of HCAL front face. This sample represents the denominator
- calculate p_n(true) / p_n(HCAL) variable, where p_n(HCAL) is reconstructed neutron momentum according to the procedure same as in data
- select events when ratio value would be within 0.8-1.2 range. This sample represents the numerator
- make 2D Y-projection vs X-projection plot
- the edges of the 2D plot will tell what is the active calorimeter area size

Figure 112 shows the distributions of p_n(true)/p_n(HCAL) variable and the 2D X-Y-projection plot made using the p+C interactions at 58 GeV/c

Figure 113 shows X and Y projections for subsample shown on Fig. 112 (right plot).

Figure 114 shows the neutron reconstruction rates depending on X and Y projections.

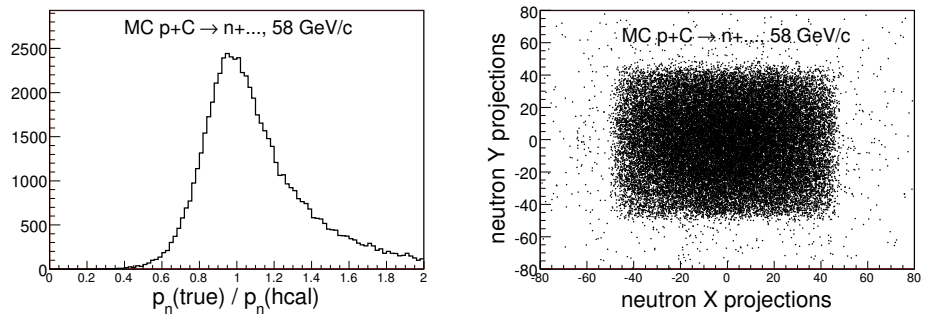

Figure 112: The distributions of p_n(true)/p_n(HCAL) variable (left) and the 2D X-Y-projection plot (right) made using the p+C interactions at 58 GeV/c

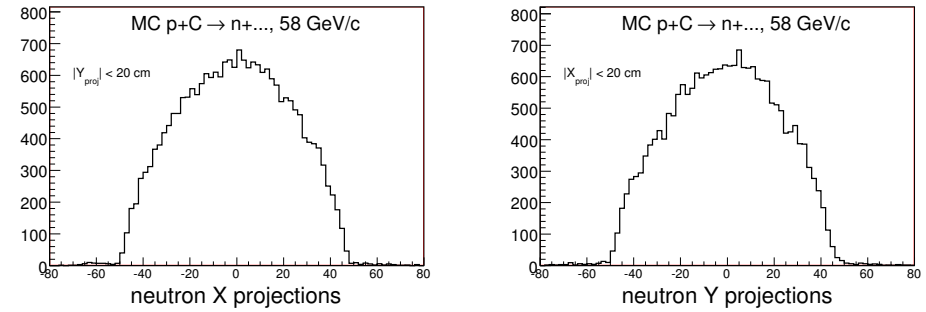

Figure 113: The X and Y projections for subsample shown on Fig. 112 (right plot).

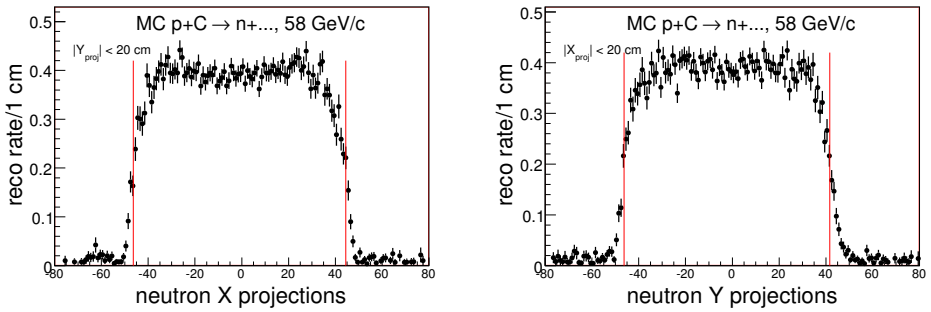

Figure 114: The neutron reconstruction rates depending on X and Y projections. The rate is a ratio of what shown on Fig. 113 over the generated sample.

The vertical red lines in Fig. 114 illustrates defined by the fit the X (or Y) position where the neutron rate reached 1/2 of it's maximum value. The active edges of the hadron calorimeter were found as: -46.39 cm and 44.47 cm in X view and -46.27 cm and 41.62 cm in Y view, respectively. Thus, the active surface area is equal to 0.9086×0.8789 = 0.79857 m^2. The uncertainty in the surface area value is ±0.001 m^2 (or 0.0005 m in single estimate). Then, the expected solid angle value for the thin target would be: $\Omega = 0.7986 / 24.76^2 = 0.001302 \pm 0.000002$ (syst) steradians.

What is an angular coverage of the calorimeter? Our calorimeter front surface is a rectangular. An equivalent radius value can be found through the formula: $S = \pi r^2$, then $r = \sqrt{\frac{S}{\pi}}$. The equivalent radius would be $r = \sqrt{\frac{0.7986}{3.141593}} = 0.5047$ m. Thus, the angular coverage: $\sin\theta = \theta = \frac{0.5047}{24.76} = 0.0204$ radians, or 20.4 mrad.

Figure 115 shows the solid angle value distributions for p+p, p+C and p+Bi interactions at 58 GeV/c

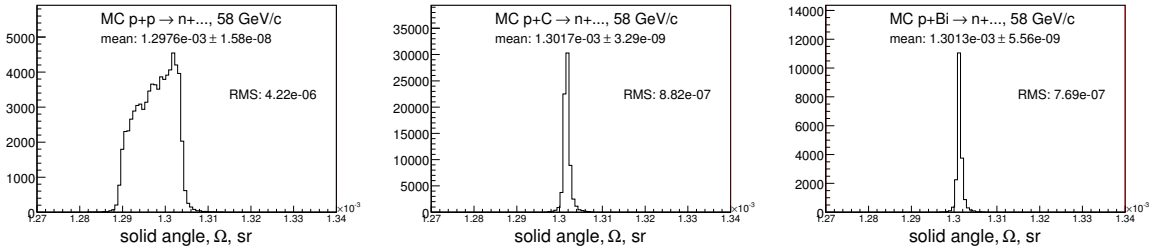

Figure 115: The solid angle value distributions for p+p, p+C and p+Bi interactions at 58 GeV/c.

Figure 116 shows the solid angle value distributions for p+p at 84 GeV/c and for p+C and p+Bi interactions at 120 GeV/c

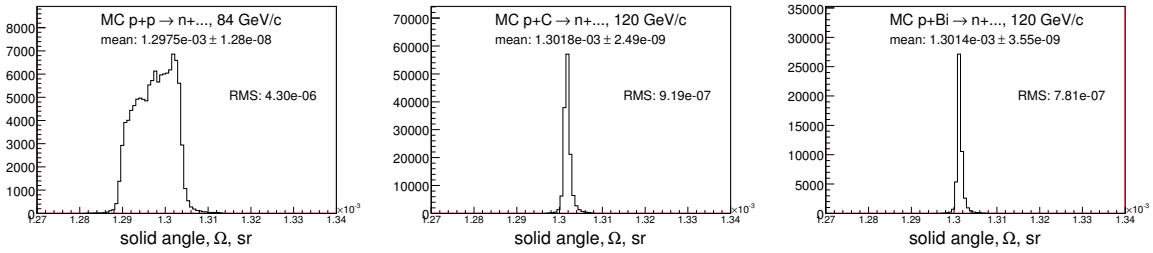

Figure 116: The solid angle value distributions for p+p at 84 GeV/c and p+C and p+Bi interactions at 120 GeV/c.

Table 31 illustrates the summary of the solid angle values calculated for the active and designed front surface area of the hadron calorimeter.

	$\Omega_{active}\times10^3$,sr	$RMS_\Omega\times10^6$	$\Omega_{design}\times10^3$,sr	$\Delta\Omega$(assign)
H_2-20	1.2986	3.89	1.5742	0.003
H_2-58	1.2976	4.22	1.5729	0.003
Be-58	1.3014	0.82	1.5775	0.002
C-58	1.3017	0.88	1.5779	0.002
Bi-58	1.3013	0.77	1.5774	0.002
U-58	1.3014	0.75	1.5775	0.002
H_2-84	1.2975	4.30	1.5728	0.003
Be-120	1.3015	0.92	1.5777	0.002
C-120	1.3018	0.92	1.5781	0.002
Bi-120	1.3014	0.78	1.5775	0.002

Table 31: Summary of Ω values depending on target. Ω_{active} - an active value of the solid angle, RMS_Ω - variations of the solid angle due to of the target length, Ω_{design} the solid angle according to the calorimeter design and $\Delta\Omega$(assign) is assigned systematic uncertainty.

20 Calorimeter Acceptance

The geometrical acceptance of the calorimeter is certain. However, as was shown on previous section that the neutron angular distribution is model dependent. Due to of this fact the calorimeter acceptance would depend on what model in use. So, we used three Monte Carlo generators: FLUKA, MARS and LAQGSM [5, 6, 7] generators to see for the possible variations in acceptance.

Figure 117 shows the calorimeter acceptance as the function of the neutron momentum for pp, pBe and pC at 58 GeV/c

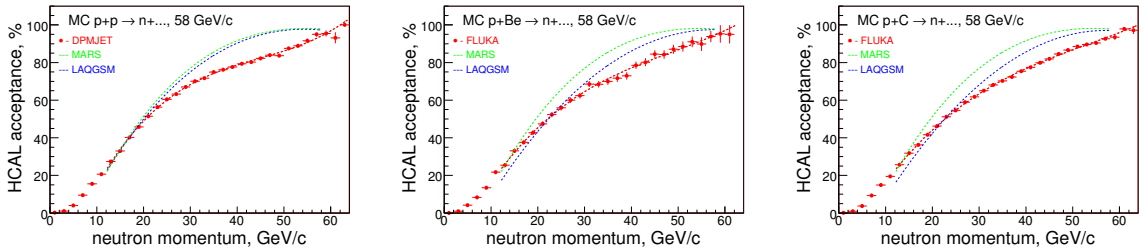

Figure 117: Calorimeter acceptances as the function of the neutron momentum for pp, pBe and pC at 58 GeV/c.

Figure 118 shows the calorimeter acceptance as the function of the neutron momentum for pBi, pU and pp at 58 and 84 GeV/c.

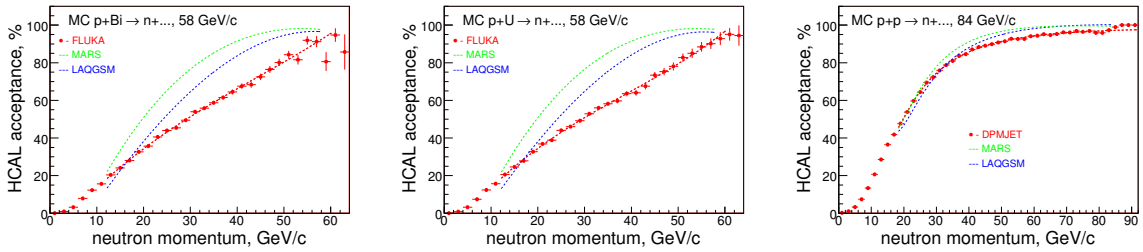

Figure 118: Calorimeter acceptances as the function of the neutron momentum for pBi, pU and pp at 58 and 84 GeV/c.

Figure 119 shows the calorimeter acceptance as the function of the neutron momentum for pBe, pC and pBi at 120 GeV/c.

21 Effect of Calorimeter Resolution to Neutron Spectrum

The calorimeter resolution, σ, as a function of the incident proton beam momenta was found to be [1]:

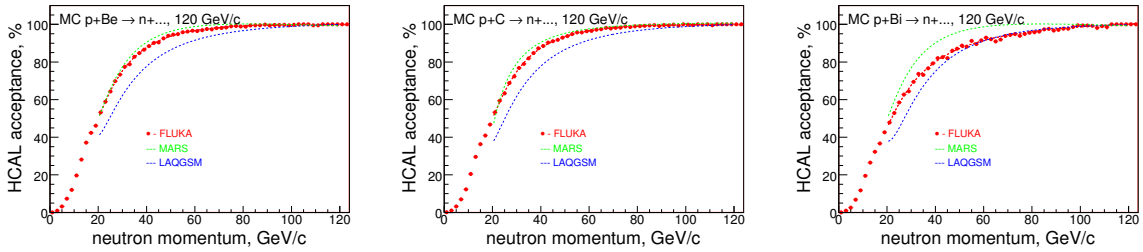

Figure 119: Calorimeter acceptances as the function of the neutron momentum for pBe, pC and pBi at 120 GeV/c.

$$\sigma = \sqrt{0.554^2 E + 0.026^2 E^2}$$

where E is proton beam energy in GeV. One can assume that the calorimeter performance for neutrons would be pretty match similar to protons. We see also a small nonlinearity there, which can be taken in account by using a second order polynomial function:

$$\sigma = \sqrt{1.98^2 + 0.2948^2 E_{ts} + 0.0558^2 E_{ts}^2}$$

In this formula E_{ts} represents the true summed neutron momentum pointing to HCAL fiducial. An actual smearing value for given event has been derived as a random number from Gaussian distribution, where σ used as an input parameter to Gauss. Thus, for each MC event we have two neutron energies: E_{ts} and $E_{ts} \pm \Delta_E$. Figure 120 illustrates the calorimeter resolution vs the proton beam energy and what used to smear neutron energy in MC.

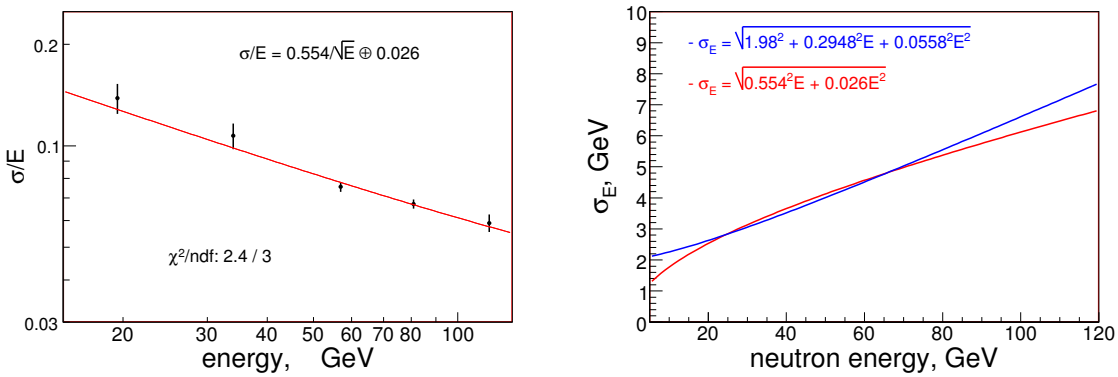

Figure 120: The hadron calorimeter energy resolution, σ/E, vs the incident proton energy (left) and how neutron energy resolution was simulated in MC (right - blue curve).

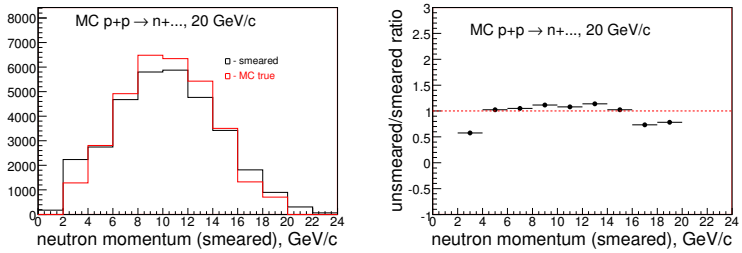

Figure 121: The effect of calorimeter resolution to the neutron spectrum using p+p interactions at 20 GeV/c: smeared and unsmeared summed neutron spectra (left) and the unsmeared over smeared ratio (right).

Figure 121 illustrates the effect of calorimeter resolution to the neutron spectrum using p+p interactions at 20 GeV/c.

Figure 122 illustrates the effect of calorimeter resolution to the neutron spectrum using p+p interactions at 58 GeV/c.

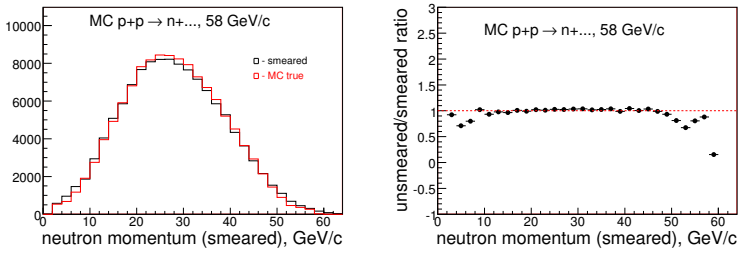

Figure 122: The effect of calorimeter resolution to the neutron spectrum using p+p interactions at 58 GeV/c: smeared and unsmeared summed neutron spectra (left) and the unsmeared over smeared ratio (right).

Figure 123 illustrates the effect of calorimeter resolution to the neutron spectrum using p+Be interactions at 58 GeV/c.

Figure 124 illustrates the effect of calorimeter resolution to the neutron spectrum using p+C interactions at 58 GeV/c.

Figure 125 illustrates the effect of calorimeter resolution to the neutron spectrum using p+Bi interactions at 58 GeV/c.

Figure 126 illustrates the effect of calorimeter resolution to the neutron spectrum using p+U interactions at 58 GeV/c.

Figure 127 illustrates the effect of calorimeter resolution to the neutron spectrum using p+p interactions at 84 GeV/c.

Figure 128 illustrates the effect of calorimeter resolution to the neutron spectrum using p+Be interactions at 120 GeV/c.

Figure 129 illustrates the effect of calorimeter resolution to the neutron spectrum using p+C interactions at 120 GeV/c.

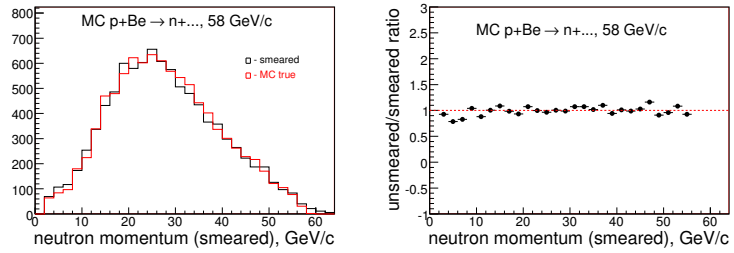

Figure 123: The effect of calorimeter resolution to the neutron spectrum using p+Be interactions at 58 GeV/c: smeared and unsmeared summed neutron spectra (left) and the unsmeared over smeared ratio (right).

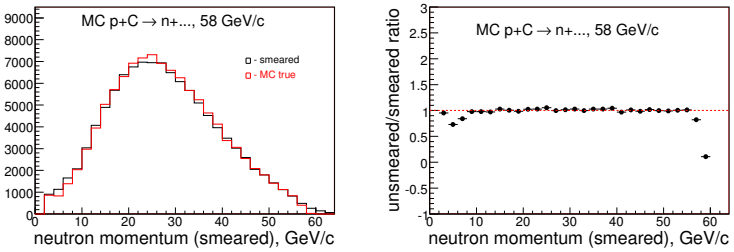

Figure 124: The effect of calorimeter resolution to the neutron spectrum using p+C interactions at 58 GeV/c: smeared and unsmeared summed neutron spectra (left) and the unsmeared over smeared ratio (right).

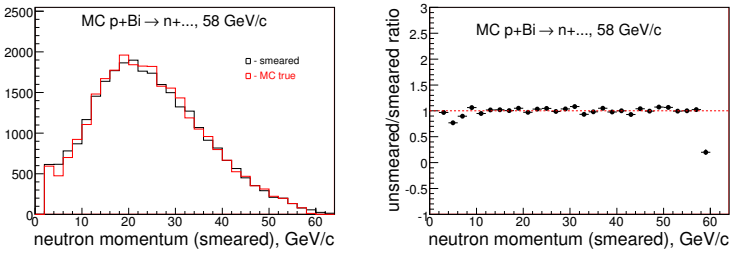

Figure 125: The effect of calorimeter resolution to the neutron spectrum using p+Bi interactions at 58 GeV/c: smeared and unsmeared summed neutron spectra (left) and the unsmeared over smeared ratio (right).

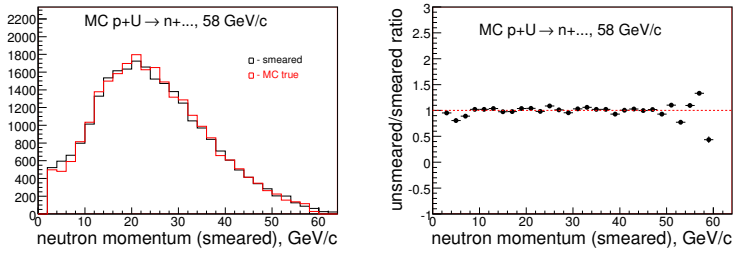

Figure 126: The effect of calorimeter resolution to the neutron spectrum using p+U interactions at 58 GeV/c: smeared and unsmeared summed neutron spectra (left) and the unsmeared over smeared ratio (right).

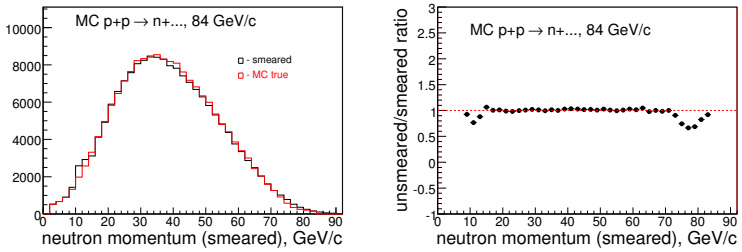

Figure 127: The effect of calorimeter resolution to the neutron spectrum using p+p interactions at 84 GeV/c: smeared and unsmeared summed neutron spectra (left) and the unsmeared over smeared ratio (right).

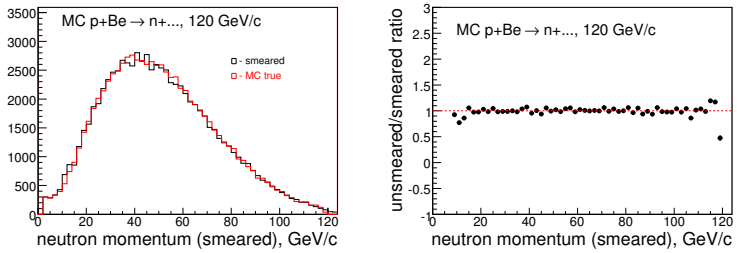

Figure 128: The effect of calorimeter resolution to the neutron spectrum using p+Be interactions at 120 GeV/c: smeared and unsmeared summed neutron spectra (left) and the unsmeared over smeared ratio (right).

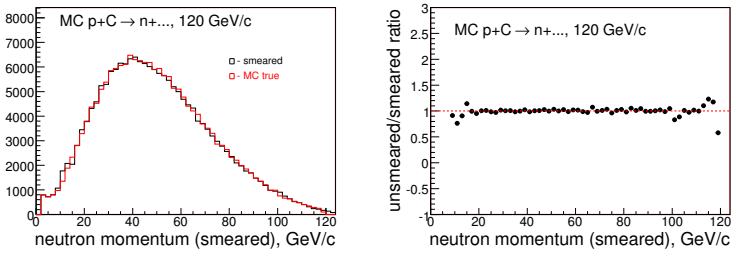

Figure 129: The effect of calorimeter resolution to the neutron spectrum using p+C interactions at 120 GeV/c: smeared and unsmeared summed neutron spectra (left) and the unsmeared over smeared ratio (right).

Figure 130 illustrates the effect of calorimeter resolution to the neutron spectrum using p+Bi interactions at 120 GeV/c.

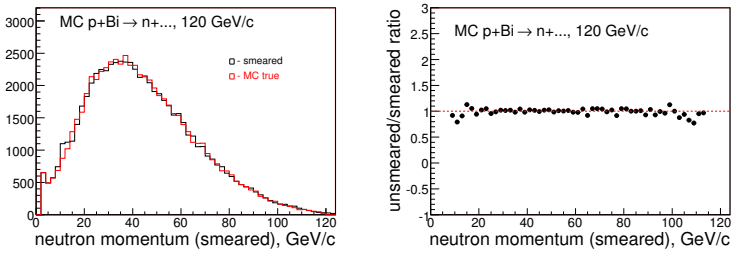

Figure 130: The effect of calorimeter resolution to the neutron spectrum using p+Bi interactions at 120 GeV/c: smeared and unsmeared summed neutron spectra (left) and the unsmeared over smeared ratio (right).

22 Neutron Selection Efficiency

On previous subsection we discussed the HCAL acceptance using Fluka and LAQGSM neutron generators. However, in analysis of the real data we applied the Z_{vtx} and Δp_T and other cuts to select neutrons. Below we will present the neutron reconstruction efficiency.

Figure 131 shows the neutron reconstruction efficiency as the function of the neutron momentum for p+p interactions at 20, 58 and 84 GeV/c.

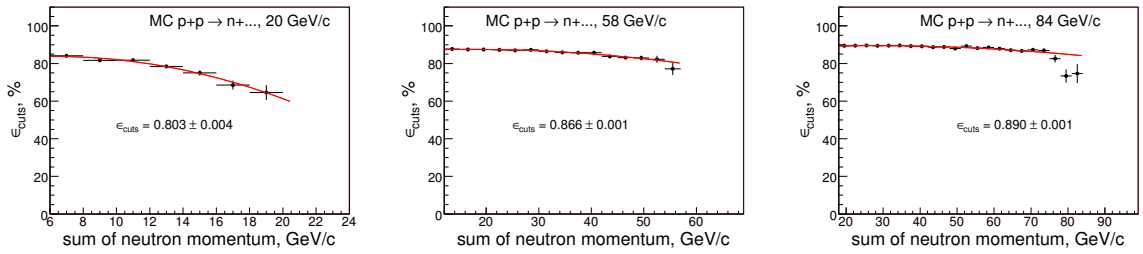

Figure 131: The neutron reconstruction efficiency as the function of the summed neutron momentum for p+p interactions at 20 GeV/c (left), 58 GeV/c (middle) and 84 GeV/c (right), respectively.

Figure 132 shows the neutron reconstruction efficiency as the function of the neutron momentum for p+Be and p+C interactions at 58 GeV/c

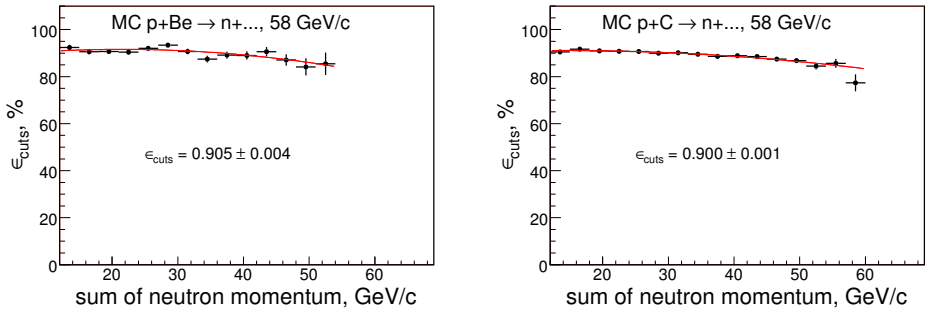

Figure 132: The neutron reconstruction efficiency as the function of the summed neutron momentum for p+Be (left) and p+C (right) interactions at 58 GeV/c.

Figure 133 shows the neutron reconstruction efficiency as the function of the neutron momentum for p+Bi and p+U interactions at 58 GeV/c

Figure 134 shows the neutron reconstruction efficiency as the function of the neutron momentum for p+Be, p+C and p+Bi interactions at 120 GeV/c

Monte Carlo the neutron reconstruction efficiency for the various targets and beam momenta are summarized in Table 32.

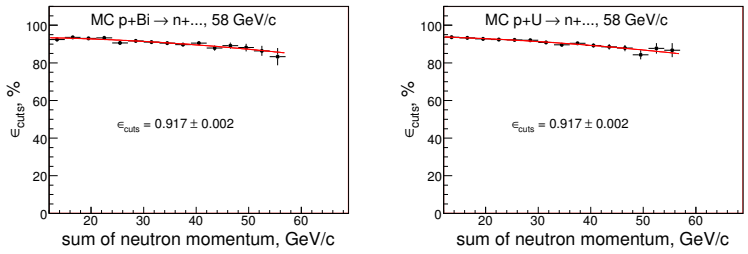

Figure 133: The neutron reconstruction efficiency as the function of the summed neutron momentum for p+Bi (left) and p+U (right) interactions at 58 GeV/c.

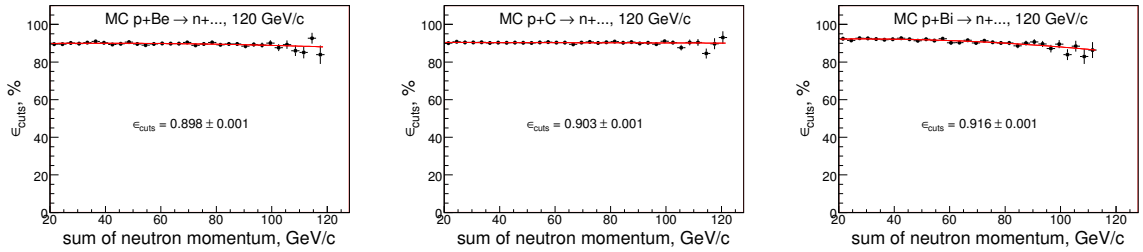

Figure 134: The neutron reconstruction efficiency as the function of the summed neutron momentum for p+Be (left), p+C (middle) and p+Bi (right) interactions at 120 GeV/c

p_{beam}	ϵ_{cuts}
H_2-20 GeV/c	0.801±0.004
H_2-58 GeV/c	0.866±0.001
Be-58 GeV/c	0.905±0.004
C-58 GeV/c	0.900±0.001
Bi-58 GeV/c	0.917±0.002
U-58 GeV/c	0.917±0.002
H_2-84 GeV/c	0.890±0.001
Be-120 GeV/c	0.898±0.001
C-120 GeV/c	0.903±0.001
Bi-120 GeV/c	0.916±0.001

Table 32: Monte Carlo the neutron selection efficiency for the various targets and beam momenta. The efficiencies were calculated with FLUKA.

23 Generated vs MC HCAL neutron spectrum

Below we will compare the generated vs MC HCAL simulated neutron spectrum. MC HCAL responses represents events, when the generated neutron is present.

Figure 135 shows the generated vs MC reconstructed neutron spectrum for p+A interactions at 58 GeV/c.

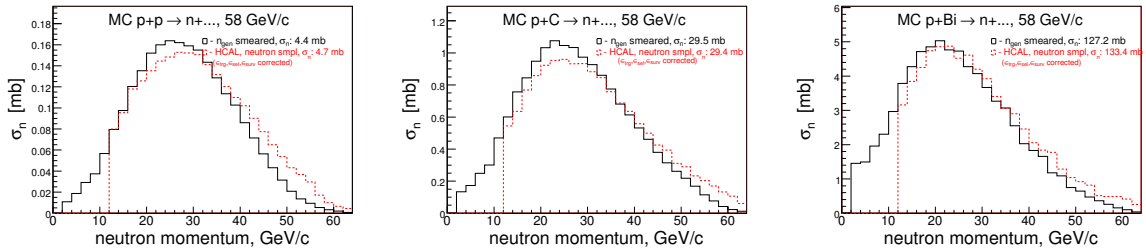

Figure 135: Comparison of the generated vs MC reconstructed neutron spectrum for p+A interactions at 58 GeV/c. Reconstructed spectrum derived from the HCAL responses for the MC events, when the generated neutron is present. It corrected for the trigger and reconstruction efficiencies, as well as for what was lost due to the interactions with setup material.

Figure 136 shows the generated vs MC reconstructed neutron spectrum for p+A interactions at 84 and 120 GeV/c.

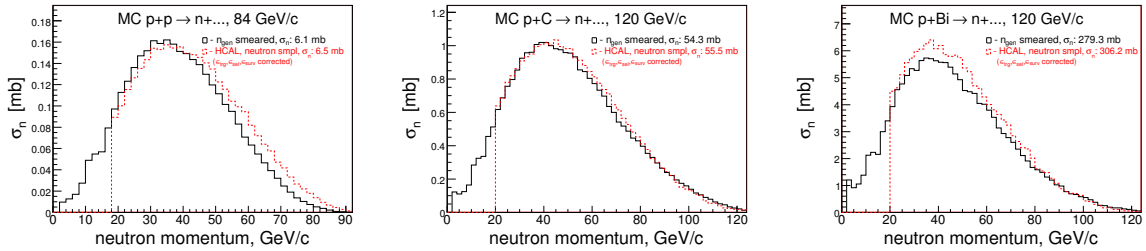

Figure 136: Comparison of the generated vs MC reconstructed neutron spectrum for p+A interactions at 84 and 120 GeV/c. Reconstructed spectrum derived from the HCAL responses for the MC events, when the generated neutron is present. It corrected for the trigger and reconstruction efficiencies, as well as for what was lost due to the interactions with setup material.

Above plots illustrates an excess in high and deficit in low neutron spectrum. Reason for this is due to of uncertainties in the trigger efficiency.

Figure 137 shows the generated vs MC reconstructed neutron spectrum for p+A interactions at 58 GeV/c when an additional trigger corrections was applied to HCAL responses.

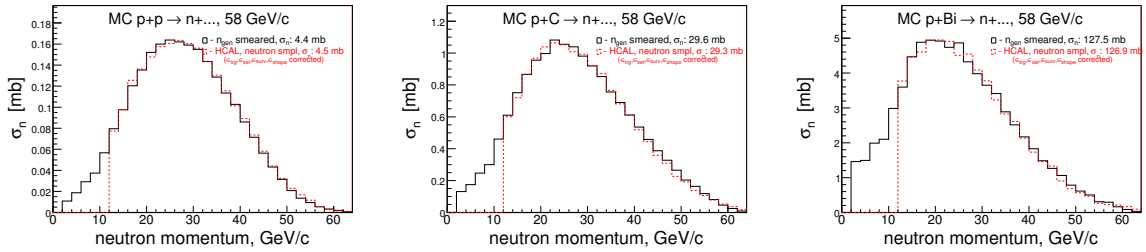

Figure 137: Comparison of the generated vs MC reconstructed neutron spectrum for p+A interactions at 58 GeV/c when an additional trigger corrections was applied. Reconstructed spectrum derived from the HCAL responses for the MC events, when the generated neutron is present.

Figure 138 shows the generated vs MC reconstructed neutron spectrum for p+A interactions at 84 and 120 GeV/c when an additional trigger corrections was applied to HCAL responses.

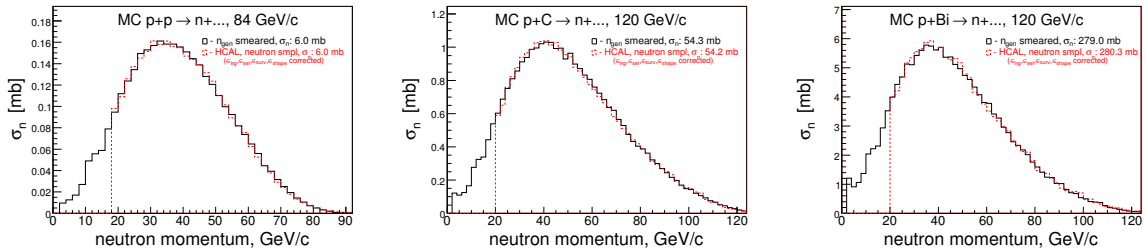

Figure 138: Comparison of the generated vs MC reconstructed neutron spectrum for p+A interactions at 84 and 120 GeV/c when an additional trigger corrections was applied. Reconstructed spectrum derived from the HCAL responses for the MC events, when the generated neutron is present.

Figure 139 shows the generated vs MC reconstructed neutron spectrum for p+A interactions at 58 GeV/c. HCAL responses are not corrected for the trigger efficiency.

Figure 140 shows the generated vs MC reconstructed neutron spectrum for p+A interactions at 84 and 120 GeV/c. HCAL responses are not corrected for the trigger efficiency.

Figure 141 shows the generated vs MC reconstructed neutron spectrum for p+A interactions at 58 GeV/c when HCAL responses are not corrected for the trigger efficiency.

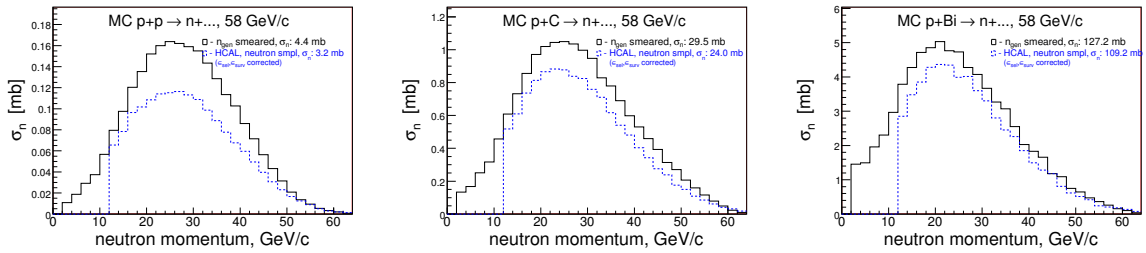

Figure 139: Comparison of the generated vs MC reconstructed neutron spectrum for p+A interactions at 58 GeV/c. Reconstructed result is based on HCAL responses, which was corrected for the reconstruction efficiency and for the neutron losses in the setup material.

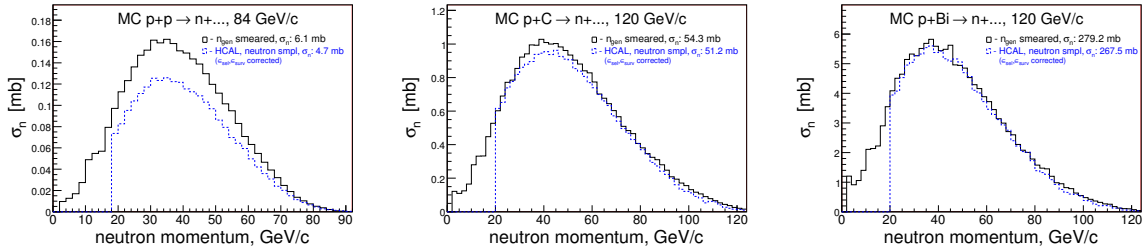

Figure 140: Comparison of the generated vs MC reconstructed neutron spectrum for p+A interactions at 84 and 120 GeV/c. Reconstructed result is based on HCAL responses, which was corrected for the reconstruction efficiency and for the neutron losses in the setup material.

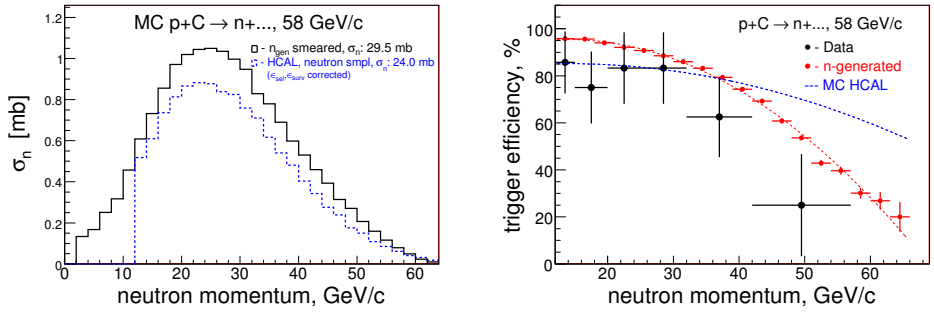

Figure 141: Left: Comparison of the generated vs MC reconstructed neutron spectrum for p+A interactions at 58 GeV/c. Reconstructed result is based on HCAL responses, which was corrected for the reconstruction efficiency and for the neutron losses in the setup material. Right: the trigger efficiency, where the blue dashed curve represents the trigger efficiency calculated as a ratio of blue over black from the left plot.

24 Neutron Backgrounds

The background can be estimated using the total MC neutron candidates, which was calculated same way as in data derived from whole MC sample. This sample consist of two subsamples: background and true neutrons. Second sample (the true neutrons) can be estimated by appling an additional requirement that the true neutron were generated. The difference between the total neutron candidates and candidates where generated neutron present is the background.

Figure 142 shows the reconstructed neutron candidates which were derived same way as in data for two conditions (left) and the predicted backgrounds (right) using pp interactions at 58 GeV/c

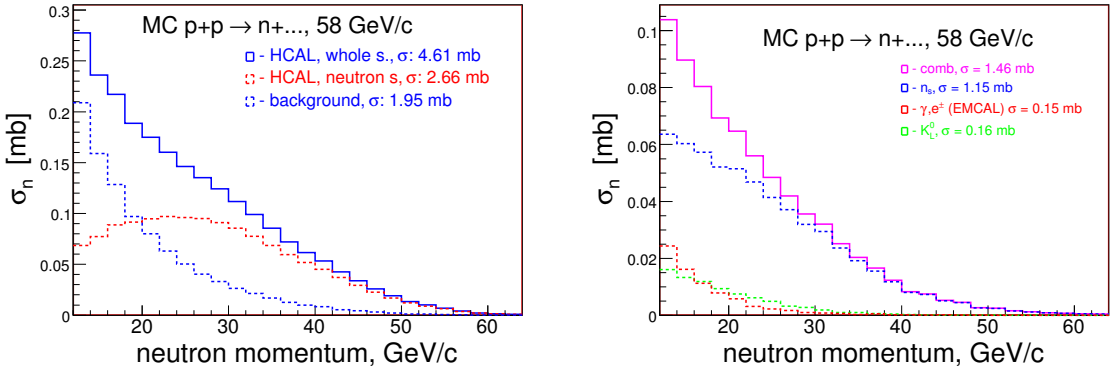

Figure 142: MC neutron candidates distributions vs the neutron momentum for pp interactions at 58 GeV/c. Left: the reconstructed neutron candidates using whole MC sample (solid blue) and those MC events when the generated neutron present (dashed red). Dashed blue - difference. Right: predicted backgrounds in front of HCAL from different sources.

Figure 143 shows the reconstructed neutron candidates which were derived same way as in data for two conditions (left) and the predicted backgrounds (right) using pBe interactions at 58 GeV/c

Figure 144 shows the reconstructed neutron candidates which were derived same way as in data for two conditions (left) and the predicted backgrounds (right) using pC interactions at 58 GeV/c.

Figure 145 shows the reconstructed neutron candidates which were derived same way as in data for two conditions (left) and the predicted backgrounds (right) using pBi interactions at 58 GeV/c.

Figure 146 shows the reconstructed neutron candidates which were derived same way as in data for two conditions (left) and the predicted backgrounds (right) using pU interactions at 58 GeV/c.

Figure 147 shows the reconstructed neutron candidates which were derived same way as in data for two conditions (left) and the predicted backgrounds (right) using

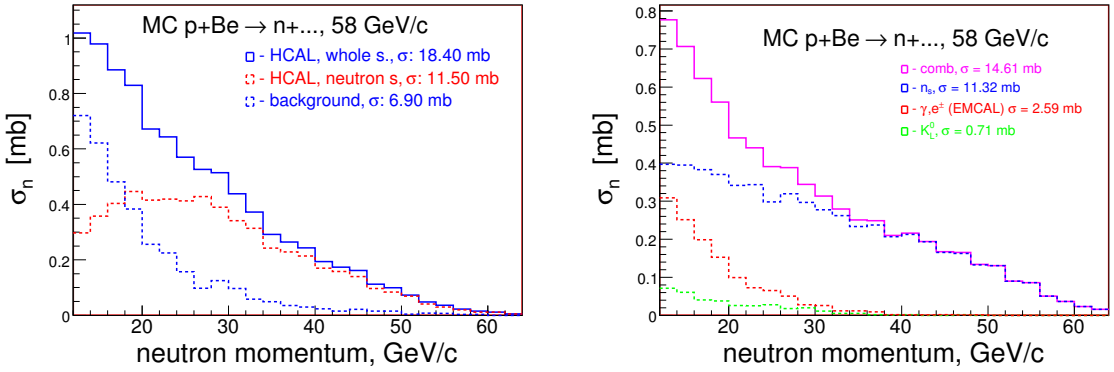

Figure 143: MC neutron candidates distributions vs the neutron momentum for pBe interactions at 58 GeV/c. Left: the reconstructed neutron candidates using whole MC sample (solid blue) and those MC events when the generated neutron present (dashed red). Dashed blue - difference. Right: predicted backgrounds in front of HCAL from different sources.

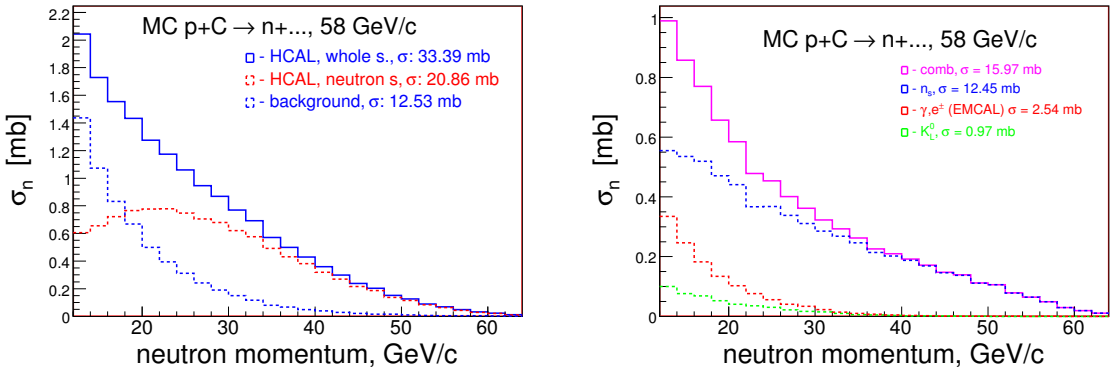

Figure 144: MC neutron candidates distributions vs the neutron momentum for pC interactions at 58 GeV/c. Left: the reconstructed neutron candidates using whole MC sample (solid blue) and those MC events when the generated neutron present (dashed red). Dashed blue - difference. Right: predicted backgrounds in front of HCAL from different sources.

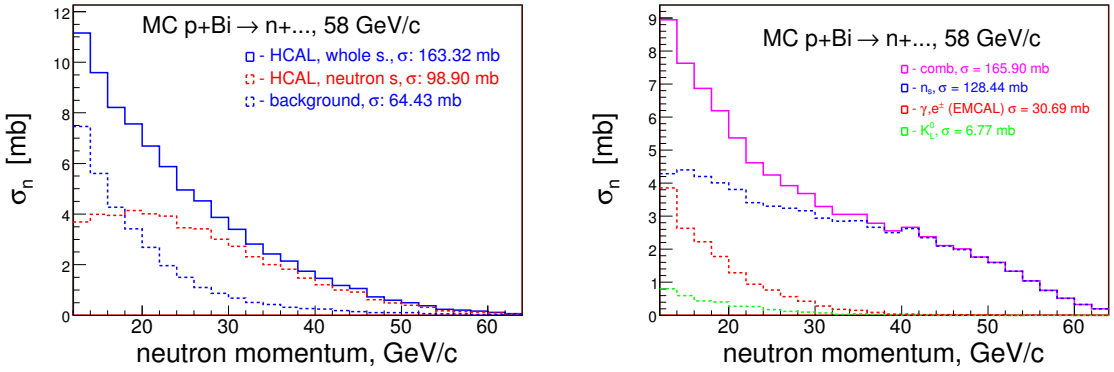

Figure 145: MC neutron candidates distributions vs the neutron momentum for pBi interactions at 58 GeV/c. Left: the reconstructed neutron candidates using whole MC sample (solid blue) and those MC events when the generated neutron present (dashed red). Dashed blue - difference. Right: predicted backgrounds in front of HCAL from different sources.

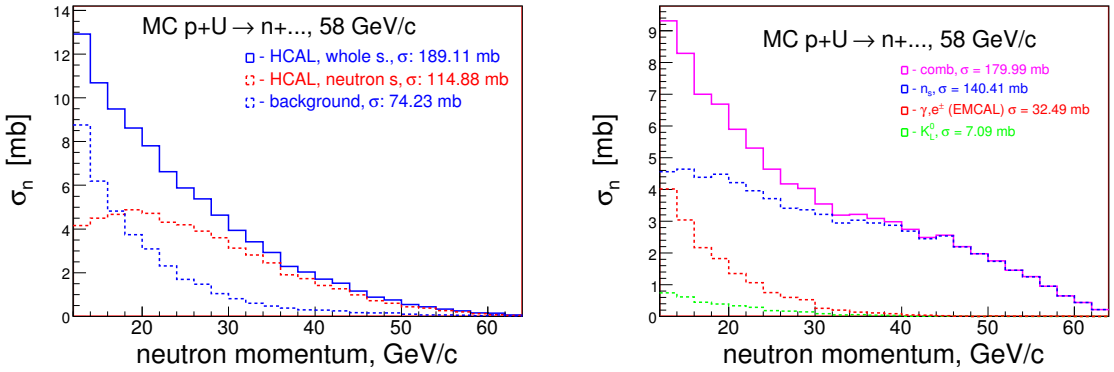

Figure 146: MC neutron candidates distributions vs the neutron momentum for pU interactions at 58 GeV/c. Left: the reconstructed neutron candidates using whole MC sample (solid blue) and those MC events when the generated neutron present (dashed red). Dashed blue - difference. Right: predicted backgrounds in front of HCAL from different sources.

pp interactions at 84 GeV/c

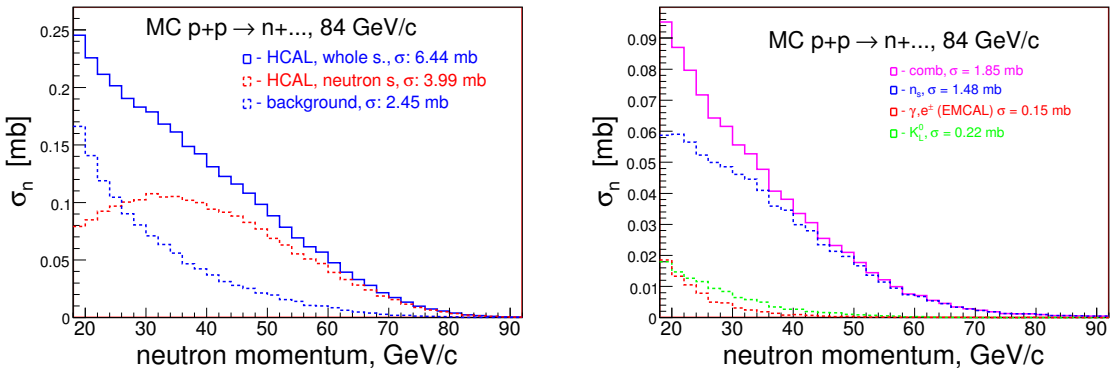

Figure 147: MC neutron candidates distributions vs the neutron momentum for pp interactions at 84 GeV/c. Left: the reconstructed neutron candidates using whole MC sample (solid blue) and those MC events when the generated neutron present (dashed red). Dashed blue - difference. Right: predicted backgrounds in front of HCAL from different sources.

Figure 148 shows the reconstructed neutron candidates which were derived same way as in data for two conditions (left) and the predicted backgrounds (right) using pBe interactions at 120 GeV/c

Figure 149 shows the reconstructed neutron candidates which were derived same way as in data for two conditions (left) and the predicted backgrounds (right) using pC interactions at 120 GeV/c.

Figure 150 shows the reconstructed neutron candidates which were derived same way as in data for two conditions (left) and the predicted backgrounds (right) using pBi interactions at 120 GeV/c.

Backgrounds are summarized in Table 33.

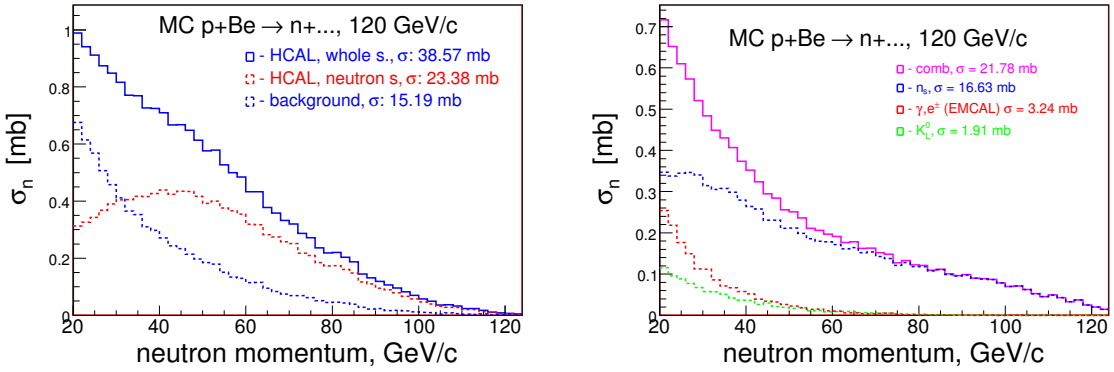

Figure 148: MC neutron candidates distributions vs the neutron momentum for pBe interactions at 120 GeV/c. Left: the reconstructed neutron candidates using whole MC sample (solid blue) and those MC events when the generated neutron present (dashed red). Dashed blue - difference. Right: predicted backgrounds in front of HCAL from different sources.

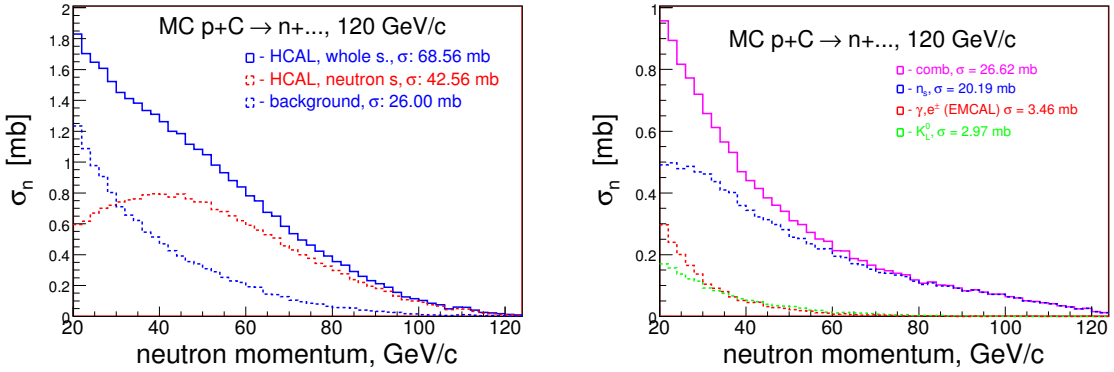

Figure 149: MC neutron candidates distributions vs the neutron momentum for pC interactions at 120 GeV/c. Left: the reconstructed neutron candidates using whole MC sample (solid blue) and those MC events when the generated neutron present (dashed red). Dashed blue - difference. Right: predicted backgrounds in front of HCAL from different sources.

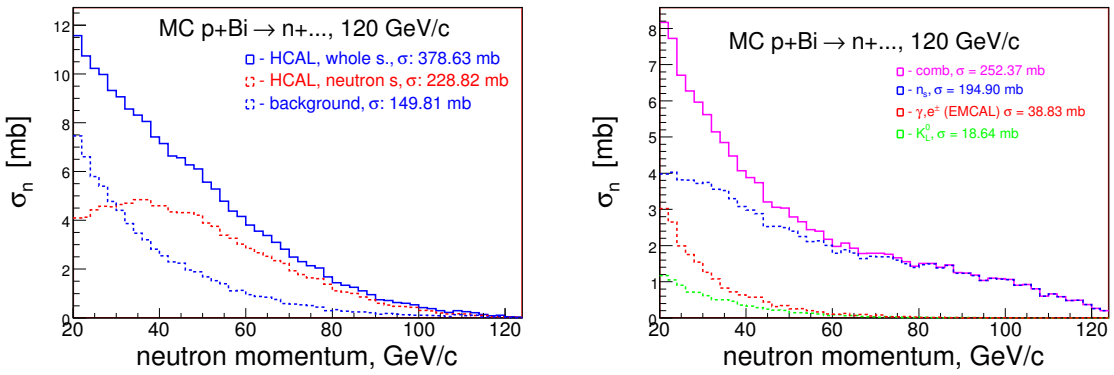

Figure 150: MC neutron candidates distributions vs the neutron momentum for pBi interactions at 120 GeV/c. Left: the reconstructed neutron candidates using whole MC sample (solid blue) and those MC events when the generated neutron present (dashed red). Dashed blue - difference. Right: predicted backgrounds in front of HCAL from different sources.

	σ_{HCAL}	$\sigma_{bkgr-HCAL}$	$\sigma_{bkgr-pred}$	Frac_{bkgr}
H_2-20	0.46	0.27	0.25	0.59
H_2-58	4.6	1.95	1.46	0.42
Be-58	18.4	6.9	14.6	0.37
C-58	33.4	12.5	16.0	0.37
Bi-58	163.3	64.4	165.9	0.39
U-58	189.1	74.2	180.0	0.39
H_2-84	6.4	2.5	2.0	0.39
Be-120	38.6	15.2	21.8	0.39
C-120	68.6	26.0	26.6	0.38
Bi-120	378.6	149.8	252.4	0.40

Table 33: Neutron backgrounds (in mb) and fraction.

25 Corrected Neutron Spectrum

One can see from Figure 52 that Monte Carlo and data uncorrected spectra shapes are identical. However, we see also that Monte Carlo generated neutron spectrum is quite differ from what was reconstructed using GEANT simulated HCAL responses for whole MC sample, see Figure 151.

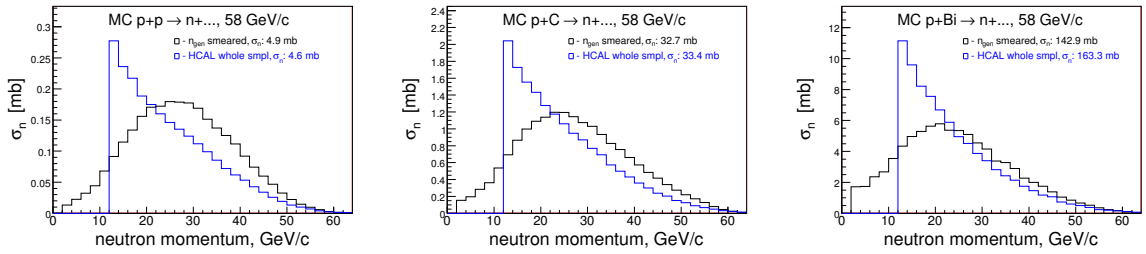

Figure 151: Neutron momentum distributions for the reconstructed neutron candidates using whole MC sample same way as in data (blue) and the generated true spectrum (black).

Why the shape of blue and black plots are differ?

- In region where the blue is below of black (p_n >23 GeV/c): it caused by the neutron losses due to of:
  - interactions with the setup material on way to HCAL
  - the trigger requirement, neutrons with momentum about of p_{beam} would have the low charged particles to pass the trigger.
  - selection requirements: Δp_T, Z_{vtx}...
- In region where the blue is above of black (p_n <23 GeV/c): because of backgrounds from different sources:
  - K^o_L produced in primary target with and/or without neutron
  - charged particles can interact with setup material and produce secondary neutrons and more K^o_L
  - if charged particle pointing to calorimeter but was not reconstructed or misreconstructed

One can assume that above mentioned processes, which makes the MC reconstructed spectrum to be much differ from what was generated, took place in data too. If this assumption is true, then we need to apply a specific correction which will bring the blue plot to the shape of the black one. Then, the similar correction need to apply for data too.

25.1 Correction procedure

The idea of the correction procedure is to calculate the ratio of the blue over the black spectra and get the fit parameters for it. Figure 152 shows how the ratio looks like for p+p interaction at 58 GeV/c

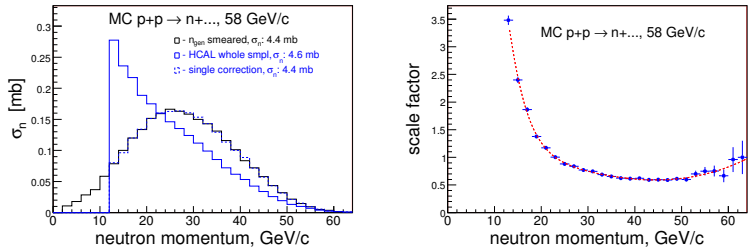

Figure 152: Left: the reconstructed neutron MC spectrum (solid blue) and the generated true spectrum (black) for p+p interactions at 58 GeV/c. Right: illustrates the ratio dependence vs the neutron momentum, where red dashed curve - fit function. The dashed blue on left plot illustrates how the solid blue spectrum would look like after the correction applied.

Figure 153 shows how the ratio looks like for p+Be interaction at 58 GeV/c

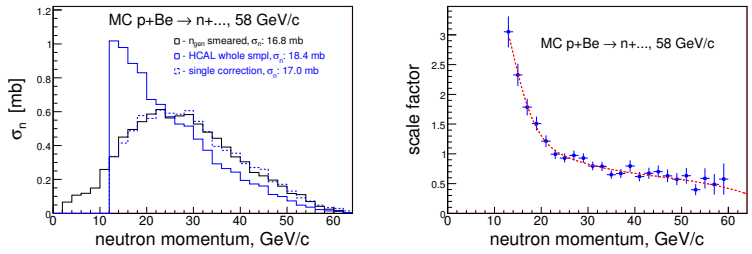

Figure 153: Left: the reconstructed neutron MC spectrum (solid blue) and the generated true spectrum (black) for p+Be interactions at 58 GeV/c. Right: illustrates the ratio dependence vs the neutron momentum, where red dashed curve - fit function. The dashed blue on left plot illustrates how the solid blue spectrum would look like after the correction applied.

Figure 154 shows how the ratio looks like for p+C interaction at 58 GeV/c
Figure 155 shows how the ratio looks like for p+Bi interaction at 58 GeV/c
Figure 156 shows how the ratio looks like for p+U interaction at 58 GeV/c
Figure 157 shows how the ratio looks like for p+p interaction at 84 GeV/c
Figure 158 shows how the ratio looks like for p+Be interaction at 120 GeV/c
Figure 159 shows how the ratio looks like for p+C interaction at 120 GeV/c
Figure 160 shows how the ratio looks like for p+Bi interaction at 120 GeV/c

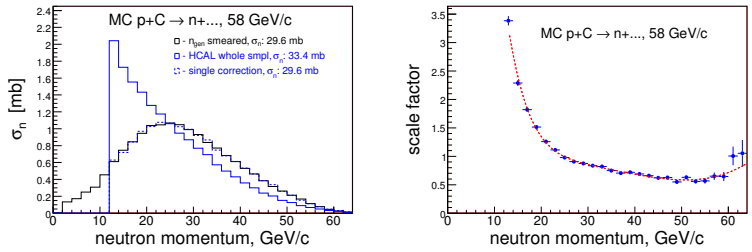

Figure 154: Left: the reconstructed neutron MC spectrum (solid blue) and the generated true spectrum (black) for p+C interactions at 58 GeV/c. Right: illustrates the ratio dependence vs the neutron momentum, where red dashed curve - fit function. The dashed blue on left plot illustrates how the solid blue spectrum would look like after the correction applied.

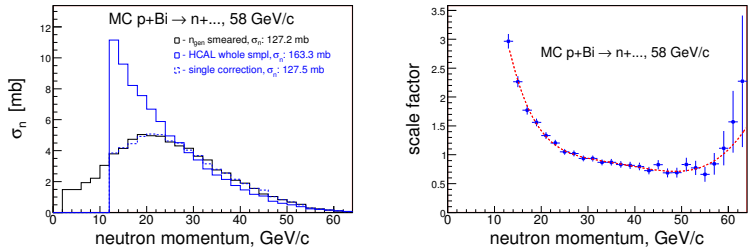

Figure 155: Left: the reconstructed neutron MC spectrum (solid blue) and the generated true spectrum (black) for p+Bi interactions at 58 GeV/c. Right: illustrates the ratio dependence vs the neutron momentum, where red dashed curve - fit function. The dashed blue on left plot illustrates how the solid blue spectrum would look like after the correction applied.

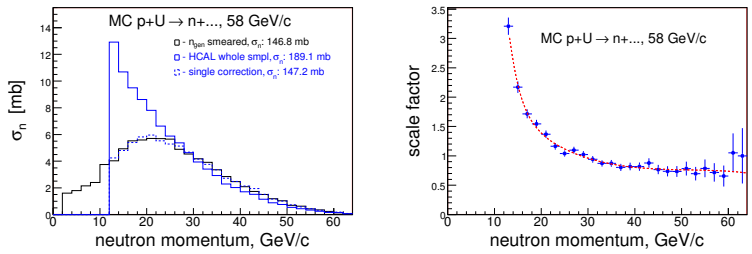

Figure 156: Left: the reconstructed neutron MC spectrum (solid blue) and the generated true spectrum (black) for p+U interactions at 58 GeV/c. Right: illustrates the ratio dependence vs the neutron momentum, where red dashed curve - fit function. The dashed blue on left plot illustrates how the solid blue spectrum would look like after the correction applied.

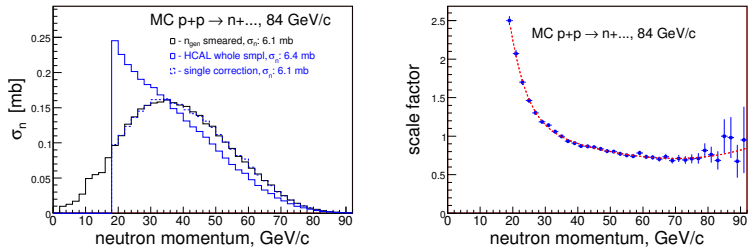

Figure 157: Left: the reconstructed neutron MC spectrum (solid blue) and the generated true spectrum (black) for p+p interactions at 84 GeV/c. Right: illustrates the ratio dependence vs the neutron momentum, where red dashed curve - fit function. The dashed blue on left plot illustrates how the solid blue spectrum would look like after the correction applied.

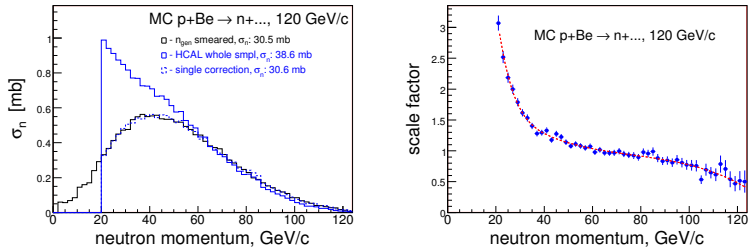

Figure 158: Left: the reconstructed neutron MC spectrum (solid blue) and the generated true spectrum (black) for p+Be interactions at 120 GeV/c. Right: illustrates the ratio dependence vs the neutron momentum, where red dashed curve - fit function. The dashed blue on left plot illustrates how the solid blue spectrum would look like after the correction applied.

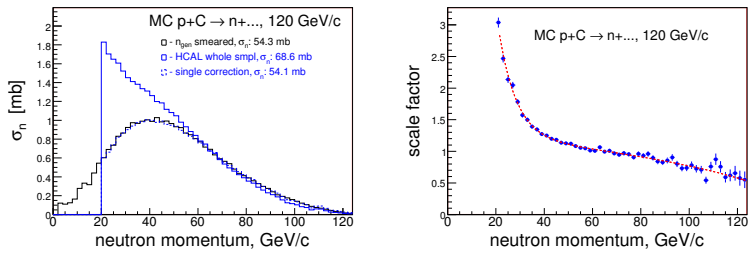

Figure 159: Left: the reconstructed neutron MC spectrum (solid blue) and the generated true spectrum (black) for p+C interactions at 120 GeV/c. Right: illustrates the ratio dependence vs the neutron momentum, where red dashed curve - fit function. The dashed blue on left plot illustrates how the solid blue spectrum would look like after the correction applied.

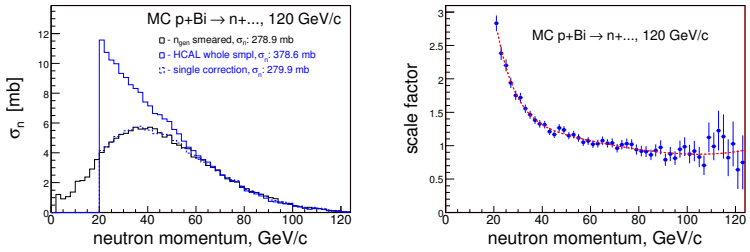

Figure 160: Left: the reconstructed neutron MC spectrum (solid blue) and the generated true spectrum (black) for p+Bi interactions at 120 GeV/c. Right: illustrates the ratio dependence vs the neutron momentum, where red dashed curve - fit function. The dashed blue on left plot illustrates how the solid blue spectrum would look like after the correction applied.

25.2 Corrected spectrum for data

Figure 161 shows the neutron spectra for data using p+p, p+Be and p+C interactions at 58 GeV GeV/c

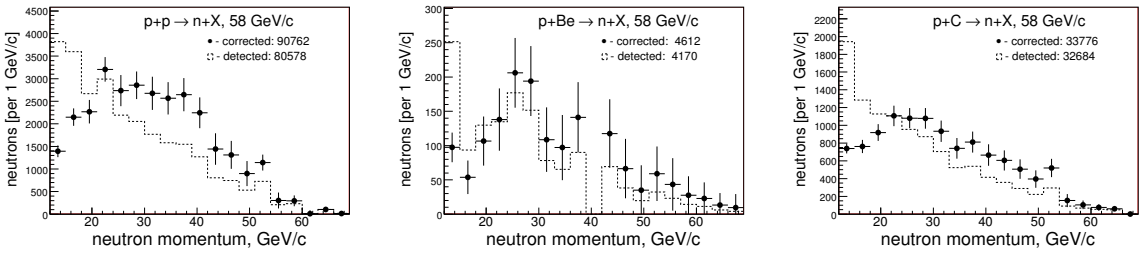

Figure 161: Neutron yields vs momentum for p+p (left), p+Be (middle) and p+C (right) interactions at 58 GeV GeV/c: dashed - uncorrected, bullet - correction applied as described on previous subsection.

Figure 162 shows the neutron spectra for data using p+Bi, p+U at 58 and p+p interactions at 84 GeV GeV/c

Figure 163 shows the neutron spectra for data using p+Be, p+C and p+Bi interactions at 120 GeV GeV/c

Corrections applied to the neutron sample sizes are summarized in Table 34.

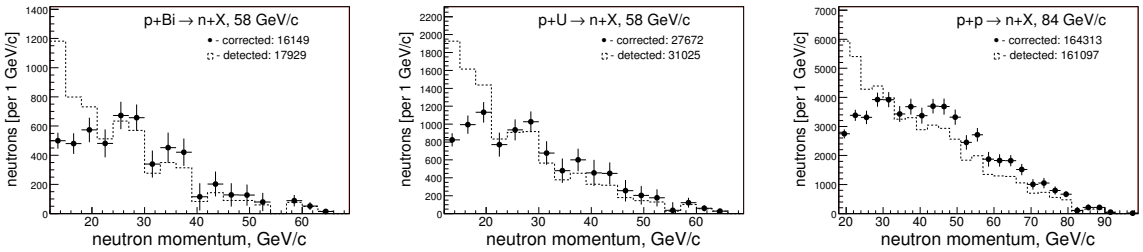

Figure 162: Neutron yields vs momentum for p+Bi (left), p+U (middle) at 58 GeV/c and p+p (right) interactions at 84 GeV GeV/c: dashed - uncorrected, bullet - correction applied as described on previous subsection.

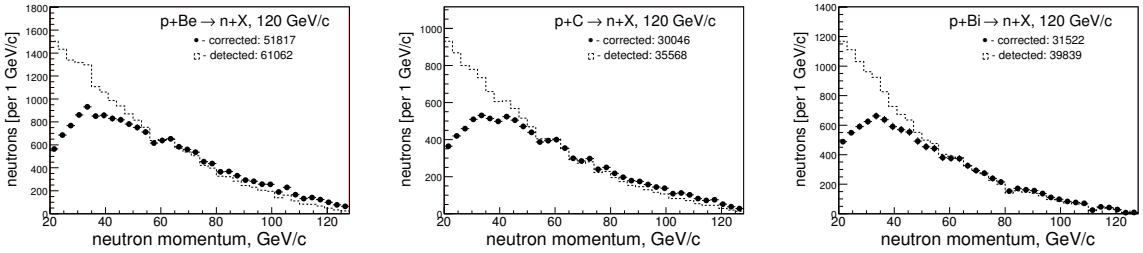

Figure 163: Neutron yields vs momentum for p+Be (left), p+C (middle) and p+Bi (right) interactions at 120 GeV GeV/c: dashed - uncorrected, bullet - correction applied as described on previous subsection.

	N_n(detected)	N_n(corrected)
H_2-20	886±79	1933±164
H_2-58	80578±2752	90762±3134
Be-58	4170±408	4612±450
C-58	32684±1076	33776±1132
Bi-58	17929±948	16150±898
U-58	31024±1339	27672±1287
H_2-84	161097±2953	164313±3003
Be-120	61062±429	51817±363
C-120	35568±235	30046±199
Bi-120	39839±414	31522±337

Table 34: Summary of corrections to the neutron sample size. Uncertainties are statistical

26 Systematic Uncertainty

We considered following sources of the systematics uncertainties:

- incident protons
- target-out subtraction
- spectrum correction function
- HCAL acceptance
- HCAL solid angle

The statistical, estimated and assigned systematic uncertainties for the incident protons are summarized in Table 35.

target	p_{beam}	stat.	estim.sys.	assigned syst.
H_2	20	0.054	±0.07	±0.10
H_2	58	0.026	±0.03	±0.10
Beryllium	58	0.052	±0.01	±0.10
Carbon	58	0.028	±0.02	±0.10
Bismuth	58	0.018	±0.05	±0.10
Uranium	58	0.015	±0.06	±0.10
H_2	84	0.009	±0.09	±0.10
Beryllium	120	0.009	±0.08	±0.10
Carbon	120	0.012	±0.07	±0.10
Bismuth	120	0.009	±0.08	±0.10

Table 35: The statistical, estimated and assigned systematic uncertainties for the incident protons. The systematic uncertainties for the target-out sample size considered separately.

The systematic uncertainty studies of the target-out subtraction procedure are summarized in Table 36.

The uncertainty of the spectrum correction function was estimated as 30% variation of the difference between with and without correction applied on momentum bin-by-bin bases. The results are summarized in Table 37.

The HCAL acceptance uncertainty was estimated by two approaches: a)by varying FLUKA results within ±30% and b)using a difference between FLUKA and other MC generators

The systematic uncertainty studies of the HCAL acceptance uncertainty varying FLUKA prediction are summarized in Table 38.

The systematic uncertainty studies of the HCAL acceptance using the differences between FLUKA and other MC predictions are summarized in Table 39.

	N_n(nominal)	CF_{t-out}	ΔF_{t-out}	N_n(variations)	$\Delta\epsilon_{t-out}$
H_2-20	1933	0.50	±0.17	$^{+2022}_{-1843}$	±0.046
H_2-58	90762	1.16	±0.10	$^{+94922}_{-86602}$	±0.046
Be-58	4612	1.47	±0.16	$^{+5057}_{-4166}$	±0.097
C-58	33776	1.39	±0.13	$^{+35196}_{-32360}$	±0.042
Bi-58	16150	1.14	±0.10	$^{+17662}_{-14636}$	±0.094
U-58	27672	1.09	±0.10	$^{+30513}_{-24831}$	±0.103
H_2-84	164313	1.11	±0.10	$^{+170774}_{-157851}$	±0.039
Be-120	51817	1.09	±0.10	$^{+54636}_{-48997}$	±0.054
C-120	30046	1.25	±0.10	$^{+30952}_{-29139}$	±0.030
Bi-120	31522	1.04	±0.10	$^{+34361}_{-28684}$	±0.090

Table 36: The systematic uncertainty studies of the target-out subtraction procedure. N_n(nominal) is the same as N_n(corrected) in Table 34. CF_{t-out} represents the correction factor to the target-out sample size applied to bring it to the same height as in target-in sample. ΔF_{t-out} represents an assigned variation level for the correction factor: 1/3 of correction value or not less than 10%. Next column represents resulting variations on the number of neutrons. Last column - the systematic uncertainty.

	N_n(nominal)	$+N_n$	$-N_n$	Frac
H_2-20	1933	2276	1590	0.177
H_2-58	90762	101524	80000	0.118
Be-58	4612	5135	4088	0.113
C-58	33776	37584	29969	0.113
Bi-58	16150	17759	14540	0.100
U-58	27672	30433	24911	0.100
H_2-84	164313	177354	151271	0.079
Be-120	51817	56315	47318	0.087
C-120	30046	32596	27496	0.085
Bi-120	31522	34375	28669	0.091

Table 37: Summary of systematic uncertainty for the spectrum correction function. It was estimated as 30% variation of the difference between with and without correction applied on momentum bin-by-bin bases.

	N_n(nom)	N_{hcal}	$+N_{hcal}$	$-N_{hcal}$	Frac
H_2-20	1933	13279	16682	9875	±0.256
H_2-58	90762	149576	167220	131932	±0.118
Be-58	4612	7863	8838	6887	±0.124
C-58	33776	60782	68883	52680	±0.133
Bi-58	16150	39149	46049	32249	±0.176
U-58	27672	67631	79619	55643	±0.177
H_2-84	164313	206091	218624	193557	±0.061
Be-120	51817	59020	61181	56859	±0.037
C-120	30046	34509	35848	33170	±0.039
Bi-120	31522	39840	42335	37345	±0.063

Table 38: The systematic uncertainty studies of the HCAL acceptance using FLUKA prediction variations. N_n(nom) - number of neutrons prior to HCAL acceptance correction. N_{hcal} - corrected for the HCAL acceptance. $\pm N_{hcal}$ represents the resulting number of neutrons due to 30% variations of the difference between using and without using of the HCAL acceptance correction. Last column - the fractional systematic uncertainty

	N_n(FL)	N_n(MA)	N_n(LA)	$\frac{FL-MA}{FL}$	$\frac{FL-LA}{FL}$
H_2-20	13279	9302	8048	0.299	0.393
H_2-58	149576	137886	140613	0.078	0.060
Be-58	7863	6989	7952	0.111	-0.011
C-58	60782	52890	61789	0.130	-0.017
Bi-58	39149	27689	36153	0.293	0.076
U-58	67631	47989	62859	0.290	0.070
H_2-84	206091	198251	206174	0.038	0.000
Be-120	59020	57877	65567	0.019	-0.111
C-120	34509	33757	38589	0.022	-0.118
Bi-120	39840	36282	43697	0.089	-0.097

Table 39: The systematic uncertainty studies of the HCAL acceptance using the differences between FLUKA and other MC models. N_n(FL), N_n(MA) and N_n(LA) - represents the number of neutrons, where the acceptance correction applied were based on FLUKA, MARS and LAQGSM, repsectively.

We calculate a three versions of the total systematic uncertainties: with and without HCAl acceptance applied and the uncertainty for the invariant cross section, see Table 40.

	w/o HCAL	with HCAL	ICS
H_2-20	±0.208	±0.330	±0.208
H_2-58	±0.162	±0.201	±0.162
Be-58	±0.179	±0.218	±0.179
C-58	±0.157	±0.205	±0.157
Bi-58	±0.170	±0.244	±0.170
U-58	±0.175	±0.249	±0.175
H_2-84	±0.133	±0.147	±0.133
Be-120	±0.143	±0.148	±0.143
C-120	±0.135	±0.140	±0.135
Bi-120	±0.162	±0.174	±0.162

Table 40: The total systematic uncertainties: with and without HCAL acceptance applied and uncertainty for the invariant cross section.

26.1 Systematics superimposed: w/o HCAL acceptance

Figure 164 shows the neutron spectra without HCAL acceptance applied from p+p, p+Be and p+C interactions at 58 GeV/c with the systematic uncertainties superimposed.

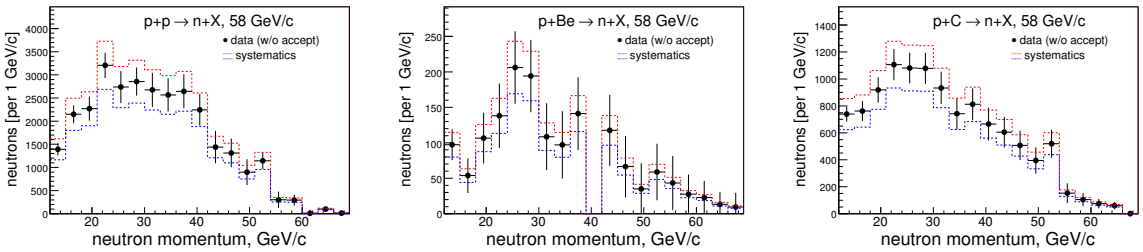

Figure 164: The neutron spectra without HCAL acceptance applied from p+p (left), p+Be (middle) and p+C (right) interactions at 58 GeV/c with the systematic uncertainties superimposed.

Figure 165 shows the neutron spectra without HCAL acceptance applied from p+Bi and p+U at 58 GeV/c and p+p interactions at 84 GeV/c with the systematic uncertainties superimposed.

Figure 166 shows the neutron spectra without HCAL acceptance applied from p+Be, p+C and p+Bi interactions at 120 GeV/c with the systematic uncertainties superimposed.

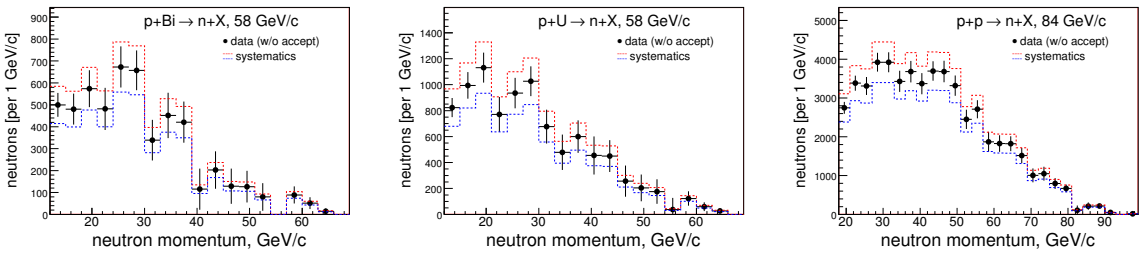

Figure 165: The neutron spectra without HCAL acceptance applied from p+Bi (left) and p+U (middle) at 58 GeV/c and p+p (right) interactions at 84 GeV/c with the systematic uncertainties superimposed.

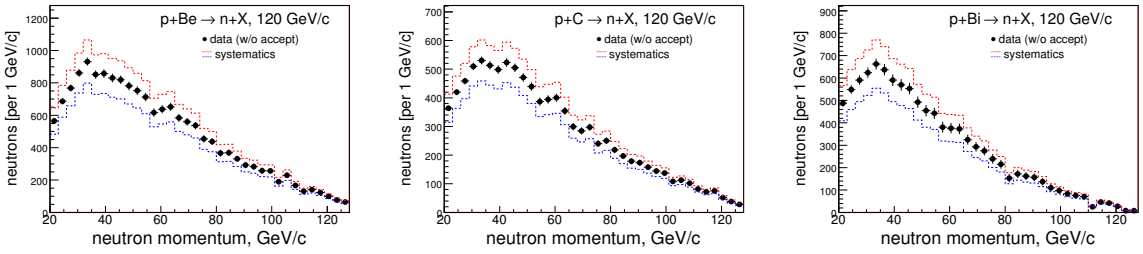

Figure 166: The neutron spectra without HCAL acceptance applied from p+Be (left), p+C (middle) and p+Bi (right) interactions at 120 GeV/c with the systematic uncertainties superimposed.

26.2 Systematics superimposed: HCAL acceptance applied

Figure 167 shows the neutron spectra with HCAL acceptance applied from p+p, p+Be and p+C interactions at 58 GeV/c with the systematic uncertainties superimposed.

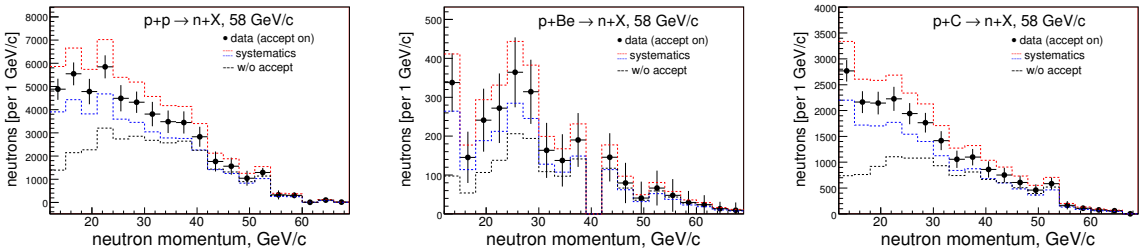

Figure 167: The neutron spectra with HCAL acceptance applied from p+p (left), p+Be (middle) and p+C (right) interactions at 58 GeV/c. The systematic uncertainties superimposed.

Figure 168 shows the neutron spectra with HCAL acceptance applied from p+Bi and p+U at 58 GeV/c and p+p interactions at 84 GeV/c with the systematic uncertainties superimposed.

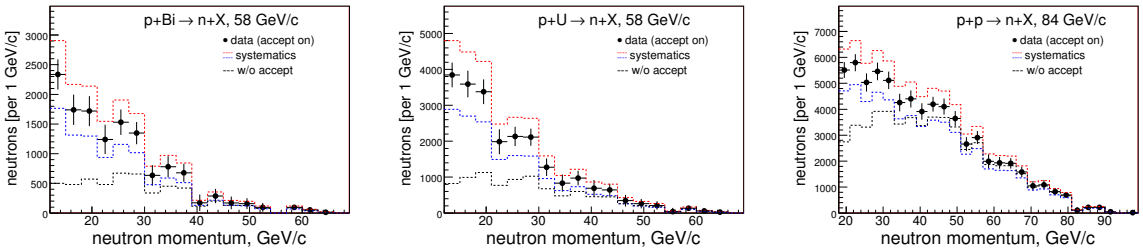

Figure 168: The neutron spectra with HCAL acceptance applied from p+Bi (left) and p+U (middle) at 58 GeV/c and p+p (right) interactions at 84 GeV/c. The systematic uncertainties superimposed.

Figure 169 shows the neutron spectra with HCAL acceptance applied from p+Be, p+C and p+Bi interactions at 120 GeV/c with the systematic uncertainties superimposed.

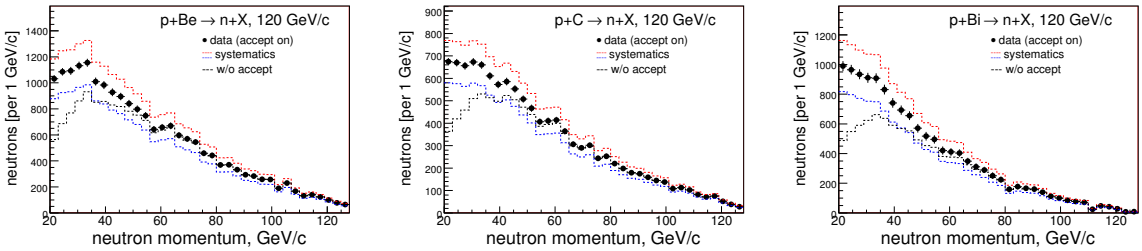

Figure 169: The neutron spectra with HCAL acceptance applied from p+Be (left), p+C (middle) and p+Bi (right) interactions at 120 GeV/c. The systematic uncertainties superimposed.

27 Inelastic Cross Section Estimate (as a cross check)

Before to discuss the neutron cross section we like to do some cross check. For example, estimate the inelastic cross section using our neutron sample and compare it with PDG. Our neutron sample represents a subsample of the inelastic processes, or σ_{inel}. If we count events prior the neutron selection, then it would be the inelastic sample. We calculate σ_{inel} as:

$$\sigma_{inel} = \frac{N_{inel}(t-in) - N_{inel}(t-out) - N_{backgr}}{N_{beam} \times \epsilon_{trig}} \times \frac{10^4}{n_t}, \text{ mb/(GeV/c)}$$

where N_{inel} are events passed Z_{vtx}, Δp_T and SciHi reqirements for both: target-in and target-out. N_{backgr} is remained elastic and straight through backgrounds (not known - not used). N_{beam} is number of incident protons, ϵ_{trig} is the trigger efficiency, . Quantity n_t is number of target particles per cm^2, details are on Table 1. The factor 10^4 is to bring the cross section in mbarns units.

We present results for both a)default events selection requirements and b)with an additional cut to reduce the straight throughs

27.0.1 Default event selection

Default event selection requirements:

- the interaction position should be around of the target
- the straight through are rejected by Δp_T >0.15 GeV/c cut
- SciHi trigger is on

Resulting input numbers and the σ_{inel} for p+p interactions at 58 GeV/c are shown in Table 41.

	Δp_T >0.15 GeV/c	Δp_T >0.25 GeV/c
N_{beam}	2.6206e+07	2.6206e+07
$N_{inel}(t-in)$	562704	507120
$N_{inel}(t-out)$	37920*5.196	34584*5.196
ϵ_{trig}	0.60±0.03	0.65±0.03
σ_{inel}, our	39.4 mb	32.6 mb
σ_{inel}, PDG	31.0 mb	31.0 mb
σ_{inel}, DPMJET	30.6 mb	30.6 mb

Table 41: The input numbers and the σ_{inel} for p+p interactions at 58 GeV/c. Factor 5.196 in $N_{inel}(t-out)$ line is to bring target-out sample size to same value as target-in. Δp_T >0.15 GeV/c cut is default value for the neutron analysis. n_t=5.922 for the liquid hydrogen.

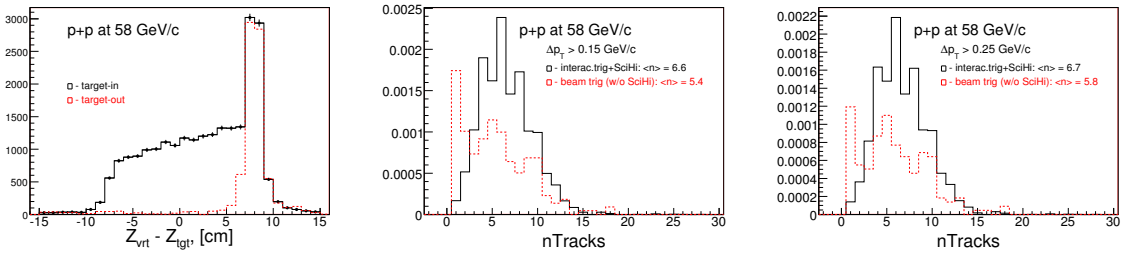

Figure 170: The Z_{vtx} (left) and charge track multiplicities (middle and right) for p+p interactions at 58 GeV/c. Multiplicities were normalized per single incident proton for events passed Z_{vtx}, Δp_T and SciHi requirements (in black) and beam trigger events passed Z_{vtx} and Δp_T cuts only (in red, not in scale). Target-out subtraction were applied. nTrks=1 in red plots illustrate the presence of the straight throughs. In black nTrks=1,2 are reduced by SciHi.

Figure 170 shows the Z_{vtx} and charged track multiplicities for p+p interactions at 58 GeV/c.

Comparison of our N_{ch} result with PDG using p+p interactions at 58 GeV/c are shown in Table 42

	Our	PDG
N_{ch}, Δp_T >0.15 GeV/c	5.4	6.0
N_{ch}, Δp_T >0.25 GeV/c	5.8	6.0

Table 42: Comparison of our N_{ch} with PDG. Our results are based on the unbias trigger data (without SciHi requirements).

The input numbers and the σ_{inel} for p+p interactions at 84 GeV/c are shown in Table 43.

Figure 171 shows the Z_{vtx} and charged track multiplicities for p+p interactions at 84 GeV/c

By viewing above results someone might come-up with an idea why we not using more tight Δp_T cut? Another possible question: If an input sample size for the neutron analysis is about 30% higher than what supposed to be, then what is possible impact to the neutron cross section? Short answer would be: In neutron selection we have an additional cut to reduce the straight throughs: Event rejected if there charged track with p_{trk} >0.7*P_{beam}. Figure 172 shed some lights on this.

Results for the neutron cross section with more tight Δp_T cut shown on Table 44

From σ_{inel} studies we might conclude:

- σ_{inel} with the default cuts appear to be about 30% higher than PDG value
- tightening of Δp_T cut, which helps to reduce the background, lead to better agreement with PDG (30% →10%).

	Δp_T >0.15 GeV/c	Δp_T >0.25 GeV/c
N_{beam}	3.1373e+07	3.1373e+07
$N_{inel}(t-in)$	771367	703865
$N_{inel}(t-out)$	79653*3.278	73626*3.278
ϵ_{trig}	0.66±0.02	0.71±0.03
σ_{inel}, our	41.7 mb	35.0 mb
σ_{inel}, PDG	31.0 mb	31.0 mb
σ_{inel}, DPMJET	30.9 mb	30.9 mb

Table 43: The input numbers and the σ_{inel} for p+p interactions at 84 GeV/c. Δp_T >0.15 GeV/c is default value for the neutron analysis.

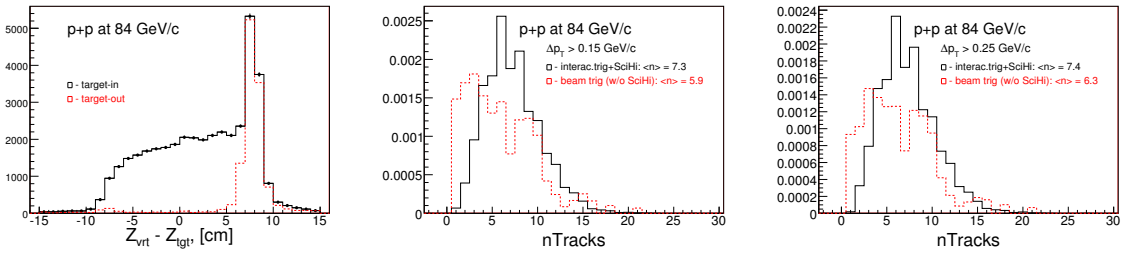

Figure 171: The Z_{vtx} (left) and charge track multiplicities (middle and right) for p+p interactions at 84 GeV/c. Multiplicities were normalized per single incident proton for events passed Z_{vtx}, Δp_T and SciHi requirements (in black) and beam trigger events passed Z_{vtx} and Δp_T cuts only (in red, not in scale). Target-out subtraction were applied. nTrks=1 in red plots illustrate the presence of the straight throughs. In black nTrks=1,2 are reduced by SciHi. N_{ch} PDG is 7.0

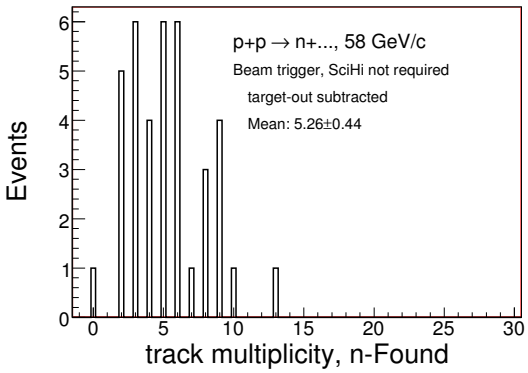

Figure 172: Charged track multiplicities for neutron candidates from p+p interactions at 58 GeV/c. Requirements: beam trigger, SciHi not required, target-out subtracted.

	Δp_T >0.15 GeV/c	Δp_T >0.25 GeV/c	variation
20 GeV/c	2.2±0.3 mb	1.9±0.3 mb	0.14±0.14
58 GeV/c	8.2±1.0 mb	7.2±0.9 mb	0.12±0.12
84 GeV/c	12.3±1.5 mb	11.0±1.4 mb	0.11±0.12

Table 44: Neutron cross section, $\int \frac{d\sigma}{dp}$ (discussed on following pages), calculated for different Δp_T cuts from p+p→n+X. NOTE: for Δp_T >0.25 GeV/c results were used the same the trigger efficiency, neutron selection efficiency and background level as for Δp_T >0.15 GeV/c case. But it might be not correct.

- tightening of Δp_T cut for the neutron analysis reduces the neutron cross section value in level of one uncertainty. This variation can be overestimated.

27.0.2 An additional cut to reject the straight throughs

For this study we implemented the additional cut to reject remained straight throughs: reject event if charged track has p_{trk} >0.7*P_{beam}. This cut is in use to select neutrons.

Results with the additional cut for p+p interactions are presented in Table 45

beam momentum	20 GeV/c	58 GeV/c	84 GeV/c
N_{beam}	2.2155e+06	2.6206e+07	3.1373e+07
$N_{inel}(t-in)$	24492	496464	697154
$N_{inel}(t-out)$	1929*3.98	32856*4.364	70581*3.347
ϵ_{trig}	0.65±0.03	0.78±0.03	0.73±0.02
σ_{inel}, our	19.6 mb	29.2 mb	33.7 mb
σ_{inel}, PDG	30.5 mb	31.0 mb	31.4 mb
σ_{inel}, DPMJET	30.5 mb	30.6 mb	30.9 mb

Table 45: Inelastic cross sections for pp interactions at 20, 58 and 84 GeV/c. Our result for the momentum of 20 GeV/c is 30% below of expectation. Partially it can be explained by presence of 25% of pions in beam, where the $\sigma_{inel}(\pi^+ p)$=20 mb

Figure 173 shows the comparison of the σ_{inel} as a function of the charged track multiplicity for data and MC using p+p interactions at 20, 58 and 84 GeV/c.

Below we present the inelastic cross section results for heavier targets. The input numbers and the σ_{inel} for pC and pBi interactions at 58 and 120 GeV/c proton beams are shown in Table 46.

Figure 174 shows the pC and pPb σ_{inel} world data presented as a function of the proton momentum.

Figure 175 shows the pC and pBi absorption rates as a function of the run number.

Figure 176 shows the comparison of the σ_{inel} as a function of the charged track multiplicity for data and MC using p+p interactions at 20, 58 and 84 GeV/c.

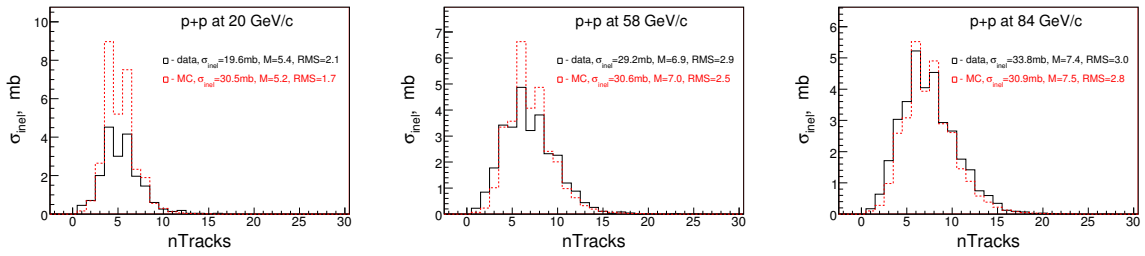

Figure 173: Comparison of the σ_{inel} as a function of the charged track multiplicity for data and MC using p+p interactions at 20, 58 and 84 GeV/c

	p+C	p+C	p+Bi	p+Bi
P_{beam}	58 GeV/c	120 GeV/c	58 GeV/c	120 GeV/c
N_{beam}	8.7518e+06	5.5421e+06	2.1832e+07	2.8955e+07
$N_{inel}(t-in)$	199944	101513	261096	282351
$N_{inel}(t-out)$	46797*0.545	26592*0.665	58942*1.239	35096*2.579
ϵ_{trig}	0.82±0.07	0.85±0.02	0.84±0.04	0.78±0.02
n_t	0.8408	0.8408	0.0487	0.0487
σ_{inel}, our	289 mb	212 mb	2108 mb	1736 mb
σ_{inel},FLUKA	286 mb	287 mb	1875 mb	1880 mb
σ_{inel},LAQGSM	265 mb	266 mb	1674 mb	1676 mb

Table 46: Inelastic cross sections for pC and pBi interactions at 58 and 120 GeV/c. Note: p+Bi data calculated w/o nTrack<30 and $p_{sum} < 1.1 * P_{beam}$ cuts.

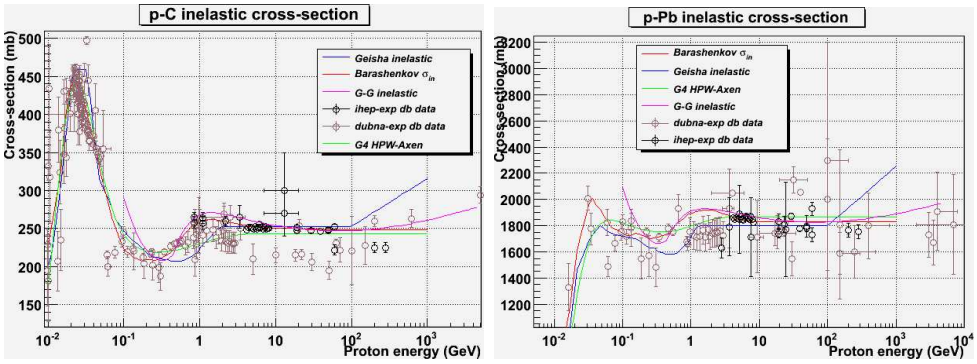

Figure 174: pC and pPb inelastic cross section world data presented as a function of the proton momentum.

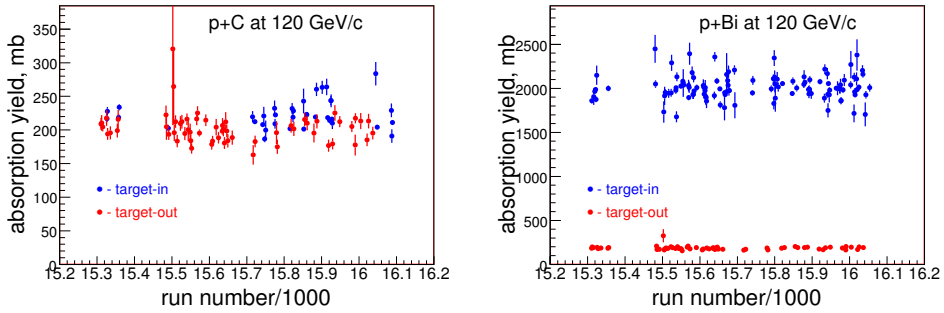

Figure 175: Absorption rate as a function of the run number for 120 GeV beam momentum. Blue: the trigger efficiency and target-out subtraction were NOT applied. Red: interactions with the trigger scintillator.

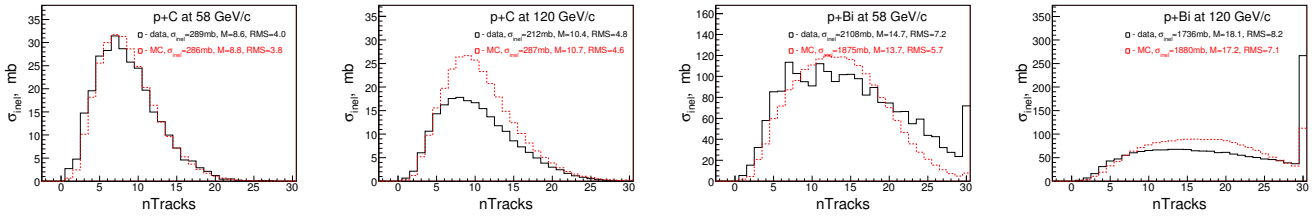

Figure 176: Comparison of the σ_{inel} as a function of the charged track multiplicity for data and MC using p+C and p+Bi interactions at 58 and 120 GeV/c

27.0.3 Neutrals total cross section: data vs MC. K^o_L background

Figure 177 shows Monte Carlo neutrals multiplicities per single pp interactions at 20 GeV/c and comparison of K^o_L with $K^{\pm}$ spectra vs x_F variable.

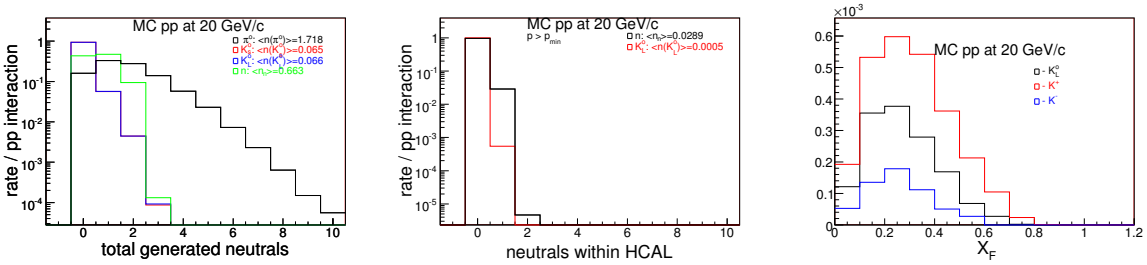

Figure 177: The neutrals multiplicities distributions per single inelastic pp interaction at 20 GeV/c: left - without cuts, middle - neutrals required to be pointing to HCAL volume and p>p_{min}. Right - comparison of K^o_L with $K^{\pm}$ spectra vs x_F variable

Neutrals average multiplicities per single pp interactions and total cross sections at 20 GeV/c are summarized in Table 47.

	$< n_{MC} >$	$< n_{data-W} >$	σ_{MC}	σ_{data-W}
π^o	1.719	1.55	52.4 mb	45±4 mb
K^o_s	0.065	0.05	2.0 mb	1.3±? mb
K^o_L	0.066	n/a	2.0 mb	1.3 mb(pred)
n	0.663	n/a	20.2 mb	n/a

Table 47: Neutrals average multiplicities per single pp interactions and total cross sections at 20 GeV/c. MC prod. cross section: 30.5 mb. $< \pi^o >$ in data was calculated as: $< \pi^o >$ = -0.82 + 0.79*ln(p_{lab}) - J.Withmore Physics Reports 27, No.5 (1976) 187-273. $\sigma_{MC} =< n_{MC} >$ * 30.5 mb

Neutron and K^o_L average multiplicities per single pp interactions and cross sections at 20 GeV/c are summarized in Table 48.

	$< n >$	σ_{MC}	$\sigma_{data}(\int \frac{d\sigma}{dp})$
n	0.0289	0.88 mb	2.2±0.3 mb
K^o_L	0.0005	0.015 mb	n/a
K^o_L/n	0.017		

Table 48: n and K^o_L are within HCAL and p>p_{min}. Background level is 0.007 per neutron. It looks like that 0.01 of K^o_L contribution is remained there.

Figure 178 shows Monte Carlo neutrals multiplicities per single pp interactions at 58 GeV/c and comparison of K^o_L with $K^{\pm}$ spectra vs x_F variable.

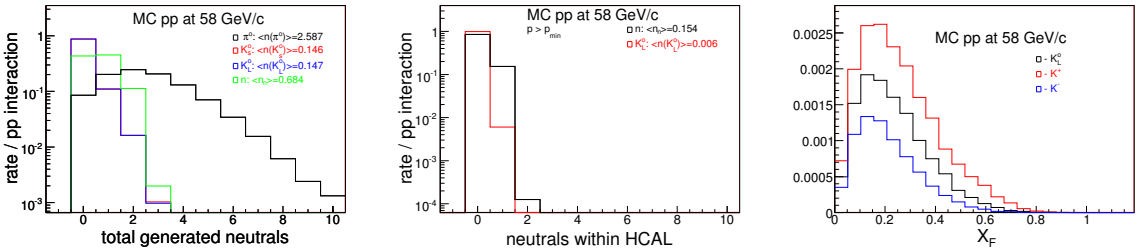

Figure 178: The neutrals multiplicities distributions per single inelastic pp interaction at 58 GeV/c: left - without cuts, middle - neutrals required to be pointing to HCAL volume and p>p_{min}. Right - comparison of K^o_L with $K^{\pm}$ spectra vs x_F variable

Neutrals average multiplicities per single pp interactions and total cross sections at 58 GeV/c are summarized in Table 49.

	$< n_{MC} >$	$< n_{data-W} >$	σ_{MC}	σ_{data-W}
π^o	2.587	2.39	79.2 mb	81±4 mb (69GeV)
K^o_s	0.146	0.13±0.03	4.5 mb	4±1 mb (69GeV)
K^o_L	0.147	n/a	4.5 mb	4±1 mb(pred)
n	0.684	n/a	20.9 mb	n/a

Table 49: Neutrals average multiplicities per single pp interactions and total cross sections at 58 GeV/c. MC prod. cross section: 30.6 mb. $< \pi^o >$ in data was calculated as: $< \pi^o >$ = -0.82 + 0.79*ln(p_{lab}). $\sigma_{MC} =< n_{MC} >$ * 30.6 mb

Neutron and K^o_L average multiplicities per single pp interactions and cross sections at 58 GeV/c are summarized in Table 50.

	$< n >$	σ_{MC}	$\sigma_{data}(\int \frac{d\sigma}{dp})$
n	0.154	4.7 mb	8.2±1.0 mb
K^o_L	0.006	0.18 mb	n/a
K^o_L/n	0.04		

Table 50: n and K^o_L are within HCAL and p>p_{min}. Estimated background level for this data is 0.082 per single neutron candidate.

Figure 179 shows Monte Carlo neutrals multiplicities per single pp interactions at 84 GeV/c and comparison of K^o_L with $K^{\pm}$ spectra vs x_F variable.

Neutrals average multiplicities per single pp interactions and total cross sections at 84 GeV/c are summarized in Table 51.

Neutron and K^o_L average multiplicities per single pp interactions and cross sections at 84 GeV/c are summarized in Table 52.

From above studies we observed:

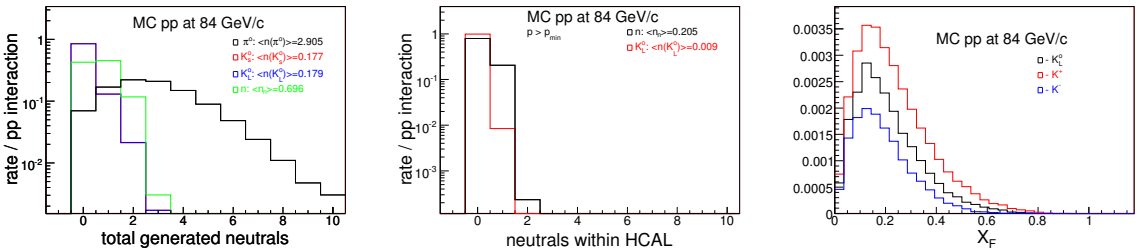

Figure 179: The neutrals multiplicities distributions per single inelastic pp interaction at 84 GeV/c: left - without cuts, middle - neutrals required to be pointing to HCAL volume and p>p_{min}. Right - comparison of K^o_L with $K^{\pm}$ spectra vs x_F variable

	$< n_{MC} >$	$< n_{data-W} >$	σ_{MC}	σ_{data-W}
π^o	2.905	2.68	89.6 mb	83±4 mb ($\frac{69+102}{2}$GeV)
K^o_s	0.177	0.14±0.02	5.5 mb	4.3±1 mb ($\frac{69+102}{2}$GeV)
K^o_L	0.179	n/a	5.5 mb	4.3±1 mb(pred)
n	0.696	n/a	21.5 mb	n/a

Table 51: Neutrals average multiplicities per single pp interactions and total cross sections at 84 GeV/c. MC prod. cross section: 30.9 mb. $< \pi^o >$ in data was calculated as: $< \pi^o >$ = -0.82 + 0.79*ln(p_{lab}). σ_{MC} =$< n_{MC} >$ * 30.9 mb

	$< n >$	σ_{MC}	$\sigma_{data}(\int \frac{d\sigma}{dp})$
n	0.205	6.5 mb	12.3±1.5 mb
K^o_L	0.009	0.28 mb	n/a
K^o_L/n	0.04		

Table 52: n and K^o_L are within HCAL and p>p_{min}. Estimated background level for this data is 0.117 per single neutron candidate.

- the neutron production cross section in our data, ($\int \frac{d\sigma}{dp}$), systematically higher than the prediction from DPMJET, by factor 2.

- K_s^o/K_L^o production cross section in DPMJET is slightly higher than the existing inclusive K_s^o production data, J.Whitmore Physics Reports 27, No.5 (1976) 187-273.

- our background estimates covers well the K_L^o contribution. It is consistent for 20 GeV/c data within 1-2% level. For 58 and 84 GeV/c data predicted K_L^o contributions are not greater than half of what we considering as the total background.

One can conclude that K_L^o contribution in our data is not underestimated.

28 Neutron Cross Section Results

We calculate the inclusive neutron production cross sections for following cases:

- spectra NOT corrected for the geometrical acceptance
- spectra were corrected for the neutrons missed due to calorimeter's geometrical acceptance
- invariant cross section with the calorimeter's solid angle included

28.1 HCAL acceptance correction was NOT applied

28.1.1 Results for data

The neutron production cross section for case without acceptance corrections was calculated as:

$$\frac{d\sigma_n}{dp} = \frac{N_n(t-in)-N_n(t-out)}{N_{beam}\cdot\epsilon_{scf}\cdot\Delta p} \times \frac{1}{n_t} \times 10^4, \text{ mb/(GeV/c)},$$

where $N_n(t-in)$ and $N_n(t-out)$ are the number of neutron candidates for target-in and target-out cases, respectively. N_{beam} - incident protons, ϵ_{scf} - the single correction function as described in sect. 25, Δp - momentum bin width.

Figure 180 shows the forward neutron production cross section for case without geometrical acceptance corrections applied using p+p, p+Be and p+C interactions at 58 GeV/c.

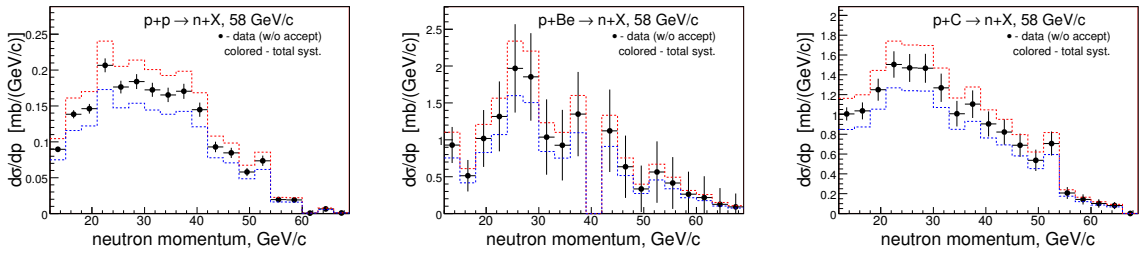

Figure 180: The forward neutron production cross section for case without geometrical acceptance corrections applied using p+p (left), p+Be (middle) and p+C interactions at 58 GeV/c.

Figure 181 shows the forward neutron production cross section for case without geometrical acceptance corrections applied using p+Bi and p+U interactions at 58 GeV/c and p+p at 84 GeV/c.

Figure 182 shows the forward neutron production cross section for case without geometrical acceptance corrections applied using p+Be, p+C and p+Bi interactions at 120 GeV/c.

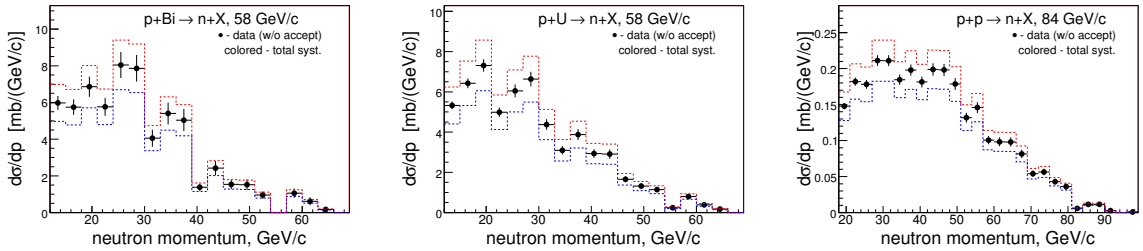

Figure 181: The forward neutron production cross section for case without geometrical acceptance corrections applied using p+Bi (left) and p+U (middle) interactions at 58 GeV/c and p+p (right) interactions at 84 GeV/c.

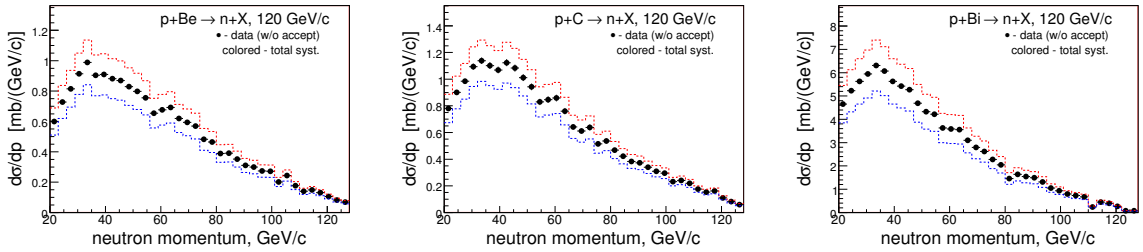

Figure 182: The forward neutron production cross section for case without geometrical acceptance corrections applied using p+Be (left), p+C (middle) and p+Bi(right) interactions at 120 GeV/c.

	σ_n	stat.	syst
H_2-20	1.5	0.1	0.3
H_2-58	5.8	0.2	1.0
Be-58	44.0	4.4	8.3
C-58	45.9	1.5	7.2
Bi-58	193.2	10.4	32.5
U-58	178.8	7.7	30.8
H_2-84	8.8	0.2	1.2
Be-120	55.0	0.4	8.2
C-120	64.5	0.4	8.8
Bi-120	300.2	3.1	52.0

Table 53: The inclusive forward neutron production cross sections. The calculations done for case, when HCAL acceptance corrections was NOT applied. Units are in mb.

The inclusive forward neutron production cross sections for case without geometrical acceptance corrections applied are summarized in Table 53.

Figure 183 shows the forward neutron production cross section dependence vs the target atomic weight. HCAL acceptance corrections NOT applied.

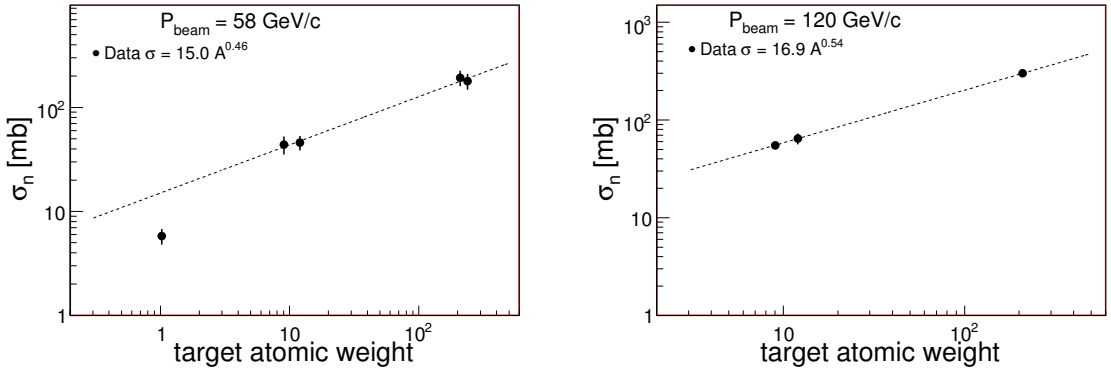

Figure 183: The forward neutron production cross section dependence vs the target atomic weight for case when HCAL acceptance corrections was NOT applied: 58 GeV/c (left) and 120 GeV/c (right).

The fit parameters are shown in Table 54.

	coefficient	power
58 GeV/c	15.1 ± 3.5	0.46 ± 0.06
120 GeV/c	16.9 ± 4.1	0.54 ± 0.05

Table 54: The fit parameters of the neutron production cross section when HCAL acceptance was NOT applied as a function of the target atomic weight.

28.1.2 Comparison with Monte Carlo

Monte Carlo cross section was calculated as:

$$\frac{d\sigma_n}{dp} = \sigma_{inel} \cdot \frac{N_n}{N_{events} \cdot \Delta p}, \text{ mb/(GeV/c) for DPMJET}$$
$$\frac{d\sigma_n}{dp} = \frac{N_n}{N_{beam} \cdot n_t \cdot \Delta p} \times CC \times 10^4, \text{ mb/(GeV/c) for FLUKA}$$

where σ_{inel} is the inelastic cross section of p+p process (note: our DPMJET samples consist from the inelastic processes only), N_n is number of observed neutrons within HCAL, N_{events} is number of total MC events in sample, Δp is bin width.

In case of Fluka N_{beam} is the number of incident protons in MC, n_t is the number of nuclei per cm^2 used in MC and CC is the correction factor for it's difference from the

	N_{files}	CF	n_t(data)	n_t(MC)	CC
Be-58	34	0.962	0.4744	0.4925	1.038
C-58	162	0.961	0.8408	1.006	1.196
Bi-58	160	0.937	0.0487	0.0487	1.000
U-58	133	0.935	0.0474	0.0479	1.011
Be-120	178	0.872	0.4744	0.4925	1.038
C-120	165	0.874	0.8408	1.006	1.196
Bi-120	185	0.797	0.0487	0.0487	1.000

Table 55: Correction factors: CF and CC

target properties used in data. $N_{beam} = N_{files} \cdot 2 \cdot 10^5 \cdot CF$, where N_{files} is the number of generated files, CF is the correction factor for fraction of events were dropped due to of the beam position and $p_{sum} > 1.2P_{beam}$ cuts. CF and CC coefficients shown in Table 55.

Below we will present comparison of the measured neutron cross section with Monte Carlo, where data NOT corrected for the HCAL acceptance. Requirements for MC: neutrons within HCAL geometry and $p_n > p_{min}$. Figure 184 shows comparison of the forward neutron production cross section with Monte Carlo results using p+p, p+C and p+Bi interactions at 58 GeV/c.

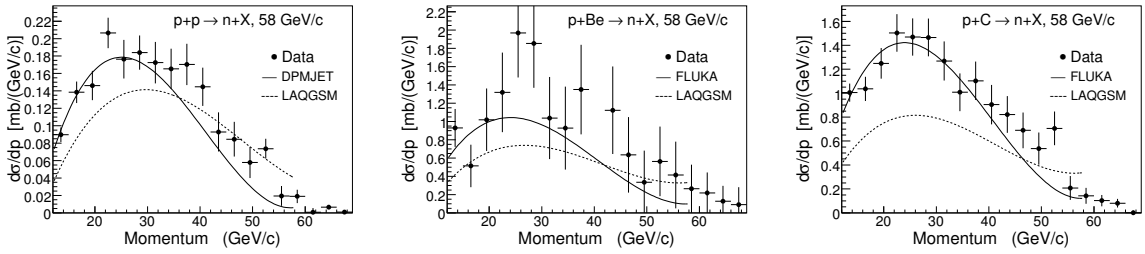

Figure 184: The comparison of forward neutron production cross section from data with Monte Carlo predictions using p+p (left), p+Be (middle) and p+C (right) interactions at 58 GeV/c. Data were NOT corrected for the HCAL acceptance. Requirements for MC: neutrons within HCAL geometry and $p_n > p_{min}$.

Figure 185 shows comparison of the forward neutron production cross section with Monte Carlo results using p+Bi, p+U at 58 GeV/c and p+p interactions at 84 GeV/c.

Figure 186 shows comparison of the forward neutron production cross section with Monte Carlo results using p+p at 84 GeV/c and p+C and p+Bi interactions at 120 GeV/c. .

Comparison of the production cross sections for case without geometrical acceptance corrections applied with Monte Carlo cross section are summarized in Table 56.

Figure 187 shows comparison of the MC neutron production cross section as function of the target atomic weight for FLUKA, LAQGSM and MARS at 58 and 120

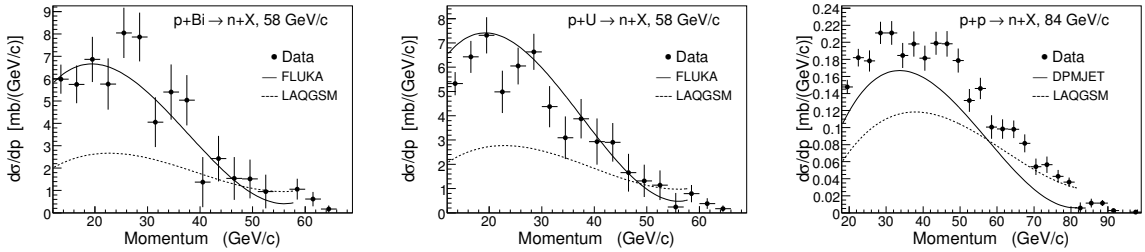

Figure 185: The comparison of forward neutron production cross section from data with Monte Carlo predictions using p+Bi (left) and p+U (middle) at 58 GeV/c and p+p (right) interactions at 84 GeV/c. Data were NOT corrected for the HCAL acceptance. Requirements for MC: neutrons within HCAL geometry and $p_n > p_{min}$.

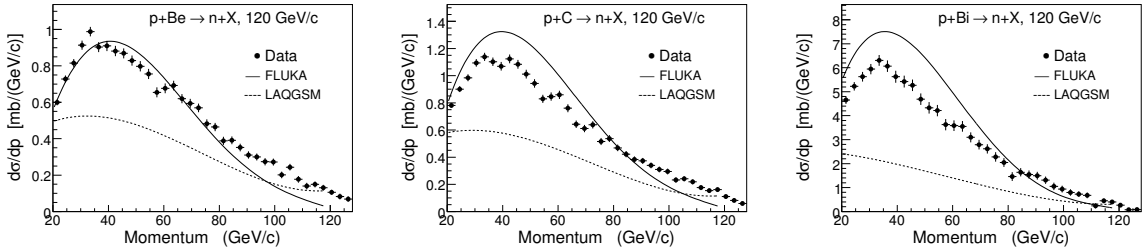

Figure 186: The comparison of forward neutron production cross section with Monte Carlo results using p+Be (left), p+C (middle) and p+Bi (right) interactions at 120 GeV/c. Data were NOT corrected for the HCAL acceptance. Requirements for MC: neutrons within HCAL geometry and $p_n > p_{min}$..

	data	stat.	syst	$\frac{DPMJET}{FLUKA}$	LAQGSM	MARS
H_2-20	1.5	0.1	0.3	0.9	1.7	2.1
H_2-58	5.8	0.2	1.0	4.9	4.7	6.8
Be-58	44.0	4.4	8.3	30.2	25.3	35.7
C-58	45.9	1.5	7.2	40.9	27.5	43.5
Bi-58	193.2	10.4	32.5	179.0	88.3	238.0
U-58	178.8	7.7	30.8	199.6	91.5	256.0
H_2-84	8.8	0.2	1.2	6.4	5.4	7.9
Be-120	55.0	0.4	8.2	51.1	33.4	44.0
C-120	64.5	0.4	8.8	70.9	36.6	53.1
Bi-120	300.2	3.1	52.0	369.1	120.1	281.1

Table 56: Comparison of the neutron production cross sections for case without geometrical acceptance corrections applied with Monte Carlo cross sections.

GeV/c beam momenta. Requirements for Monte Carlo neutrons: within HCAL geometry and $p_n > p_{min}$.

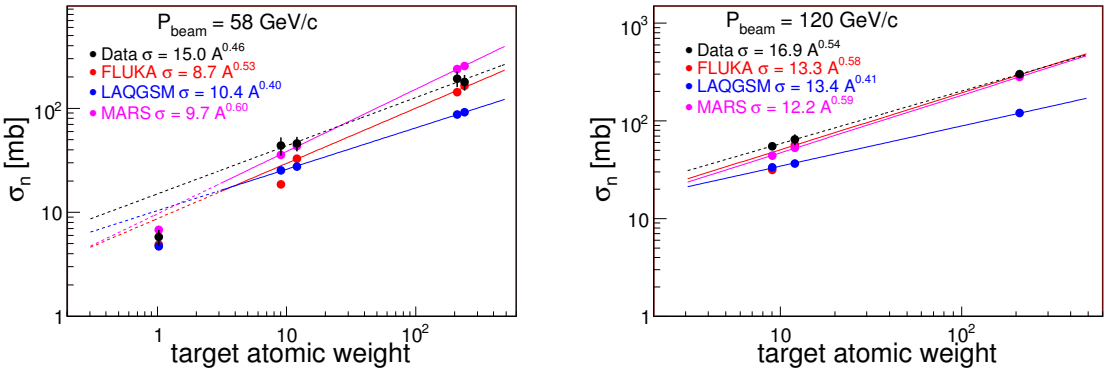

Figure 187: The data vs MC comparison of the neutron production cross section as function of the target atomic weight at 58 (left) and 120 (right) GeV/c beam momenta. Data were NOT corrected for the HCAL acceptance. Requirements for Monte Carlo neutrons: within HCAL geometry and $p_n > p_{min}$.

From above comparison one can conclude:

- FLUKA predictions looks almost consistent with data for many targets, except for Be, where prediction is lower by factor 2
- the central values for MARS predictions is in reasonable agreement with data, however the shape of spectra in high neutron momentum looks unreasonable. It is in controversy with both: data and the proton behaviour
- LAQGSM predictions looks consistent with data, however for the havier targets it off, for example, factor 2 for Bi

28.2 Calorimeter Acceptance correction applied

The forward neutron production cross section with the calorimeter acceptance correction applied was calculated as:

$$\frac{d\sigma_n}{dp} = \frac{N_n(t-in)-N_n(t-out)}{N_{beam}\cdot\epsilon_{scf}\cdot\epsilon_{hcal}\cdot\Delta p} \times \frac{1}{n_t} \times 10^4, \text{ mb/(GeV/c)}$$

where, N_n is number of the neutron candidates passing the selection requirements, where t-in and t-out are target-in and target-out respectively. N_{beam} is the number of incident protons, ϵ_{scf} is the single correction function, ϵ_{hcal} is the calorimeter acceptance as described in section 20, Δp is momentum bin width. Quantity n_t is number of target particles per cm^2, details are on Table 1. The factor 10^4 is to bring the cross section in mb units.

The inclusive forward neutron production cross sections with HCAL acceptance applied are summarized in Table 57.

	σ_{scf}	$\sigma_{scf*hcal}$	stat.	syst.
H_2-20	1.5	10.1	0.6	0.7
H_2-58	5.8	9.6	0.1	1.9
Be-58	44.0	75.1	4.5	16.9
C-58	45.9	82.6	2.0	17.0
Bi-58	193.2	468.3	10.6	114.0
U-58	178.8	437.1	6.0	107.9
H_2-84	8.8	11.1	0.1	1.6
Be-120	55.0	62.6	0.2	9.6
C-120	64.5	74.1	0.3	10.5
Bi-120	300.2	379.5	1.4	69.9

Table 57: The inclusive forward neutron production cross sections: σ_{scf} - only the single correction function was applied, $\sigma_{scf*hcal}$ - both: the single correction function and HCAL acceptance corrections were applied. The cross section units are in mb.

Figure 188 shows the forward neutron production cross section with HCAL acceptance applied for p+p, p+Be and p+C interactions at 58 GeV/c.

Figure 189 shows the forward neutron production cross section with HCAL acceptance applied for p+Bi and p+U at 58 GeV/c and p+p interactions at 84 GeV/c.

Figure 190 shows the forward neutron production cross section with HCAL acceptance applied for p+Be, p+C and p+Bi interactions at 120 GeV/c.

Figure 191 shows the forward neutron production cross section as a function of the target atomic weight.

The fit parameters are shown in Table 58.

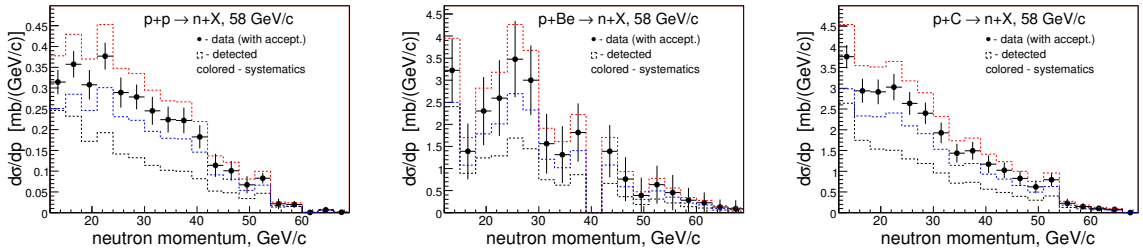

Figure 188: The forward neutron production cross section with HCAL acceptance applied for p+p (left), p+Be (middle) and p+C (right) interactions at 58 GeV/c.

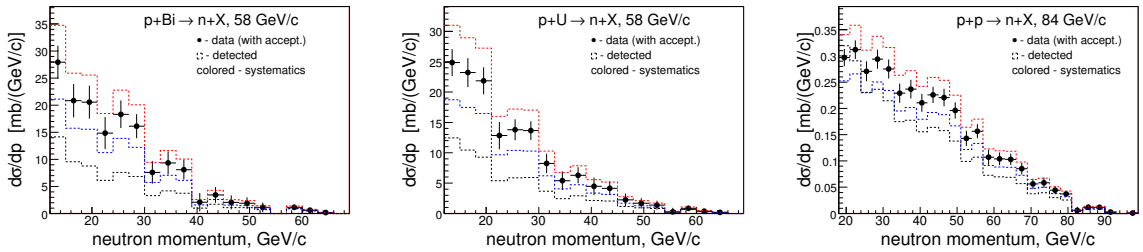

Figure 189: The forward neutron production cross section with HCAL acceptance applied for p+Bi (left) and p+U (middle) at 58 GeV/c and p+p (right) interactions at 84 GeV/c.

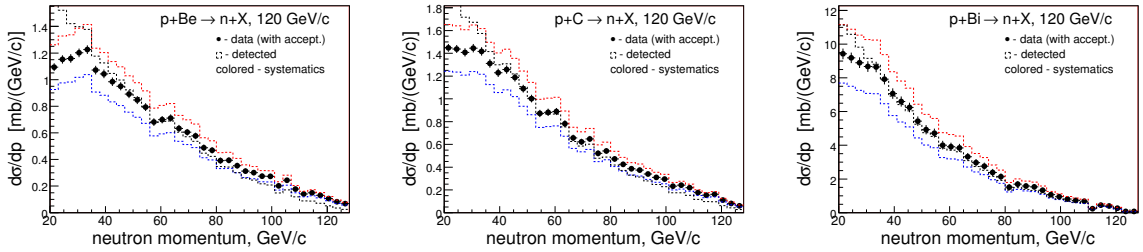

Figure 190: The forward neutron production cross section with HCAL acceptance applied for p+Be (left), p+C (middle) and p+Bi (right) interactions at 120 GeV/c.

	coefficient	power
58 GeV/c	20.8 ± 6.2	0.57 ± 0.08
120 GeV/c	17.8 ± 4.2	0.57 ± 0.07

Table 58: The fit parameters of the neutron production cross section with HCAL acceptance applied as a function of the target atomic weight.

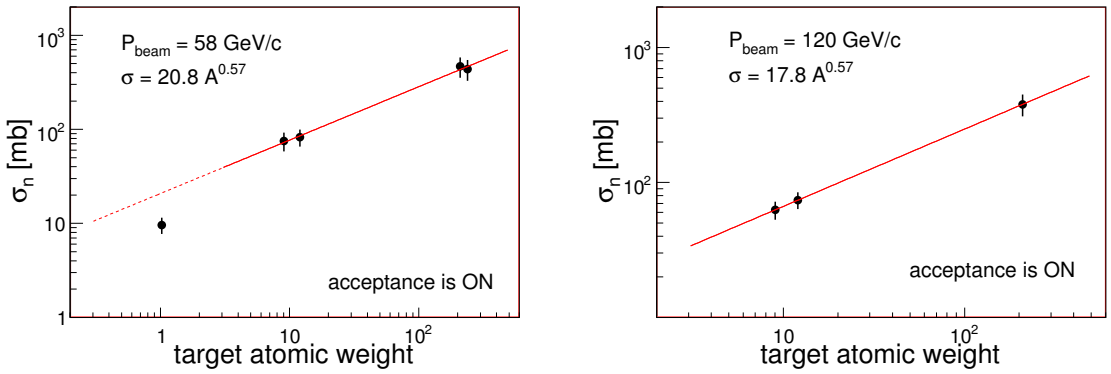

Figure 191: The forward neutron production cross section with HCAL acceptance applied as a function of the target atomic weight: 58 GeV/c (left) and 120 GeV/c (right), respectively. On left plot H_2 data point is not included to the fit.

28.3 Invariant cross section with the calorimeter's solid angle included

The invariant inclusive neutron production cross section was calculated as:

$$\frac{E}{p^2\Omega}\frac{d\sigma}{dp} = \frac{E}{p^2\Omega} \times \frac{N_n(t-in)-N_n(t-out)}{N_{beam}\cdot\epsilon_{scf}\cdot\Delta p} \times \frac{1}{n_t} \times 10^4, \text{ mb/(GeV/c)}^2\text{/sr}$$

where p and E are neutron momentum and energy, Ω is the calorimeter's solid angle, presented in Table 31, $\frac{d\sigma}{dp}$ is the same as described in section 28.1.1.

Figure 192 shows the invariant neutron production cross section as the function of neutron momentum for p+p, p+Be and p+C interactions at 58 GeV/c.

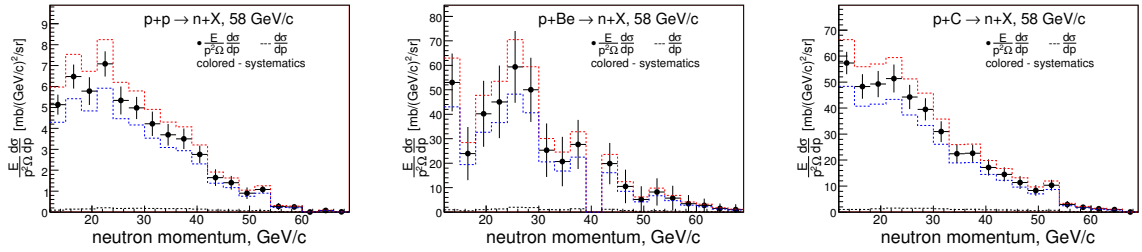

Figure 192: The invariant neutron production cross section as the function of neutron momentum for p+p (left), p+Be (middle) and p+C (right) interactions at 58 GeV/c with the total systematic uncertainties superimposed.

Figure 193 shows the invariant neutron production cross section as the function of neutron momentum for p+Bi and p+U at 58 GeV/c and p+p interactions at 84 GeV/c.

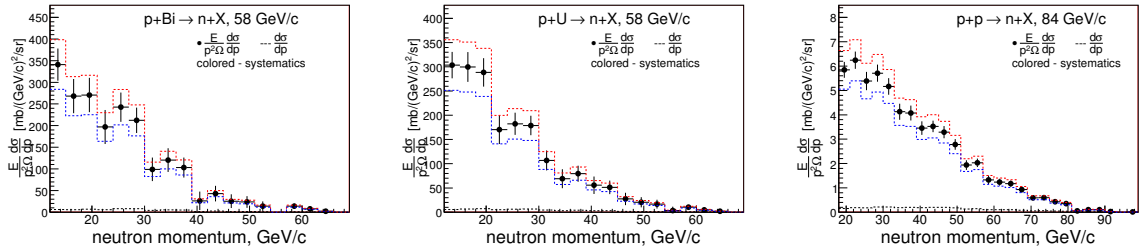

Figure 193: The invariant neutron production cross section as the function of neutron momentum for p+Bi (left) and p+U (middle) at 58 GeV/c and p+p (right) interactions at 84 GeV/c with the total systematic uncertainties superimposed.

Figure 194 shows the invariant neutron production cross section as the function of neutron momentum for p+Be, p+C and p+Bi interactions at 120 GeV/c with the total systematic uncertainties superimposed.

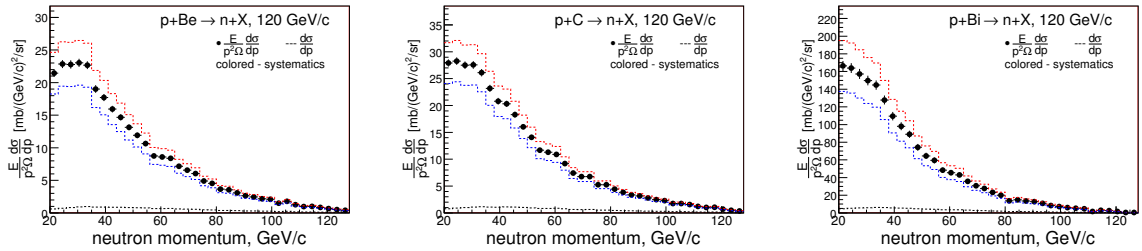

Figure 194: The invariant neutron production cross section as the function of neutron momentum for p+Be (left), p+C (middle) and p+Bi(right) interactions at 120 GeV/c with the total systematic uncertainties superimposed.

28.4 Cross section as a function of the variable x_F

The x_F is calculated in cm frame with the bin width of 0.05: $x_F = \frac{p_{\parallel,n}cm}{p_{max}cm}$, here $p_{\parallel,n}$cm is the neutron longitudinal momentum component in the center of mass system and p_{max}cm is maximum incident momentum in cm frame.

28.4.1 HCAL acceptance NOT applied

The neutron production cross section (without acceptance corrections) as a function of variable x_F was calculated as:

$$\frac{d\sigma}{dx_F} = \frac{N_n(t-in)-N_n(t-out)}{N_{beam}\cdot\epsilon_{scf}\cdot\Delta x_F} \times \frac{1}{n_t} \times 10^4, \text{ mb}$$

Figure 195 shows the forward neutron production cross section vs variable x_F using p+p, p+Be and p+C interactions at 58 GeV/c. The geometrical acceptance corrections NOT applied.

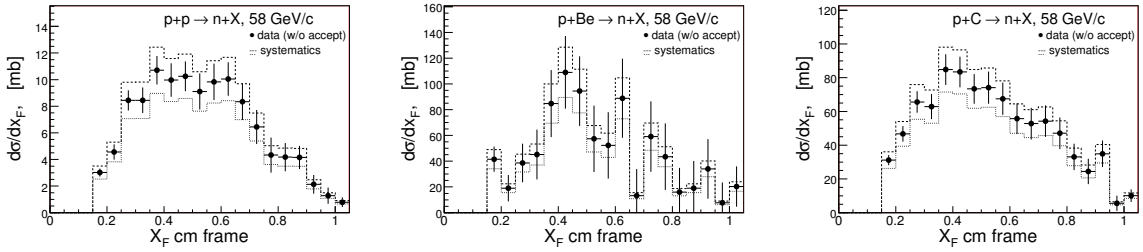

Figure 195: The forward neutron production cross section vs variable x_F using p+p (left), p+Be (middle) and p+C (right) interactions at 58 GeV/c. The geometrical acceptance corrections NOT applied.

Figure 196 shows the forward neutron production cross section vs variable x_F using p+Bi and p+U interactions at 58 GeV/c and p+p interactions at 84 GeV/c. The geometrical acceptance corrections NOT applied.

Figure 197 shows the forward neutron production cross section vs variable x_F using p+Be, p+C and p+Bi interactions at 120 GeV/c. The geometrical acceptance corrections NOT applied.

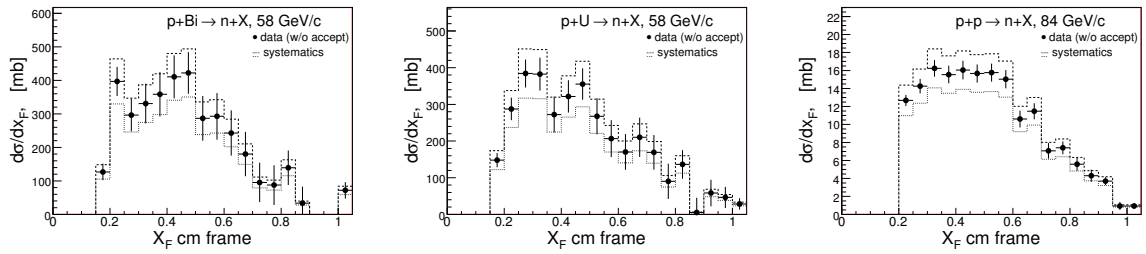

Figure 196: The forward neutron production cross section vs variable x_F using p+Bi (left) and p+U (right) interactions at 58 GeV/c and p+p interactions at 84 GeV/c. The geometrical acceptance corrections NOT applied.

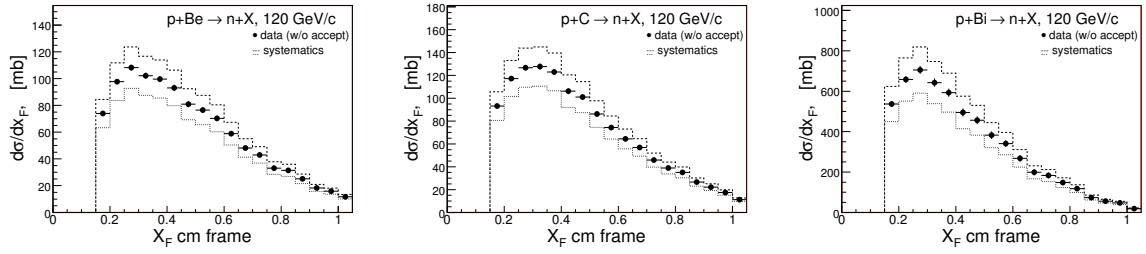

Figure 197: The forward neutron production cross section vs variable x_F using p+Be (left), p+C (center) and p+Bi (right) interactions at 120 GeV/c. The geometrical acceptance corrections NOT applied.

28.4.2 HCAL acceptance correction applied

The neutron production cross section with acceptance corrections applied as a function of variable x_F was calculated as:

$$\frac{d\sigma}{dx_F} = \frac{N_n(t-in) - N_n(t-out)}{N_{beam} \cdot \epsilon_{scf} \cdot \epsilon_{hcal} \cdot \Delta x_F} \times \frac{1}{n_t} \times 10^4, \text{ mb}$$

Figure 198 shows the forward neutron production cross section vs variable x_F using p+p, p+Be and p+C interactions 58 GeV/c. The geometrical acceptance corrections were applied.

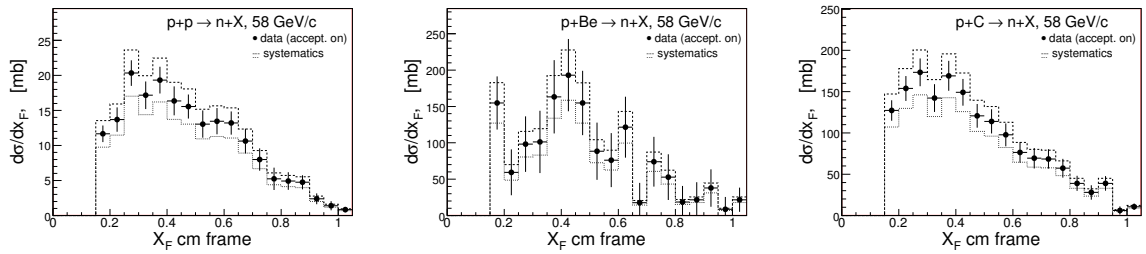

Figure 198: The forward neutron production cross section vs variable x_F using p+p (left), p+Be (middle) and p+C (right) interactions at 58 GeV/c. The geometrical acceptance corrections were applied.

Figure 199 shows the forward neutron production cross section vs variable x_F using p+Bi and p+U interactions at 58 GeV/c and p+p interactions at 84 GeV/c. The geometrical acceptance corrections were applied.

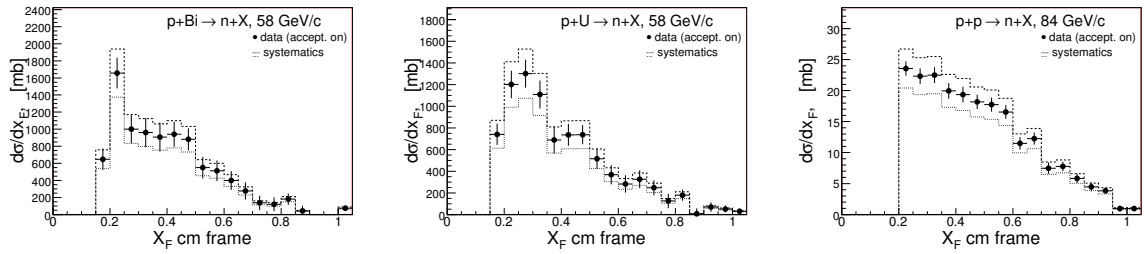

Figure 199: The forward neutron production cross section vs variable x_F using p+Bi (left) and p+U (middle) interactions at 58 GeV/c and p+p (right) interactions at 84 GeV/c. The geometrical acceptance corrections were applied.

Figure 200 shows the forward neutron production cross section vs variable x_F using p+Be, p+C and p+Bi interactions at 120 GeV/c. The geometrical acceptance corrections were applied.

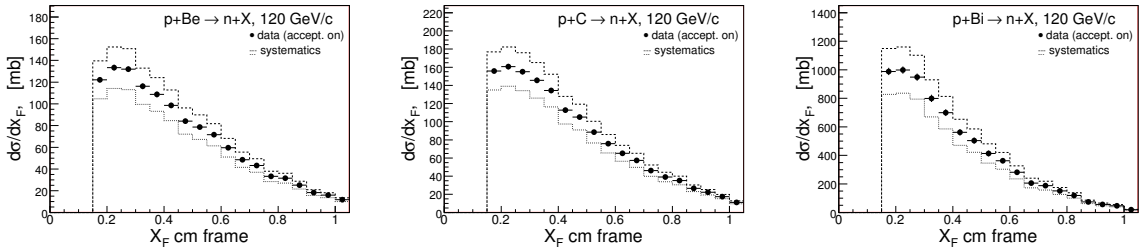

Figure 200: The forward neutron production cross section vs variable x_F using p+Be (left), p+C (center) and p+Bi (right) interactions at 120 GeV/c. The geometrical acceptance corrections were applied.

28.4.3 P_{beam} dependence for HCAL acceptance applied

Figure 201 shows the comparison of the forward neutron production cross section vs variable x_F for two P_{beam} momenta using p+p, p+C and p+Bi interactions. The geometrical acceptance corrections were applied.

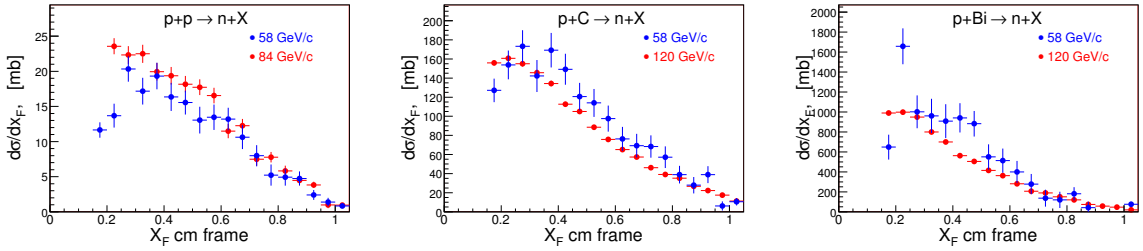

Figure 201: The comparison of the forward neutron production cross section vs variable x_F for two P_{beam} momenta using p+p, p+C and p+Bi interactions. The geometrical acceptance corrections were applied.

28.4.4 dn_n/dx_F distribution: HCAL acceptance applied

The dn_n/dx_F distribution allow to view the neutron yield per single proton-nucleon interaction, so A dependence is canceled. Then the results for different targets should be similar. The neutron yield per single pN interaction vs variable x_F was calculated as:

$$\frac{dn_n}{dx_F} = \frac{1}{\sigma_{inel}} \cdot \frac{d\sigma_n}{dx_F} = \frac{1}{\sigma_{inel}} \cdot \frac{N_n(t-in) - N_n(t-out)}{N_{beam} \cdot \epsilon_{scf} \cdot \epsilon_{hcal} \cdot \Delta x_F} \cdot \frac{1}{n_t} \cdot 10^4$$

Figure 202 shows the neutron yield distribution vs variable x_F using p+p, p+Be and p+C interactions at 58 GeV/c.

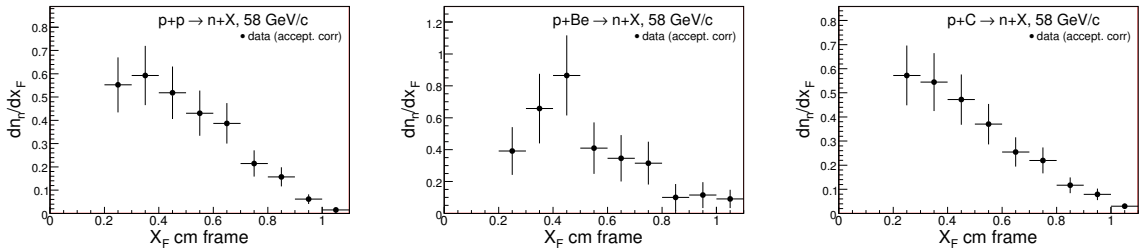

Figure 202: The neutron yield distribution vs variable x_F using p+p (left), p+Be (middle) and p+C (right) interactions at 58 GeV/c. The geometrical acceptance corrections were applied. The error bars represents both: statistical and systematical combined in quadrature.

Figure 203 shows the neutron yield distribution vs variable x_F using p+Bi and p+U at 58 GeV/c and p+p interactions at 84 GeV/c.

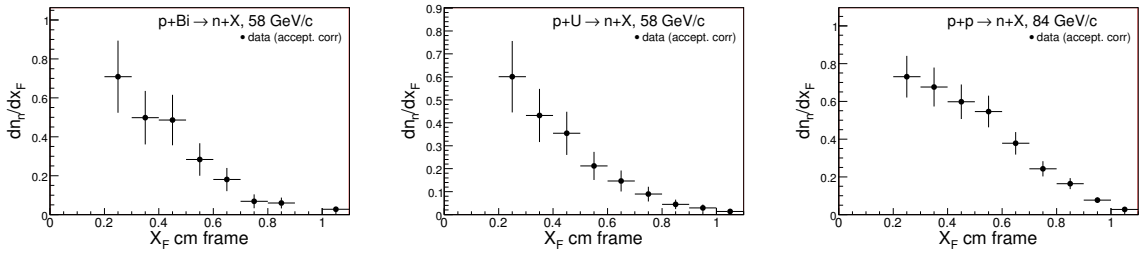

Figure 203: The neutron yield distribution vs variable x_F using p+Bi (left) and p+U (middle) at 58 GeV/c and p+p (right) interactions at 84 GeV/c. The geometrical acceptance corrections were applied. The error bars represents both: statistical and systematical combined in quadrature.

Figure 204 shows the neutron yield distribution vs variable x_F using p+Be, p+C and p+Bi interactions at 120 GeV/c.

Above used the σ_{inel} values are the same as in FLUKA, see Table 59.

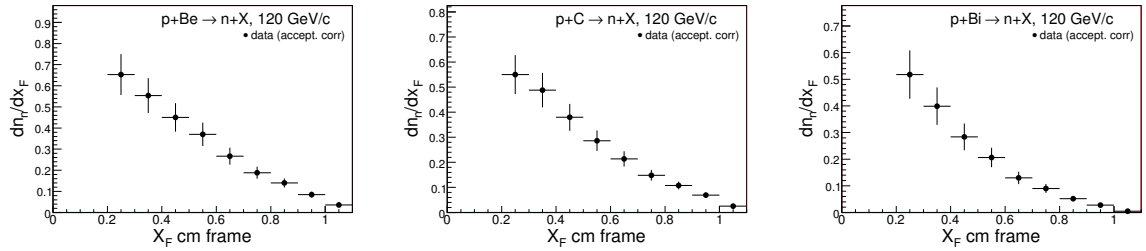

Figure 204: The neutron yield distribution vs variable x_F using p+Be (left), p+C (middle) and p+Bi (right) interactions at 120 GeV/c. The geometrical acceptance corrections were applied. The error bars represents both: statistical and systematical combined in quadrature.

	58 GeV/c	84 GeV/c	120 GeV/c
p+p	30.8	31.4	-
p+Be	201	-	203
p+C	286	-	287
p+Bi	1875	-	1880
p+U	2081	-	-

Table 59: The σ_{inel} values, mb, used to calculate above presented dn_n/dx_F distributions.

Figure 205 shows the neutron yield distribution vs variable x_F using p+p, p+Be and p+C interactions at 58 GeV/c.

The intergated values for dn/dx_F distributions are summarized in Table 60.

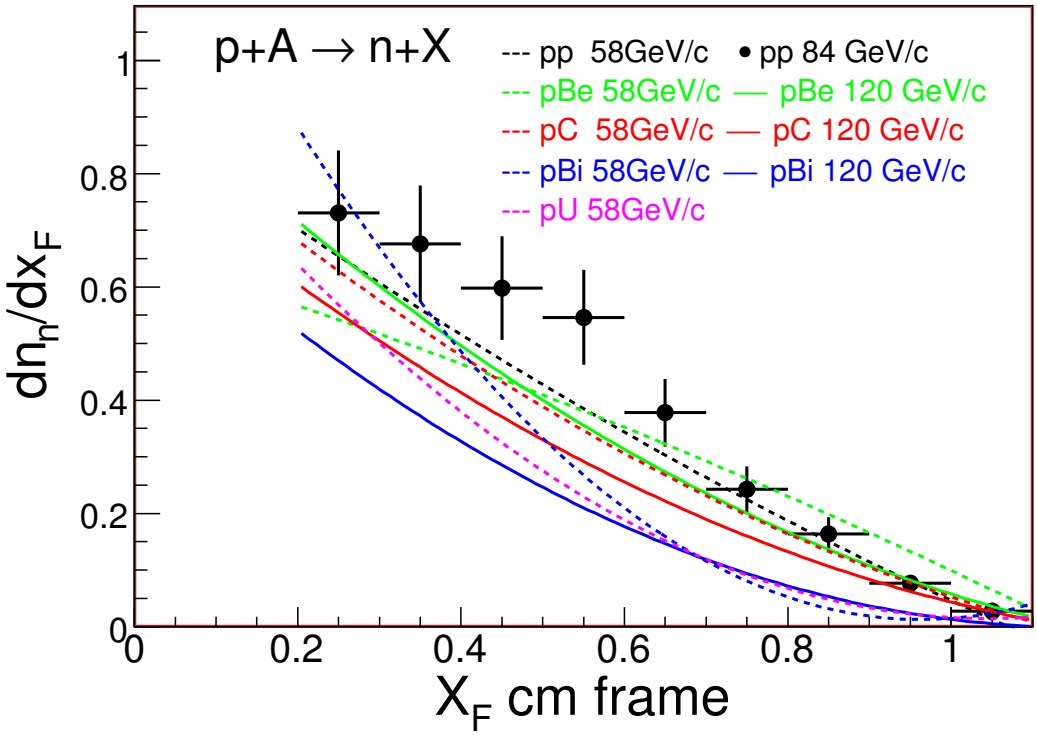

Figure 205: The dn_n/dx_F distributions. All available data are superimposed.

	$\int \frac{dn}{dx_F}$	Δ
H_2-58	2.93	0.59
Be-58	3.29	0.79
C-58	2.66	0.55
Bi-58	2.31	0.58
U-58	1.92	0.49
H_2-84	3.44	0.51
Be-120	2.74	0.41
C-120	2.27	0.32
Bi-120	1.71	0.30

Table 60: The intergated value for dn/dx_F distributions.

28.4.5 Comparison with NA49 results

NA49 experiment [2] performed the neutron production measurements from pp interactions at 158 GeV/c. The results were presented as dn_n/dx_F distribution:

$\frac{dn_n}{dx_F} = \frac{\pi}{\sigma_{inel}} \cdot \frac{\sqrt{s}}{2} \cdot \int \frac{f}{E} \cdot dp_T^2$, where $f = \mathrm{E}\frac{d^3\sigma}{dp^3} = \pi \mathrm{E}\frac{d^3\sigma}{dp_T^2 dp_{\|}}$ is invariant cross section

Figure 206 shows the dn_n/dx_F distributions using p+p at 58 GeV/c and p+p interactions at 84 GeV/c. The neutron yield was calculated without acceptance correction applied. NA49 results are superimposed

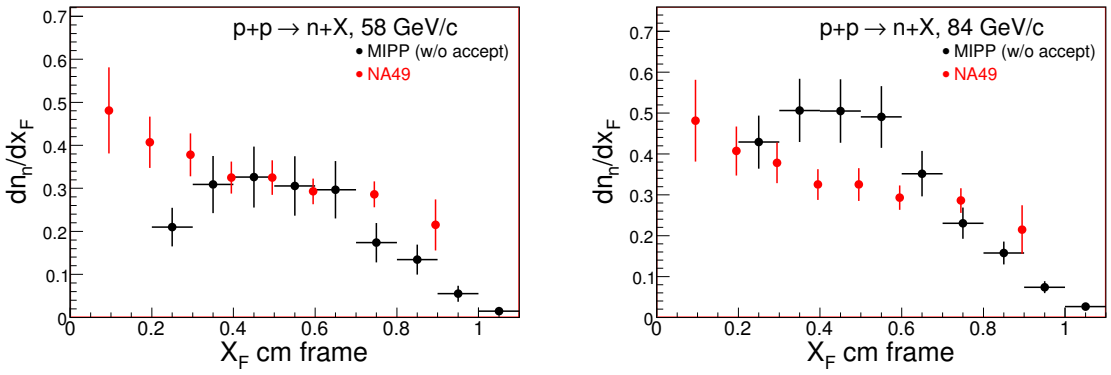

Figure 206: The dn_n/dx_F distributions for neutrons using p+p at 58 GeV/c (left) and p+p interactions at 84 GeV/c (right). The neutron yield was calculated without HCAL acceptance correction applied. NA49 results are superimposed

Plots for the case, when the HCAL acceptance correction applied, are shown in Figure 207.

Figure 208 illustrates the expected NA49 calorimeter's acceptance.

Figure 209 illustrates the expected NA49 calorimeter's acceptance.

We can compare NA49 results for protons with our Monte Carlo proton distribution, see Figure 210.

Comparison of NA49 results for protons with FLUKA proton distributions using the nuclear targets are shown in Figure 211.

Figure 212 illustrates NA49 dn/dx_F distributions for the inclusive production of π^+, π^- and $\bar{p}$.

Figure 213 illustrates NA49 neutron distributions.

Figure 214 illustrates the comparison with other experiments.

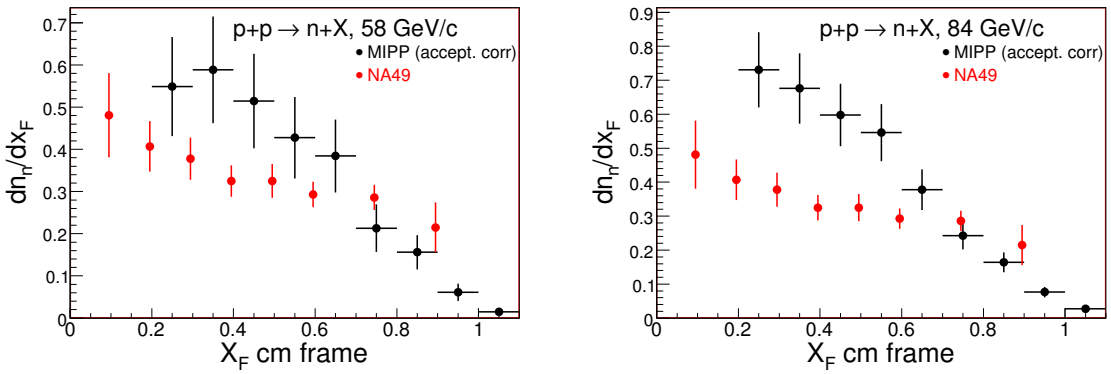

Figure 207: The dn_n/dx_F distributions for neutrons using p+p at 58 GeV/c (left) and p+p interactions at 84 GeV/c (right). The HCAL acceptance correction applied. NA49 results are superimposed

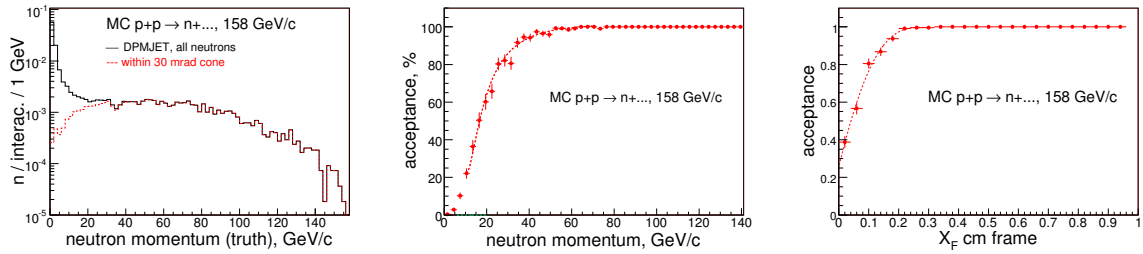

Figure 208: The expected NA49 neutron spectrum (left) and calorimeter's acceptance estimate using a special MC. In these calculations the NA49 calorimeter's an angular coverage assumed to be 30 mrad cone in forward direction.

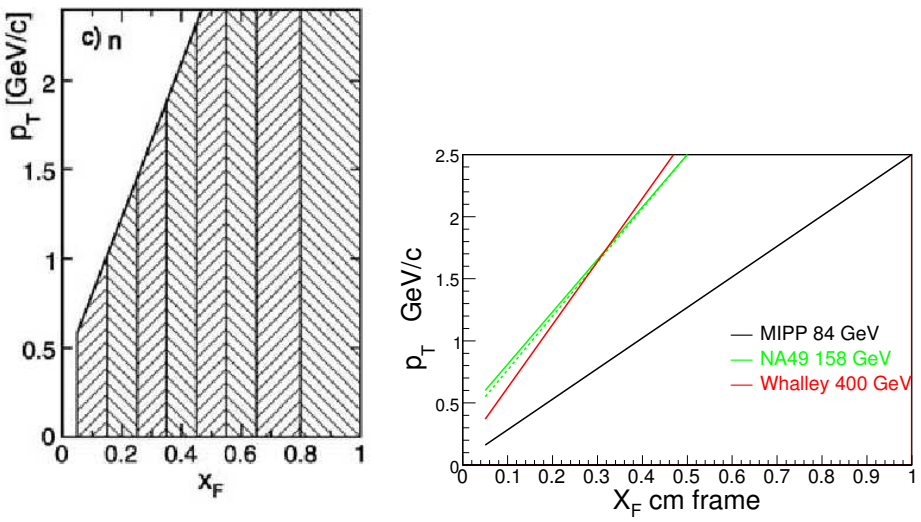

Figure 209: NA49 p_T vs X_F acceptance (left) and similar plot for the other experiments (right).

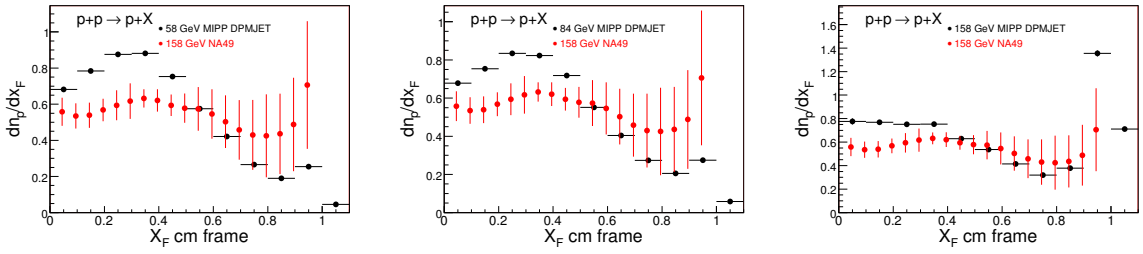

Figure 210: The dn_p/dx_F distributions for Monte Carlo protons using p+p at 58 GeV/c (left), at GeV/c (middle) and at 158 GeV/c (right). Reconstructed track was identified as proton using MC truth info. The calorimeter fiducial not required. NA49 results are superimposed

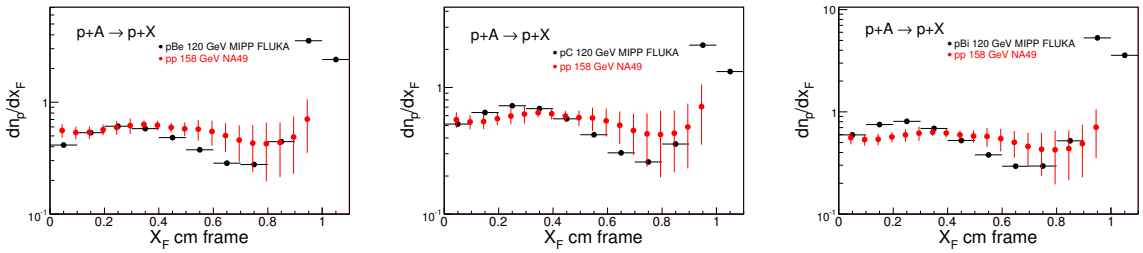

Figure 211: The dn_p/dx_F distributions for FLUKA protons using p+Be (left), p+C (middle) and p+Bi (right) at 120 GeV/c. Reconstructed track was identified as proton using MC truth info. There are no any cuts downstream of the target were applied. The calorimeter fiducial not required. NA49 results are superimposed

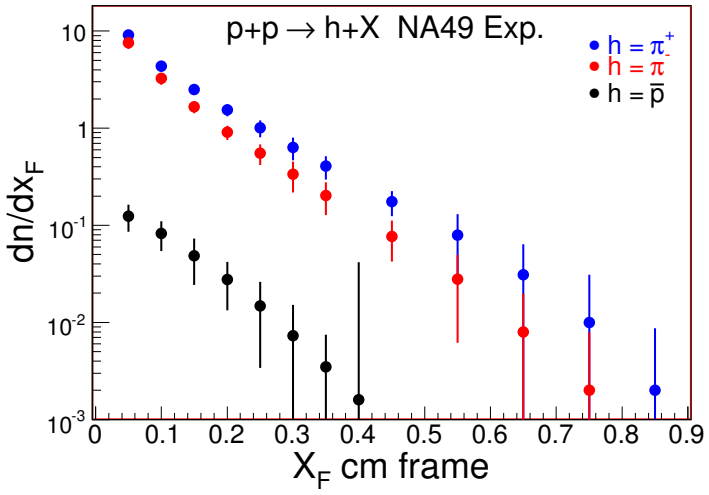

Figure 212: The dn_p/dx_F distributions for the inclusive production of π^+, π^- and $\bar{p}$ measured by NA49 experiment. This gives an answer to the question: "Should neutron distribution be a flat or declining?".

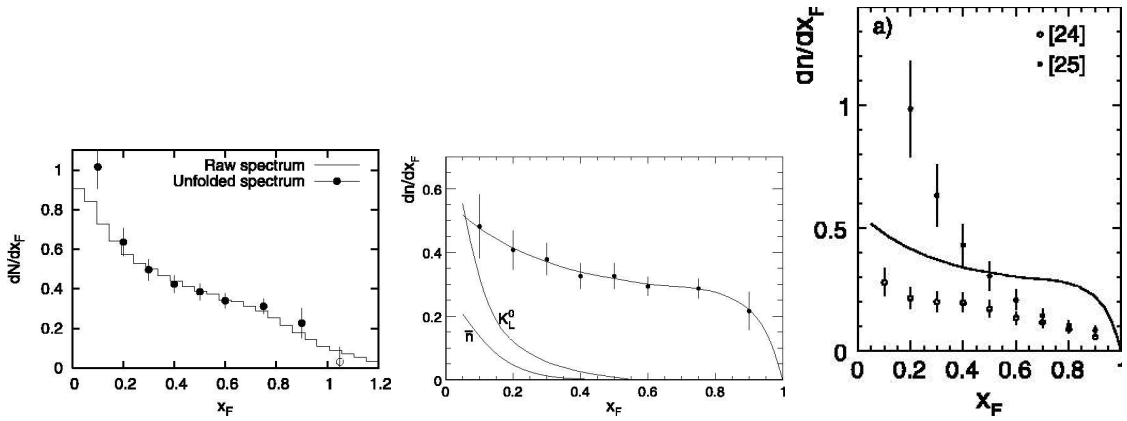

Figure 213: NA49 neutron related plots copied from Eur.Phys.J.C (2010)65:9-63. LEFT: same as Fig.7 - Raw measured energy distribution of neutrons compare with the unfolded neutron distribution. The increase of the latter at x_F <0.1 is due to reduction in transverse acceptance. *The open circle* indicates the consistency of the unfolded spectra with zero beyond the kinematic limit. MIDDLE: same as Fig.63 - p_T integrated density distribution dn/dx_F as a function of x_F of neutron produced in p+p interactions at 158 GeV/c. The subtracted K^o_L and anti-neutron distributions are also shown. RIGHT: same as Fig.66a - Comparison as a function of x_F of the NA49 results on neutron density with ISR [8] and Fermilab [9] measurements, the full line is NA49.

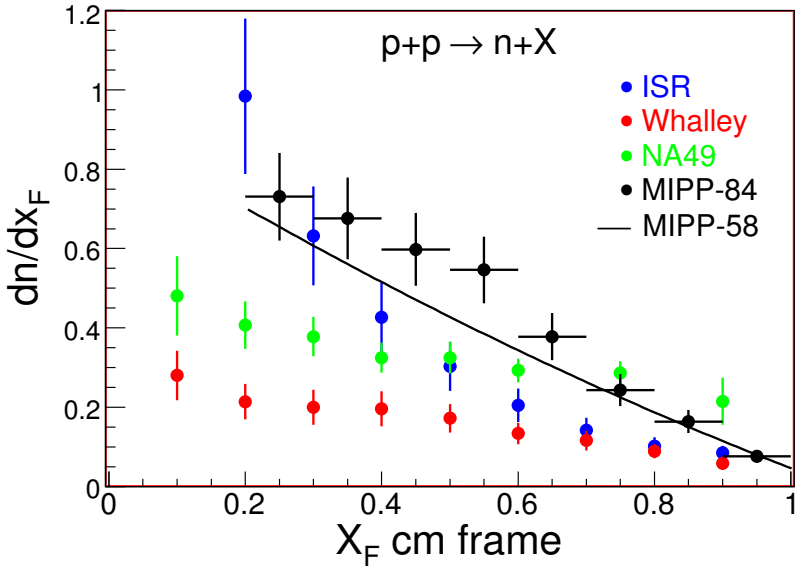

Figure 214: Comparison with other experiments. Our results were superimposed onto the right plot of Fig. 213

28.4.6 Invariant cross section

The invariant inclusive neutron production cross section as the function of variable x_F was calculated as:

$$\frac{E}{p^2\Omega}\frac{d\sigma}{dp} = \frac{E}{p^2\Omega} \times \frac{N_n(t-in)-N_n(t-out)}{N_{beam}\times\epsilon_{scf}\times\Delta p} \times \frac{1}{n_t} \times 10^4, \text{ mb/(GeV/c)/sr},$$

above formula is the same as described in section 28.3

Figure 215 shows the forward neutron production invariant cross section for p+p, p+Be and p+C interactions at 58 GeV/c as the function of variable x_F.

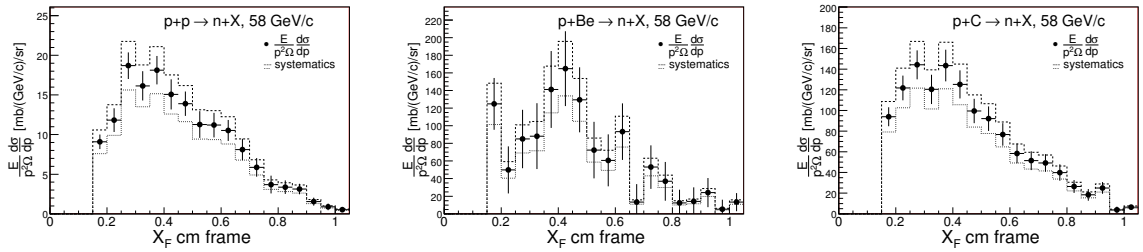

Figure 215: The neutron invariant cross section for p+p (left), p+Be (middle) and p+C (right) interactions at 58 GeV/c as the function of variable x_F.

Figure 216 shows the forward neutron production cross section for p+Bi and p+U interactions at 58 GeV/c and p+p interactions at 84 GeV/c as the function of variable x_F.

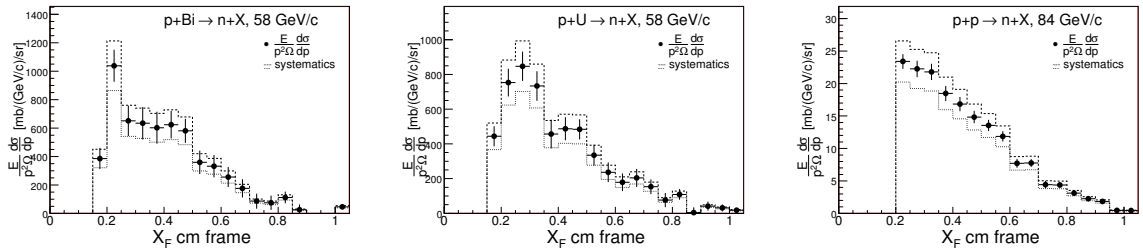

Figure 216: The neutron invariant cross section for p+Bi (left) and p+U (middle) interactions at 58 GeV/c and p+p (right) interactions at 84 GeV/cas the function of variable x_F.

Figure 217 shows the forward neutron production cross section for p+Be, p+C and p+Bi interactions at 120 GeV/c as the function of variable x_F.

28.4.7 P_{beam} dependence for the invariant cross section

Figure 218 shows the comparison of neutron invariant cross section vs variable x_F for two P_{beam} momenta using p+p, p+C and p+Bi interactions.

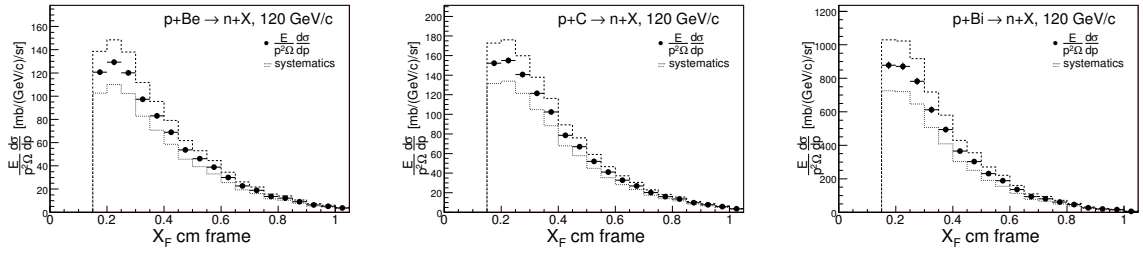

Figure 217: The neutron invariant cross section for p+Be (left), p+C (middle) and p+Bi(right) interactions at 120 GeV/c as the function of variable x_F.

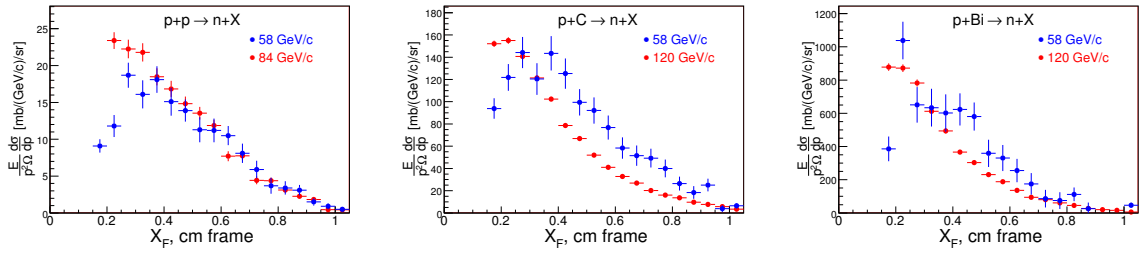

Figure 218: The comparison of the neutron invariant cross section vs variable x_F for two P_{beam} momenta using p+p, p+C and p+Bi interactions.

29 Neutron Angular Distribution

29.1 Measurements with data

The neutron angular measurements using data is based on the unmatched shower position at EMCAL. All events passed the neutron selection requirements.

The angular distributions of the neutrons from the Be and C targets at 58 GeV/c are shown in Figure 219.

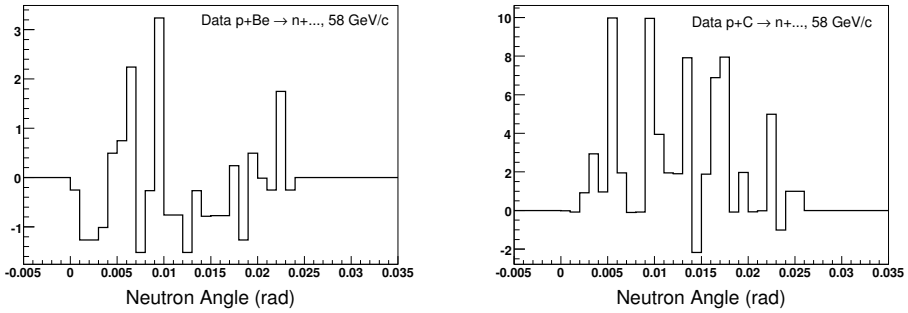

Figure 219: The neutron angular distributions from the Be and C targets at 58 GeV/c. The neutron angular measurements using data is based on the unmatched shower position at EMCAL. All events passed the neutron selection requirements.

The angular distributions of the neutrons from the Bi and U targets at 58 GeV/c are shown in Figure 220.

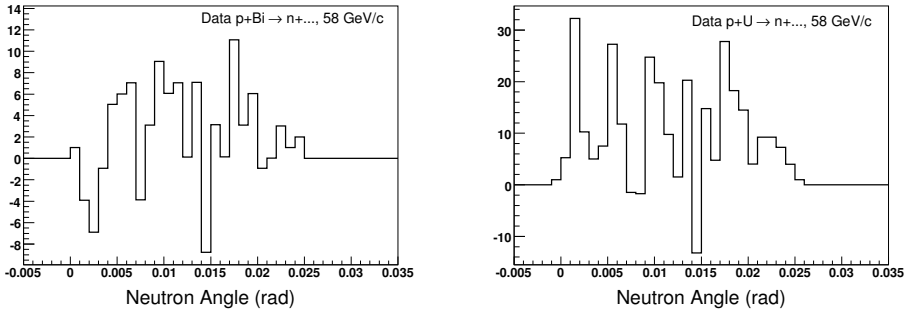

Figure 220: The neutron angular distributions from the Bi and U targets at 58 GeV/c. The neutron angular measurements using data is based on the unmatched shower position at EMCAL. All events passed the neutron selection requirements.

The angular distributions for the liquid hydrogen, 58 and 84 GeV/c momenta (on left), and thin targets at 120 GeV/c (on right) are shown in Figure 221.

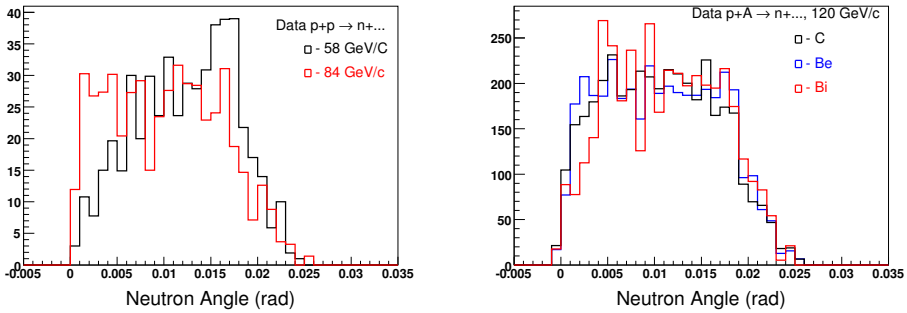

Figure 221: The neutron angular distributions for the liquid hydrogen target at 58 and 84 GeV/c (on left) and Be, C and Bi targets at 120 GeV/c (on right). The neutron angular measurements using data is based on the unmatched shower position at EMCAL. All events passed the neutron selection requirements. All distributions are brought to the same area size.

29.2 Neutron angle: data vs Monte Carlo

Below we will compare the neutron angular distributions from data with Monte Carlo. The angular distributions of the neutrons from Be, C and Bi targets at 120 GeV/c proton beam momentum are shown in Figure 222.

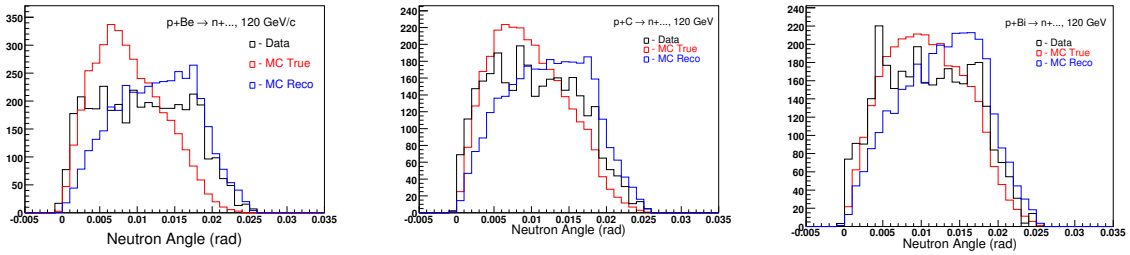

Figure 222: The neutron angular distributions for data and MC superimposed: from p+Be (left), p+C (middle) and p+Bi (right) interactions, respectively. The proton beam momentum is 120 GeV/c.

The neutron angular distributions, true vs reco MC comparison, from p+C and p+Bi interactions at 120 GeV/c are shown in Figure 223.

Unmatched shower position distributions in X-view from p+C and p+Bi interactions at 120 GeV/c are shown in Figure 224.

Unmatched shower position distributions in Y-view from p+C and p+Bi interactions at 120 GeV/c are shown in Figure 225.

Unmatched shower width distributions in X-view from p+C and p+Bi interactions at 120 GeV/c are shown in Figure 226.

Unmatched shower width distributions in Y-view from p+C and p+Bi interactions

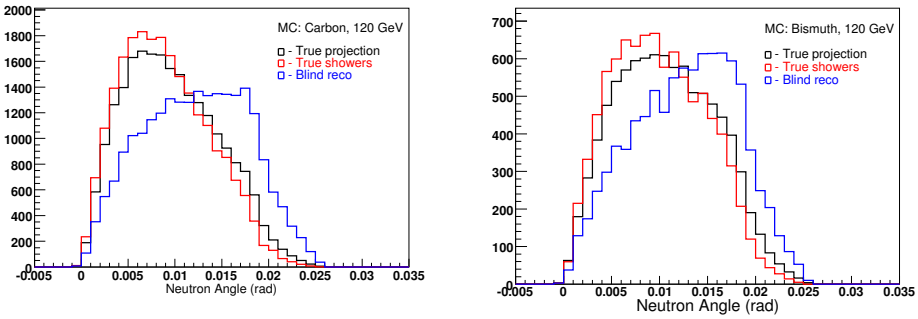

Figure 223: The neutron angular distributions, true vs reco MC comparison, from p+C and p+Bi interactions at 120 GeV/c. Fraction of neutrons that have a shower matched with projection = 23%.

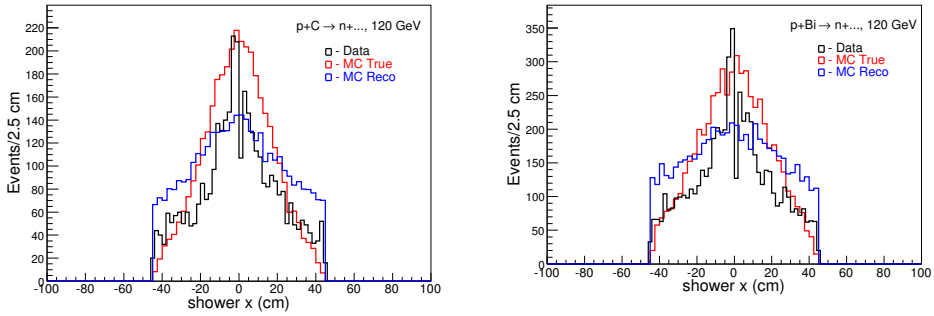

Figure 224: Unmatched shower position distributions in X-view from p+C and p+Bi interactions at 120 GeV/c

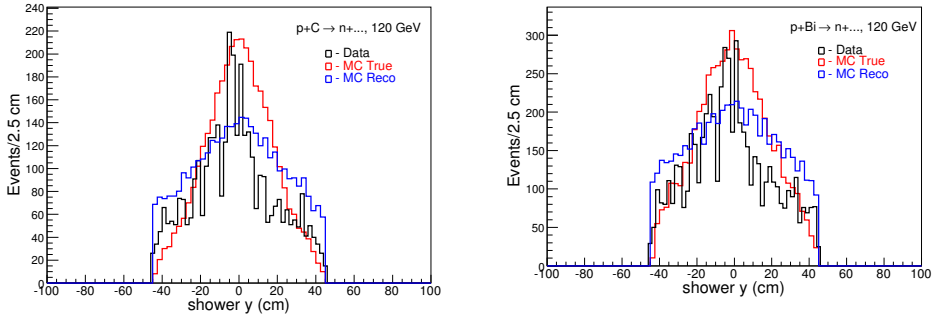

Figure 225: Unmatched shower position distributions in Y-view from p+C and p+Bi interactions at 120 GeV/c

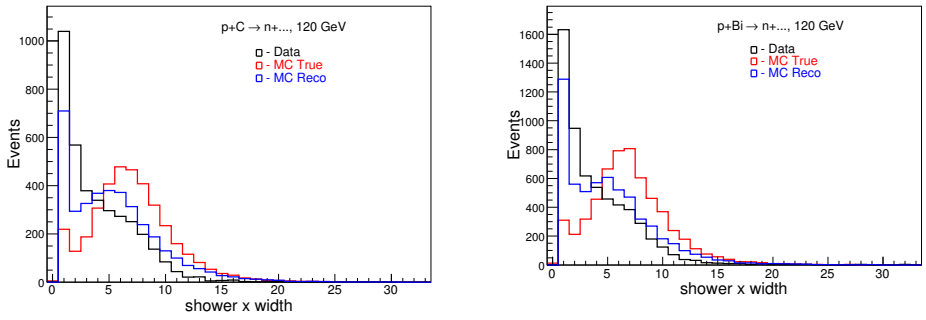

Figure 226: Unmatched shower width distributions in X-view from p+C and p+Bi interactions at 120 GeV/c

at 120 GeV/c are shown in Figure 227.

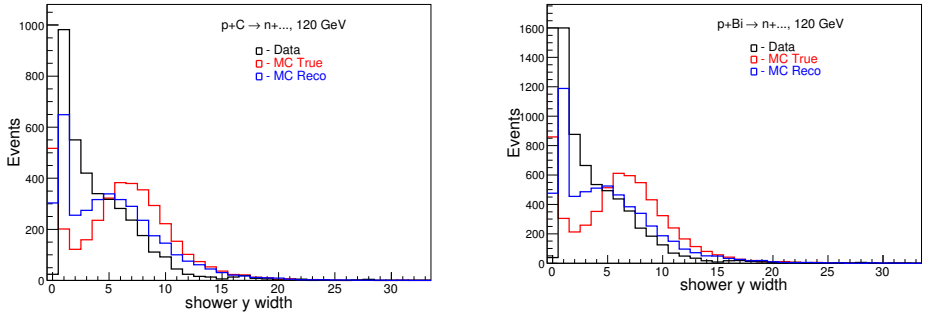

Figure 227: Unmatched shower width distributions in Y-view from p+C and p+Bi interactions at 120 GeV/c

Unmatched shower energy fractions, EMCAL/HCAL ratio, distributions from p+C and p+Bi interactions at 120 GeV/c are shown in Figure 228.

Unmatched shower energy fractions, EMCAL/HCAL ratio, distributions from p+C and p+Bi interactions at 120 GeV/c are shown in Figure 229.

Unmatched shower longitudinal profile in EMCal from p+C and p+Bi interactions at 120 GeV/c are shown in Figure 230.

30 Conclusion

We have performed...

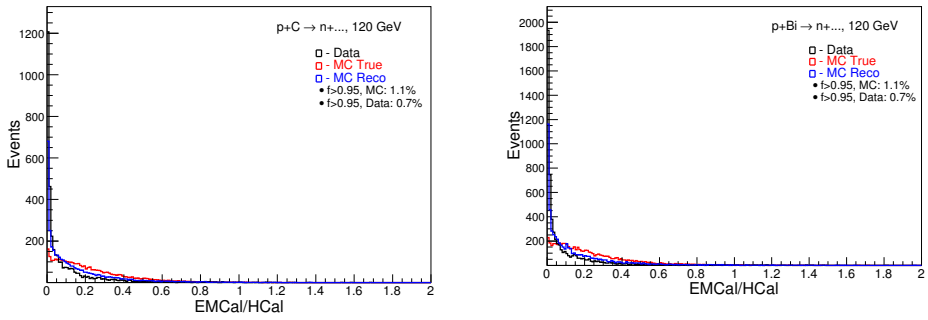

Figure 228: Unmatched shower energy fractions, EMCAL/HCAL ratio, distributions from p+C and p+Bi interactions at 120 GeV/c

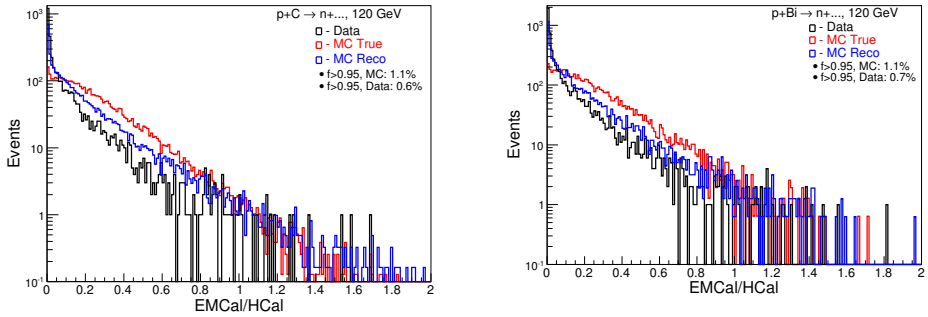

Figure 229: Unmatched shower energy fractions, EMCAL/HCAL ratio, distributions from p+C and p+Bi interactions at 120 GeV/c

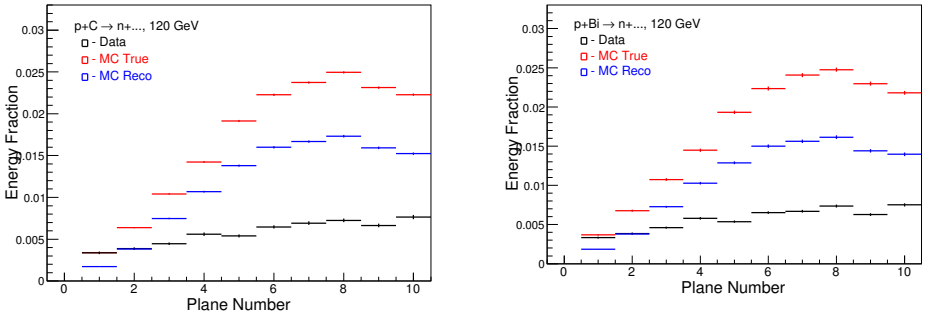

Figure 230: Unmatched shower longitudinal profile in EMCal from p+C and p+Bi interactions at 120 GeV/c

References

[1] T.S.Nigmanov et al. Electromagnetic and Hadron calorimeters in the MIPP experiment. NIM A 598 (2009) 394-399.

[2] T.Anticic at al. Inclusive production of protons, anti-protons and neutrons in p+p collisions at 158 GeV/c beam momentum. The NA49 Collaboration. Eur.Phys.J.C(2010)65: 9-63 and arXiv:0904.2708v1 [hep-ex] 17 Apr 2009.

[3] Holger Meyer, MIPP software analysis meeting 3-27-09, page 8

[4] Jon Paley, MIPP software library - add summaries of unmatched segment tracks to DST., Dec., 2008.

[5] K.K. Gudima, S.G. Mashnik, and A.J. Sierk, User Manual for the Code LAQGSM, LANL Report LA-UR-01-6804, Los Alamos, 2001.

[6] S.G. Mashnik, K.K. Gudima, R.E. Prael, A.J. Sierk, M.I. Baznat, and N.V. Mokhov, EM03.03 and LAQGSM03.03 Event Generators for the MCNP6, MCNPX, and MARS15 Transport Codes,Invited lectures presented at the Joint ICTP-IAEA Advanced Workshop on Model Codes for Spallation Reactions, February 4, 2008, ICTP, Trieste, Italy, LA-UR-08-2931, Los Alamos (2008); E-print: arXiv:0805.0751v2 [nucl-th]; IAEA Report INDC(NDS)-0530, Distr. SC, Vienna, Austria, August 2008, p.51.

[7] S.G. Mashnik, K.K. Gudima, N.V. Mokhov, and R.E. Prael, AQGSM03.03 Upgrade and Its Validation,LANL Research Note X-3-RN(U)07-15, August 27, 2007; LANL Report LA-UR-07-6198, E-print: arXiv:0709.173.

[8] J.Engler et al. Nucl.Phys.B 84, 70(1975)

[9] M.R.Whalley. UM HE, 79-14 (1979)

Appendix

A Transverse position cut for the liquid hydrogen data

Figure 231 shows the longitudinal vertex position distributions for the interactions with the empty cryo target using π, K and p beam and interaction triggers.

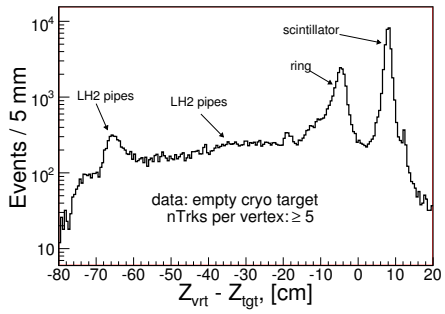

Figure 231: The longitudinal vertex position distributions for the interactions with the empty cryo target using π, K and p beam and interaction triggers

Figure 232 shows the transverse vertex position distributions for the interactions with the empty cryo target using π, K and p beam and interaction triggers.

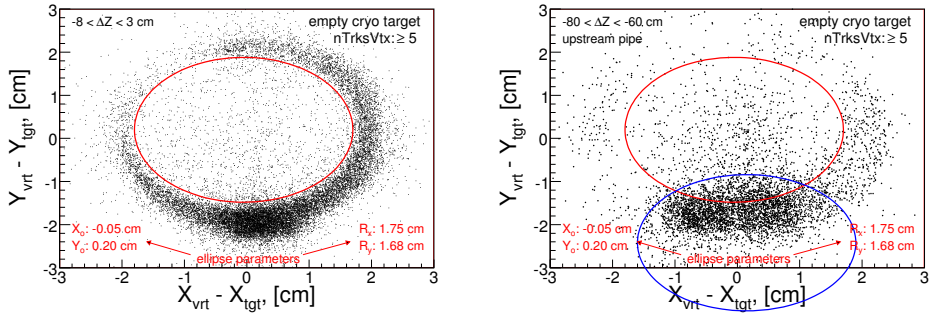

Figure 232: The transverse vertex position distributions for the interactions with the empty cryo target using π, K and p beam and interaction triggers. Plots made with different ΔZ_{vtx} cuts: -8< ΔZ_{vtx} <3 cm for the left plot which reflects the transverse slice of the hydrogen flask and -80< ΔZ_{vtx} <-60 cm for the right plot which represents the transverse slice at region of where a most upstream location of the transport pipes is appears to be close to the beam line.

Left plot on Figure 232 allow to see the interactions with the supporting aluminum(?) ring which holds the target flask. An ellipse (red circle) illustrates the

area which can be account as a liquid hydrogen volume. Right plot indicates that the liquid hydrogen transport pipes some how entering to the liquid hydrogen volume, see an overlapped area by both ellipses. The beam track transverse position cut would be: use those data points which is within the red ellipse and NOT within blue one.

The beam transverse positions at Z=Z_{tgt} shown in Figure 233 for 58 GeV/c liquid hydrogen and empty cryo target data. The red lines show what was selected as hydrogen flask center in horizontal and vertical plane, respectively. Their were defined from the empty cryo studies.

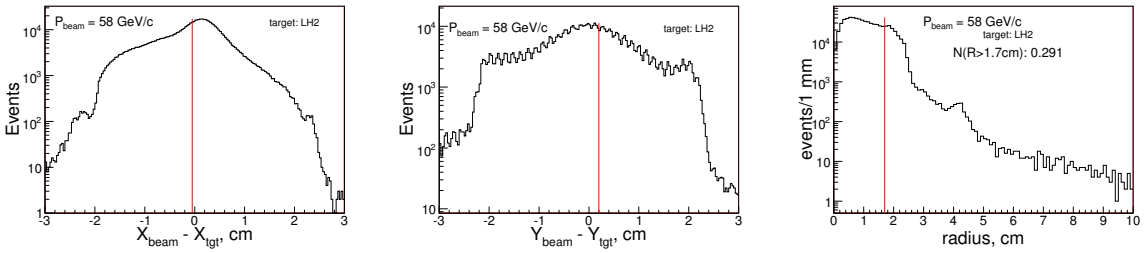

Figure 233: The beam track position distributions at Z of liquid hydrogen target center using 58 GeV/c particles. The red lines on left and in middle plots illustrate the horizontal and vertical centers of hydrogen flask. The right plot shows the distance between target center and the position of the particle distribution. The red line there shows the ellipse radius cut position.

B Calorimeter's Energy Scale in data

B.1 Projected neutron energy losses in EMCAL

The projected neutron energy losses in EMCAL was estimated with an assumption that it is the same as proton losses. Figure 234 shows the proton energy losses in calorimeters and momentum distribution of 20 GeV/c beam tracks.

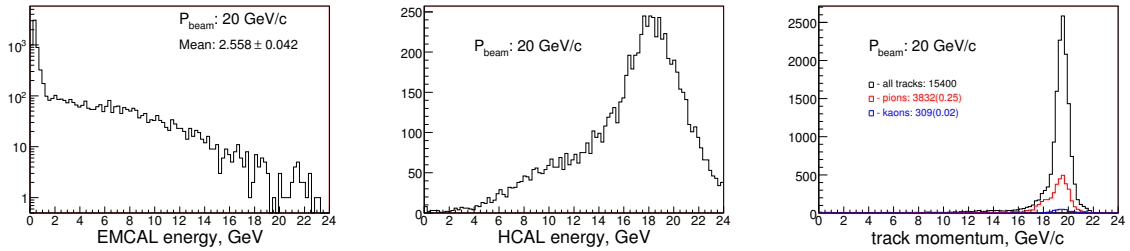

Figure 234: The proton energy losses in calorimeters and momentum distribution of 20 GeV/c beam tracks. Requirements: proton beam trigger, single track, LH2 target. The track momentum plot (left) shows the pion (red) and kaon (blue) contamination in proton beam which was identified by RICH detector.

Figure 235 shows the proton energy losses in calorimeters and momentum distribution of 58 GeV/c beam tracks.

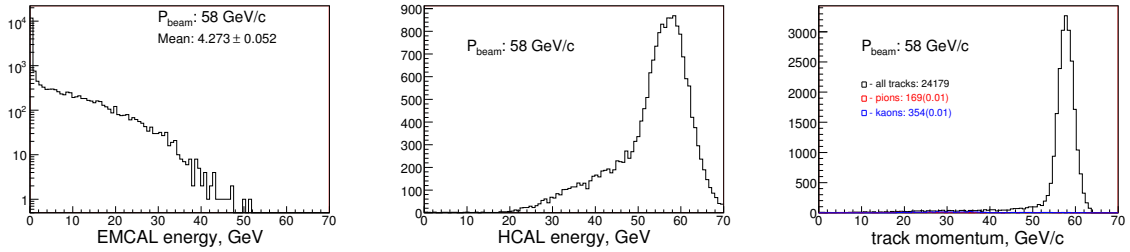

Figure 235: The proton energy losses in calorimeters and momentum distribution of 58 GeV/c beam tracks. Requirements: proton beam trigger, single track, U target

Figure 236 shows the proton energy losses in calorimeters and momentum distribution of 84 GeV/c beam tracks.

Figure 237 shows the proton energy losses in calorimeters and momentum distribution of 120 GeV/c beam tracks.

Figure 238 shows the proton energy mean losses in EMCAL as the function of the proton momentum.

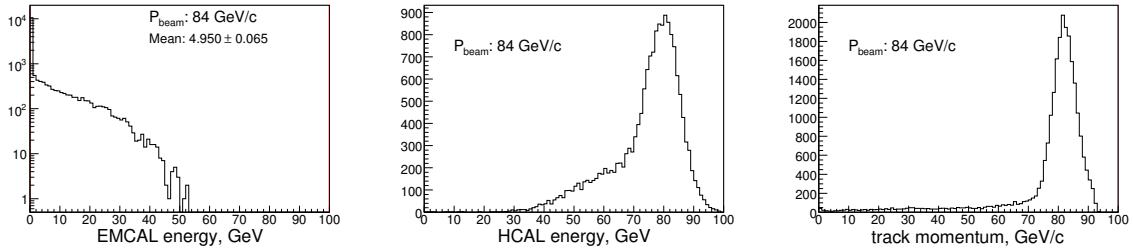

Figure 236: The proton energy losses in calorimeters and momentum distribution of 84 GeV/c beam tracks. Requirements: proton beam trigger, single track, LH2 target

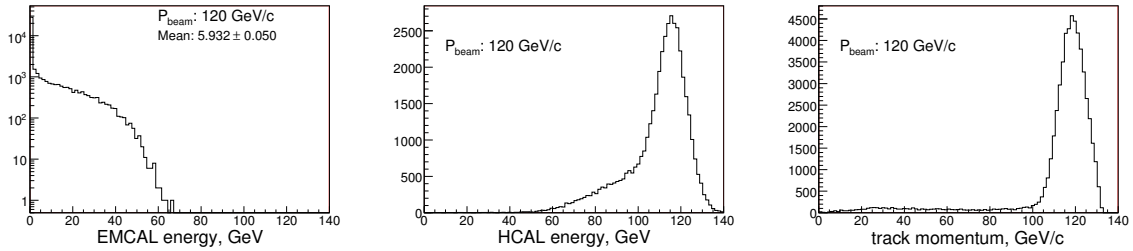

Figure 237: The proton energy losses in calorimeters and momentum distribution of 120 GeV/c beam tracks. Requirements: proton beam trigger, single track, Bi target

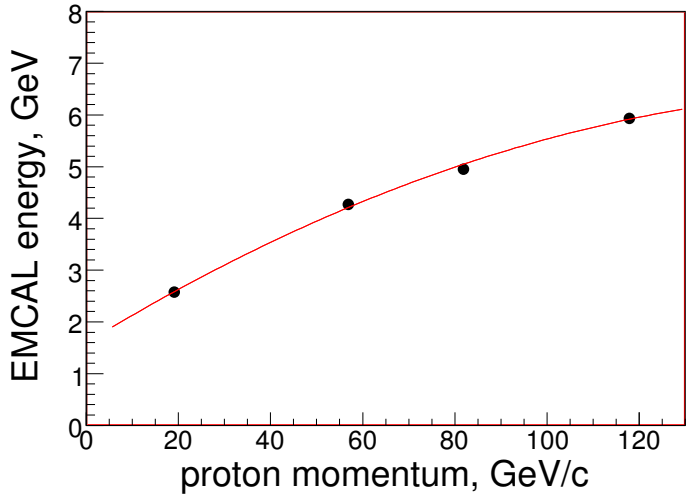

Figure 238: The proton energy mean losses in EMCAL as the function of the proton momentum. Red curve is fit with 2-nd order polynomial. Fit parameters: a free parameter is 1.60±0.08, linear term is 0.055±0.003 and quadratic term is -0.00015±0.00002.

B.2 How well the Calorimeter's energy scale?

How well the neutron/calorimeters energy scale was tuned can be viewed through the E_{e+h}/p_{trk} ratio. If tuning was done correctly, then this ratio would be equal to 1. Figure 239 shows the E_{e+h}/p_{trk} ratio distributions for 20 and 58 GeV/c proton beams.

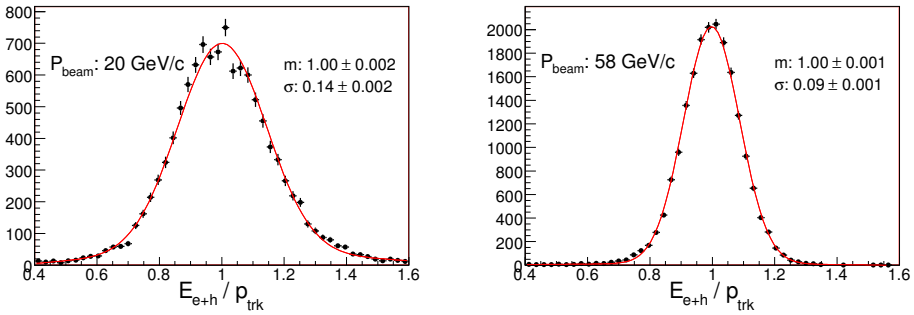

Figure 239: The E_{e+h}/p_{trk} ratio distributions for 20 and 58 GeV/c proton beams. The captions in plots indicates that the mean values of the E_{e+h}/p_{trk} are equal to 1 within given uncertainties.

Figure 240 shows the E_{e+h}/p_{trk} ratio distributions for 84 and 120 GeV/c proton beams.

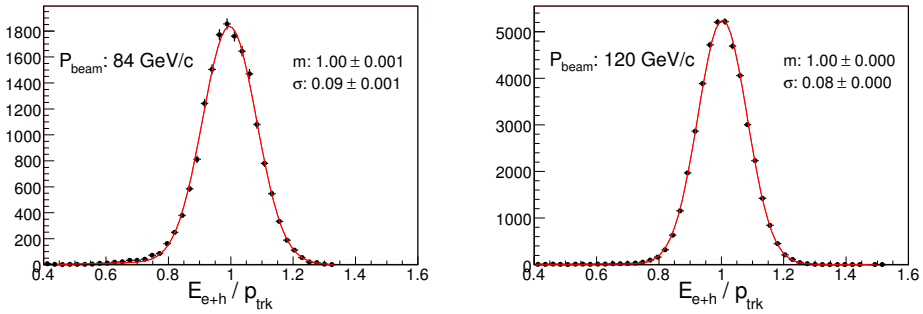

Figure 240: The E_{e+h}/p_{trk} ratio distributions for 84 and 120 GeV/c proton beams. The captions in plots indicates that the mean values of the E_{e+h}/p_{trk} are equal to 1 within given uncertainties.

B.3 Pion contamination in proton beam triggers

The track momentum plot on 20 GeV/c data shows about 25% of pion contamination in proton beam which was identified by RICH detector, see Figure 234. What the beam Cerenkov detectors tells about the pions?

C Calorimeter's energy scale in MC

C.1 Updated EMCal gas material

Figure 241 shows the EMCal and HCAL responses and E_{e+h}/E_p ratio distribution for the beam momentum protons both data and MC using pC interactions at 58 GeV/c. EMCal gas material in MC has been updated.

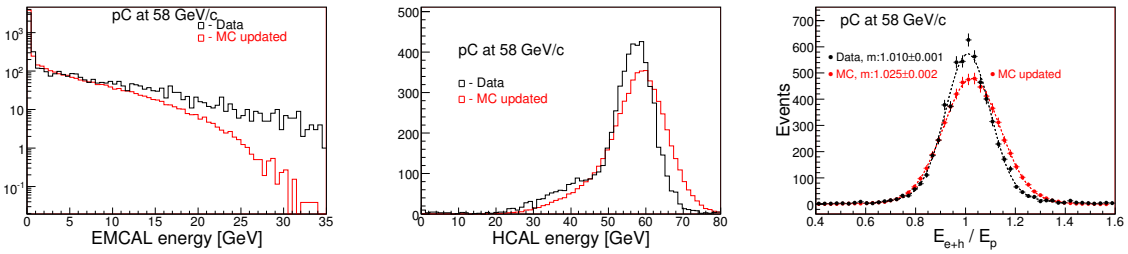

Figure 241: The EMCal and HCAL responses and E_{e+h}/E_p ratio distribution for the beam momentum protons both data and MC using pC interactions at 58 GeV/c. EMCal gas material in MC has been updated.

Figure 242 shows the EMCal and HCAL responses and E_{e+h}/E_p ratio distribution for the beam momentum protons both data and MC using pC interactions at 120 GeV/c. EMCal gas material in MC has been updated.

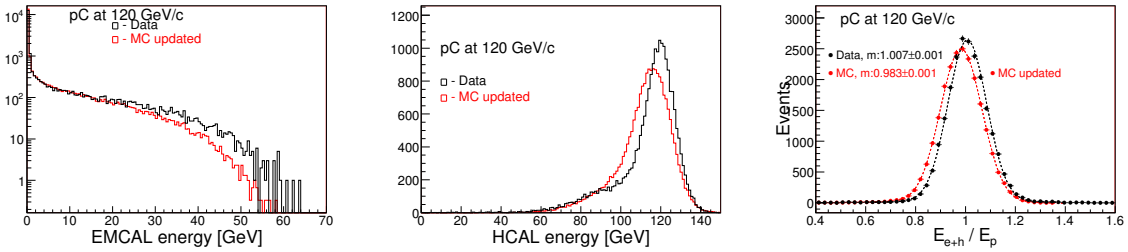

Figure 242: The EMCal and HCAL responses and E_{e+h}/E_p ratio distribution for the beam momentum protons both data and MC using pC interactions at 120 GeV/c. EMCal gas material in MC has been updated.

C.2 With previous EMCal gas material assignment

Figure 243 shows the EMCal and HCAL responses and E_{e+h}/E_p ratio distribution for the beam momentum protons both data and MC using pC interactions at 58 GeV/c. Previous EMCal gas material assignment.

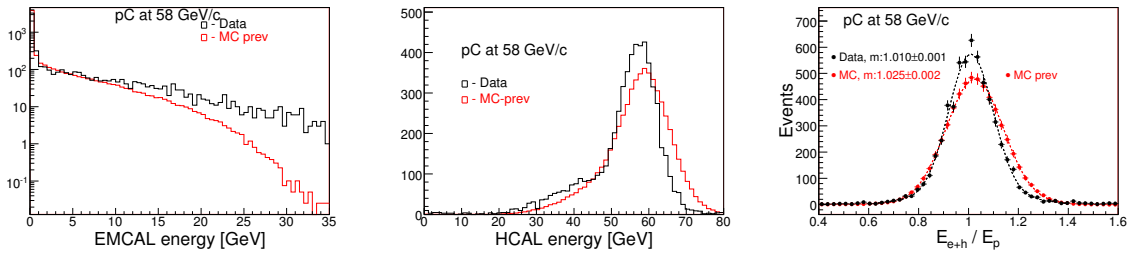

Figure 243: The EMCal and HCAL responses and E_{e+h}/E_p ratio distribution for the beam momentum protons both data and MC using pC interactions at 58 GeV/c. Previous EMCal gas material assignment.

Figure 244 shows the EMCal and HCAL responses and E_{e+h}/E_p ratio distribution for the beam momentum protons both data and MC using pC interactions at 120 GeV/c. Previous EMCal gas material assignment

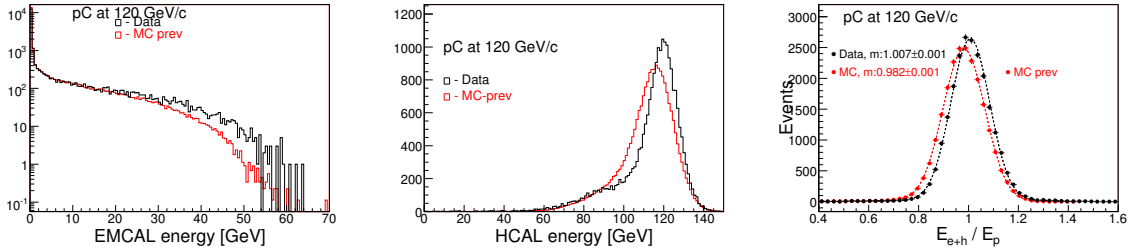

Figure 244: The EMCal and HCAL responses and E_{e+h}/E_p ratio distribution for the beam momentum protons both data and MC using pC interactions at 120 GeV/c. Previous EMCal gas material assignment

Table 61 summarizes the calorimeter's energy scale for previous and updated versions of Monte Carlo.

	previous MC	updated MC
C-58 GeV/c	+0.025	+0.025
C-120 GeV/c	-0.018	-0.017

Table 61: Summary of the calorimeter's energy scale offsets for previous and updated versions of Monte Carlo.

Figure 245 shows the E_{e+h}/E_p ratio distributions with MC HCAL energy scale corrected. Updated EMCal gas material assignment.

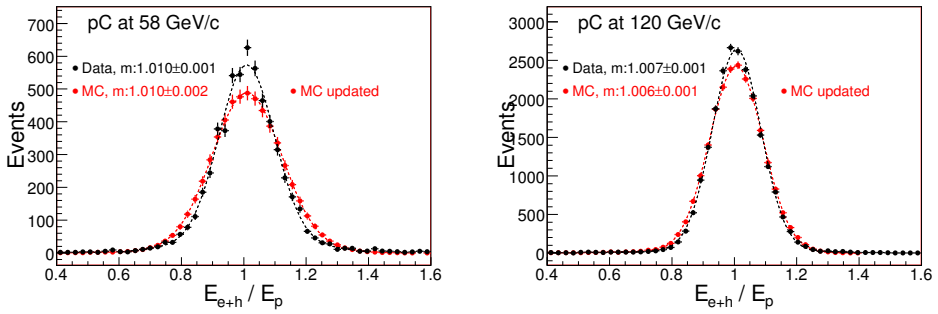

Figure 245: E_{e+h}/E_p ratio distributions with MC HCAL energy scale corrected. Updated EMCal gas material assignment.

D Track Multiplicity for Data: proton interactions

The trigger efficiency is a function depending on the track multiplicity and the trigger scintillator acceptance. Due to of that we will consider the multiplicity for those tracks, which passed through the scintillator.

Below we present the charged track multiplicity for different targets and beam momenta using the transverse momentum cut as Δp_T >0.15 GeV/c. Figure 246 shows the charged track multiplicity for p+p interactions at 58 GeV/c for both target-in and target-out (on left) and the case when target-out subtraction is applied (on right).

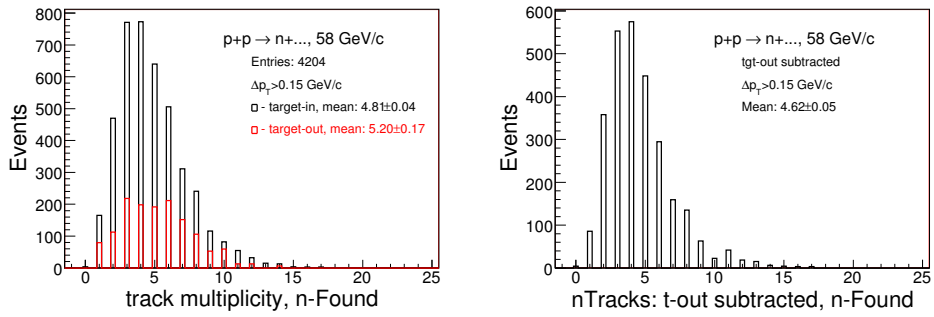

Figure 246: The charged track multiplicity for p+p interactions at 58 GeV/c for both target-in and target-out (on left) and the case when target-out subtraction is applied (on right). Requirements: all events passed the neutron selection cuts.

Figure 247 shows the charged track multiplicity for p+Be interactions at 58 GeV/c for both target-in and target-out (on left) and the case when target-out subtraction is applied (on right).

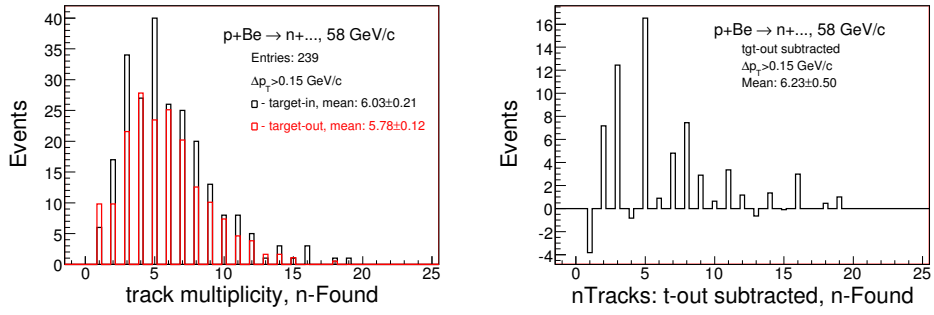

Figure 247: The charged track multiplicity for p+Be interactions at 58 GeV/c for both target-in and target-out (on left) and the case when target-out subtraction is applied (on right). Requirements: all events passed the neutron selection cuts.

Figure 248 shows the charged track multiplicity for p+C interactions at 58 GeV/c for both target-in and target-out (on left) and the case when target-out subtraction

is applied (on right).

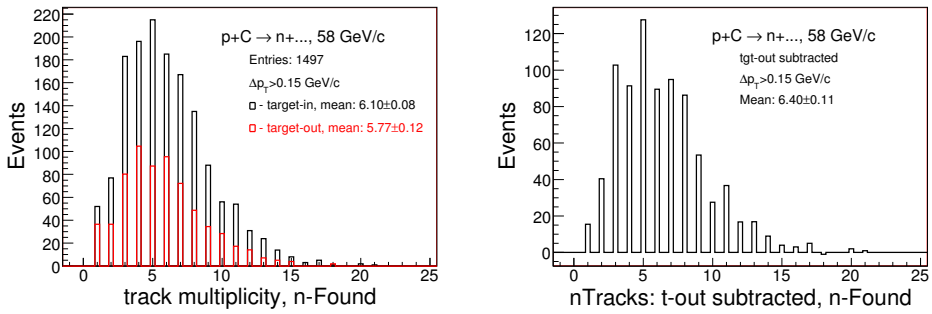

Figure 248: The charged track multiplicity for p+C interactions at 58 GeV/c for both target-in and target-out (on left) and the case when target-out subtraction is applied (on right). Requirements: all events passed the neutron selection cuts.

Figure 249 shows the charged track multiplicity for p+Bi interactions at 58 GeV/c for both target-in and target-out (on left) and the case when target-out subtraction is applied (on right).

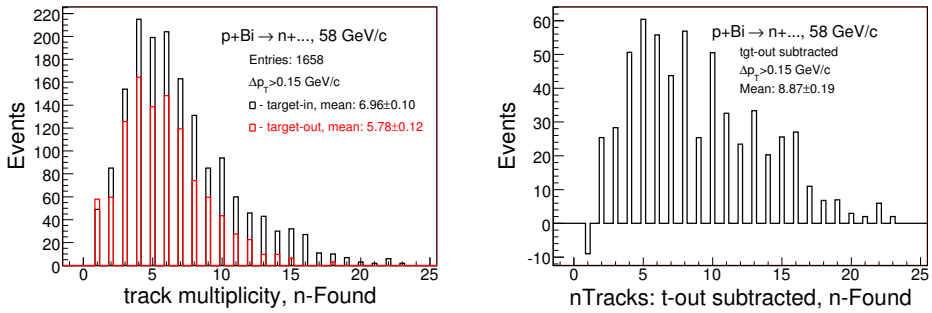

Figure 249: The charged track multiplicity for p+Bi interactions at 58 GeV/c for both target-in and target-out (on left) and the case when target-out subtraction is applied (on right). Requirements: all events passed the neutron selection cuts.

Figure 250 shows the charged track multiplicity for p+U interactions at 58 GeV/c for both target-in and target-out (on left) and the case when target-out subtraction is applied (on right).

Figure 251 shows the charged track multiplicity for p+p interactions at 84 GeV/c for both target-in and target-out (on left) and the case when target-out subtraction is applied (on right).

Figure 252 shows the charged track multiplicity for p+Be interactions at 120 GeV/c for both target-in and target-out (on left) and the case when target-out subtraction is applied (on right).

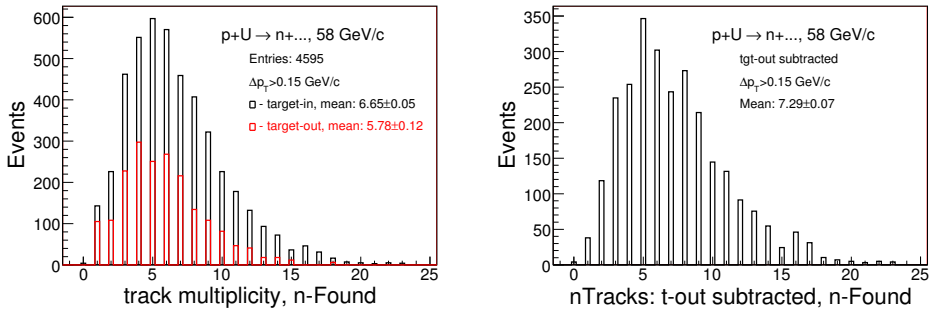

Figure 250: The charged track multiplicity for p+U interactions at 58 GeV/c for both target-in and target-out (on left) and the case when target-out subtraction is applied (on right). Requirements: all events passed the neutron selection cuts.

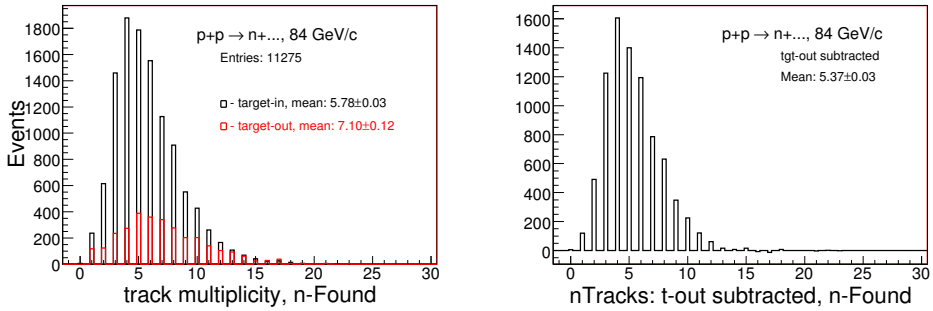

Figure 251: The charged track multiplicity for p+p interactions at 84 GeV/c for both target-in and target-out (on left) and the case when target-out subtraction is applied (on right). Requirements: all events passed the neutron selection cuts.

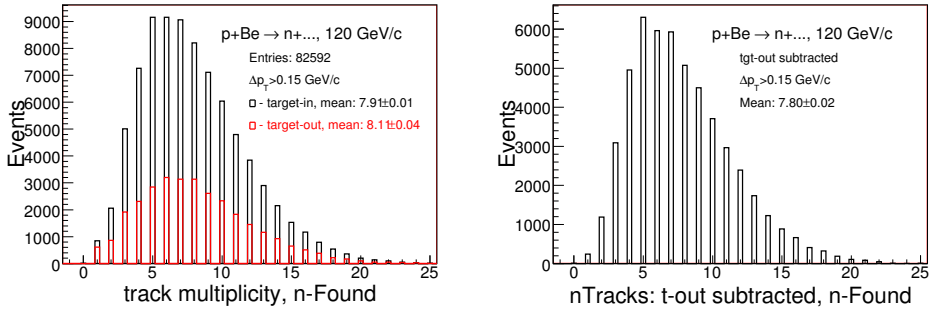

Figure 252: The charged track multiplicity for p+Be interactions at 120 GeV/c for both target-in and target-out (on left) and the case when target-out subtraction is applied (on right). Requirements: all events passed the neutron selection cuts.

Figure 253 shows the charged track multiplicity for p+C interactions at 120 GeV/c for both target-in and target-out (on left) and the case when target-out subtraction is applied (on right).

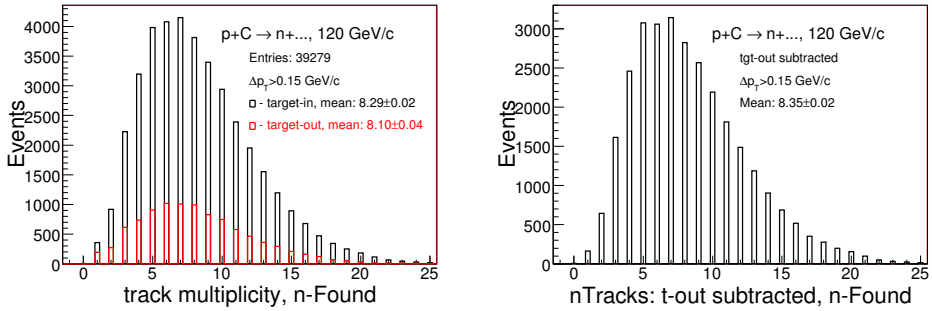

Figure 253: The charged track multiplicity for p+C interactions at 120 GeV/c for both target-in and target-out (on left) and the case when target-out subtraction is applied (on right). Requirements: all events passed the neutron selection cuts.

Figure 254 shows the charged track multiplicity for p+Bi interactions at 120 GeV/c for both target-in and target-out (on left) and the case when target-out subtraction is applied (on right).

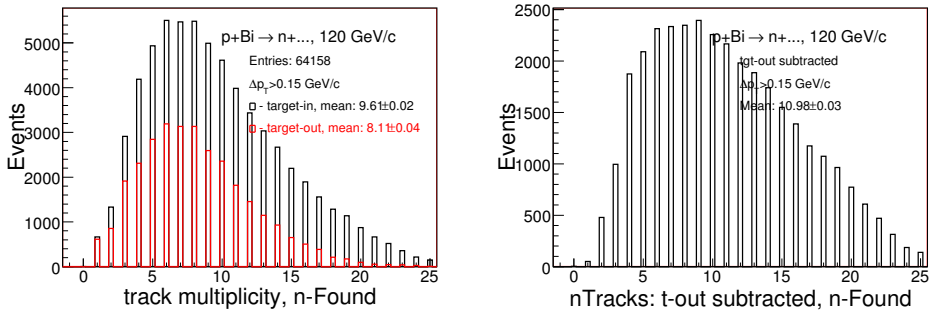

Figure 254: The charged track multiplicity for p+Bi interactions at 120 GeV/c for both target-in and target-out (on left) and the case when target-out subtraction is applied (on right). Requirements: all events passed the neutron selection cuts.

The charged track multiplicity for the proton interaction trigger data with SciHi is on are summarized in Table 62.

E Non-neutron multiplicities

Figure 255 shows the multiplicities for p+C at 58 GeV/c and at 120 GeV/c.

	target-in	target-out	Subtr.	beamTrig
H_2-58 GeV/c	4.81±0.04	5.20±0.17	4.62±0.04	4.6(5.1)±0.4
Be-58 GeV/c	6.03±0.08	5.78±0.12	6.23±0.32	8.7(8.1)±3.0
C-58 GeV/c	6.10±0.08	5.77±0.12	6.40±0.10	5.0(5.4)±1.7
Bi-58 GeV/c	6.96±0.10	5.78±0.12	8.87±0.20	7.6(6.8)±2.9
U-58 GeV/c	6.65±0.05	5.78±0.12	7.29±0.07	5.2(5.7)±0.5
H_2-84 GeV/c	5.78±0.03	7.10±0.12	5.37±0.03	3.7(5.5)±0.2
Be-120 GeV/c	7.91±0.01	8.11±0.04	7.80±0.02	7.1(7.2)±0.3
C-120 GeV/c	8.29±0.02	8.10±0.04	8.35±0.02	7.2(7.4)±0.4
Bi-120 GeV/c	9.61±0.02	8.10±0.04	10.98±0.03	8.5(10.1)±0.4

Table 62: The charged track multiplicity passing through the trigger scintillator using the proton interaction trigger data with SciHi is on. The multiplicities are shown for target-in, target-out and subtraction applied cases using the transverse momentum cut as Δp_T >0.15 GeV/c. Last column represents the multiplicities for the beam trigger without SciHi requirements. All events passed the neutron selection cuts.

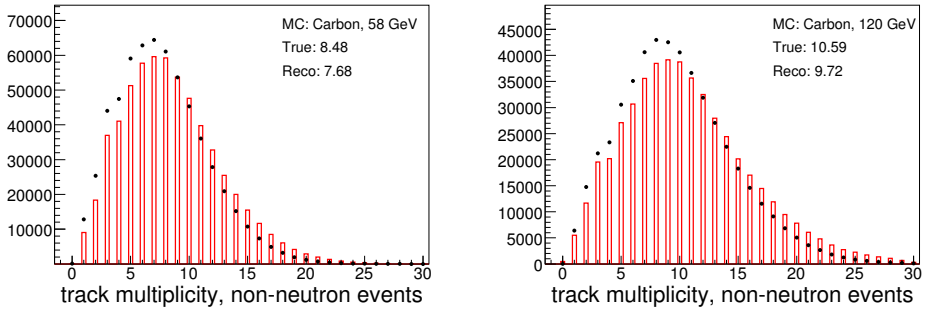

Figure 255: The multiplicities for p+C at 58 GeV/c (left) and at 120 GeV/c (right), respectively.

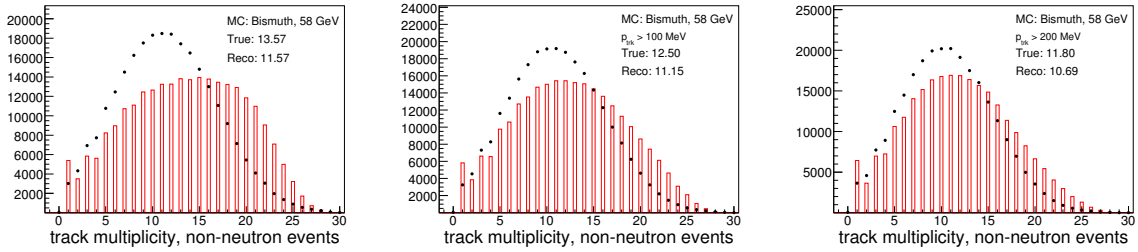

Figure 256: The multiplicities for p+Bi at 58 GeV/c interactions with different track momentum cut: 0 MeV/c (left), 100 MeV/c (middle) and 200 MeV/c (right), respectively.

Figure 256 shows the multiplicities for p+Bi at 58 GeV/c with different track momentum cut: 0 MeV/c, 100 MeV/c and 200 MeV/c.

Figure 257 shows the multiplicities for p+U at 58 GeV/c with different track momentum cut: 0 MeV/c, 100 MeV/c and 200 MeV/c.

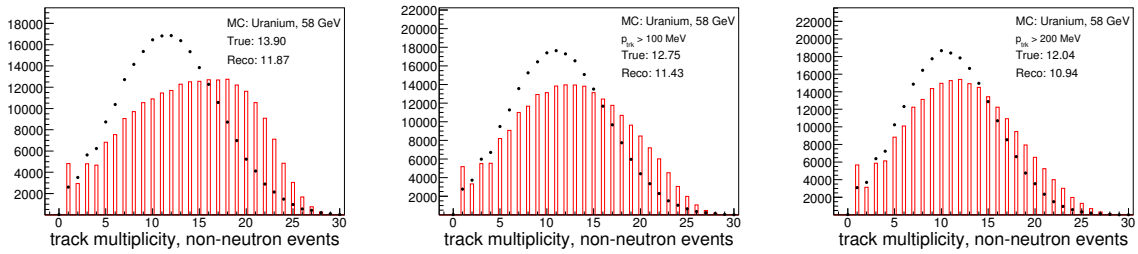

Figure 257: The multiplicities for p+U at 58 GeV/c interactions with different track momentum cut: 0 MeV/c (left), 100 MeV/c (middle) and 200 MeV/c (right), respectively.

Figure 258 shows the multiplicities for p+Bi at 120 GeV/c with different track momentum cut: 0 MeV/c, 100 MeV/c and 200 MeV/c.

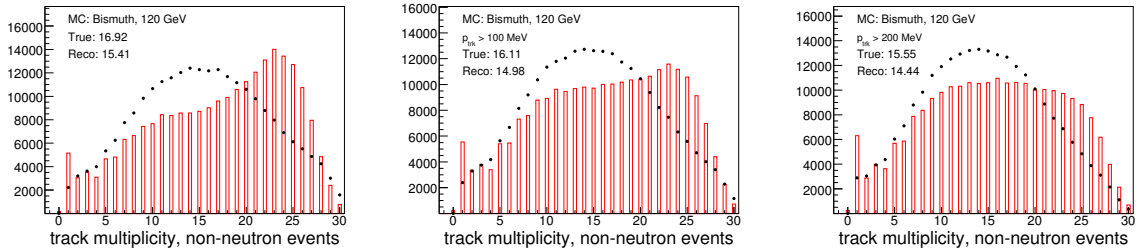

Figure 258: The multiplicities for p+Bi at 120 GeV/c interactions with different track momentum cut: 0 MeV/c (left), 100 MeV/c (middle) and 200 MeV/c (right), respectively.

The charged track multiplicities for the non-neutron samples are summarized in Table 63.

	True(Reco), 0 GeV/c	100 MeV/c	200 MeV/c
C-58 GeV/c	8.5 (7.7)	-	-
Bi-58 GeV/c	13.6 (11.6)	12.5 (11.1)	11.8 (10.7)
U-58 GeV/c	13.9 (11.9)	12.8 (11.4)	12.0 (10.9)
C-120 GeV/c	10.6 (9.7)	-	-
Bi-120 GeV/c	16.9 (15.4)	16.1 (15.0)	15.6 (14.4)

Table 63: The charged track multiplicities for the non-neutron samples with the different track momentum cuts: 0 MeV/c, 100 MeV/c and 200 MeV/c, respectively

F Neutron yield vs the TOF interaction length variation

Figure 259 illustrates the primary neutron production and interaction Z positions using FLUKA p+C sample at 58 GeV/c. Plots made for the different interaction length of TOF wall: nominal, up and down by 25%.

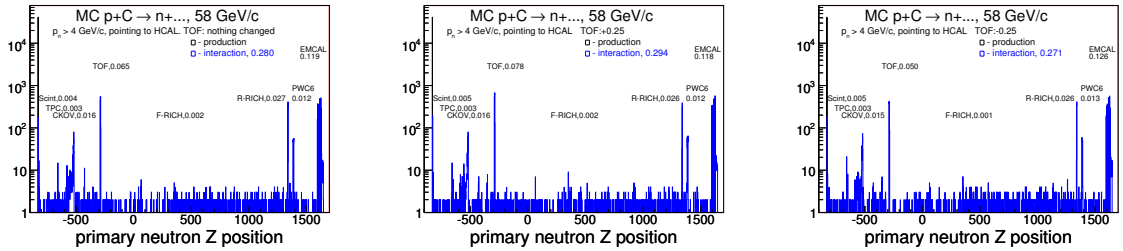

Figure 259: The primary neutron production and interaction Z positions using FLUKA p+C sample at 58 GeV/c. Plots made for the different interaction length of TOF wall: nominal (left), up (middle) and down (right) by 25% of the nominal value. The fractions of the primary neutron losses in TOF wall are 6.5%, 7.8% and 5.0%, respectively.

Variation of the TOF wall's interaction length might lead to the different correction functions, see Figure 260

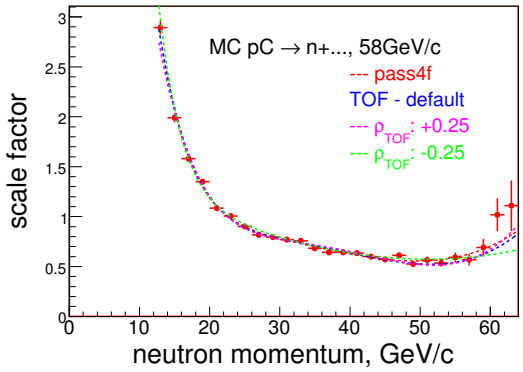

Figure 260: The single correction functions for the different interaction length assignments of the TOF wall using FLUKA p+C 4 samples at 58 GeV/c

Resulting the neutron cross section variations are summarized in Table 64.

Above numbers illustrates how stable the central value of cross section in data vs variations of TOF interaction length assignments:

- $^{+0.3}_{-0.6}$ mb (or $^{+0.007}_{-0.013}$) if TOF interaction length varied by ±25%

	σ_n	Δ
pass4f	45.90±1.51	
ToF IL: default	46.17±1.52	+0.27 mb
ToF IL: +25%	46.21±1.52	+0.31 mb
ToF IL: -25%	45.31±1.49	-0.59 mb

Table 64: Neutron cross section results for ToF interaction length variation using FLUKA 4 p+C samples at 58 GeV/c.

G MC neutron's true spectrum vs reconstructed proton spectrum

Figure 261 illustrates the comparison of the neutron and proton spectra from p+p, p+Be and p+C interactions at 58 GeV/c.

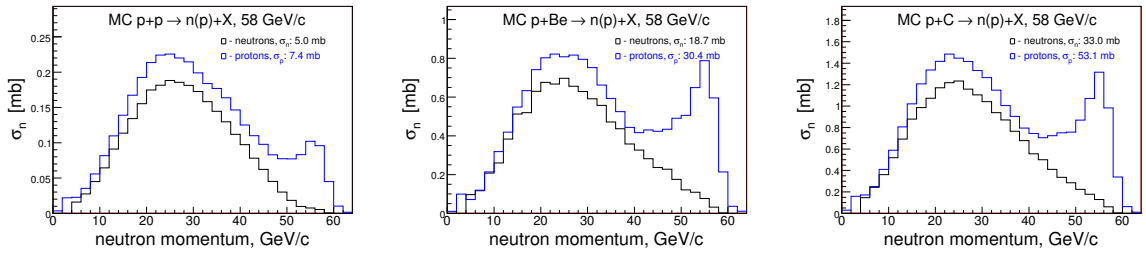

Figure 261: Comparison of the neutron and proton spectra at the same beam momentum using p+p (left), p+Be (middle) and p+C (right) interactions at 58 GeV/c. Neutrons - true, protons - reconstructed with id from MC truth info. Proton tracks are within HCAL fiducial

Figure 262 illustrates the comparison of the neutron and proton spectra from p+Bi and p+U at 58 GeV/c and p+p interactions at 84 GeV/c.

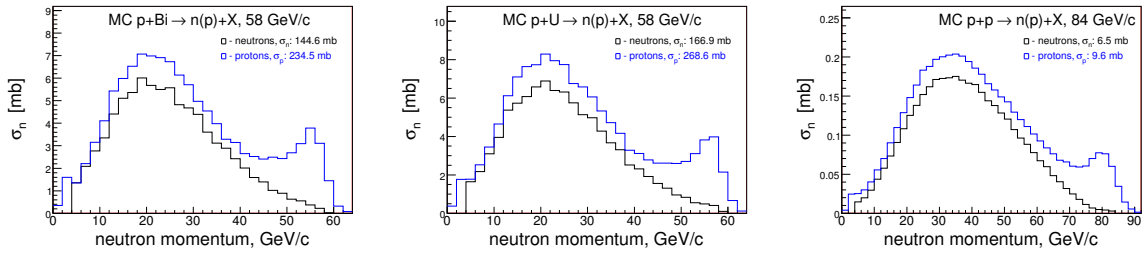

Figure 262: Comparison of the neutron and proton spectra at the same beam momentum using p+Bi (left) and p+U (middle) interactions at 58 GeV/c and p+p (right) interactions at 84 GeV/c. Neutrons - true, protons - reconstructed with id from MC truth info. Proton tracks are within HCAL fiducial

Figure 263 illustrates the comparison of the neutron and proton spectra from p+Be, p+C and p+Bi interactions at 120 GeV/c.

Figure 264 shows the proton and neutron production cross section dependence vs the target atomic weight.

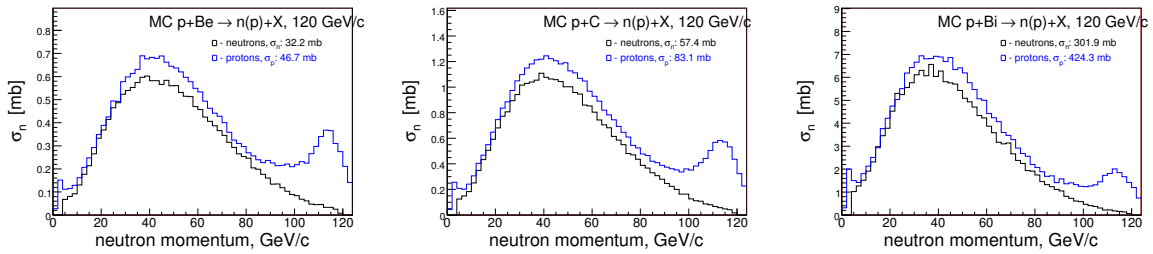

Figure 263: Comparison of the neutron and proton spectra at the same beam momentum using p+Be (left), p+C (middle) and p+Bi (right) interactions at 120 GeV/c. Neutrons - true, protons - reconstructed with id from MC truth info. Proton tracks are within HCAL fiducial

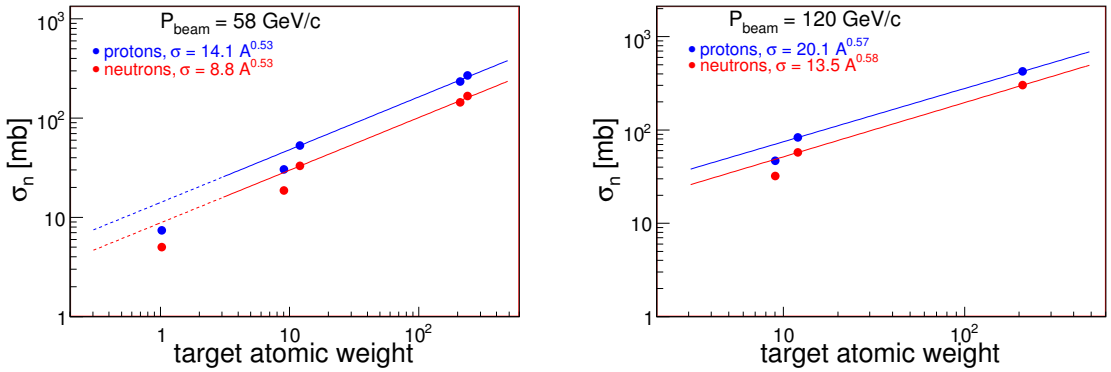

Figure 264: Monte Carlo neutron and proton production cross section dependence vs the target atomic weight. Requirements for neutrons: produced in the primary target, identified as neutron using truth info and it pointing to HCAL. Requirements for protons: reconstructed track was identified as a proton using MC info and it pointing to HCAL. Blue and red lines represents the fit results. For both plots the fit procedure was constrained not to use the result from Be target.

H More on Be issue with FLUKA: v.06 vs v.08

Figure 265 illustrates the neutron and proton yields from FLUKA06 and 08 using pure MC p+Be interactions at 58 GeV/c.

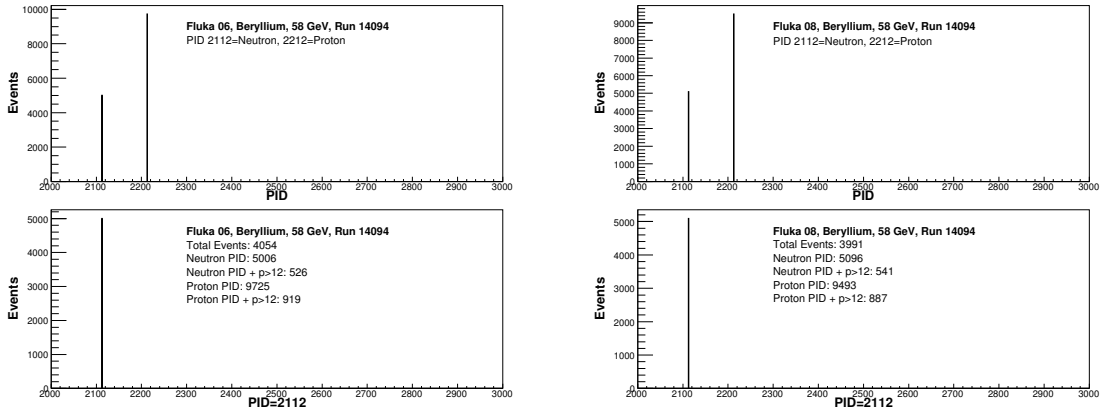

Figure 265: The illustrations on the neutron yields from p+Be interations at 58 GeV/c using FLUKA06 (left) and 08 (right). p_n >12 GeV/c, HCAL fiducial is not required. The results based on the pure MC info using p+Be interactions at 58 GeV/c.

Figure 266 illustrates the neutron and proton yields from FLUKA06 and 08 using pure MC p+C interactions at 58 GeV/c.

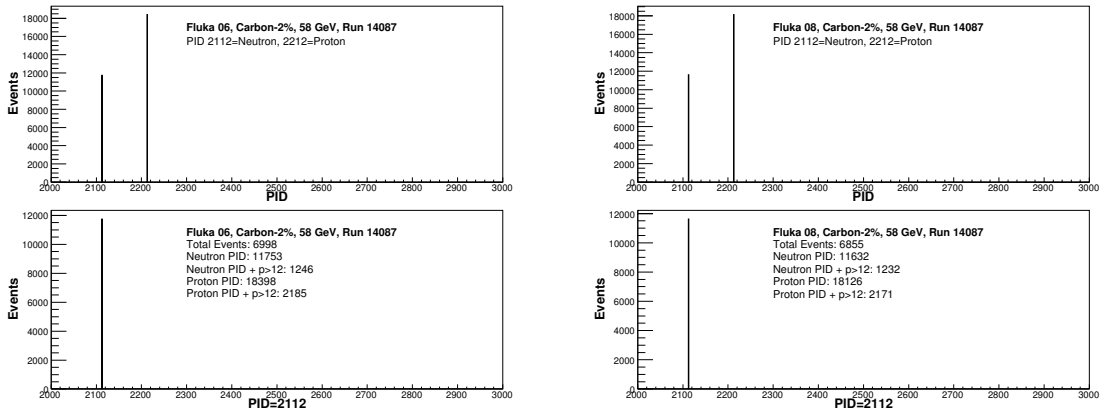

Figure 266: The illustrations on the neutron yields from p+C interations at 120 GeV/c using FLUKA06 (left) and 08 (right). p_n >12 GeV/c, HCAL fiducial is not required. The results based on the pure MC info using p+Be interactions at 58 GeV/c.

Figure 267 illustrates the neutron and proton yields from FLUKA06 and 08 using pure MC p+Bi interactions at 58 GeV/c.

Figure 268 illustrates the neutron and proton yields from FLUKA06 and 08 using pure MC p+Be interactions at 120 GeV/c.

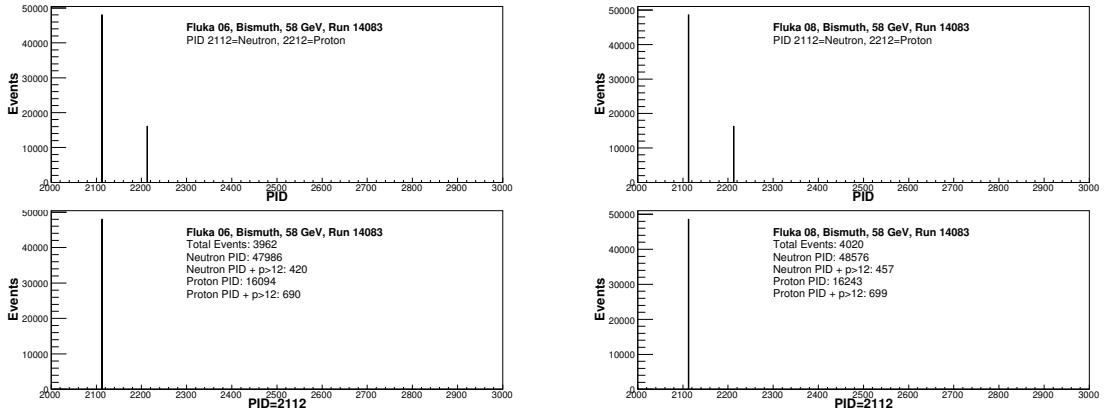

Figure 267: The illustrations on the neutron yields from p+Bi interations at 58 GeV/c using FLUKA06 (left) and 08 (right). p_n >12 GeV/c, HCAL fiducial is not required. The results based on the pure MC info using p+Be interactions at 58 GeV/c.

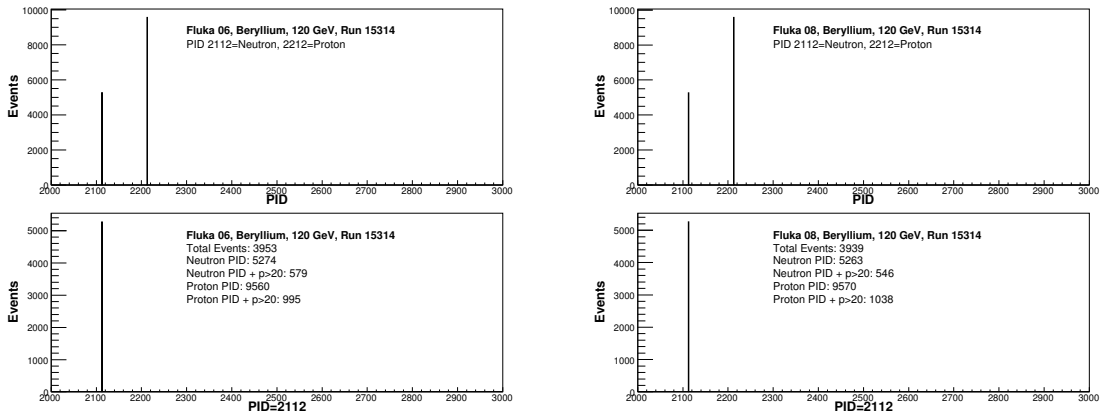

Figure 268: The illustrations on the neutron yields from p+Be interations at 120 GeV/c using FLUKA06 (left) and 08 (right). p_n >20 GeV/c, HCAL fiducial is not required. The results based on the pure MC info using p+Be interactions at 120 GeV/c.

Figure 269 illustrates the neutron and proton yields from FLUKA06 and 08 using pure MC p+C interactions at 120 GeV/c.

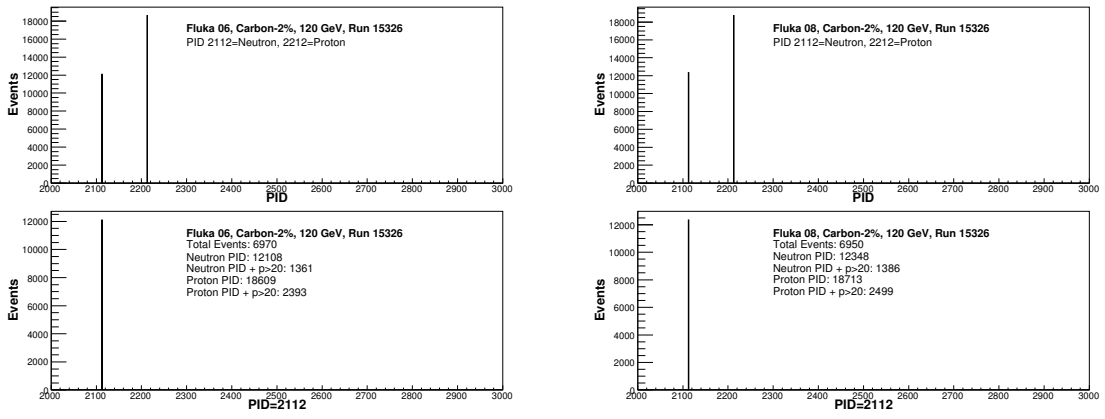

Figure 269: The illustrations on the neutron yields from p+C interations at 120 GeV/c using FLUKA06 (left) and 08 (right). p_n >20 GeV/c, HCAL fiducial is not required. The results based on the pure MC info using p+Be interactions at 120 GeV/c.

Figure 270 illustrates the neutron and proton yields from FLUKA06 and 08 using pure MC p+Bi interactions at 120 GeV/c.

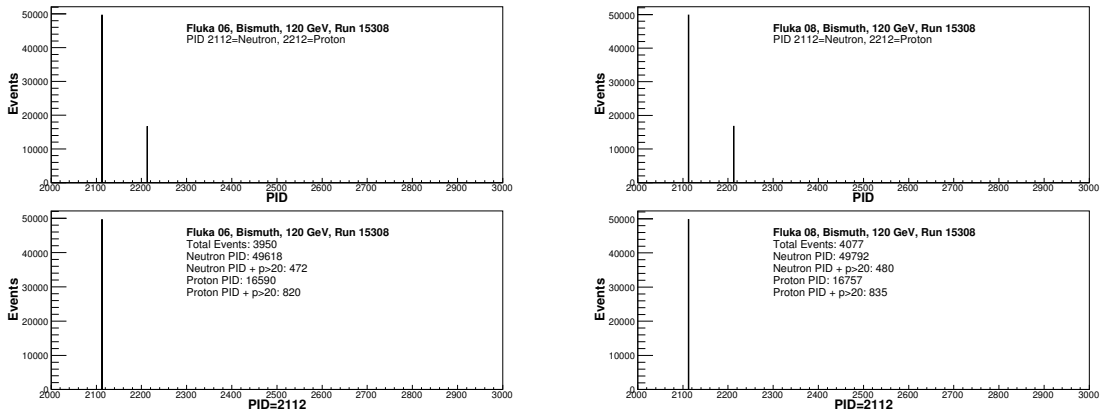

Figure 270: The illustrations on the neutron yields from p+Bi interations at 120 GeV/c using FLUKA06 (left) and 08 (right). p_n >20 GeV/c, HCAL fiducial is not required. The results based on the pure MC info using p+Be interactions at 120 GeV/c.

The results for neutron yields are summarized in Table 65.
The proton yields are summarized in Table 66.

	FLUKA06	FLUKA08
Be 58 GeV/c	526*258/4054→33.5 mb	541*258/3991→35.0 mb
C 58 GeV/c	1246*330/6998→58.8 mb	1232*330/6855→59.3 mb
Bi 58 GeV/c	420*3246/3962→344 mb	457*3246/4020→369 mb
Be 120 GeV/c	579*260/3953→38.1 mb	546*260/3939→36.0 mb
C 120 GeV/c	1361*332/6970→64.8 mb	1386*332/6950→66.2 mb
Bi 58 GeV/c	472*3255/3950→389 mb	480*3255/4077→383 mb

Table 65: The summary of neutron yields from p+Be, p+C and p+Bi interactions at 58 and 120 GeV/c using FLUKA06 and 08.

	FLUKA06	FLUKA08
Be 58 GeV/c	919*258/4054→58.5 mb	887*258/3991→57.3 mb
C 58 GeV/c	2185*330/6998→103 mb	2171*330/6855→105 mb
Bi 58 GeV/c	690*3246/3962→565 mb	699*3246/4020→564 mb
Be 120 GeV/c	995*260/3953→65.4 mb	1038*260/3939→68.5 mb
C 120 GeV/c	2393*332/6970→114 mb	2499*332/6950→119 mb
Bi 58 GeV/c	820*3255/3950→676 mb	835*3255/4077→667 mb

Table 66: The summary of proton yields from p+Be, p+C and p+Bi interactions at 58 and 120 GeV/c using FLUKA06 and 08.

I Are elastic events in FLUKA generator?

What was found in first 100 events of p+p and p+C MC samples are summarized in Table 67.

	p+p,58 GeV/c	p+C 58 GeV/c
single proton exiting target	0	26
quasi elastic	0	4
hadron production	100	70

Table 67: